University of Canterbury

Department of Civil and Natural Resources Engineering

Seismic Performance Assessment of a Base Isolated Building

Thesis for Master's Degree

Candidate:

Alvin Yang

Supervisors:

Professor Timothy J. Sullivan

Professor Brendon A. Bradley

Adjunct Professor J. Didier Pettinga

Earthquake Engineering Programme

University of Canterbury

Christchurch, New Zealand

2020

Abstract

Recent studies have demonstrated the practical usage of the Pacific Earthquake Engineering Research Performance-Based Earthquake Engineering (PEER-PBEE) framework to quantify performance measures, such as monetary losses and downtime, for buildings under seismic conditions. However, in most of these studies the PEER-PBEE framework was applied for traditional buildings.

This research aims, firstly, to provide evidence on the effectiveness in seismic performance of structures with base isolation compared to a fixed base, in terms of the expected annual loss and expected downtime, by performing loss assessment of a case study building that is base isolated. The research finds that the EAL of the base isolated building is 0.0012% with a standard deviation of 0.00028% the building replacement cost. This was found to be around 50-100 times lower than the EAL of a 12-storey and 4-storey traditional steel moment resisting frame office buildings.

Secondly, the cost of inviting a structural engineer to manually inspect and assess the building is considered in the loss analysis. Installing smartphones on the building to function as seismic monitoring system was found to help in reducing the cost of post-earthquake investigation by reducing the cost and downtime associated with manual inspection, and is likely to be beneficial in the long term for reducing cost and downtime.

Keywords: PEER-PBEE, loss estimation, base isolation, reinforced concrete structural walls, seismic monitoring.

Acknowledgements

Firstly, I would like to thank my supervisors, Professor Tim Sullivan, Professor Brendon Bradley, and Dr. Didier Pettinga, for giving lots of feedback and guidance throughout my research. They lead the way on my research direction and helped me a lot along the way during execution. Without their teaching and patience, I would have never completed this research and thesis.

I would like to give special thanks to Amir Orumiyehei and Fransiscus Asisi Arifin for providing information and assistance for the research.

I would also like to acknowledge Muhammad Rashid for allowing me to perform experiment on the shaketable.

Special thanks also to my parents and sister for supporting me throughout this master's degree.

Table of Contents

Table of Figures

Table of Tables

1. Introduction

1.1. Background

Earthquakes are usually associated with the collapse of a building, especially if the magnitude of the earthquake is large. However, current building codes are advanced enough to prevent major structural failures and loss of life through techniques such as capacity design. This is proven by the fact that many modern buildings in New Zealand designed after the 1970s survived the February 2011 Earthquake in Christchurch that was reported as being almost twice the design intensity (Kam et al., 2011).

The focus of current codes is not on limiting damage or maintaining function of the building post-earthquake. However, life safety alone is not enough because the costs of repair or replacement due to damage were observed to be a major issue.

This study will use the PEER-PBEE (FEMA P-58) framework to perform a loss analysis on a case study building that is base isolated. The PEER-PBEE framework is chosen because it is able to account for uncertainty and randomness in ground motions, constructional material, labour costs, etc., in its computation. Moreover, it allows the building performance to be expressed in terms of monetary loss which may assist with seismic risk communication.

The case study building is a base isolated multi-storey residential building located in central Christchurch, New Zealand. A 3D structural model of the case study building is developed will be Ruaumoko 3D (Carr, 2005) to generate engineering demand parameters (EDPs) for computing losses. Since a rigorous application of the PEER-PBEE framework is time consuming, the SLAT software (Bradley, 2009) will be used to speed up the calculations.

The seismic performance of the case study building will be compared in terms of the direct losses to traditional buildings from the literatures. The key objective is to quantify the cost-saving that results from having base isolation

through comparing the expected annual losses (EALs) of the case study building and traditional buildings.

The value of having seismic instrumentation in terms of reducing the cost and downtime associated is investigated. Firstly, the benefits of installing accelerometer sensors to measure structural integrity after earthquakes is investigated by comparing the reduction of the cost and downtime associated with manual inspections. Next, a cheaper alternative of using smartphones as seismic sensors will be investigated because seismic accelerometers are generally expensive. Finally, a procedure to estimate the storey stiffness from accelerometer data is devised to help engineers in performing post-earthquake inspection for reducing downtime.

1.2. Description of the Case Study Building

The building footprint of the case study building are 22.59 m along the East-West direction, 18.5 m along the North-South direction, and a height of 45.21 m. Figure 1 illustrates the apartment building as viewed from different angles.

Figure 1. Pictures of the apartment building used in the study

The building has a total of nine levels. The ground level units are gallery units with two storeys, where the first two levels are denoted as ground (G) and upper

ground (UG) floors. The next few levels above are the first level (L1) to the fifth level (L5) consisting of standard single storey units. Finally, the penthouse units starting from the eighth storey are gallery units that are each two storeys high, where the lower level is denoted as penthouse ground (PG) and the upper level as penthouse first floor (P1). In addition to the roof level (R), the building has ten levels structurally. The base isolators are located at the basement below the ground floor. The basement is not used for anything else except to accommodate services that allow for extra seismic movement, such as for the sprinkler pipes.

At each level, the building consists of two residential units separated at the middle along the North-South axis. Every residential unit is serviced by its own elevator, meaning that there are two elevator shafts in the building. Additionally, a common stairwell at the southern side of the building provides service from the ground floor to all levels except the penthouse first level (P1).

1.3. Objectives

This research investigates the cost-efficiency of base isolation for a building with reinforced concrete structural walls as the main lateral resisting system considering seismic risk in terms of expected annual loss (EAL). Therefore, the main objective of this research is to provide empirical evidence that base isolation can provide substantial cost-savings.

Another aspect of this study will be to research the cost and downtime associated with inviting a structural engineer to perform inspection of the building after an earthquake. This is motivated by the number of building demolitions that occurred after the Christchurch earthquakes due to difficulties in assessing damages in the buildings (Marquis et al., 2017).

1.4. General Performance of Reinforced Concrete Buildings

As explained previously, the objective of this research is to examine the cost-effectiveness of the case study apartment building. In this study, the apartment building will be analysed and used as the basis to answer the research questions formulated in this chapter regarding cost-effectiveness of base isolation and

seismic instrumentation. Since the case study building is a reinforced concrete building, the first task is to review the general performance of reinforced concrete buildings.

The 4 September 2010 and 22 February 2011 Christchurch earthquakes are important for showing the performances of many reinforced concrete buildings, and particularly for structural walls, due to earthquakes. In the Christchurch CBD, it is reported that the 4 September earthquake response spectral ordinates were generally exceeding the 500-years return period design level and the 22 February 2011 earthquake the seismic demands for buildings with periods between 0.5 s to 1.8 s and 2.8 s to 3.5 s were close to or above the 2,500-year return-period design spectra (Kam et al., 2011).

The 4 September earthquake showed that, even if a building is structurally sound, the direct repair costs of non-structural elements represented a major component in the total loss. The main issue is that non-structural components are sensitive to the building responses. Base isolation may be able to provide an effective solution to this by reducing the superstructure response and thereby lowering the total loss. Thus, a key aspect of this research will contribute to addressing the effectiveness of this system.

A large majority of modern (post-1976) RC buildings performed as expected during the 22 February earthquake (Kam et al., 2011). In particular, the colour-tagging distribution for RC structural wall buildings saw green tags at 48.4%, yellow tags at 31.9%, and red tags at 19.8%. In general, buildings designed previous to 1976 have a higher proportion of being red tagged compared to modern buildings.

It is noteworthy that some of the RC buildings were deemed uneconomical to be repaired, even though they exhibited good ductile behaviour. This was attributed to a general lack of confidence in the structural integrity of these potentially damaged structures in the event of one or more severe aftershocks.

As a result, many of these modern buildings that could have been reused were demolished.

Because of the large number of potentially unsafe structures, the uncertainty in their structural integrity also caused a significant delay that resulted in a substantial downtime for many buildings. An effective solution to address this issue might be to install seismic instrumentation to the buildings, so that a reliable and relatively inexpensive assessment of the structural integrity can be quickly performed after a major earthquake or aftershock. A part of this research will investigate how seismic instrumentation might reduce the cost and downtime associated with manual inspections after a major earthquake.

Another advantage of seismic instrumentation is that it could provide a more accurate assessment of the structural integrity than visual inspection. Based on the experience of the 22 February earthquake, the demolition of a multi-storey building can involve quite an extensive amount of time and non-negligible cost. Moreover, the demolition of a single building can affect the accessibility or operation of adjacent or close-by buildings. These and other factors showed that having an accurate assessment can be very important. It is undesirable that a building is deemed unsafe and subsequently tagged for demolition due to a lack of information when making the post-earthquake decision. The time-series history of the building response that seismic instrumentation provides may assist engineers make better post-earthquake decision.

1.5. Research Questions and Objectives

This research will investigate the cost effectiveness of a base isolated structure when compared to traditional buildings. In this research, a case study building will be examined and used as a basis for comparison. This case study building is a base isolated apartment building with reinforced concrete walls as its primary lateral resisting system in the superstructure. The modelling and analysis will be explained in detail in the following chapters.

The primary objectives of this study are to:

1. Perform loss analysis assessment on the base isolated building.
   This entails:
   1.1. Building a 3D structural model in Ruaumoko (Carr, 2005).
   1.2. Verifying the structural model and conducting structural analyses.
   1.3. Performing loss analysis based on the PEER-PBEE framework and the literature.

2. Investigate how different structural typologies can change the seismic performance.
   This entails:
   2.1. Comparing the Expected Annual Loss (EAL) of the base isolated building to traditional constructions by referring to results from the literature.

3. Explore the benefits of seismic instrumentation on the expected repair costs of a building and investigate cheaper alternatives.
   This entails:
   3.1. Identifying the typical time and cost of a post-earthquake inspection.
   3.2. Establishing a value case for instrumentation of buildings in terms of repairability assessment by comparing repair costs with and without instrumentation.
   3.3. Investigating the potential of smartphones as cheaper alternative to accelerometer sensors in recording acceleration data.

To achieve the objectives of this research, the scope of this research is limited to:

- This research will focus on just a single case study building. This is justified because the objective is not to compare the loss analysis of base isolated buildings against tradition construction in general but rather to provide a point of reference for engineers and future decision makers when considering base isolation.
- Multi-stripe non-linear response history analyses (NLRHA) will be performed at nine intensity levels for a time-based loss analysis. The ground motions were provided by Yeow, Orumiyehei, et al. (2018) and

were selected by using the GCIM approach (Bradley, 2010) based on PSHA at Christchurch City Centre.

With these scopes and objectives, this research will attempt to answer the following questions:

1. What is the expected annual loss of a typical New Zealand base isolated building?

* The earthquake performance of the building will be analysed prior to performing a time-based loss analysis following the PEER-PBEE framework.

2. How does the expected annual loss of the case study building compare with other structural typologies?

* As discussed previously, damage to non-structural components represented a major contribution to the total loss. The main benefit of base isolation is in reducing the superstructure responses, thereby reducing damages in non-structural components.

3. Can seismic monitoring significantly reduce cost and downtime associated with manual inspection of a building after earthquakes?

* As highlighted previously, seismic instrumentation may help to reduce cost and downtime after an earthquake by providing valuable response history data so that decision can be made quickly and more reliably.

2. Literature Review

2.1. Seismic Performance

2.1.1. Current Seismic Performance Objectives in New Zealand

In a conventional seismic design approach, a building is designed to prevent failure of individual structural components. This is done through consideration of the system, with design requirements such as the strong-column-weak-beam requirement (Porter, 2003). A design is believed to be satisfactory when the member forces and lateral displacements of the building from analysis are below some predefined limits. However, standards such as the AS/NZS1170.5:2002 usually provided limited accuracy in deriving the design accelerations for analysis. Another downside is that the approach is binary and deterministic (Porter, 2003). Consequently, the inherent variations in the risk of collapse, fatalities, repair costs and downtime are not always available to the decision makers.

To improve this shortcoming, the ASCE-41 standard was developed to allow engineers to better quantify the seismic engineering performance of a building under selected ground motion intensities. The standard was applied during the design, by Holmes Consulting, of the base isolated building used in this study by selecting four well-defined limit states, with each being associated to a specific ground motion intensity or return period chosen by the structural engineer.

The SLS1 limit state based on ASCE-41 standard (Pekelnicky & Poland, 2012) is defined as follows:

- No damage should be expected, except for very minor damage (e.g. cracking of brittle masonry and concrete which would generally not require any repair).

The DCLS or Immediate Occupancy limit state based on the ASCE-41 standard (Pekelnicky & Poland, 2012) is defined as follows:

- Expect minimal or no damage to structural and minor damage to non-structural components. Although immediate occupancy is possible, it might need some repair or clean ups to restore the non-structural components to their original state.
- Some utility services, such as power, water and natural gas might be impaired.
- Structural components retained no permanent drift, while sustaining original strength and stiffness.
- Some cracking of facades, partitions and ceilings might happen.
- Minor diagonal cracking of the walls, especially in the coupling beam of wall openings. However, repairs to the concrete shear wall are anticipated to be limited to epoxy injection and patch repair of minor areas of concrete spalling.
- The walls were designed to remain nominally elastic after the DCLS level earthquakes.
- The isolators were designed such that replacement will not be required following a DCLS level earthquake. The engineers also noted that the isolators were designed to sustain earthquake loading in excess of 200% required for ULS (Oliver, 2016).

The ULS or Life Safety limit state based on the ASCE-41 standard (Pekelnicky & Poland, 2012) is defined as follows:

- Some structural and non-structural components are extensively damaged.
- There are damages around the wall openings with extensive flexural and shear cracks at the coupling beams. Some crushing of concrete, but generally remains intact.
- Only minor injuries to occupants and no life threatening injuries are expected. Damaged structural and non-structural components are

designed such that no large falling debris hazard to the occupants will be caused.

- Repairs for buildings experiencing this damage state may not necessarily be economical.
- Capacity design principles were used when designing this building to meet the life safety objective (Oliver, 2016). The walls are the primary lateral resisting elements and so capacity design was applied for yielding at their base.

The Collapse Prevention (CP) limit state based on the ASCE-41 standard (Pekelnicky & Poland, 2012) is defined as follows:

- Building on the verge of collapse. Significant degradation of stiffness and strength in lateral force resisting system and large residual displacement. However, critical gravity carrying components must continue to be able to carry their gravity loads.
- Significant risk of falling debris hazard exists from structural and non-structural components.
- Buildings can collapse under aftershocks and should not be reoccupied.
- The AS/NZS 1170.5 standard does not require explicit check of building performance level beyond the ULS or Life Safety limit state, including the Collapse Prevention limit state. Oliver (2016) argues that this is because structures designed according to the New Zealand material standards (i.e. NZS 3101:2006) are expected to have structural resilience to resist loads 1.5-1.8x the ULS loads.

For the four limit states described above, the following return period intensity levels were used:

Limit state	Design return period (1/years)
DCLS	475
ULS	475

CP	2000

The buildings were designed to limit drift and deformation at each limit state as follows:

- For DCLS, the engineers specified a superstructure drift of 0.5% to simplify detailing of non-structural partition walls.
- For ULS, the inter-storey drift limits between adjacent levels considered in the design were adopted in accordance with the AS/NZS1170.0:2002 standard. The standard specified an inter-storey drift limit of 2.5%. The design acceleration (g) for components at each storey above the isolation for both ULS and SLS were computed using equations from AS/NZS1170.5.

It is notable that both the DCLS and ULS limit states were defined for a 1 in 475 years return period. However, the DCLS limit state specified an inter-storey drift limit of 0.5%, whereas the ULS limit state was 2.5%. Therefore, the DCLS limit state governed in the design process of the building.

2.1.2. Performance Based Earthquake Engineering Methodology

In contrast to the conventional design approach, a Performance Based Earthquake Engineering (PBEE) methodology permits quantification of performance metrics that are considered more relevant to decision makers. These metrics are probabilistic estimates of the repair and restoration costs, risk of casualties, and loss in functionality (Deirlein et al., 2003). Doing this allows the extraction of useful information for the client, including the expected annual monetary loss and probability of collapse. Base isolated buildings should entail lower expected losses compared to traditional construction when analysed using the PBEE methodology (Sullivan et al., 2014). This information can potentially aid building owners in justifying the higher initial cost associated with the installation of a base isolation system.

The PBEE framework starts with defining the structural type and the site location, followed by four analysis stages. Namely, these are the hazard analysis stage, structural analysis stage, damage analysis stage and loss analysis stage, as showcased by Figure 2. A primary advantage in dividing into stages is that each stage becomes well encapsulated. Hence, expertise of the entire methodology will not be required by the practicing engineers and stakeholders (Porter, 2003).

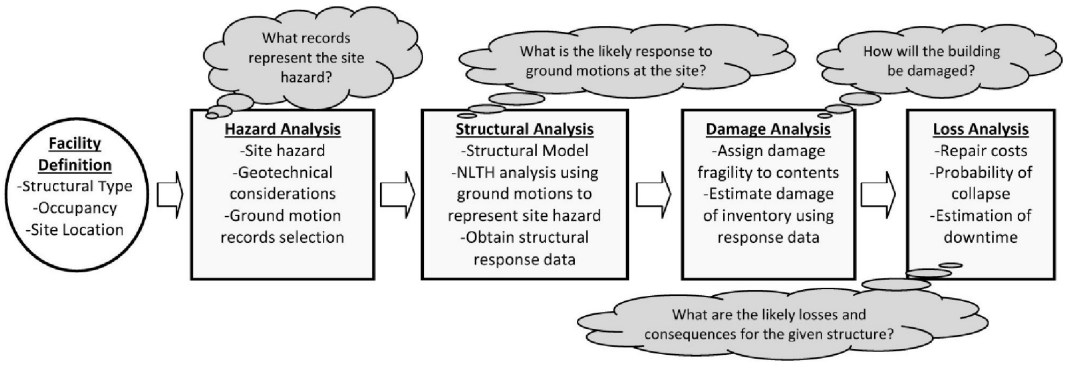

Figure 2. Description of the four analysis stages in PBEE (Sullivan et al., 2014)

To begin with, the site hazard curve can be generated through a Probabilistic Seismic Hazard Analysis. The Probabilistic Seismic Hazard Analysis predicts the probabilistic distribution of ground motion intensity as a function of the fault type, distance to epicentre and path effects, and local site effect and amplifications. Thus, the outputs of this stage are characteristic ground motions that represent the different intensity levels as well as their annual frequency of exceedance. The engineering demand parameters (EDPs) are then obtained by using these ground motions into non-linear computer analyses of a computer model of the building structure. These EDPs are structural responses such as the storey drifts and floor accelerations.

The probabilities of various damage states occurring in a structural or non-structural component can be computed through fragility functions (Ramirez, 2009). A component with multiple damage states can be related to the EDPs

through fragility functions. Furthermore, using a fragility function is advantageous because the failure of a component can be entirely measured from experimental data, without the need to consult expert opinions (Porter, 2003).

Finally, the expected annual loss (EAL) of the building can be calculated as a performance measurement to assist decision makers (Bradley et al., 2008). The EAL is defined as the expected monetary loss associated with repair of damaged structural or non-structural components a building is likely to experience on average each year. It can be computed by integrating the product of the mean repair cost for a given seismic intensity and its associated annual frequency of exceedance over the seismic intensity levels of interest (Bradley et al., 2008).

Aside from monetary losses, the likelihood for fatalities or injury from a given seismic intensity level may be estimated by relating the damage states of a structure to the number of lives exposed to those damage states. This process is typically done by utilising the collapse fragility function, which established the risk of collapse over a range of seismic intensity levels, and a population model to estimate the likelihood of fatalities or injury (Sullivan et al., 2014).

2.1.3. Cost-benefit of Base Isolated Buildings

The cost-benefit of base isolated buildings and conventional buildings in New Zealand was compared in the study by Cutfield et al. (2014). The study examined two hypothetical three-story steel braced office buildings, one base isolated with LRBs and the other with conventional foundation. The conventional building was designed as a SCBF (Special Concentrically Braced Frame) with force reduction factor of $R = 6$, while the base isolated building was designed as an OCBF (Ordinary Concentrically Braced Frame) with force reduction factor of $R = 1$. Three-dimensional models of the base isolated building and conventional building were created and analysed using a non-linear finite element analysis software. Notably, two models were created for the base isolated building, one with consideration of a moat wall and another without.

Multi-stripe NLTH analyses for a range of ten intensity levels were performed on these structural models. It was found that base isolation significantly reduced both peak floor acceleration and peak inter-storey drifts when compared with conventional foundation. The simulations also showed that pounding of the base isolated building against moat wall generally increased in frequency with intensity levels. Moreover, it was found that pounding typically amplified the peak floor accelerations at the superstructure.

Loss analysis was performed on both the base isolated building, with and without a moat wall, and the conventional building. It was assumed that the buildings were designed for office use and the damageable component inventory included structural components, non-structural components, and building contents. The quantities of each item as well as the fragility curves and repair costs were assumed from the FEMA P-58 guidelines. It was found that at the same hazard level, the significant contribution to financial losses in the isolated OCBF was from repair cost to minor damage in interior partitions. Furthermore, losses in the isolated building become particularly significant at higher intensity levels, where occurrence of moat wall pounding resulted in a large contribution to losses. Nevertheless, the EAL for conventional SCBF was $20,500, for isolated OCBF with consideration of moat wall the EAL was $2,000, whereas for the isolated OCBF without consideration of moat wall the EAL was $160.

From the study by Cutfield et al. (2014), it can be seen that an expected annual cost saving of almost 130 times can be achieved if there is no moat wall pounding. The study concluded that the performance of the isolated building models was far superior to the conventional building model, although this performance degraded somewhat in the unlikely event of structural pounding against the building's moat wall.

This research will conduct a similar study to contribute to the knowledge of cost saving for base isolation versus conventional structural systems. The difference

is that this research will consider an existing residential building in Christchurch, with a focus on its direct loss.

2.2. Base Isolation Systems

2.2.1. Elastomeric Rubber Bearings

Base isolation is a commonly implemented technique for mitigating structural and non-structural damage during earthquakes. The primary function of an isolation system is to shift the fundamental frequency of the structure to a value below the range of frequencies in dominating earthquake input (Al-Azawi et al., 2017). One well-known example of its excellent performance is the base-isolated USC hospital building in Los Angeles. During the 1994 Northridge earthquake, the building remained undamaged and had a superstructure drift ratio below 10% of the limit (Celebi, 1996).

Elastomeric bearings are composed of alternating layers of laminated rubber layers and steel shims. The purpose of the steel shim plates is to restrain the rubber at the bond interface and provide vertical stiffness to the rubber bearing. Traditionally, the compression stiffness of typical elastomeric bearings is several thousand times greater than its horizontal stiffness (Warn & Ryan, 2012).

Low damping natural or synthetic rubber bearings usually requires external dampers, such as a linear viscous damper, to provide additional damping (Al-Azawi et al., 2017). Although high damping rubber can provide significant damping, lead-rubber bearing can provide a more stable bilinear hysteresis behaviour (Yang & Zhang, 2018).

2.2.2. Lead Rubber Bearings

Modern lead-rubber bearings (LRB) differ from high damping rubber bearings only by the lead plug inserted at the centre of the bearing. The addition of the lead plug enhances the energy dissipation in comparison to low damping elastomeric bearings (Warn & Ryan, 2012) and provides a bilinear hysteretic

behaviour. In a typical structural system, the lead plug approximately increases damping to 10-15% of critical damping (Nagarajaiah et al., 1991). Thus, there is usually no need to supplement with external damping devices. Like elastomeric bearings, the vertical stiffness is several thousand times higher than horizontal stiffness. Therefore, lead-rubber bearings provide effective isolation only in the horizontal direction (Warn & Ryan, 2012).

The LRB may fail in buckling when there is large presence of compressive axial load originating from the superstructure's gravity load and associated overturning forces from the lateral load (Sanchez et al., 2012). The bearing will lose its shear and axial resistance when buckling occurs. Therefore, the design of elastomeric bearings must account for buckling to prevent catastrophic failure of the building.

A model to account for the shear force and axial force interaction was developed by Koh & Kelly (1988). At a given point of time, the vertical stiffness of the lead-rubber bearing is modelled as a function of shear deformation, while its shear stiffness is a function of the axial load and critical buckling load. The overlapping area between the uppermost and lowermost layers is reduced as the lead-rubber bearing is subjected to shear displacement resulting in a reduction of the critical buckling load (Buckle & Liu, 1994).

In addition to buckling failure, there are also some models that have been developed to account for second order (P-delta) effects. However, these models have not been widely used due to the need for a large amount of experimental data to calibrate the model parameters (Warn & Ryan, 2012).

Uplift or tension is resisted by the combined action of the rubber and lead plug. The lead-rubber bearing under tensile load will respond non-linearly due to the yielding of the lead plug up to the design tensile elongation, which depends on the size of the bearing and lead plug. Beyond this load, cavitation will form in the rubber, leading to permanent damage. Pietra and Park (2017) recommended

the effective tensile stiffness of the lead-rubber bearing be assigned as the secant stiffness to the design tensile elongation.

2.2.3. Steel-PTFE Friction Slider Bearings

Steel-PTFE flat sliding bearings have been used as part of seismic isolation systems to provide vertical load carrying capacity of the superstructure, while allowing shear deformation due to their low horizontal stiffness (Dolce et al., 2005). However, the flat slider bearing must rely on separate mechanisms, such as lead-rubber bearings, to provide re-centring and additional energy dissipation capacity (Dolce et al., 2007).

In past studies and current design practices, analytical models of steel-PTFE sliding bearings are assumed to have a constant friction coefficient for computing the horizontal shear resistance (Dolce et al., 2005). This is sometimes is considered to be an unconservative assumption, as experimental observations (Constantinou et al., 1987; Mokha et al., 1990) have shown that friction coefficients are correlated with sliding velocity, surface temperature, normal pressure and cyclic loadings.

In 1990, Constantinou et al. (1990) proposed an exponential model of the friction coefficient, as derived from experimental observations. The friction coefficient for a given velocity became a function of the minimum and maximum friction coefficients, which are properties of the slider bearings that can be determined experimentally. However, peak velocity typically ranges between 160 mm/s to 400 mm/s during earthquake. For practical purposes, the sliding friction coefficient may be assumed to be constant during design (Dolce et al., 2005) and it was found that velocity-dependence of the friction coefficient has no noticeable impact on the peak responses (Su et al., 1990).

Other than exceeding the design maximum displacement, the steel-PTFE slider bearings can fail from extreme cyclic loadings resulting in the wear of PTFE and increased surface temperature. Increased temperature had been experimentally observed to temporarily decrease the friction coefficient

(Constantinou et al., 1987), which can potentially lead to a higher horizontal displacement. However, the probability of the bearing failing from either of these two conditions during a seismic event are unlikely, as a typical earthquake produces only a few cycles at maximum displacement (Dolce et al., 2005).

2.3. Structural Modelling and Analysis

2.3.1. Modelling of RC Walls

The case study building includes several RC walls and hence, literature relevant to the modelling of RC walls is examined here. One way to model reinforced concrete (RC) wall sections is to reduce the wall section shape into a one-dimensional column in the so-called stick model (Mazars et al., 2006). A drawback is that even though a stick model can yield the total sectional forces, it is not able to differentiate the force distribution among the planar subsections (Beyer et al., 2008).

Another more computationally intensive approach is to model the RC wall using shell elements. This element type can capture the in-plane shear and bending moment, as well as the out-of-plane force (Bathe & Dvorkin, 1986). Mesh discretisation should be done to ensure that the model responses converges to its true behaviour (Fahjan et al., 2010). However, this resulted in an increased computational cost that can be a significant drawback for practicing engineers and is difficult to get accurate deformation prediction and hysteresis behaviour.

Meanwhile, a study (Arnott, 2005) has shown that the equivalent beam model is just as effective in simulating wall behaviour in the elastic range as the most refined shell elements. In the equivalent frame model, a planar wall is modelled using a vertical frame element. Other structural elements, such as another wall or beams connecting to the vertical element can be modelled using similar frame elements which are then connected using horizontal links. Arnott (2005) found that with increasing stiffness of the horizontal link, the equivalent frame model started to converge in their results with a refined shell element model. However,

making a link element infinitely stiff also has its disadvantages, such as numerical problems that can arise during analysis.

The vertical spacing of horizontal links is an important modelling variable. Reducing the vertical spacing is desired because it can minimise the development of parasitic moments in the equivalent frame model (Beyer et al., 2008). A parasitic moment is a coupling moment between the top and bottom horizontal links which tends to resist the continuous shear stress applied on the wall edges (Kwan, 1993). This parasitic moment induces additional lateral deflection that is not observable in the physical wall. Additionally, displacement-based fibre element models have a linear curvature distribution along the elements. The more elements there are along the height of wall, the more accurate their representation of curvature non-linearity associated with inelastic deformation (Beyer et al., 2008). Therefore, shorter vertical spacing will help to reduce the effect of parasitic moments as well as increasing their capability to represent inelastic deformation.

The section properties of the horizontal link are also important modelling variables (Beyer et al., 2008). The elastic torsional stiffness of horizontal links should be reduced to account for the effects of concrete cracking and yielding of reinforcement on the wall section. Moreover, the section of the walls must remain plane even with increasing deformation. This can be achieved by increasing the link in-plane stiffness to make the in-plane behaviour rigid (Beyer et al., 2008). Finally, the in-plane shear area of links must be set to zero in analyses to eliminate the in-plane shear deformation.

The in-plane shear stiffness of the vertical element will change with increasing ductility demand due to the onset of cracking along the section. This is usually not accounted for if a single equivalent elastic shear stiffness is assigned to the wall element for analysis. To overcome this, Beyer et al (2008) recommended setting the elastic stiffness to the average stiffness found in the physical wall when subjected to a whole range of ductility demands.

2.3.2. Modelling of Base Isolated Structures

The preliminary design of the apartment building used for the research was done in two parts (Oliver, 2016). The first part was the design of the isolation system using the equivalent force method. For this, the superstructure is treated as a lumped mass with a single degree of freedom and its stiffness as the equivalent horizontal stiffness of the isolation system (Yang & Zhang, 2018). The second part was the design of the superstructure itself, with the response spectrum procedure carried out on the superstructure with 5% damping to be consistent with a fixed base structure (Standards New Zealand, 2004)

There are several analytical modelling methods suggested in a past study (Nagarajaiah et al., 1991) for time-history analysis. One such method is the equivalent linear method. In this method, the superstructure and isolation system are assumed to respond elastically throughout the analysis. The nonlinear behaviour of a bearing can be linearized by assuming an effective stiffness equal to the post-yield secant stiffness and the addition of damping to capture its energy dissipation mechanism. The drawback of this approach is that sliding isolators cannot be modelled.

Another method involves modelling the lateral resisting system two-dimensionally. In exchange of lower computational demand, the torsional response and biaxial effects in the isolation system are neglected from the analysis. The superstructure elements can be modelled as elastic or inelastic. However, this method is clearly not suitable where torsional response arising from building asymmetry is important, especially at locations where the corner isolator can experience excessive drift beyond its design limit.

In light of the above, a three-dimensional nonlinear dynamic analysis may be conducted to overcome limitations with other approaches. For this, the isolation system is modelled with non-linear hysteretic behaviour, while the superstructure elements are modelled as either elastic or inelastic. However, the estimation of inelastic displacements using a more detailed non-linear analysis

may produce very different displacement demands, which in turn may cause large differences in loss estimates (Ramirez, 2009).

2.4. Structural Integrity

2.4.1. Repairability

After the 2011 Christchurch earthquake, engineers, building owners, and insurers were facing challenges when conducting post-earthquake assessments due to the lack of repairability guidelines (Elwood et al., 2015). This generally resulted in a more conservative assessment of the residual capacity in many damaged RC buildings. In addition, the lack of knowledge of the structural integrity to resist future earthquakes led to the demolition of many buildings after the Christchurch earthquake (Marquis et al., 2017).

For the case where a structure is damaged but not destroyed, the current definition of reinstatement by New Zealand insurance companies included reference to restoring the building to a "condition when new" (Elwood et al., 2015). However, it also mentioned that any extra cost to comply with current earthquake standards will not be included in the reinstatement. The "condition when new" clause of insurance policies remained poorly defined and difficult to quantify, especially when there are large uncertainties surrounding the assessment of residual capacity in RC buildings to begin with. As a result, many buildings were demolished because of the difficulty for engineers to recover the "when new" conditions (Brown et al., 2013).

To address these shortcomings, Elwood et al (Elwood et al., 2016) proposed a guideline framework, as showcased by Figure 3, to guide engineers in doing a detailed assessment of RC buildings. The objective of the framework is to assess the residual capacity of the building when considering future design level earthquake and to identify whether repair is feasible, as compared to the replacement of the building.

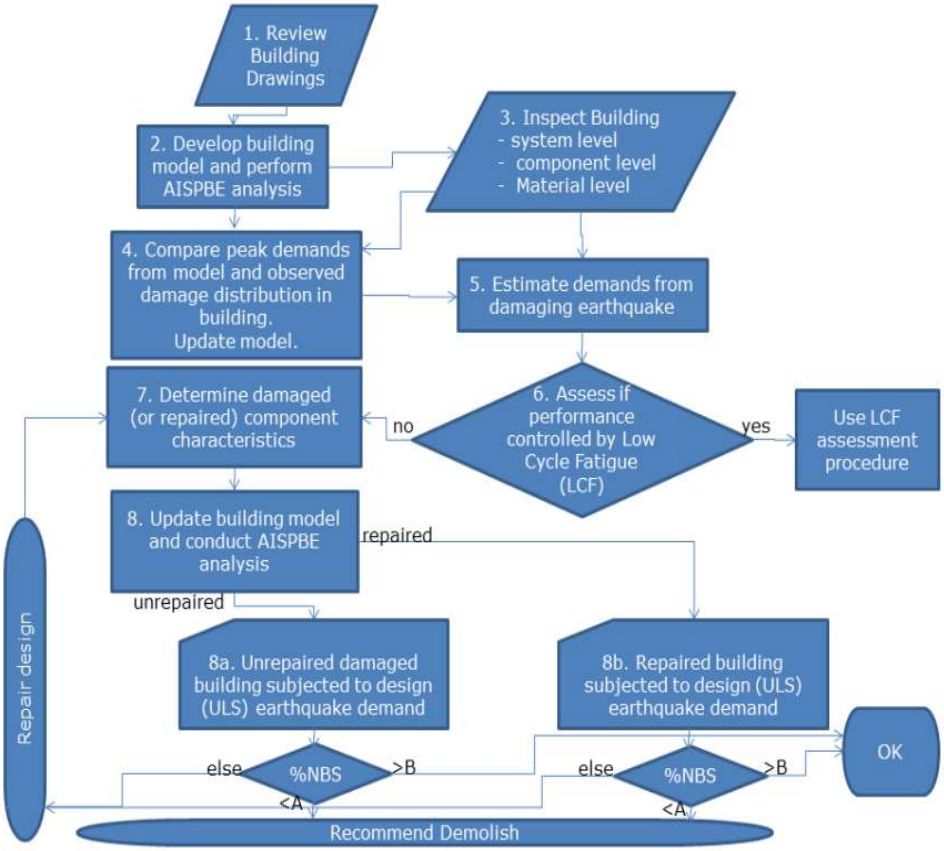

Figure 3. Proposed guideline for repairability assessment of RC buildings (Elwood et al., 2016)

The repairability guideline begins with reviewing the structural drawings to identify the likely locations of plastic hinges and potential damages in the gravity resisting system. Next, a numerical model is developed with the objective to confirm locations of plastic hinges and identify expected building mechanism. The building model will also be used to estimate the peak demands experienced by the building under the damaging ground motion through either linear or non-linear analysis.

Engineers should then perform a building inspection before the building is further damaged by aftershocks. The building inspection stage can be divided into three main levels. Beginning on the system level, the primary mechanism of the building should be confirmed and residual displacements at each storey

estimated. Afterwards, the locations of plastic hinge should be confirmed. Moving on to the component level, the length of the plastic hinge is then estimated from the measured crack widths and axial loads. It is important to consider the presence of axial load because it can close the crack widths. Lastly, the residual strain in the reinforcements can be determined by measuring crack widths and the strain penetration. A strain hardening test should also follow through undertaking a procedure such as the one proposed by Loporcaro et al (2015). However, if the component experienced a high-level damage, then comprehensive material testing should be undertaken.

Subsequently, the building model should be updated to reflect the new information gained from the building survey. The actual peak displacements can be inferred from the observed damages in various key components, which can serve as reference by comparing the outputs from the existing model.

The engineers should check whether low cycle fatigue (LCF) controls the performance of the damaged building. LCF is a failure resulting from repeated plastic deformations in a low number of cycles (Homan, 2018). Although the design of structural system is usually done by considering peak demands, it doesn't usually consider the number of cycles (Elwood et al., 2016). Thus, it is important to assess the residual capacity of a building in terms of the number of cycles left to LCF failure.

The residual stiffness, strength and deformation capacity of damaged components are then estimated from the peak and residual deformation demands. Afterwards, a new model will be created based on the damaged state of the building. The damaged building model will then be analysed to a design level earthquake. Should its performance, measured in terms of the percentage of the New Building Standard (NBS), be below some predefined threshold, then the building is recommended to be demolished. Whereas if its performance is above the threshold, then repair will be deemed as acceptable.

Alternatively, the performance of damaged structure can be computed based on the probability of failure (Elwood et al., 2015). This approach utilises part of the PEER PBEE methodology, in which the building collapse fragility curve is developed. The advantage of this approach is that it provides a more holistic assessment of the damaged building (Elwood et al., 2016). This benefits the insurance companies and building owners in the process of deciding the insurance reinstatement. The cost can be used by the stakeholders to decide on whether to repair or replace the building. Moreover, a repair strategy can then be carefully selected by the building owner to optimally results in a lower probability of collapse compared to the original building.

Orthogonal to the issue of performing repairability assessment is the improvement of post-earthquake repairability by improving the consideration of non-structural elements in seismic design. There are two areas this can be done: (a) improve the design and detailing of non-structural elements, and (b) improve the conceptual design decisions on the relative positioning of structural and non-structural elements (Sullivan, 2020).

With respect to drift-sensitive components, plasterboard partitions are one of the most vulnerable non-structural components in the building. Their performance can be improved by using gapped wall systems or partly sliding partition wall systems (Sullivan, 2020). On the other hand, the performance of acceleration-sensitive components can be improved by providing adequate bracing or through innovative design (Sullivan, 2020).

The conceptual design stage has an important impact on the post-earthquake repairability. A case study by Sullivan (2020) showed that improving the accessibility of post-earthquake repair of steel EBF links for a hypothetical building may cost as much as 4.7% of the estimated replacement cost of the building. The author concluded that a considerable saving in time and repair cost could be achieved by formulating a repair strategy as part of the concept design phase to provide access for inspection and repair post-earthquake.

In this research, the benefits of base-isolation for post-earthquake repairability will be considered.

2.4.2. Seismic Monitoring through Machine Learning

Many studies in the past (Worden & Manson, 2006; Ying et al., 2012) have utilised machine learning algorithms to assess the structural health of a building after an earthquake. In vibration-based structural health monitoring, the integrity of a structural system can be instantly reported to the building occupants and owners after an earthquake by utilising damage detection algorithms. Thereby, the downtime and fees associated with inviting engineers for manual inspection can be reduced or eliminated. In addition, visual inspection has certain risk of misidentifying damages in RC components due to the axial loads closing the cracks (Elwood et al., 2016) or the damages being visually obstructed by other non-structural components (Chang et al., 2018).

Structural damage can be assessed by observing any deviations in dynamic characteristics of the structure, such as the change in natural frequencies, damping and mode shapes (Farrar & Worden, 2006). For example, Chang et al. (2018) utilised natural frequencies as the function to identify structural variations in the model updating process. Although variations in the properties of a structure can be identified, its residual capacity remained difficult to obtain. This, along with the limited number of sensor measurements, means that there are many difficulties in modelling actual damages in a structure. Therefore, a simplified model that well represents the dynamic behaviour of a structure may be the key to assessing its post-earthquake structural integrity.

In recent times, Artificial Neural Network (ANN) with backpropagation is a popular machine learning algorithm that has found many applications. ANN is a type of machine learning algorithm that can map any arbitrarily complex relationship between the inputs and outputs. Its primary function is to perform regression analysis by minimising the error involved in the mapping process (Rosenblatt, 1958). Hence, much training data is required before the regression

model can be used to predict outputs that have sufficient accuracy. Figure 4 demonstrates the underlying mechanics of the ANN.

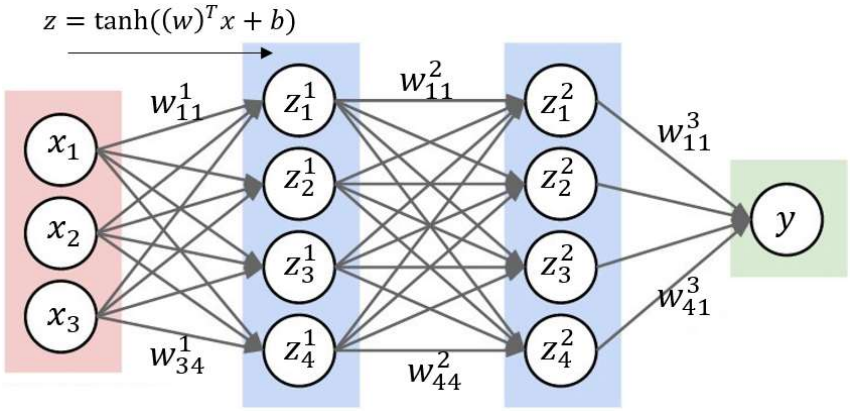

Figure 4. The computation process in the ANN model

Chang et al (2018) trained an ANN model to establish the relationship between mode shapes and reduction of stiffness at different storeys of the structure. Firstly, the Stochastic Subspace Identification (SSI) method was adopted in their study to monitor the modal frequency and mode shapes based on the structural response to ambient vibration. The modal frequency and mode shapes were then inputted into the ANN model to determine the reduction in storey stiffness of the building. However, a drawback of this approach is that damages in the structure might not necessarily change the mode shapes. This could happen if the damage happened to non-structural components or when the damages are equally distributed across the height.

To overcome this, another study by Zhang et al (2018) utilised a different machine learning algorithm to predict the increased collapse vulnerability of building after a damaging earthquake. This was done by allowing the algorithm to compute the ratio κ based on measured response from sensors installed throughout the building. The ratio κ measures the remaining structural integrity after an earthquake. It is defined between the seismic intensity level ($S_{a,int}$) causing collapse at its undamaged state normalised by the seismic intensity level

($S_{a,dmg}$) causing collapse at its damaged state. The damaged building can then be classified as safe or unsafe for occupancy by comparing the ratio κ to a pre-established threshold (κ_{min}), which represents the minimum acceptable reduction in collapse safety.

To sum up, it has been claimed that a machine learning framework allows for rapid probabilistic assessment of whether the building is safe to reoccupy after an earthquake (Zhang et al., 2018). Given this, the topic is considered to the study of post-earthquake repairability of the case study building. An instrument-based assessment will reduce or eliminate the downtime and costs associated with hiring engineers to perform manual inspection. It will also give occupants and building owners a sense of security after moderate earthquakes. Additionally, the outputs from the machine learning algorithm could be incorporated into repairability assessment to help engineers directly identify possible locations of damage, thereby saving a lot of time for engineers in a busy post-earthquake event.

2.4.3. Seismic Instrumentation with Smartphones

The purposes of implementing a seismic instrumentation program to an existing structure are to monitor and analyse. Seismic instrumentation can give insight on the behaviour and potential locations of damage in a structure under earthquake loadings. It could also provide important data to assist engineers and decision makers on the status of its operability or repairability. Moreover, seismic monitoring may help to improve our current design procedure by verifying the various assumptions made during the design of the building.

Celebi (2002) recommended the ideal instrumentation scheme as described in Figure 5 below. For base-isolated buildings, the behaviour of the isolation system is best captured by placing acceleration sensors at the top and bottom of the isolation plane along with sensors on the superstructure.

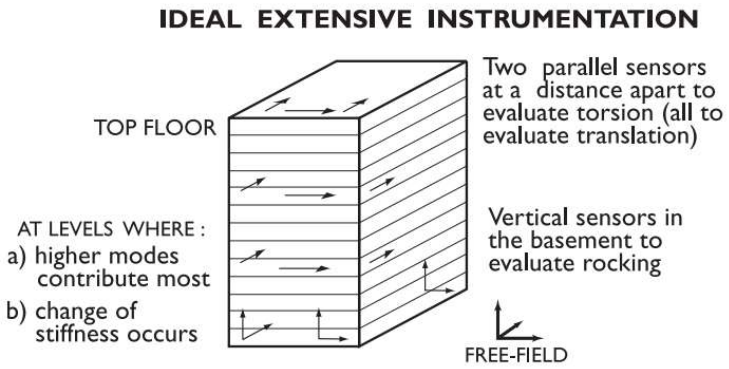

Figure 5. The ideal sensor locations scheme for recording seismic data (Celebi, 2002)

The introduction of wireless technology allowed the distribution of many Internet of Things (IoT) sensors easily in the space, thereby increasing the amount of monitoring and reducing hardware costs compared to wired sensors (Lamonaca et al., 2018). In recent years, there are an increasing number of smartphones that have built-in acceleration sensors. Hence, smartphones may be a suitable low-cost alternative to implement seismic monitoring by acting as the IoT sensors. Moreover, most modern smartphones have high computational power to do signal processing tasks. They also possess communicative ability to the internet, which allows the storage of the recorded data to external servers.

Furthermore, the accelerometers in most modern smartphones tend to have a high sampling rate in the tri-axial directions. For example, the Nokia N95 8GB smartphone can achieve sampling rate of around 60-70 Hz (Lau & David, 2010). Meanwhile, the recommended sampling rate for recording seismic data is 20 Hz (Bolt & Hudson, 1975). Thus, modern smartphones appear to have more than enough capacity to record seismic data in high resolution.

To easily develop and deploy IoT solutions, IBM created the IBM Watson IoT Platform (Livigni, 2016). The aim of the platform is to turn any Android smartphone into a sensor for reading and sending acceleration data to a server

for further data processing. The smartphone must be provided a continuous WiFi connection so that it can send live acceleration data into the cloud for storage. Afterwards, the user can utilise the Node-RED flow drag-and-drop approach to design the data pipeline. For example, the user might set a minimum acceleration threshold to filter out ambient vibration input to maximise the storage space.

The possibility of using smartphones and instrumentation has been discussed here because it is believed that they can reduce the cost and downtime associated with inviting structural engineers for inspection of damages of a building after an earthquake.

3. PEER-PBEE Assessment

3.1. Introduction

3.1.1. Loss Analysis of the Case Study Building

The objective of this chapter is to investigate the expected annual loss (EAL) for a typical base-isolated building located in Christchurch, New Zealand. The EAL will be computed by performing time-based assessment in accordance to the PEER-PBEE framework (Deirlein et al., 2003).

A structural model of the building is first created in Ruaumoko 3D (Carr, 2005) with lumped plasticity. Next, a multi-stripe NLRHA analysis is performed on the structural model with selected ground motions for nine intensity levels. Sensitivity analyses will then be performed by varying design parameters and assumptions to investigate their impact on the analysis results.

The obtained engineering demand parameters (EDPs) will be run through damage measure-fragility curve analyses with SLAT (Bradley, 2009). This is done to produce a decision variable of the expected annual loss by integrating together the loss due to certain intensity level and its associated rate of exceedance over all intensity levels.

Finally, the computed EAL for this base isolated building will be compared with the EALs reported by past studies evaluated on structures in New Zealand with different structural typologies. The aim of this exercise is to provide information to future engineers and decision makers on the relative performance of base isolation compared to traditional construction.

3.1.2. Hazard Analysis

The first step in a time-based loss analysis is to quantify the seismic hazard, which is a relationship between the rate of exceeding various ground motion intensity levels at a site and a measure of the ground motion (e.g. spectral acceleration for a given period). However, the quantification of seismic hazard

is a difficult task because of its inherent variability. Firstly, it is difficult to precisely determine the time and location of future ruptures. This is because the intensity, frequency content, and duration of ground motions at a particular site are influenced by the seismic wave propagation and site effects. These uncertainties arising from strong ground motions in turn result in uncertainty in the level of structural response and associated damage in the structure.

This research will not cover the process of hazard analysis. Instead, the work will rely on probabilistic seismic hazard analysis (PSHA) performed by Yeow et al. (2018) for the Central Business District in Christchurch, New Zealand with soil class D, using New Zealand specific rupture forecast models and attenuation relationships for spectral acceleration at the fundamental period of 2.0 s. This was selected in part because it is an efficient IM with respect to reducing the uncertainty in the structural response, which will in turn reduce the uncertainty in the direct losses output by a subsequent loss analysis.

The seismic hazard curve is shown in Figure 6, along with the design hazard curve in NZS 1170.5 (Standards New Zealand, 2004). It can be observed that the seismic hazards are lower than the design hazard curve. Several reasons for the differences include overestimating the effect of small-to-moderate earthquakes and simplifications of the spectral curve shape in NZS 1170.5 (Yeow, Orumiyehei, et al., 2018).

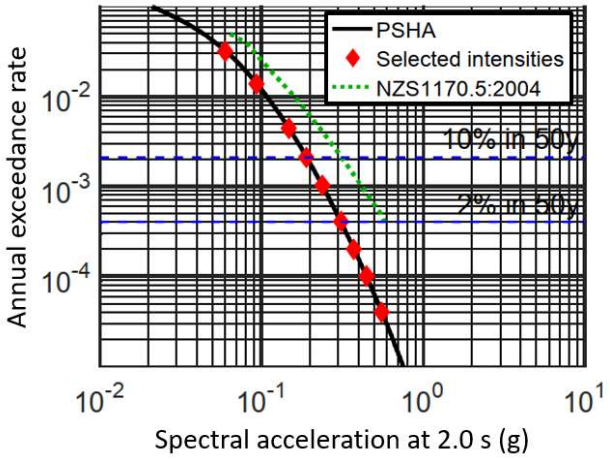

Figure 6. Seismic hazard curves for structures with $T = 2.0\ s$ in Christchurch and on soil class D (Yeow, Orumiyehei, et al., 2018)

For structural analysis, twenty representative ground motions over a range of nine intensity levels were selected based on the hazard curve outputted by PSHA. The representativeness of the ground motion suite with respect to a certain intensity measure must be quantified using statistical tests. Thus, the generalised conditional intensity measure (GCIM) method proposed by Bradley (2010) was employed by Yeow et al. (2018) for selecting the suite of ground motions used in the subsequent structural analysis.

In this study, nine intensity levels were selected that approximately corresponded to the return periods of one in: (1) 31 years, (2) 72 years, (3) 224 years, (4) 475 years, (5) 975 years, (6) 2475 years, (7) 4975 years, (8) 10,000 years, and (9) 25,000 years. For each intensity level, twenty representative ground motions were selected by Yeow et al. (2018) using the GCIM method as previously described.

3.1.3. Structural System

The building structure was designed by Holmes Consulting by following the Low Damage Design (LDD) principles (Oliver, 2016). The primary objective of LDD is to mitigate the extents of earthquake damage in the building, such

that the building may be easily and economically repaired with minimal disruption after an earthquake.

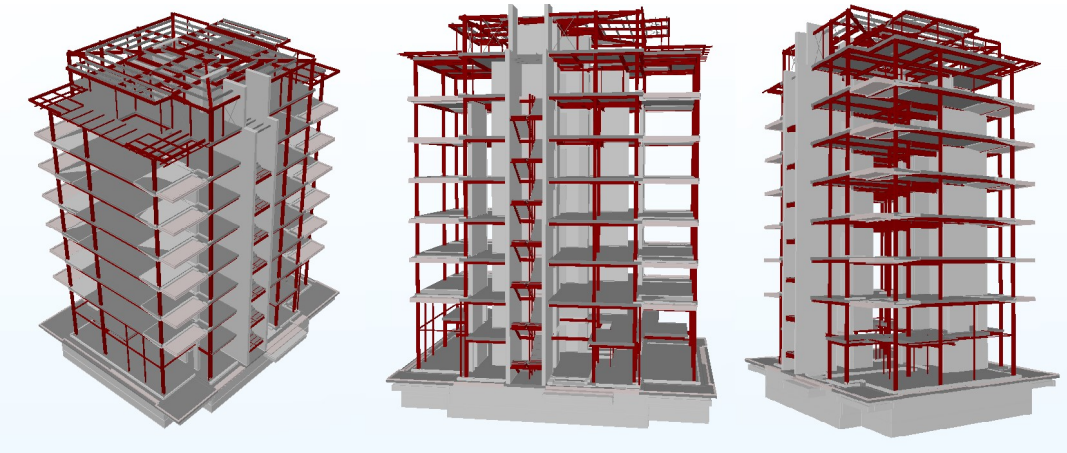

Figure 7. BIM model of the structure as viewed from different angles (Oliver, 2016)

The superstructure of the building consisted of both steel framing and reinforced concrete walls. However, the roof level is distinct from the other levels in that it is constructed using light-weight steel framing and steel bracing. The steel framing in a typical floor was designed to provide gravity load resisting capacity and not for resisting lateral loads. This is evident from the engineering drawings of the beam and column joints. Except where it was explicitly noted to be moment connections, the beam and column joints are assumed as pinned. Realistically, however, the "pinned" connections might transfer some moment between connected elements. This study will attempt to account for such behaviour when modelling the structure.

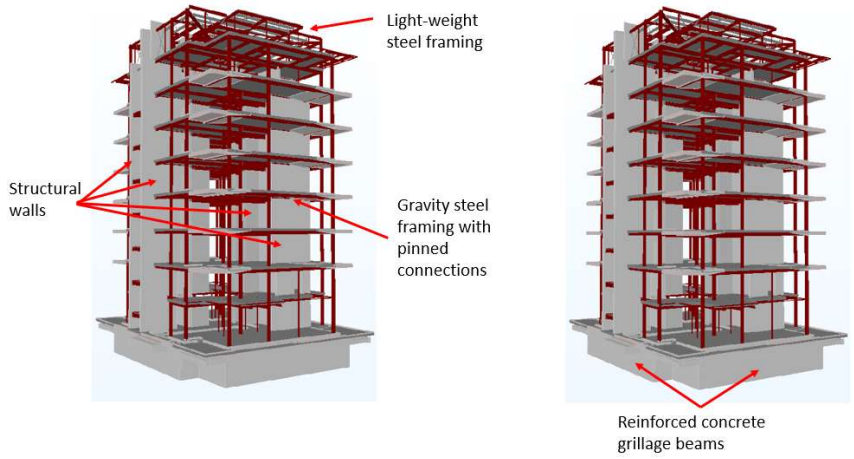

Figure 8. Structural system of the building

Meanwhile, the structural walls provide both gravity and lateral load resisting capacity within the superstructure. Figure 9 shows the location of the five lateral resisting walls in a typical floor plan. The reinforced concrete T-walls extended from ground floor to the roof level, whereas the straight walls extended only up to the seventh storey. Furthermore, the lateral load resisting system is structurally symmetrical in both the North-South and East-West directions and as such, the structure is considered a torsional stable system. It is also interesting to note that the total length of the structural walls in the North-South direction is almost twice that in the East-West direction.

Figure 9. Plan view of a typical floor with the structural walls highlighted in red

The floor levels are taken at the top of the concrete slab of a one-way composite flooring system. The general floor area has a 210 mm thick concrete slab, while the balcony is a cantilevered two-way concrete slab that is 400 mm thick. To accommodate for the moment demand from the cantilevered balcony slab, the adjacent slab is tapered from 210 mm to 400 mm. Furthermore, there are also openings in certain area of the slab to provide vertical access for the stairwell and the two hanging lift shafts.

At ground level, the superstructure is supported by reinforced concrete grillage beams that are in turn supported by base isolators. The purpose of the grillage beams is to resist p-delta actions associated with the isolators and to redistribute the discrete overturning moments and shear developed within the structural walls to the isolation system.

The base isolators are each supported by a stiff plinth that sits on top of the concrete raft foundation. There are two types of base isolator utilised in this building, the lead rubber bearings (LRBs) and steel-PTFE slider bearings (SBs). The slider bearings are used for two reasons. The first is to support the high vertical loads directly below the structural walls, while the second is to provide additional damping to the structure in the horizontal direction. However, the slider bearings offer no re-centring capability as the sliders have a flat surface. Re-centring after excitation is mainly provided by the elastomeric rubber in lead rubber bearings.

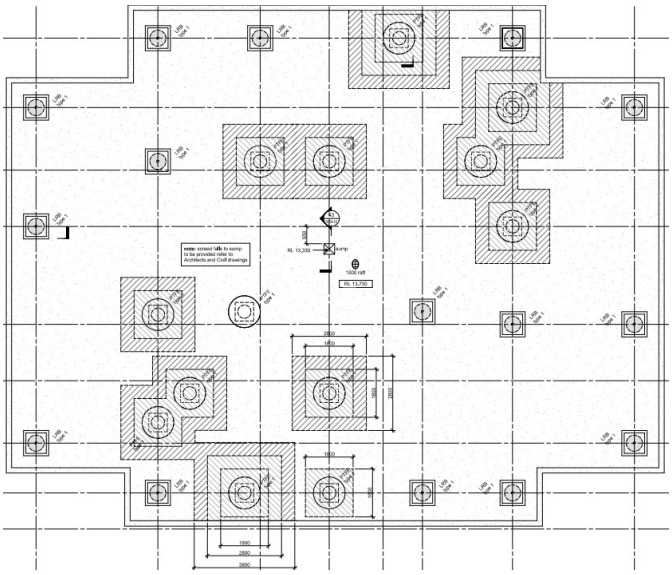

Figure 10. Floor plan at the foundation level showing the base isolators

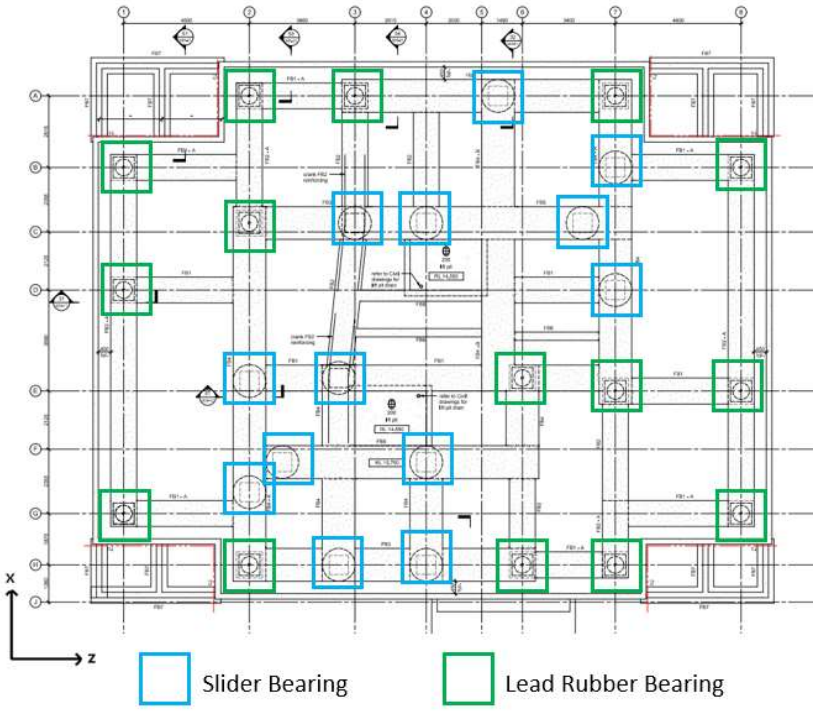

Figure 11. Floor plan at the ground floor showing the grillage beams and base isolators

Figure 10 shows the distribution of the LRBs and SBs beneath the superstructure. As can be observed by comparing with Figure 11, the SBs are mostly located underneath the structural walls (refer to Figure 15 at page 51), whereas the LRBs are located underneath the steel gravity columns. This is because SBs are rigid in the vertical direction, while the lead core of LRBs has some vertical flexibility. In addition, the LRBs are positioned close to the perimeters to provide the recentring capability as well as to limit torsional deformation.

3.1.4. Non-Structural Components

In addition to the structural system described previously, the non-structural components are of great importance when considering loss assessment. The apartment building was described by the Architect as being "a very high-quality development with many firsts and notable features incorporated". The building contains many high-quality non-structural components that may be expensive to repair or replace after a damaging earthquake. Fortunately, the building is base isolated, and hence the demands on the superstructure will be lower than ordinary buildings for the same earthquake. Nevertheless, the non-structural components that are of interest for post-earthquake repair costs included the external cladding, interior partitions, suspended ceilings, and other building services, such as piping, ducts, and mechanical equipment.

The external cladding is a unitised curtain wall system supported by the main structure with slotted connections attached to the outrigger panels casted into the floor slab at each level. The curtain wall unit consisted of three different types. The first two types are glazing, and their only difference is that the glass can be either clear or frosted. The other type is a boxed neolith panel, which has a hollow core and two layers of neolith slab laminated onto the aluminium framing at three sides.

The interior partitions are drywall with timber framing as the support. The common drywall panels are acoustic and fire rated GIB boards, while some rooms have natural stone tiles and wood veneer as wall finishes.

Generally, the suspended ceiling consisted of a GIB board panel of 13 mm thickness fixed to the aluminium grids that are supported by vertical wires. Because of the high requirement in acoustic performance, some parts of the suspended ceiling have two layers of 13 mm GIB board which totalled to 26 mm in thickness. This difference in weight mainly affected the spacing of the grids. The fixed-floating system of suspended ceiling is used in rooms with smaller ceiling area, whereas the suspended ceiling is fully floating with back bracing as required when the ceiling area became sufficiently large.

The horizontal non-structural components for hydraulics and mechanical services are usually hidden within the plenum space of the suspended ceiling. Some exceptions are the compressors and fan coil units (FCUs) that are attached to the slab level. Every hydraulic and mechanical equipment had been detailed such that it will perform well in earthquakes by providing seismic restraints and vibration isolators.

3.1.5. Seismic Instrumentation

The building is monitored through a seismic instrumentation system consisting of six triaxial accelerometers. Four accelerometers were attached to the superstructure at different levels and two on the concrete raft foundation for measuring the ground motion at the site. This configuration will allow an accurate estimation of the demands on the isolation system and the superstructure itself. Two accelerometers were placed at the seventh storey. It was assumed that the eighth storey and the lightweight roof do not contribute significantly in terms of seismic mass, hence the response at this level can be taken as equivalent to that of the roof level. The two accelerometers are placed diagonally across each other, one at the North-Western side and the other at the South-Eastern side of the building. This configuration was chosen to maximise

the recording of accelerations for computing the torsional response. Moreover, two accelerometers are placed at the underside of the reinforced concrete grillage beams located at the ground floor. The purpose of these two accelerometers is to measure the response of the isolation system by comparing accelerations with the two accelerometers attached to the concrete raft slab directly underneath. Likewise, the accelerometers were placed diagonally opposite to each other.

The accelerometers are of tri-axial MEMs silicon type with range of ± 5g and a sampling rate of 200 Hz. The sensor network is connected to a GPS controller unit that provides a global reference position for synchronising the recording time across the sensors. This arrangement will reduce time delay among sensors up to a maximum of 4 ms.

In order to trigger recording, at least three accelerometers must record motions larger than the predefined threshold of 0.3 cm/s^2. There is a rolling buffer of 30 seconds providing the pre-event and post-event data. These are useful for determining the signal-to-noise ratio later when processing the data. Note that the data is being recorded in the CUSP-Me central recorder as well as in the individual sensors in case of power outage.

Due to the limited number of sensors, with only one level being monitored in the superstructure, the information on the structural response that can be obtained after an earthquake will be quite limited. Although there are techniques (Koh et al., 2006) to estimate the response at each storey by assuming the distribution of storey stiffnesses, this will require a prior knowledge of the stiffness distribution that can be difficult to accurately determine. To overcome this issue, a greater number of sensors can be installed to provide a higher resolution of the data. However, this is currently not optimal because of the high cost associated with accelerometer sensors. Therefore, a part of this research will be spent investigating the feasibility of using smartphones to substitute

accelerometer sensors for recording and storing acceleration data to the cloud. This idea will be discussed in greater detail at a later section of this Thesis.

3.2. Structural Modelling

3.2.1. General Modelling Strategy

The building structure was idealised as a three-dimensional MDOF system and a lumped plasticity model was created in the software Ruaumoko 3D (Carr, 2005) to carry out nonlinear time history analyses. Ruaumoko 3D is a software designed to produce a piece-wise time-history response of non-linear general structures to ground accelerations, ground displacements or time varying force excitations. It can also be used to compute the modal periods and mode shapes of the structure.

For an overview of the structural model created in Ruaumoko 3D, refer to Figure 12. Each node in the model has 6 degrees of freedom that are associated with translations and rotations in the three-dimensional space. For the boundary conditions, all degrees of freedom of the nodes connected below the base isolators were restrained. Although each base isolator is placed on a shear plinth of varying heights, it is assumed that both the shear plinths and the concrete raft foundation are fully rigid.

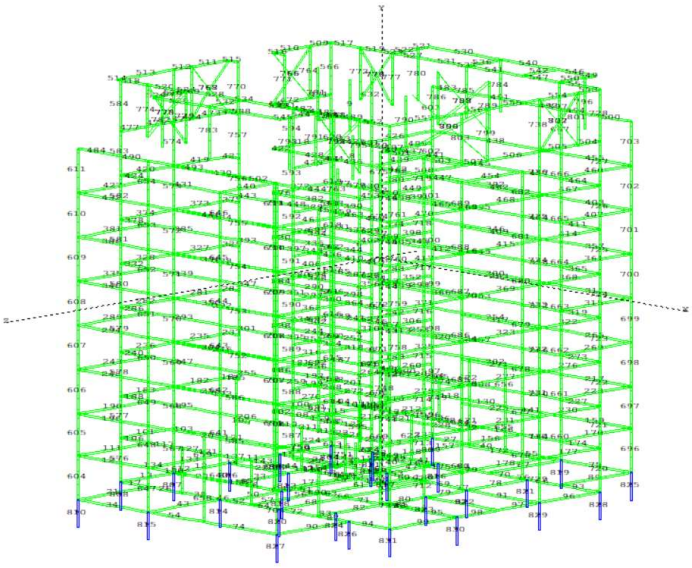

Figure 12. Structural model of the apartment in Ruaumoko 3D (Carr, 2005)

The weight of each storey was lumped at the centre of each floor at nine levels. Mass was defined in the orthogonal translational directions as well as the rotational inertia of the storey as discussed further in Section 4.2.2. The main advantage of using a lumped weight model is the reduction in the size of the mass matrix resulting in a large saving in computational time. At each storey, the nodes at the level are enslaved to a master node by coupling the degrees of freedom in the horizontal translations and vertical rotation directions. This will, in effect, result in a rigid diaphragm behaviour at each storey.

All structural elements, including the steel beams and columns as well as concrete walls, are modelled using a two-node frame member with the one-component beam element type (Giberson, 1969) in Ruaumoko 3D. This element type enables the formation of plastic hinges near one of the two ends of the beams and columns. The stiffness of the hinge is set such that the rotation of the hinge, together with the rotation associated with the elastic curvature of the beam over the beam length, are equal to the rotation associated with inelastic properties of the plastic hinge zone in the actual beam. This meant that the

stiffness of the plastic hinge spring approaches infinity when the hinge is in the elastic range, thereby ceasing to exist.

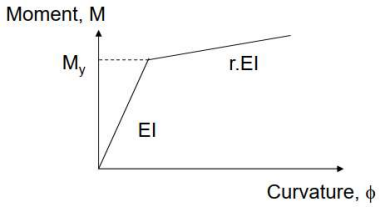

Figure 13. M-φ relationship for the one-component beam (Giberson, 1969)

The damping model adopted in the structural analysis is the Caughey damping model with linear variation. Ruaumoko 3D allows the damping ratio to be specified as a constant over a range of modes. With the Caughey damping model, the computed damping matrix will vary throughout the time-history analysis as the elements in the model progressively yield. A damping ratio of 5% of the critical damping is assumed for the overall structure, which is in line with the expectation of the structural engineer responsible for the design. In Ruaumoko 3D, this corresponds to an ICTYPE of 2 with 5% damping ratio specified at mode 1 and 3, which are the torsional and translational modes.

To account for P-Delta effects in the analyses, the P-delta analysis option in Ruaumoko was used and the constant average acceleration method developed by Newmark (1959) utilised to solve the equation of dynamic equilibrium at each time step. An integration timestep of 0.01s was used but sensitivity analyses were conducted to check that results were not affected with a smaller integration timestep of 0.001s.

Following is a list of additional assumptions that were made during the structural modelling:

- Overstrength of the bearings is not considered and hence some member demands may be underestimated.

- The superstructure is modelled as linear elastic because the base isolators are expected to reach failure before any non-linearity can develop in the superstructure. This was checked during post-processing of results.
- Gravity columns for supporting the lumped masses are modelled as pinned at both ends and are axially rigid. These columns connect the centres of mass between the floors.
- Stairs were not modelled because they were assumed to be less stiff than the adjacent concrete walls.

3.2.2. Floor Diaphragms

Composite flooring is used at each level of the building starting from the ground level (G) to the penthouse first level (P1) just below the roof level. Composite floor slabs use metal decking to support concrete that is pumped onto the decking to make up the composite system.

The concrete slab is assumed to transfer the dead and live loads in a one-way manner along the East-West axis to the secondary steel beams. A positive moment applied to the composite flooring is resisted by a combined action of the concrete slab in compression and the steel beams in tension, with shear studs transferring the loads between them. In addition, the concrete slab penetrated the concrete structural walls. Because of this, the concrete slab ties the building together and can be assumed to act as a rigid diaphragm for distributing horizontal forces to the lateral load resisting system, which is mainly the structural walls with some minor resistance expected from the steel gravity frame.

A lumped mass assumption was used for the structural model in Ruaumoko 3D. This means that the seismic weight at each level of the building is concentrated at a specific point on that floor level. The centre of mass has translational masses in the two horizontal directions and a rotational mass about the vertical axis. Vertical translations of the building with respect to each floor due to vertical

excitation was not considered in this research, while rotations about the horizontal axes were considered negligible.

Recall that the master node at each floor is free horizontally in the X and Z directions as well as rotationally in the Y direction. It is also defined as the reference point for data (i.e. drifts and acceleration) observation. Since all the other nodes in a given floor are constrained as a rigid diaphragm to the master node of that floor, it is expected that the master node represents the floor response. The position of the centre of mass at each storey is summarised in Table 1.

Table 1. Coordinate of the centre of mass at each level

Storey	X-axis (m)	Z-axis (m)	Y-axis (m)
G	10.876	9.607	15.75
UG	11.333	9.696	18.98
Level 1	11.151	9.777	22.04
Level 2	11.18	9.769	25.27
Level 3	11.18	9.769	28.5
Level 4	11.18	9.769	31.73
Level 5	11.18	9.769	34.96
PG	11.18	9.769	38.19
P1	11.414	9.584	41.42
Roof	10.78	8.747	45.21

The centre of mass at each level is computed based on:

- Tributary dead load of the gravity and lateral resisting elements of the floor.
- Dead load of the composite flooring.
- Applied live load reduced by a factor for the value expected during an earthquake (Standards New Zealand, 2004).
- The façade load applied to perimeter steel beams.

3.2.3. Seismic Weights

According to NZS 1170.5:2004 (Standards New Zealand, 2004), the seismic weight at each storey can be computed using the following equation:

$$W_i = G_i + \sum \Psi_E Q_i \quad \text{(Eq. 1)}$$

Note that Ψ_E is taken as equal to 0.3 for normal buildings and is equal to 0 for roofs without public access and the live loads are taken from the tables listed in the standard.

The general floor area consisted of one-way composite flooring using the ComFlor 60 system and concrete slab with 210 mm thickness. The build-up for both dead and live loads is summarised below:

Metal decking: 0.10 kPa
Concrete slab: 2.73 kPa
Concrete screed: 1.47 kPa
SDL: 1.5 kPa
Dead load: 5.8 kPa
Live load: 2.0 kPa

The build-up of service dead load (SDL) is as follows:

Suspended ceiling: 0.15 kPa
Services: 0.1 kPa
Internal timber walls: 0.15 kPa
Blockwork walls: 0.5 kPa
Tiling (assumed): 0.6 kPa
Total: 1.5 kPa

At the tapered slab regions supporting the cantilevered balconies, the concrete slab of the ComFlor 60 system increased in thickness from 210 mm to 400 mm. To simplify the calculation, a uniform slab thickness of 300 mm was assumed

over such region. The rest of calculations are like the ComFlor with the 210 mm concrete slab.

The stairs arriving at a given level have their weights lumped into that level to simplify modelling. Therefore, the weight contribution to a level is made up of the ascent, the descent, and the landing slab. The build-up for dead and live loads is summarised below:

Concrete landing slab (170 mm thick) = 0.17 × 24.5 = 4.165 kPa
Self-weight of treads = 0.5 kPa
SDL for stairs = 0.1 kPa
Handrail loads (C3 from Table 3.3 NZS1170) = 0.75 kPa
Dead load = 0.5 + 0.1 + 0.75 = 1.35 kPa
Live load (C3 from Table 3.1 NZS1170) = 4.0 kPa

The roof of the building is made up of light weight steel framing, where the roof material is structurally supported by DHS 250/13 purlin with a weight of 0.048 kN/m at a maximum spacing of 1.2 m. The roof SDL and live load are applied uniformly as area load instead of individually for each purlin. Since the loaded area was calculated based on the maximum span of the purlins, this will likely overestimate the purlin weights, but it should not be significant. Moreover, the live load is taken as zero for roofs without public access as per NZS 1170.5.

Roof material = 0.55 kPa
Purlin weight = 0.04 kPa
SDL for roof: 0.05 kPa
Suspended ceiling: 0.15 kPa
Dead load = 0.8 kPa

The balconies are 200 mm thick precast concrete slab with tiling on top. The build-up for the dead and live loads is as following:

Precast slab: 0.2 × 24.5 = 4.9 kPa

SDL (allowance for tiles): 0.5 kPa

Dead load: 5.4 kPa

Live load: 2.0 kPa

A complete summary of the dead and live loads for different types of floor are given in Table 2 and Table 3, respectively.

Table 2. List of dead loads applied to different floor types

Floor type	Weight (kPa)
ComFlor 60 (210 mm)	5.8
ComFlor 60 (300 mm)	8.05
Balcony	5.4
Roof	0.8
Stairs	1.35
Landing	4.17

Table 3. List of live loads applied to different floor types

Floor type	Weight (kPa)
ComFlor 60 (210 mm)	2
ComFlor 60 (300 mm)	2
Balcony	2
Roof	0
Stairs	4
Landing	4

In addition, the curtain walls will contribute dead loads to the perimeter steel beams based on the tributary area and the storey heights. The uniformly distributed loads (UDL) applied to the perimeter beams at different storeys are:

Ground floor = $0.7 \times \frac{3.23}{2} m = 1.131\ kN/m$

Upper ground floor = $0.7 \times (\frac{3.06}{2} m + \frac{3.23}{2} m) = 2.202\ kN/m$

Level 1 to penthouse ground floors = $0.7 \times 3.23m = 2.261\ kN/m$

Penthouse 1st floor = $0.7 \times (\frac{3.79}{2}m + \frac{3.23}{2}m) = 2.457\ kN/m$

Roof = $0.7 \times \frac{3.79}{2}m = 1.327\ kN/m$

A structural model that incorporates the entire gravity load resisting system was created in SAP2000 to compute the seismic weight at each storey. The floor slab was modelled using area elements so that the applied load can be directed onto the supporting elements, including the steel framing and the centroids of structural walls. The translational weights or horizontal weights are obtained by summing the nodal masses outputted by SAP2000 for a given storey over all storeys, which are summarized in Table 4. The rotational inertia at each level is then computed internally in SAP2000 and summarised in Table 5. These rotational inertias were specified in the Ruaumoko 3D model.

Table 4. Translational weights in the X and Z directions at each level

Storey	Translational weight (kN)
G	12057.9
UG	4263.658
Level 1	4690.964
Level 2	4677.604
Level 3	4677.604
Level 4	4677.604
Level 5	4677.604
PG	4403.326
P1	4956.34
Roof	1307.399

Table 5. Rotational inertia in the Y direction at each level

Storey	Rotational inertia (kNm^2)
G	821474.8
UG	265398.2
Level 1	330045.1
Level 2	323845.4
Level 3	323845.4
Level 4	323845.4
Level 5	323845.4
PG	307687.4
P1	312580.4
Roof	65070.28

3.2.4. Reinforced Concrete Walls

The reinforced concrete walls are the main lateral resisting elements of the building above the isolation level. In Ruaumoko 3D, the walls are implemented using an equivalent frame model (refer to Section 2.3.1). This means that a straight wall is represented by a column member at the geometric centroid of the wall with its longitudinal reinforcement symmetrical about it. The column member has the same elastic cracked section properties as the wall.

The cracked section properties of a single straight wall were obtained by modelling the concrete section along with its longitudinal reinforcement in the Section Designer tool of SAP2000. A moment-curvature analysis was then performed using the built-in function, and its cracked moment of inertia along with its other section properties (e.g. torsional constant, shear area, etc.) were output by the program. This was repeated for each of the reinforced concrete walls and their elastic section properties were then input into Ruaumoko 3D.

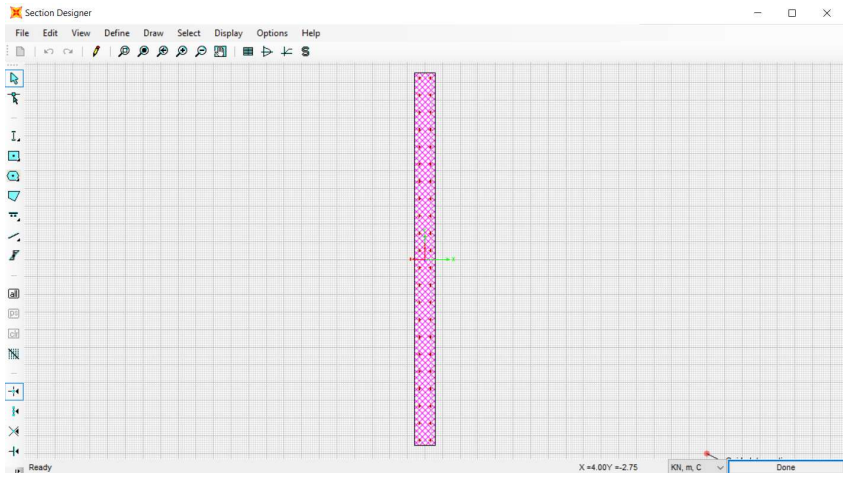

Figure 14. Modelling of a straight wall section in SAP2000 (SAP, 2013)

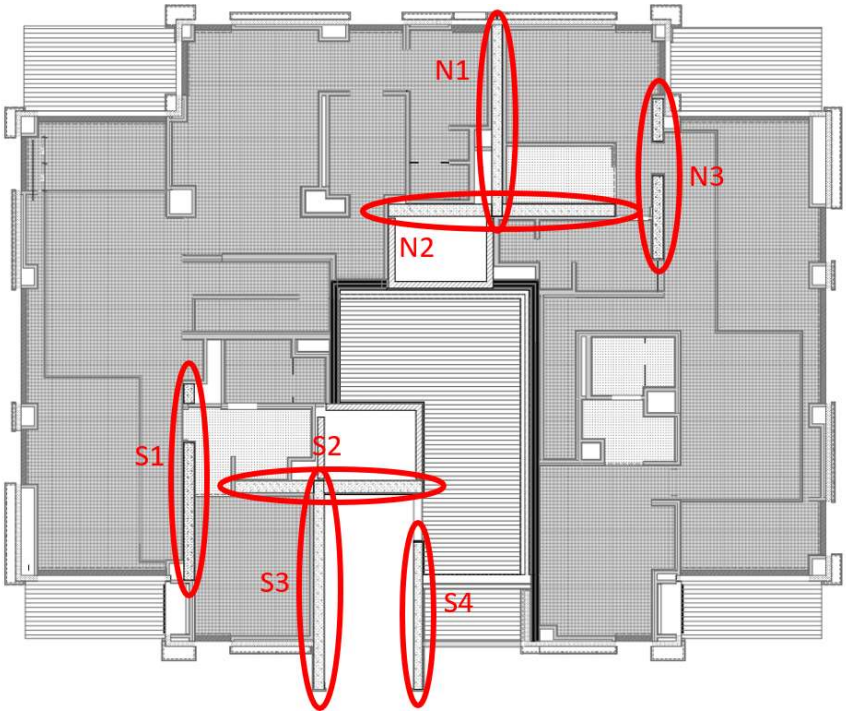

Figure 15. Plan view of the UG floor and labels of the structural walls

Figure 15 shows a plan view of the structural walls in the building at the upper ground level (UG) along with their relative positions and designations used in this Thesis. For example, walls N1 and N2 are straight wall sections that made up the northern T-shaped wall. Although they are modelled as separate column

members in Ruaumoko 3D, in reality they act together as one section when resisting flexure. To obtain this behaviour, horizontal links were used to connect between the N1 column member and the N2 column member at each level. Similarly, the S2 and S3 column members are connected via horizontal links to model the behaviour of the southern T-wall.

The horizontal link serves as a rigid link to directly transfer bending moments and shear forces between the connecting members. It is rigid for the in-plane deformation to ensure the section of T-wall will remain plane with increasing deformation. Additionally, its torsional stiffness is reduced significantly to account for concrete cracking in the wall section. The modifications to the elastic section properties of the horizontal link follows the recommendation set by Arnott (2005), as described below in Figure 16.

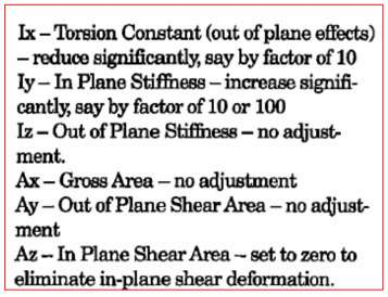
Ix – Torsion Constant (out of plane effects) – reduce significantly, say by factor of 10
Iy – In Plane Stiffness – increase significantly, say by factor of 10 or 100
Iz – Out of Plane Stiffness – no adjustment.
Ax – Gross Area – no adjustment
Ay – Out of Plane Shear Area – no adjustment
Az – In Plane Shear Area – set to zero to eliminate in-plane shear deformation.

Figure 16. Modification to horizontal links (Arnott, 2005)

Furthermore, the effective area of the column (A_e) is reduced to account for cracking of the wall section using Equation 2, where I_{cr} is the cracked moment of inertia about the major axis, whereas A_g and I_g are the gross area and moment of inertia about the major axis, respectively. It is assumed that the gross cross section area will act to resist compressive axial load. However, a reduced cross section area proportional to the ratio of cracked moment of inertia and gross moment of inertia is assumed to act for tensile axial loads. The A_e is therefore taken as the average of the two cross section areas in tension and compression. This approach is deemed reasonable for estimation of the global response of the building.

$$A_e = \frac{\frac{EI_{cr}}{EI_g} A_g + A_g}{2} \quad \text{(Eqn. 2)}$$

By modelling two column members together with horizontal links to form a T-wall, the local elemental response cannot be directly obtained from the analysis results. For example, the curvature of the T-section wall has to be derived considering both the axial loads and curvatures of the individual column members making up the T-section wall. However, the global responses of the walls, including their contribution to the inter-storey drift ratios and peak floor accelerations, should be reasonably captured. Since the main interest lies in the global response of the building rather than the local element deformations, the use of the equivalent frame model with horizontal links is considered justified.

The straight walls such as N3 and S1 have irregular openings to allow for doors. The wall openings can be modelled by subdividing the wall into pier and spandrel elements. The piers are vertical elements encasing an opening, while the spandrel is a horizontal element tying the piers together. With respect to Figure 17, the piers in Wall N3 for all storeys except between UG and level 1 are column members having the same elastic cracked section properties as the actual wall. Between UG and level 1, the piers are divided into two to accommodate an opening between them. The spandrels were made rigid in the plane of the wall by my modifying its section properties as previously described. Although this will result in unrealistic local element deformations, the main interest is in the global responses of the walls. Hence, using the pier and rigid spandrel approach was considered justified.

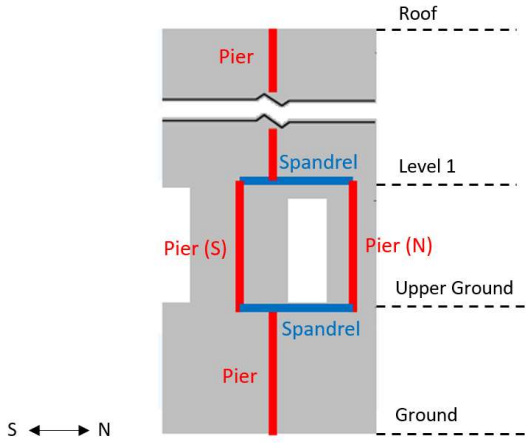

Figure 17. Modelling Wall N3 with piers and rigid spandrels

In addition to the above, the following assumptions were made when modelling the structural walls:

- Walls are elastic axially.
- The concrete material was assumed to be 30 MPa and has a weight of 24 kN/m^3. The modulus of elasticity and shear modulus of concrete were calculated as per NZS 3101:1:2006 (Standards New Zealand, 2006):

$$E = \left[4700\sqrt{f_c'}\right]\left(\frac{\rho}{2300}\right)^{1.5} = 28241\ MPa$$

$$G = 11767.1\ MPa$$

- Rigid links, as defined previously, are used to model any connections between steel beams and the concrete wall at a given storey to transfer vertical shear force from the beams.
- The rigid link is sufficiently rigid to constraint the beams to the wall and will not deform by any significant degree (see Figure 16).

3.2.5. Steel Framing

Aside from the structural walls, the steel framing is the primary system for resisting gravity loads. The steel framing consisted of steel beams and columns with their joints designed as being "pinned". In other words, the steel framing

was not designed to resist lateral forces. This is evident by the detailing of the typical joints given by the drawing shown in Figure 18.

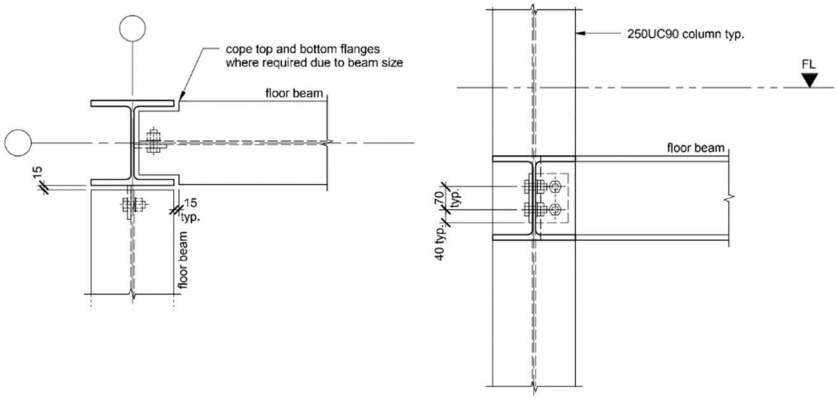

Figure 18. Typical beam-column joint at (a) roof level and (b) typical floor

As can be seen, only the web of an I-beam has angles with bolts connected to the column for transferring the shear force, while its flanges are not welded or connected via bolted angles to the column. However, it is impossible to achieve a perfectly pinned joint condition in the real world. Hence, the steel frames are expected to provide some lateral resistance, even if minimal, when the building is subjected to lateral loadings. Given the extensive use of steel framing to support gravity loads in the building, it is possible that the steel framing might contribute a non-negligible resistance to the lateral forces. To investigate this, this study will model the beam-column joints as non-perfectly pinned by modifying the rotational stiffness of the springs at both ends of the one-component beam elements (Giberson, 1969).

A sensitivity study is performed (reported in Section 3.3.3) to evaluate whether the assumption that non-perfectly pinned connections in steel framing for this particular building did contribute significantly to the structural response and subsequent loss analysis.

The general equation of the rotational stiffness for the end spring can be described by Equation 3.

$$k_{rot} = \alpha \frac{EI}{L} \quad \text{(Eqn. 3)}$$

If the beam-column joint is perfectly pinned, then $\alpha = 0$ and the end springs would have zero rotational stiffness. On the other hand, if $\alpha = \infty$, then the beam-column joint would be fully fixed.

For the purpose of this study, a value of $\alpha = 1.0$ was assumed. Assuming that E is the same for all steel members, Equation 3 was evaluated for each steel member with different cross sections and lengths to compute their rotational stiffness at both ends.

Example calculation for the major axis rotational stiffness of a 250UC90 beam with a length of 4.6 m and moment of inertia (I) of 1.407×10^{-4}:

$$K_{rot} = 1.0 \times \frac{(2 \times 10^8\ kPa) \times (1.407 \times 10^{-4}\ m^4)}{4.6\ m} = 6117\ kNm/rad$$

The rotational stiffness is then converted into end flexibility in Ruaumoko 3D by inverting the rotational stiffness, i.e. $f_{rot} = \frac{1}{K_{rot}}$.

In addition to the above assumptions, the following were made:

- The steel frame members were assumed to have an elastic modulus of 205 GPa, a shear modulus of 78.8 GPa, and Poisson's ratio of 0.2.
- The shear deformations of the members are considered in the analysis by using the effective shear area of the member sections.
- The centroids of all steel beams are located on the horizontal line with heights equalling to the storey levels.

3.2.6. Lead Rubber Bearings

The building is base isolated with a total of 28 isolator units, consisting of 15 units of lead rubber bearings (LRB) and 13 units of steel-PTFE slider bearings (SB). Each LRB unit is circular having 680 mm diameter and a lead core of 75 mm in diameter. The overall isolator height is 322 mm including the top and bottom steel plates that are 20 mm in height and has alternating layers of steel

shims and G50 rubber with thickness of 2 mm and 10 mm, respectively. The top steel plate is bolted into the concrete grillage at the top and the bottom steel plate to the concrete plinth below. It is assumed that the concrete plinth is rigid and thus the bottom of the LRB is fully restrained.

The LRB is modelled in Ruaumoko 3D as a spring element with no interactions between the local X, Y and Z components in both translations and rotations. It is modelled with no strength degradation, as earthquakes typically have relatively short durations.

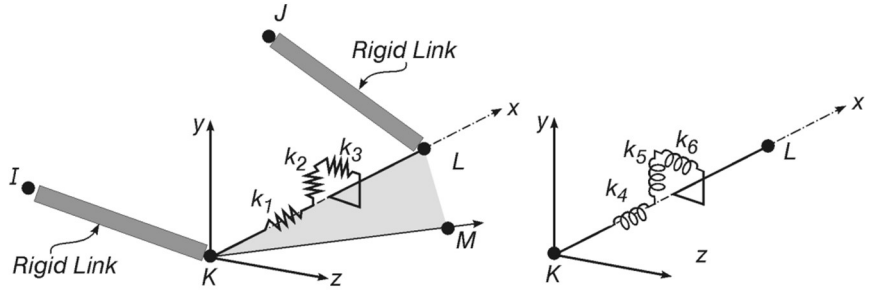

Figure 19. Local axes of the spring element for (A) translations and (B) rotations (Carr, 2005)

Previous studies (e.g. (Warn & Ryan, 2012)) have shown that the horizontal behaviour of LRB can be effectively modelled using a bilinear hysteresis model and hence the bilinear hysteresis model is adopted to model the LRBs. Experimental data provided by the LRB manufacturer was used to obtain the parameters of the spring element in Ruaumoko 3D. The initial stiffness, yield force, and bilinear factor (Ramberg-Osgood factor) of the spring element in the two horizontal directions was directly taken from the pushover curve based on the results of prototype testing.

Table 6. Characteristics of LRBs in the building

Characteristic	Value
Vertical stiffness	894,000 kN/m
Horizontal stiffness	6,563 kN/m

Rotational stiffness	10,290 kN-m/rad
Bilinear factor	0.13036
Horizontal yield force	42 kN

Figure 20. Photo of LRB subjected to compressive and shear loadings during prototype testing

Two sets of experiments were performed in the prototype testing. In the first set, the LRB was subjected to lateral force at low velocity increments to simulate a quasi-static response, while the second test subjected the LRB to the expected velocity. Tests were conducted at the manufacturer testing centre in Kuala Lumpur, Malaysia. The results from using the expected velocity test were selected over the quasi-static test to capture the interactions between horizontal stiffness and velocity. An approximate pushover curve was then derived by taking the average from the set of experimental data, as can be seen in Figure 21.

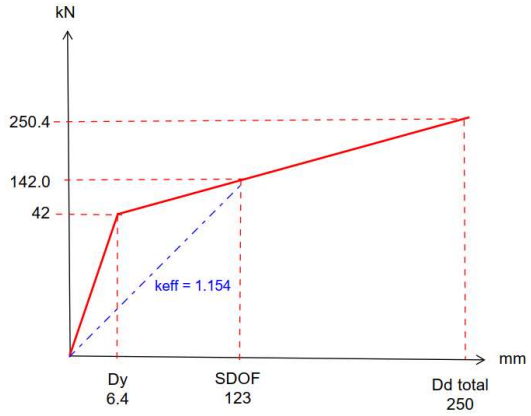

Figure 21. Experimental pushover curve with LRB subjected to the expected velocity (Robinson Seismic Limited, 2016)

Based on Figure 21, the initial horizontal stiffness was computed to be 0.853 kN/m and this value was adopted in the spring element in Ruaumoko 3D. The rotational stiffness of the LRB about the horizontal axis was included in the structural model because it could contribute to resisting p-delta actions. Rotation is mainly resisted by the elastomeric rubber and can be calculated using Equation 4, where E_b is the effective bending modulus of the rubber, I is the second moment of inertia of the rubber only section, and T_r is the total thickness of the rubber.

$$K_\theta = \frac{E_b I}{T_r} \qquad \text{(Eqn. 4)}$$

The compressive stiffness can be taken equal to the value observed by the manufacturer during the prototype test. Hence, it was set to 894,000 kN/m in the structural model. The critical buckling load of the lead core is an important design factor and was computed to equal 8,419 kN at zero horizontal displacement. However, the critical buckling load will decrease as a function of the horizontal displacement due to the reduction in the effective area of LRB resulting in a greater axial load taken by the lead core. The critical buckling load will decrease until it reaches 20% of its undeformed value before it plateaus

(Buckle & Liu, 1994). A loss in the vertical supports of the LRBs may cause significant damage and could potentially result in the building collapse. However, as the study is mainly focused on the loss analysis of the building given no collapse and because deformation demands on the beams were limited even for large intensity earthquakes, the compressive stiffness of the LRB was set to remain elastic throughout the NLTH analysis.

The tensile behaviour of an LRB can be assumed to be bi-linear (Pietra & Park, 2017). Based on the tensile force versus axial elongation curve from the prototype testing, a bi-linear curve was fit to the data approximately. The initial tensile stiffness was observed to be similar in magnitude to the compressive stiffness (894,000 kN/m) and hence, the tensile stiffness is set to equal the compressive stiffness. The tensile yield force can be directly read from the experimental curve. After yielding, the LRB is expected to have only 13% of its initial stiffness.

The horizontal stiffness of the bearings was modelled as a constant even though axial loads on the bearings may change during the response. This is deemed as reasonable for global response predictions because when lateral loads are applied on one side of the building the bearings may experience additional compression but on the other side they will experience tension and hence, the overall lateral stiffness should not be affected.

In addition to the above, the following assumptions were made while modelling:

- The torsional stiffness or rotation about the vertical axis of individual bearing is neglected.
- A rigid diaphragm at the ground level ties all isolator elements together.
- Under a maximum credible earthquake, the maximum compression load on the LRB is expected to be 2,475 kN. This value is taken as the compressive yield force of the spring element, although it is assumed that this value will never be exceeded in this study.

- The preload axial force of an individual LRB is assigned to equal the contributions of dead load and live load from the superstructure above.

3.2.7. Steel-PTFE Slider Bearings

The steel-PTFE slider bearing (SB) is a flat friction slider with a steel-PTFE sliding interface. It connects the grillage at the top to the concrete plinth below. It is assumed that the concrete plinth is rigid and thus the bottom of the SB is fully restrained.

The upper steel plate of the bearing is faced by a polished stainless steel plate underneath that is 1,200 mm in diameter. The lower steel plate of the bearing has a Teflon disc, 300 mm in diameter, recessed on its top. The bearing allows a movement of 450 mm from the centre of the bearing for a total movement of 900 mm.

Each individual SB is modelled as a spring element in Ruaumoko. Its horizontal or shear resistance, as described in Equation 5, is related to the applied axial load and the friction coefficient.

$$F = \mu N \qquad \text{(Eqn. 5)}$$

Research has shown that the friction coefficient of a SB is correlated with the sliding velocity, surface temperature, surface normal pressure, and the number of cyclic loadings (Constantinou et al., 1987). However, the sliding velocity can be taken to remain constant in a typical earthquake (Dolce et al., 2005), while the other factors are assumed to be negligible given the short duration of most earthquakes. For this study, the coefficient of friction will be assumed constant throughout the analysis and hence the shear resistance of a SB is simply a function of the normal axial load.

The manufacturer provided two values of coefficient of friction; 4% for sliding at low speed and 10% for sliding at high speed. In Ruaumoko 3D, the spring

element is modelled using only the low speed coefficient of friction, i.e., 4%, to provide a conservative estimate of the superstructure demands.

Each spring element has a constant preload shear force resistance. This is required because in lumped mass analysis, the individual elements are not assigned with weights and the axial load acting on the SB is zero. Hence, there is a need to explicitly account for the contributions of dead load and live load from the superstructure above to the shear resistance of the SB. This constant force is computed using Equation 5 when the SB is subjected to static loads applied to the superstructure for the seismic case (i.e., $G + 0.3Q$).

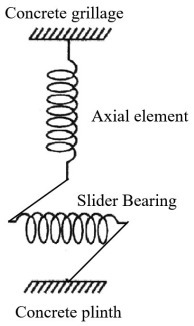

Figure 22. Spring concept used for modelling slider bearings (SBs) in Ruaumoko 3D

The SB is assumed to behave elastically in compression and its compressive stiffness is taken as ten times that of the LRB. It is also assumed that the SB is not effective in tension because it will act like a gap element in the axial direction. However, Ruaumoko 3D only allowed a single axial stiffness for the spring element. To overcome this, a spring element was introduced to connect each SB spring element in series between the node representing the concrete grillage above and the node representing rigid concrete plinth below, as shown in Figure 22. This spring element, called the SB axial element, is set to behave in a rigid manner in all three translational directions by setting the horizontal stiffness to ten times the axial stiffness. Meanwhile, its tensile yield force in the axial direction is set to a very low value to simulate the gap behaviour.

In addition to the above, the following assumptions were made while modelling:

- The torsional stiffness of individual SBs has been neglected.
- There exists a rigid diaphragm at the ground level that ties all isolator elements together.
- The vertical preload acting on individual SBs does not change throughout the analysis.

3.2.8. Reinforced Concrete Grillage

The main purpose of the grillage beams is to resist p-delta actions associated with the isolators and to redistribute the discrete overturning moments and shear developed within the structural walls to the isolation system.

The rectangular grillages below the ground floor were cast in-situ to support the superstructure above and are in turn supported by lead rubber bearings and slider bearings. The grillage beams are expected to carry shear forces and bending moments from the structural walls and the steel gravity frame, then transfer the loads to the base isolators as axial loads. It is assumed that the grillage beams can transfer some moments to the LRBs, whereas the SBs are perfectly pinned to the grillage beams.

The rectangular reinforced concrete beams are cast together with the concrete slab on top. Hence, the grillage beam can be considered as a reinforced concrete T-beam for resisting bending moments. The computation of the effective flange width of the T-beam follows the equation outlined in NZS 3101:1:2006 (Standards New Zealand, 2006). The equation for the effective flange width is a function of the dimensions of the grillage beam, the slab thickness, and the distance to adjacent beams.

An example calculation is presented below for a rectangular beam with height and width equalling 1.4 m and 1.2 m, with a span of 6.355 m, as well as a slab thickness of 0.15 m on its top. It has an adjacent rectangular beam that has a

height of 1.05 m and a distance of 3.4 m between the centrelines of these two beams.

Criterion 1: $b_{eff} = \frac{L}{8} = \frac{6.355\ m}{8} = 0.79\ m$

Criterion 2: $b_{eff} = 8\ t_{slab} = 8 \times 0.15\ m = 1.2\ m$

Criterion 3: $b_{eff} = h_{b1} = 1.4\ m$

Criterion 4: $b_{eff} = dist \times \left(\frac{h_{b1}}{h_{b1} + h_{b2}}\right) = 1.94\ m$

The maximum flange to one side of a beam that is effective in resisting flexural forces is taken as the minimum of the computed b_{eff}, which is equal to 0.79 m. Thus, the effective flange width of this grillage beam is $0.79\ m + 1.2\ m + 0.79\ m = 2.78\ m$.

In the NLTH analyses, it is assumed that the grillage beams are cracked prior to the start of every analysis. The Section Designer tool in SAP2000 was used to obtain the cracked moments of inertia about the major axis of the individual T-beams with the different effective dimensions.

Meanwhile, the torsion constant (J) was assumed to remain elastic throughout the analysis and is equal to the uncracked concrete beam section. This is because the grillage beams were not designed to carry torsional forces for satisfying the equilibrium condition. Instead, minimum torsional reinforcement was provided for compatibility purposes as dictated by the NZS 3101:1:2006 standard (Standards New Zealand, 2006).

3.3. Structural Analysis

3.3.1. Modal and Pushover Analysis

Modal analysis was done using Ruaumoko 3D. The first ten modes of the base isolated structure are used in the modal analysis to ensure that all important modes of vibration, including both translational and rotational, have been identified. The participation factors and effective masses of the first ten modes were computed in Ruaumoko and the results are summarised in Table 7.

Table 7. Participation factors and effective masses for the first ten modes of vibration

Mode	X			Z			Direction
	Participation Factor	Effective Mass (kg)	% Mass	Participation Factor	Effective Mass (kg)	% Mass	
1	-0.01215	0.1711	0	1.572	2863	78	Z
2	-0.03257	25.94	1	0.09784	234.1	85	Y
3	1.402	3442	95	0.04495	3.536	85	X
4	0.01791	0.3613	95	-0.6947	543.8	100	Z
5	0.005127	1.04	95	-0.00482	0.9206	100	Y
6	-0.4335	177	100	-0.0116	0.1267	100	X
7	0.000591	0.000969	100	0.01061	0.3128	100	Y
8	-0.00137	0.001109	100	0.04965	1.455	100	Z
9	0.03444	0.3999	100	0.000878	0.00026	100	X
10	9.75E-05	0.0000125	100	-0.00158	0.00328	100	Y

Note that the X-direction corresponds to N-S translation, the Z-direction to E-W translation, and the Y-direction indicates torsion here.

The first six modes already have the total participating mass larger than 90%, suggesting that considering only ten modes is sufficient in capturing the global response of the structure.

The results of the modal analysis returned a set of ten modes of vibration as presented in Table 8. Although the periods appeared to be low for a base isolated building, the reason is that the initial stiffness of the lead rubber bearings and slider bearings were used in the modal analysis. Hence, the periods displayed in Table 8 are not necessarily reflective of the building response in an actual earthquake.

Table 8. Modal analysis results from Ruaumoko

Mode	Frequency	Period (s)	Damping
1	0.7015	1.425	5%
2	0.7271	1.375	5%
3	0.8398	1.191	5%
4	1.846	0.5417	5%

5	2.031	0.4923	5%
6	2.369	0.4222	5%
7	6.028	0.1659	5%
8	6.923	0.1444	5%
9	9.582	0.1044	5%
10	11.19	0.08935	5%

A pushover analysis was done in Ruaumoko by gradually increasing a small increment of acceleration until the base isolators are close to failure. This was done by creating a ramp excitation starting from 0 to 0.22 g in 200 steps as shown in Figure 23.

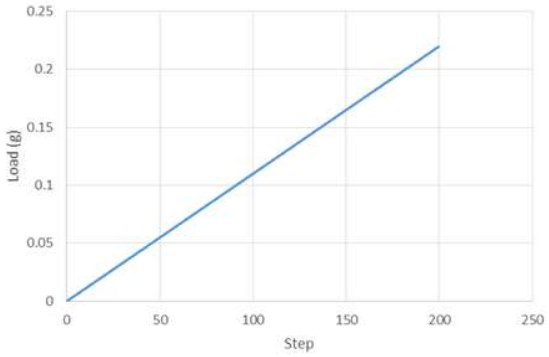

Figure 23. Ramp acceleration used as the pushover load

The pushover curves in both the X and Z directions are given in Figure 24 (a) and (b), respectively.

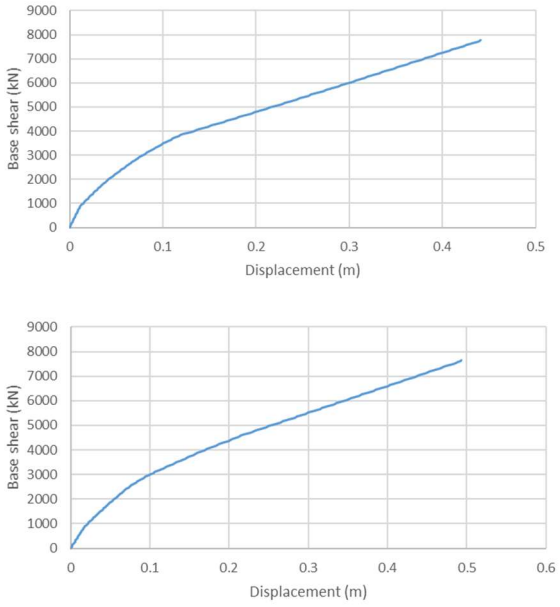

Figure 24. Pushover in the (a) X-direction and (b) Z-direction

Initially, the pushover curves maintained a linear profile until the base shear reached an approximate value of 830 kN that corresponded to a very low displacement. Then the structure responded non-linearly with each base isolator yielding in succession until all have yielded. After this point, the profile became linear again before the isolators reached their maximum displacement capacity.

At the maximum base shear, the secant stiffness in the X-direction was computed to be 17,601 kN/m, while in the Z-direction it was 15,512 kN/m. Hence, the structure is stiffer in the X-direction than in the Z-direction. This is because the length of wall in the X-direction is twice that of the Z-direction.

Furthermore, this building was designed with a DCLS performance limit of 0.5% drift in the superstructure. The superstructure never exceeded this drift limit during pushover in both directions. However, it was noted that cracked section properties for the concrete walls were not used since the gross moment of inertia was used throughout the pushover analysis. This may not be reflective of the actual building response, hence subsequent NLTH analysis will use the cracked section properties for the concrete walls.

3.3.2. Time-Based Structural Analysis Results

Time-based structural analysis was performed in Ruaumoko 3D by subjecting the same structural model to twenty representative ground motions for each of the nine intensity levels, as outlined in Section 4.1.1.

The engineering demand parameters (EDP) of interest included the peak floor accelerations (PFA), inter-storey drift ratio (IDR), the maximum displacements of the LRBs and SBs, the maximum compressive and tensile loads of the LRBs, and maximum wall curvatures at the base. The results of analyses consisting of the 25th percentile, median, 75th percentile of each EDP are summarised in the figures below from Figure 25 to Figure 32 for the two intensity levels associated with the return periods of 475 years and 2475 years. The results are expected for a "control" structural model as sensitivity analyses are conducted to investigate the impact of different modelling assumptions in Section 4.3.3.

The EDPs for the other intensity levels are not shown here for brevity. Instead, the EDPs for the other intensity levels can be found in Appendix A.

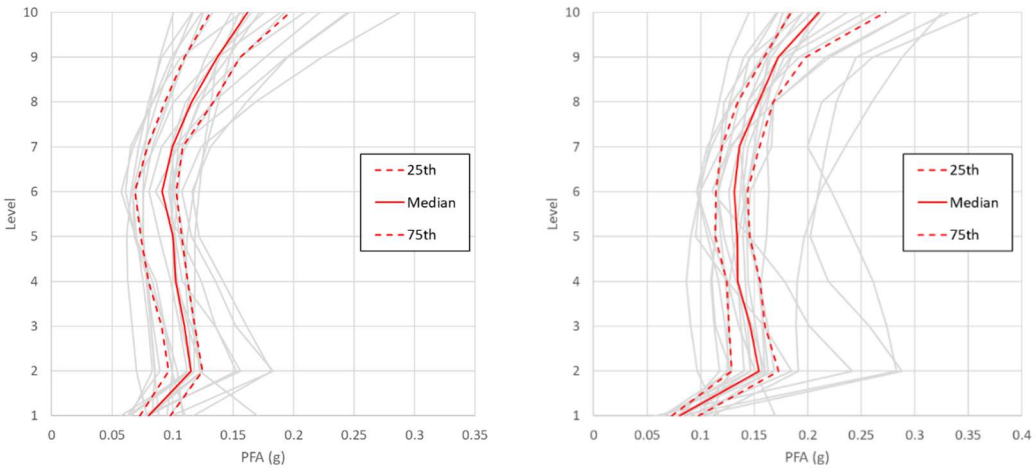

(a) (b)

Figure 25. Peak floor accelerations (PFA) of the control structural model subjected to 20 ground motions for the intensity levels of (a) 1 in 475 years and (b) 1 in 2475 years

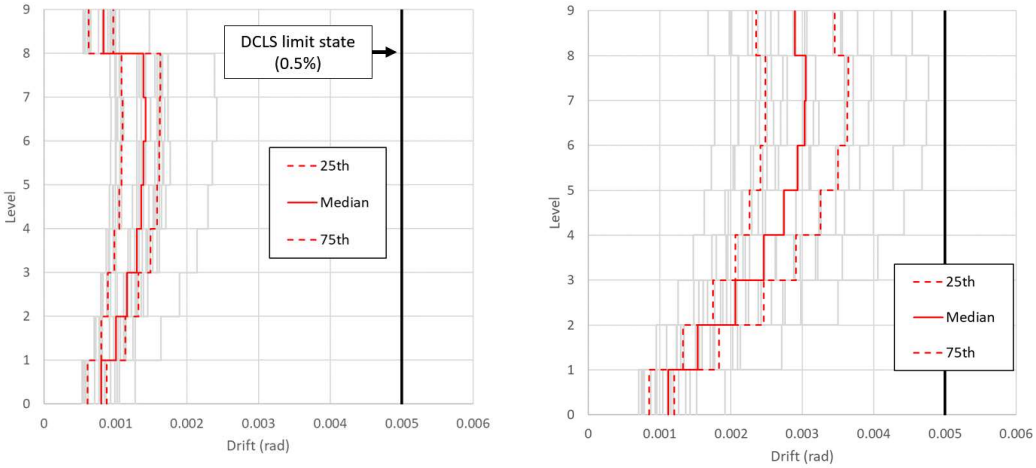

(a) (b)

Figure 26. Inter-storey drift ratio (IDR) of the control structural model subjected to 20 ground motions for the intensity level of 1 in 475 years in the (a) X-direction and (b) Z-direction

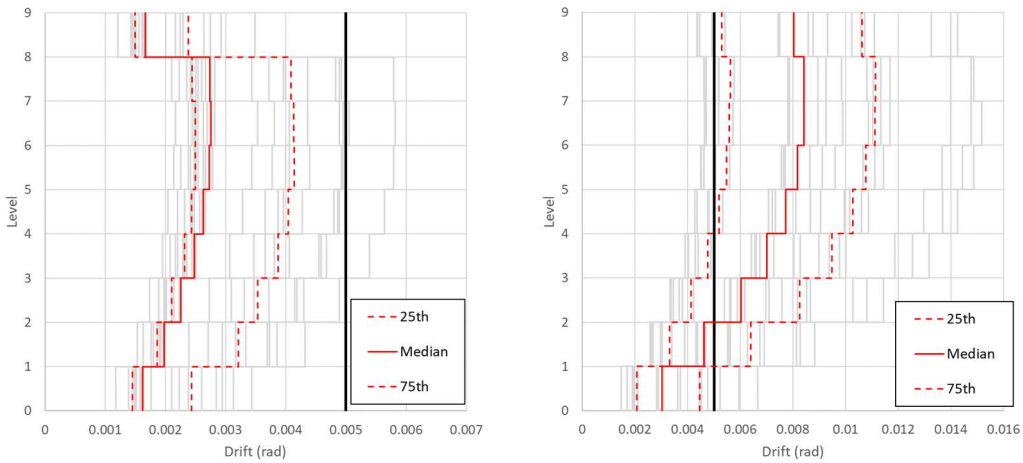

(a) (b)

Figure 27. Inter-storey drift ratio (IDR) of the control structural model subjected to 20 ground motions for the intensity level of 1 in 2475 years in the (a) X-direction and (b) Z-direction

Note that the vertical black bar on each of the IDR plot represents the DCLS limit state for drift (0.5%).

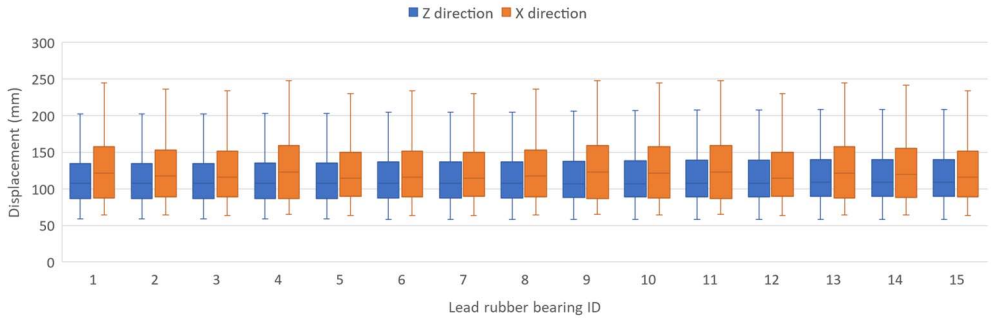

(a)

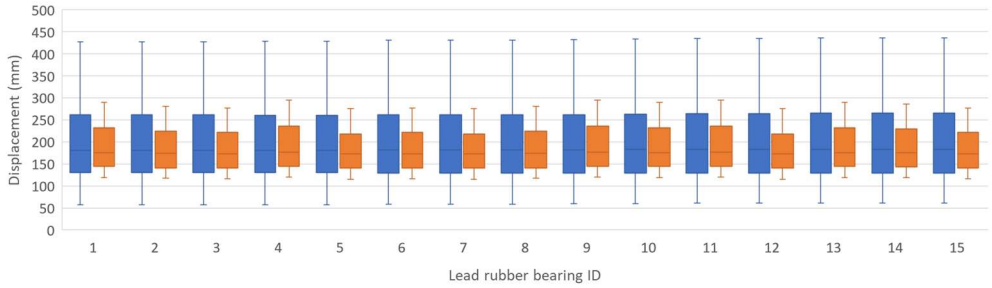

(b)

Figure 28. Maximum displacements of the lead rubber bearing (LRB) in the two horizontal directions for the intensity levels of (a) 1 in 475 years and (b) 1 in 2475 years

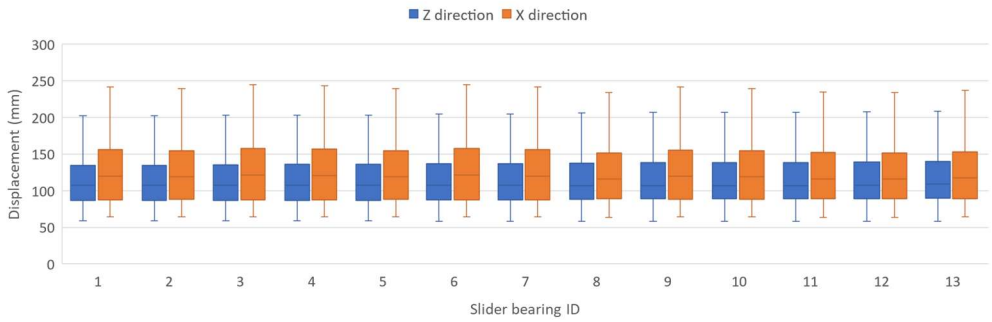

(a)

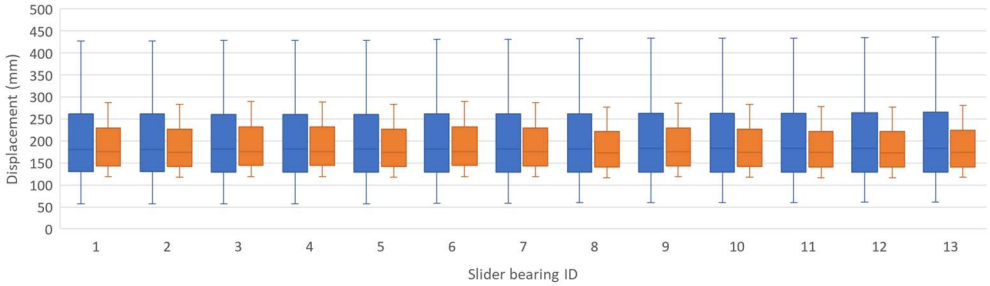

(b)

Figure 29. Maximum displacements of the slider bearing (SB) in the two horizontal directions for the intensity levels of (a) 1 in 475 years and (b) 1 in 2475 years

The box plot above defines the 25th percentile, 50th percentile (median), and 75th percentile values for maximum displacements of individual LRBs and SBs.

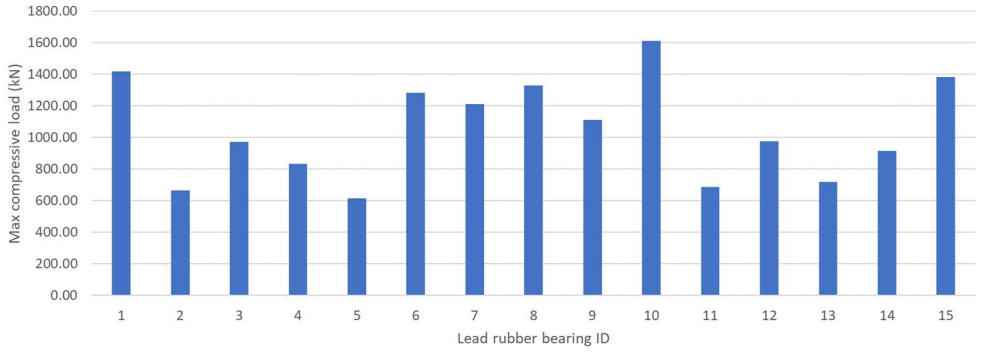

(a)

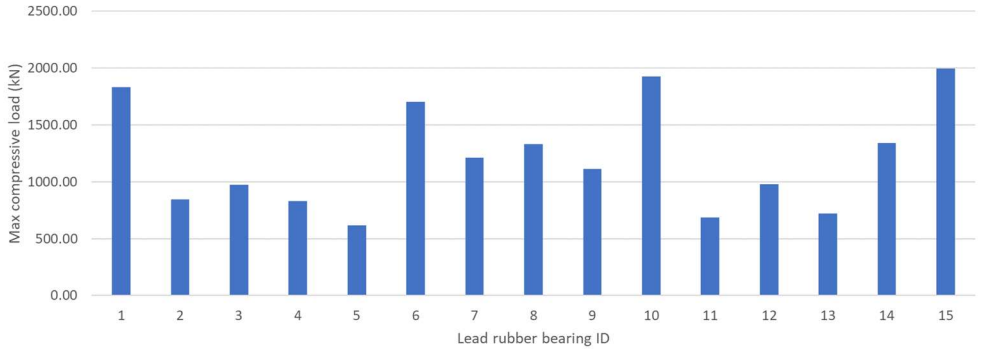

(b)

Figure 30. Maximum compressive axial loads of the lead rubber bearings (LRB) for the intensity levels of (a) 1 in 475 years and (b) 1 in 2475 years

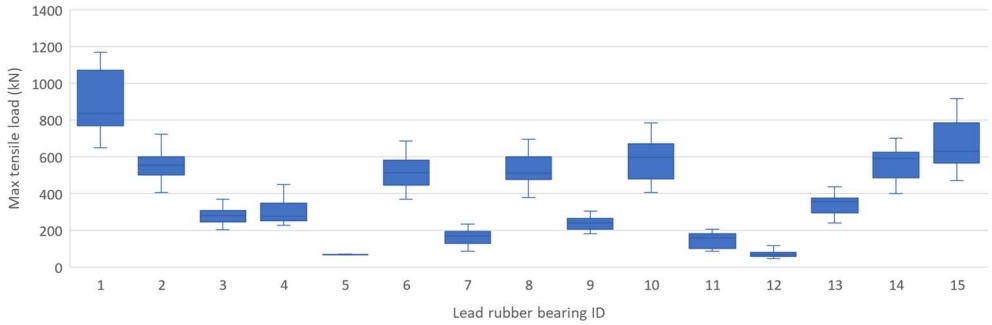

(a)

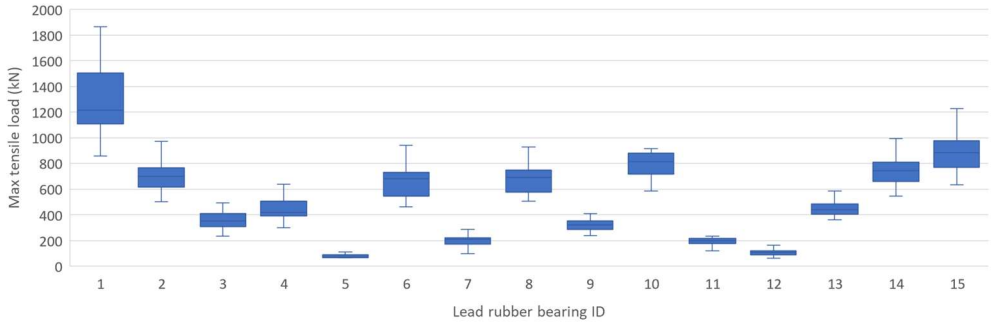

(b)

Figure 31. Maximum tensile axial loads of the lead rubber bearings (LRB) for the intensity levels of (a) 1 in 475 years and (b) 1 in 2475 years

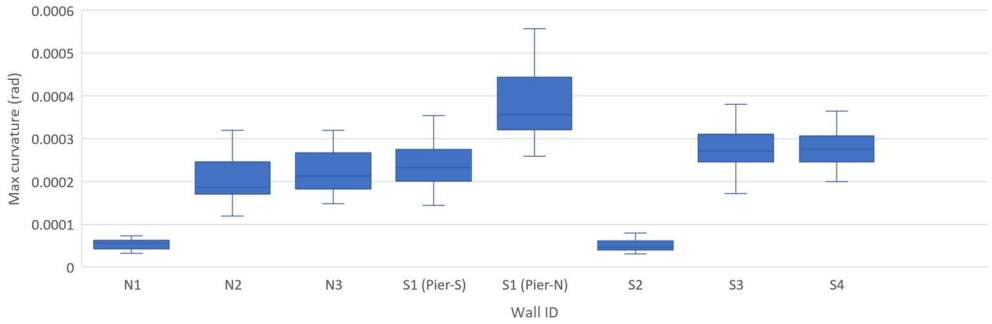

(a)

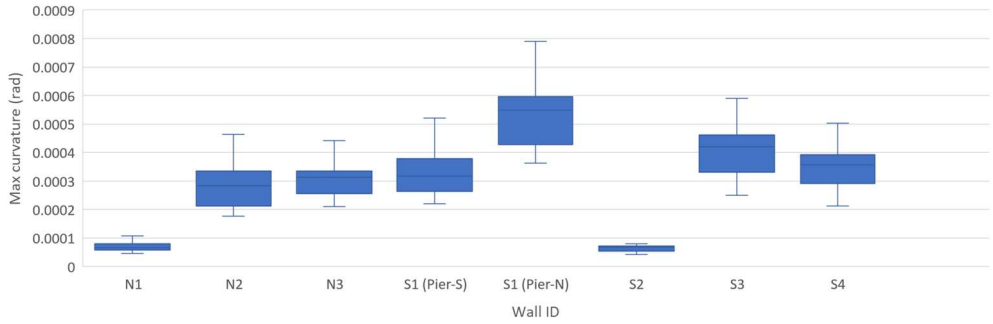

(b)

Figure 32. Maximum curvature at the base of the walls for the intensity levels of (a) 1 in 475 years and (b) 1 in 2475 years

3.3.3. Sensitivity Analyses

As outlined in previous sections, the structural model of the base isolated building incorporated many modelling assumptions and approximations. Hence, sensitivity analyses are performed to investigate their impacts on the results of the structural analyses. Specifically, the main interest is to study the uncertainty in the engineering demand parameters (EDP) that will be used as inputs in the subsequent loss analysis.

Four parameters of interest that may result in large discrepancies in the results were investigated, including:

- **Damping model:**
  The control model used a Caughey damping model with linear variation as suggested by Carr (2005). There are also other damping models available, such as the Rayleigh damping model with tangent stiffness, that are commonly used due to its computational efficiency. The original design of the building used Rayleigh damping when performing NLTH analyses. Thus, a model using the Rayleigh damping model with tangent stiffness (ICTYPE = 2) will be analysed in Ruaumoko 3D.
- **Gravity framing:**

As mentioned in Section 4.2.5, the beam-column joints of the steel gravity framing are modelled with some rotational stiffness to account for the non-perfectly pinned connections condition. To model this behaviour, rotational springs were introduced at both ends of every beam element. The rotational spring has rotational stiffness proportional to its sectional properties and the length of beam. It was assumed that this will influence the structural responses of the building and will subsequently affect the loss analysis process and expected annual loss. Therefore, to check whether this assumption is valid, another model with perfectly pinned joint connections (i.e., the rotational stiffness of the springs set to zero) will be analysed.

- **Slab weight:**
  The seismic weight of the structure is an important parameter in NLTHA. The biggest contribution to the total seismic weight is the slab weight at each floor. Due to the existence of heavy tiling and other services, it had been assumed that the service dead load acting on the slab is 1.5 kPa. To check the sensitivity of the analysis results on this assumption, the SDL equalling to 1.0 kPa and 2.0 kPa at each floor were also investigated.
- **Uncracked walls:**
  An important assumption that was made is the section properties of the reinforced concrete walls. The control model uses the cracked stiffness properties for the walls, which are conservative because they are the main lateral resisting system in the superstructure. However, sensitivity analysis will be done using the uncracked wall stiffnesses in the analysis.

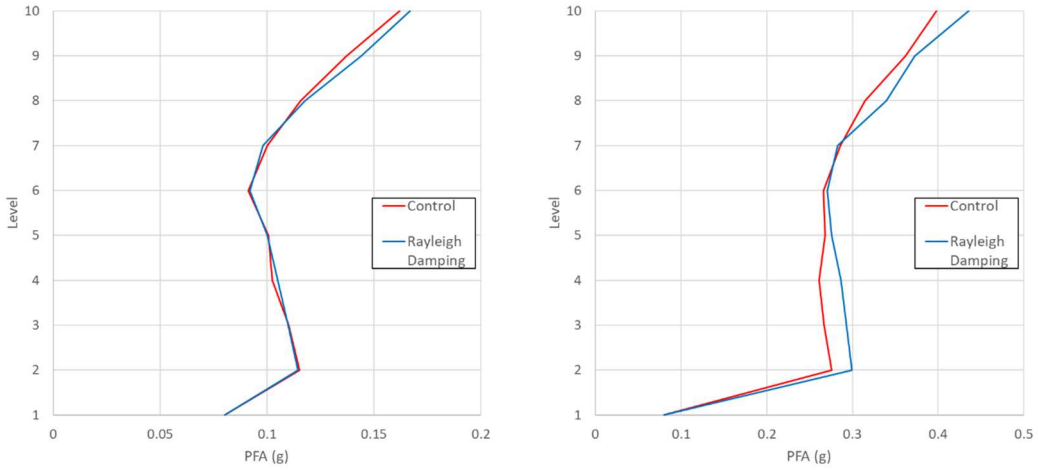

Figure 33. Damping model - Peak floor accelerations (median) for the intensity levels of (a) 1 in 475 years and (b) 1 in 2475 years

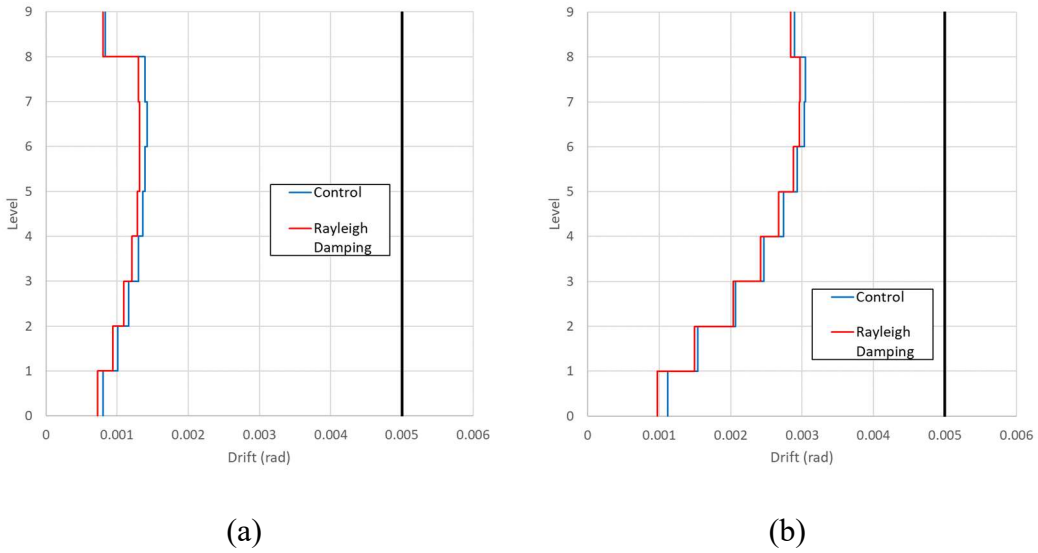

Figure 34. Damping model - Inter-storey drift ratio (median) for the intensity level of 1 in 475 years in the (a) X-direction and (b) Z-direction

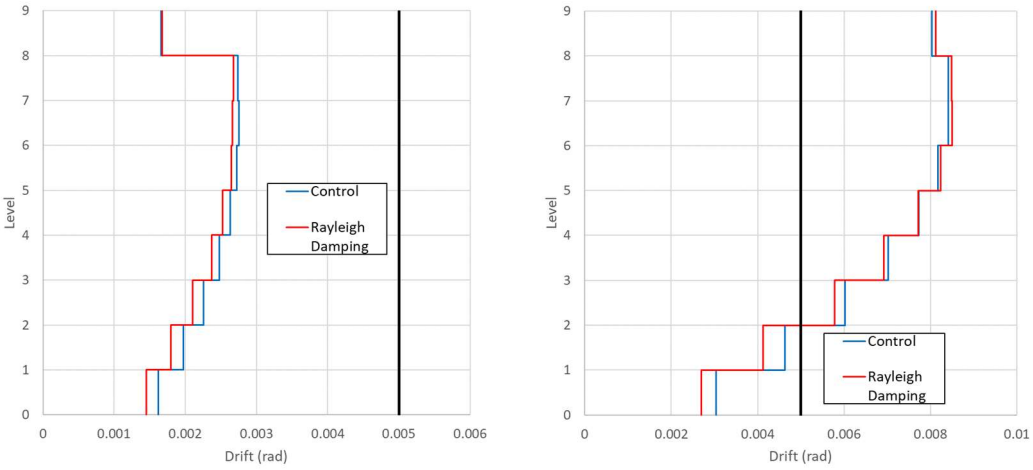

(a) (b)

Figure 35. Damping model - Inter-storey drift ratio (median) for the intensity level of 1 in 2475 years in the (a) X-direction and (b) Z-direction

Note that the vertical black bar on each of the IDR plot represents the DCLS limit state for drift (0.5%).

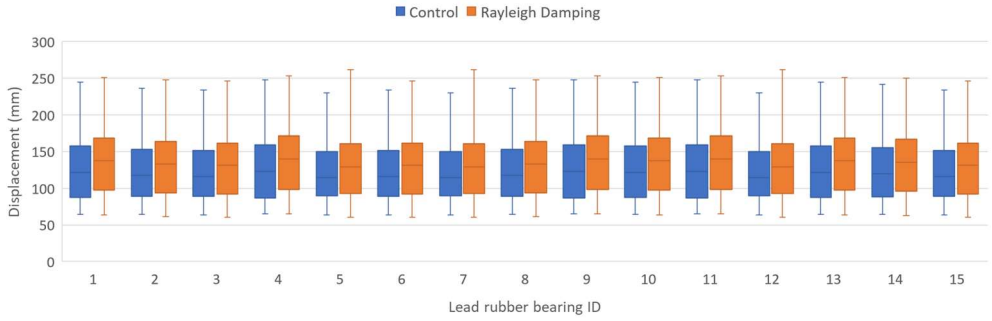

(a)

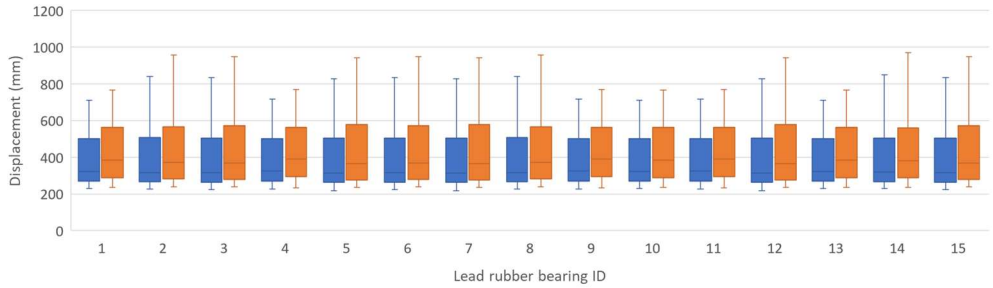

(b)

Figure 36. Damping model - Maximum displacements of the lead rubber bearing in the X-direction for the intensity levels of (a) 1 in 475 years and (b) 1 in 2475 years

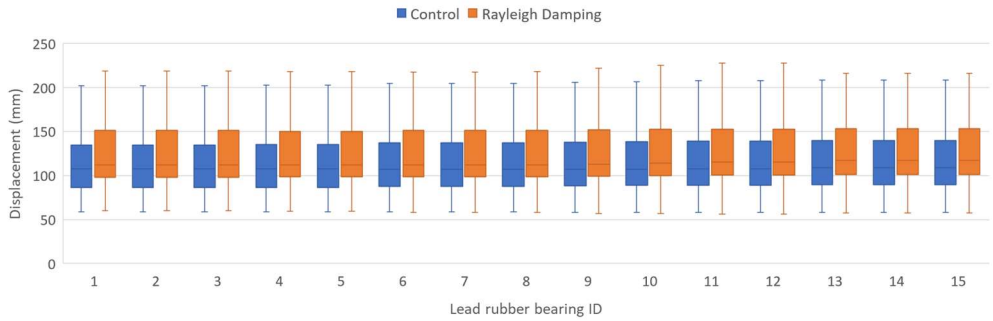

(a)

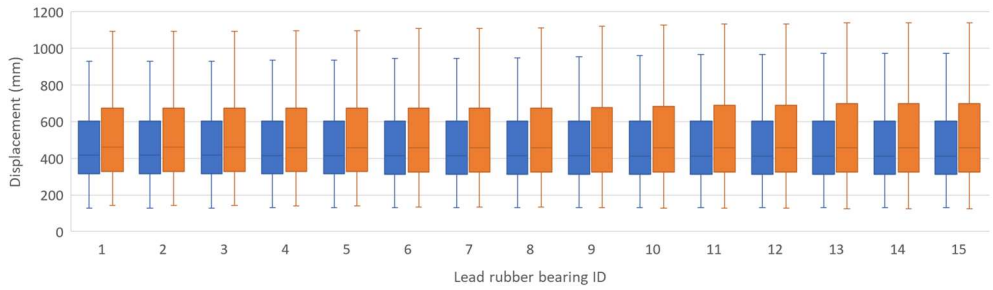

(b)

Figure 37. Damping model - Maximum displacements of the lead rubber bearing in the Z-direction for the intensity levels of (a) 1 in 475 years and (b) 1 in 2475 years

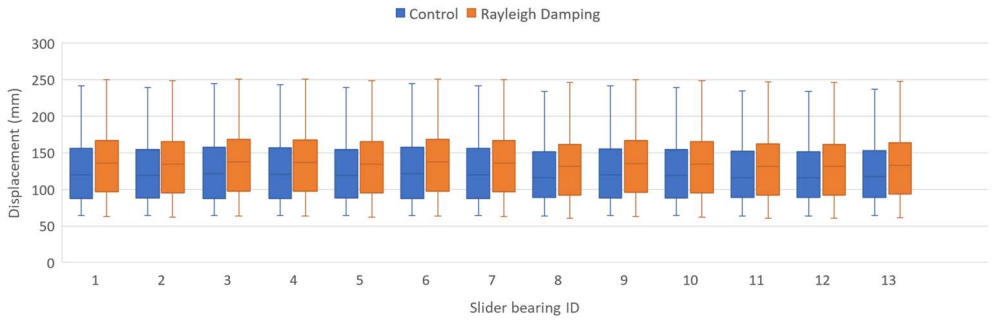

(a)

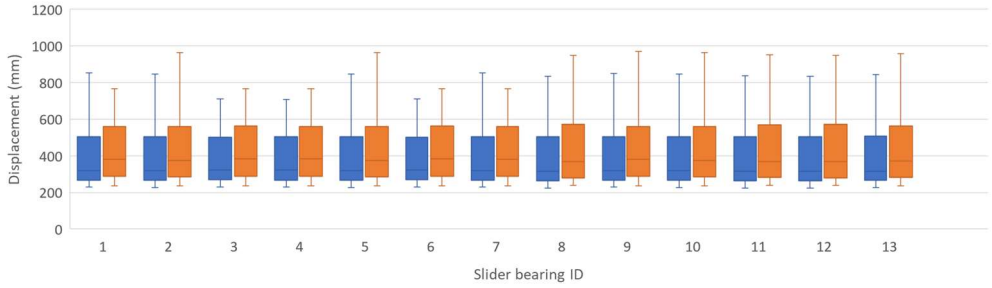

(b)

Figure 38. Damping model - Maximum displacements of the slider bearing in the X-direction for the intensity levels of (a) 1 in 475 years and (b) 1 in 2475 years

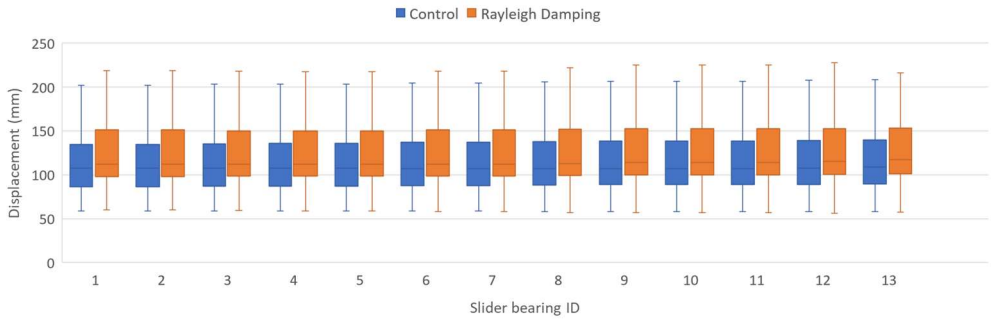

(a)

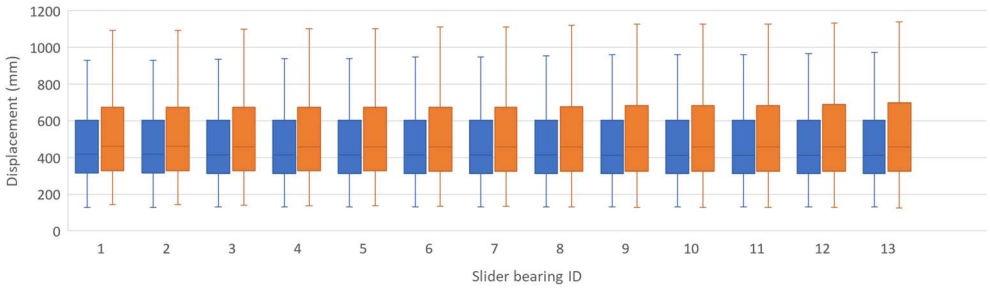

(b)

Figure 39. Damping model - Maximum displacements of the slider bearing in the Z-direction for the intensity levels of (a) 1 in 475 years and (b) 1 in 2475 years

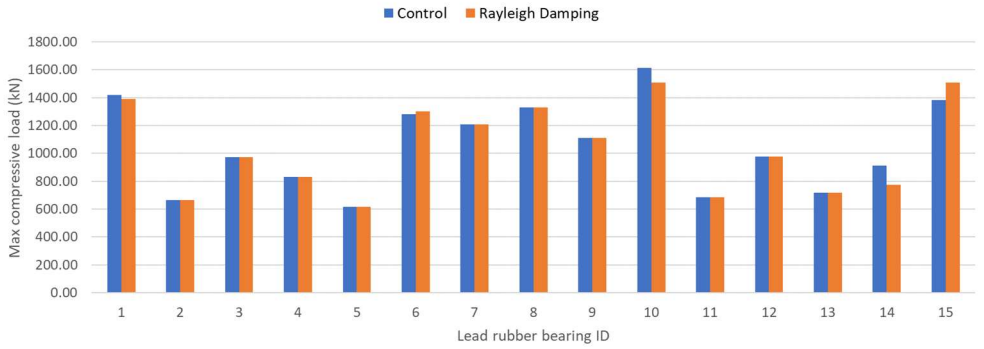

(a)

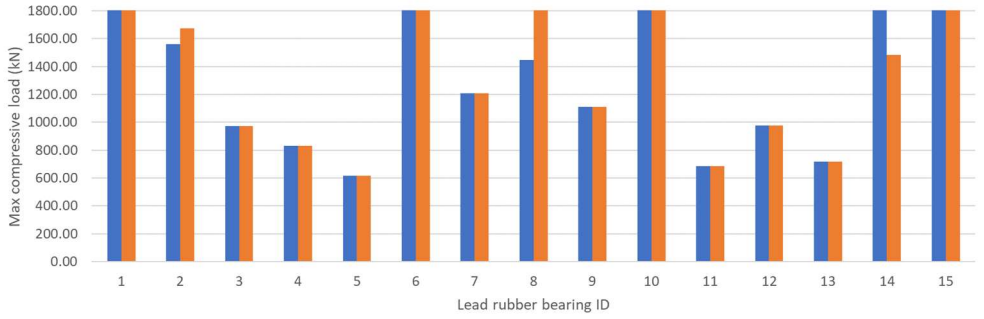

(b)

Figure 40. Damping model - Maximum compressive axial loads of the lead rubber bearings for the intensity levels of (a) 1 in 475 years and (b) 1 in 2475 years

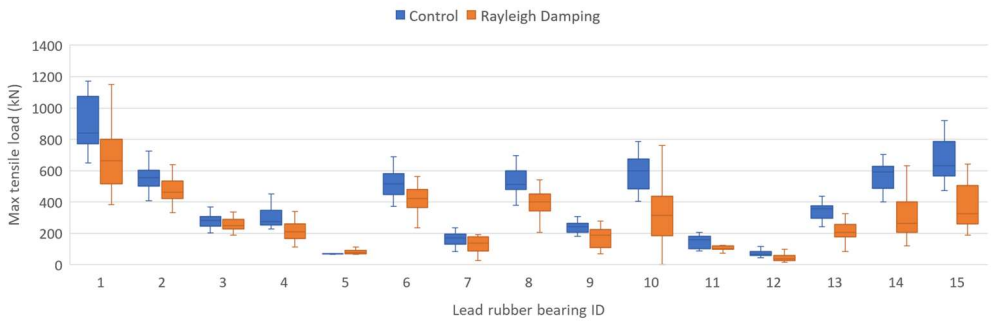

(a)

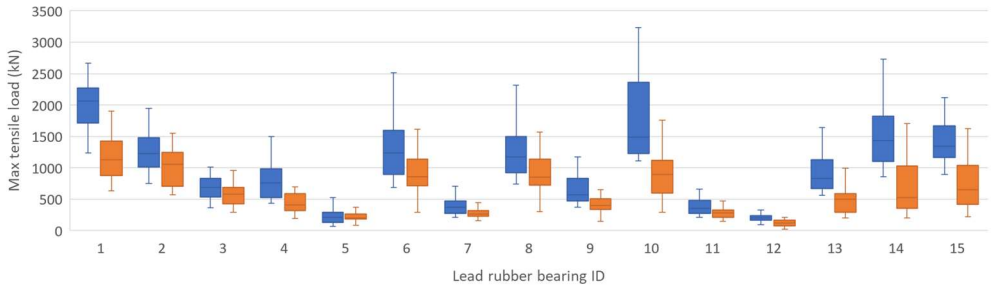

(b)

Figure 41. Damping model - Maximum tensile axial loads of the lead rubber bearings for the intensity levels of (a) 1 in 475 years and (b) 1 in 2475 years

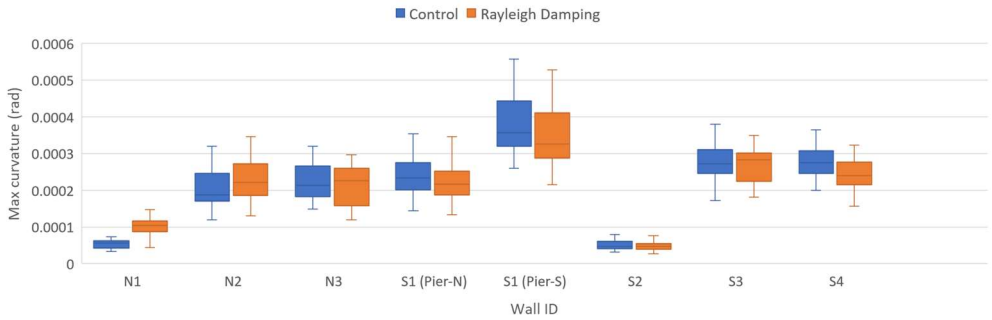

(a)

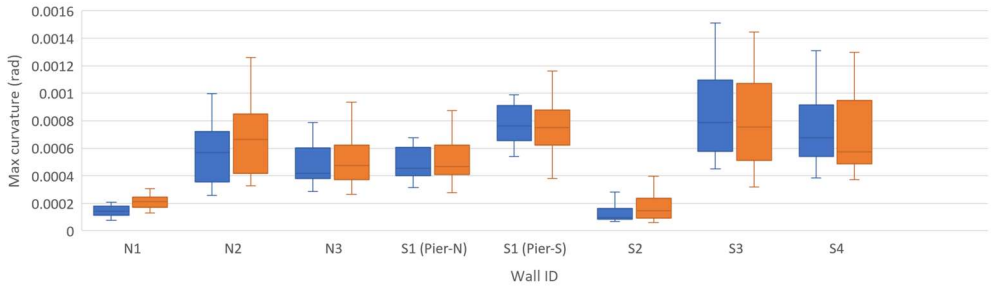

(b)

Figure 42. Damping model - Maximum curvature at the base of the walls for the intensity levels of (a) 1 in 475 years and (b) 1 in 2475 years

As can be seen from Figure 33 to Figure 42, changing the damping model affected the acceleration in the superstructure and the maximum tensile loads in the LRBs more than the inter-storey drift. The acceleration of the tangent damping is slightly higher than the control model and is more evident in the higher intensity level. This is due to the fact that Rayleigh damping with tangent stiffness slightly reduces damping in between the specified periods, which are the first and the fifth modes. Note that the fifth mode accounted for at least 95% of the effective mass.

For some bearings, the tensile forces increased significantly. However, the bearings had larger capacity in tension than these loads and hence this uncertainty is not expected to affect research.

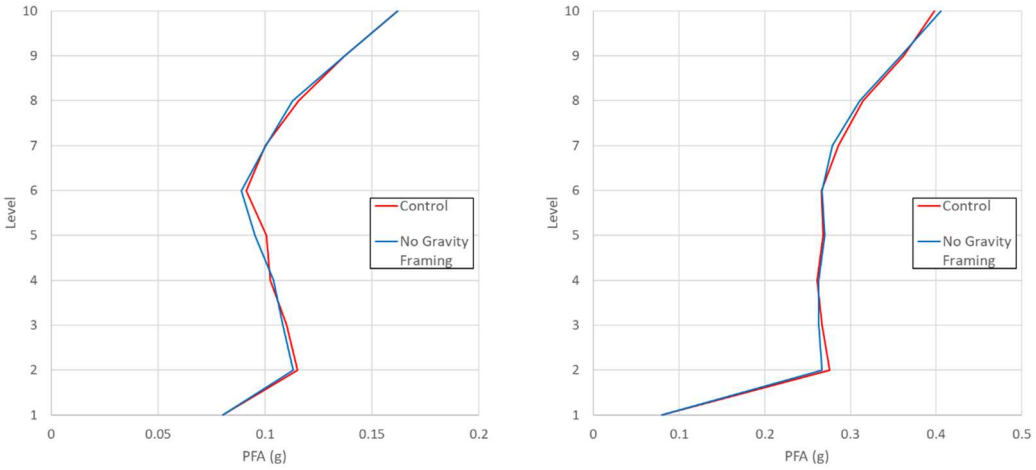

(a) (b)

Figure 43. No gravity framing - Peak floor accelerations (median) for the intensity levels of (a) 1 in 475 years and (b) 1 in 2475 years

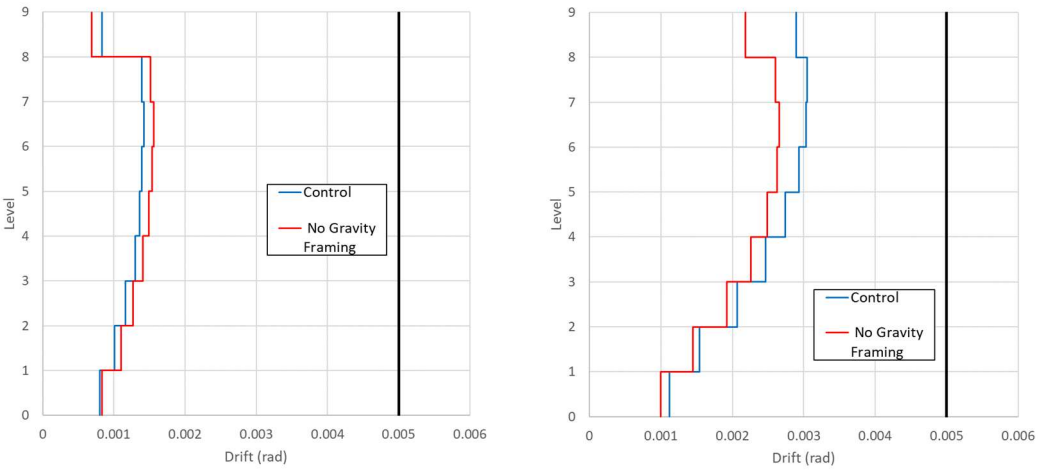

(a) (b)

Figure 44. No gravity framing - Inter-storey drift ratio (median) for the intensity level of 1 in 475 years in the (a) X-direction and (b) Z-direction

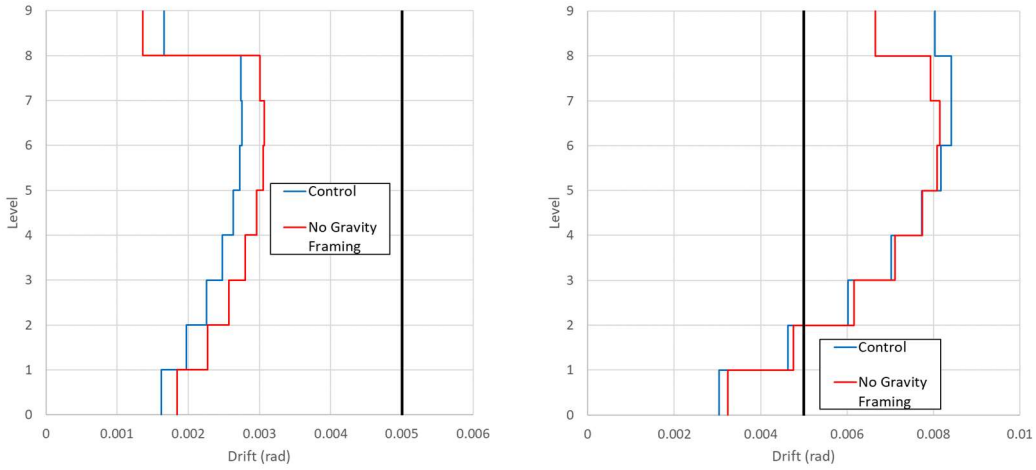

(a) (b)

Figure 45. No gravity framing - Inter-storey drift ratio (median) for the intensity level of 1 in 2475 years in the (a) X-direction and (b) Z-direction

Notice that the IDR of the top floor differed from the rest of superstructure. This is because the top floor is a lightweight steel roof that uses bracing as the main lateral resisting system in addition to a small section of structural walls.

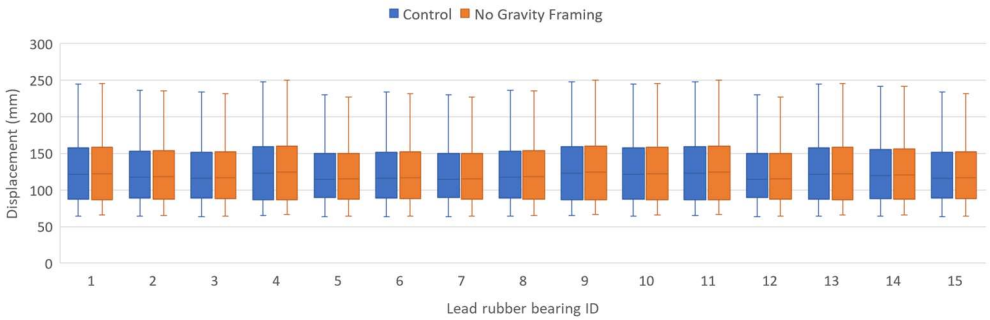

(a)

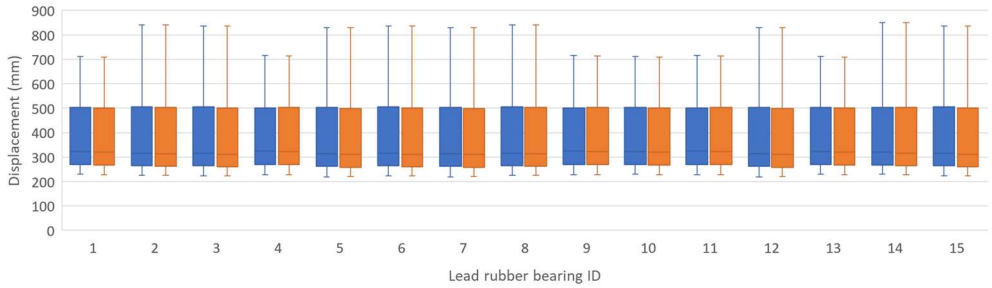

(b)

Figure 46. No gravity framing - Maximum displacements of the lead rubber bearing in the X-direction for the intensity levels of (a) 1 in 475 years and (b) 1 in 2475 years

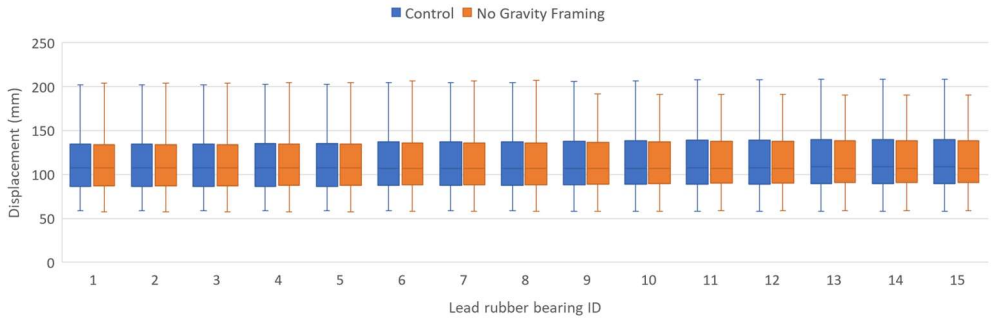

(a)

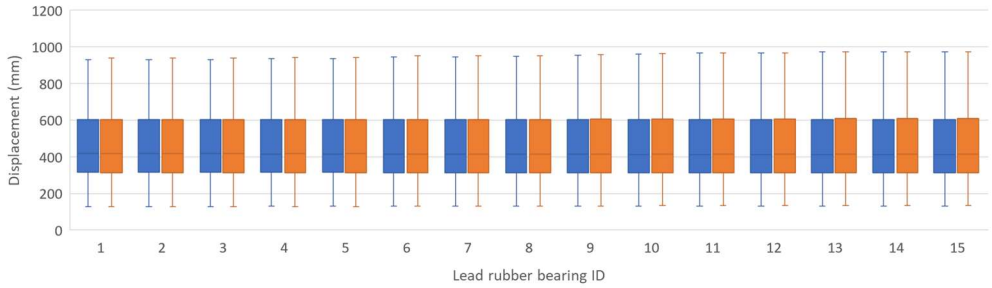

(b)

Figure 47. No gravity framing - Maximum displacements of the lead rubber bearing in the Z-direction for the intensity levels of (a) 1 in 475 years and (b) 1 in 2475 years

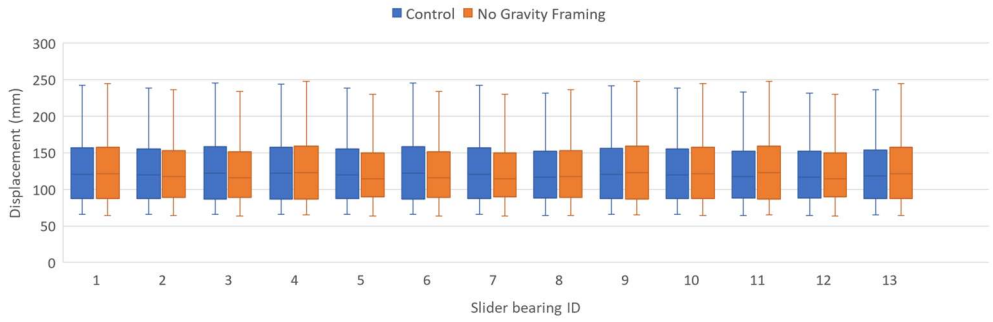

(a)

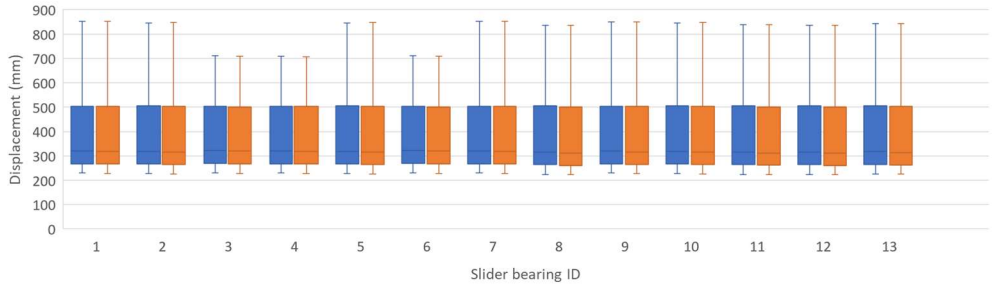

(b)

Figure 48. No gravity framing - Maximum displacements of the slider bearing in the X-direction for the intensity levels of (a) 1 in 475 years and (b) 1 in 2475 years

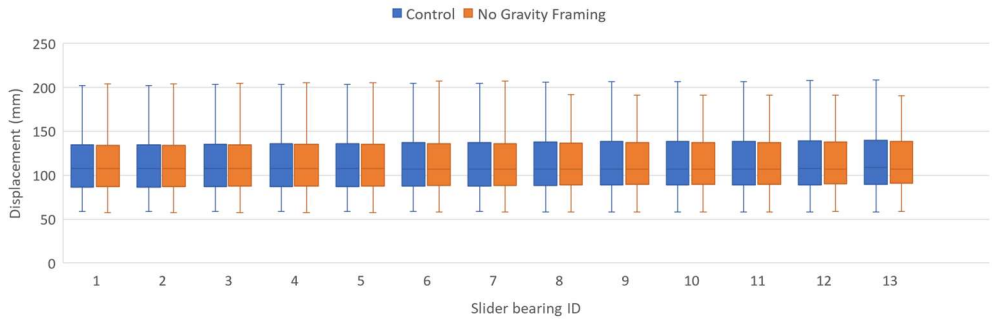

(a)

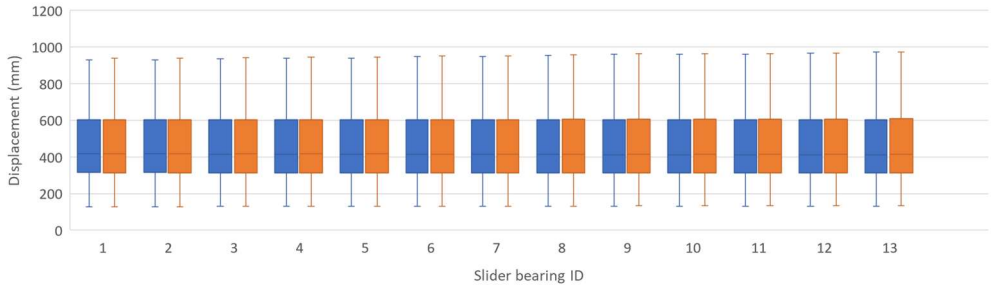

(b)

Figure 49. No gravity framing - Maximum displacements of the slider bearing in the Z-direction for the intensity levels of (a) 1 in 475 years and (b) 1 in 2475 years

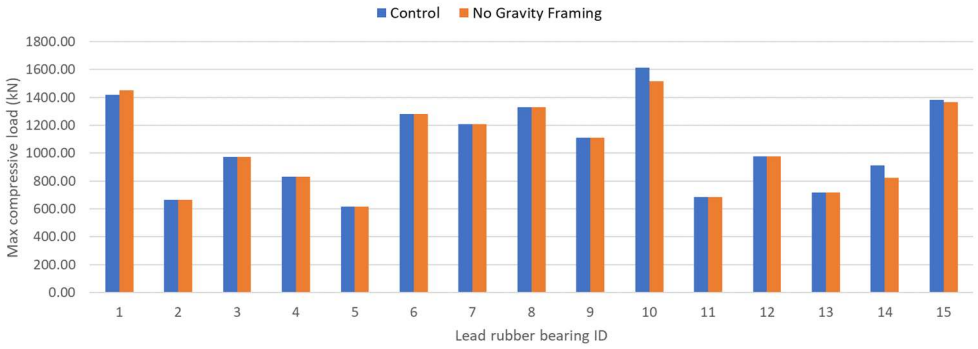

(a)

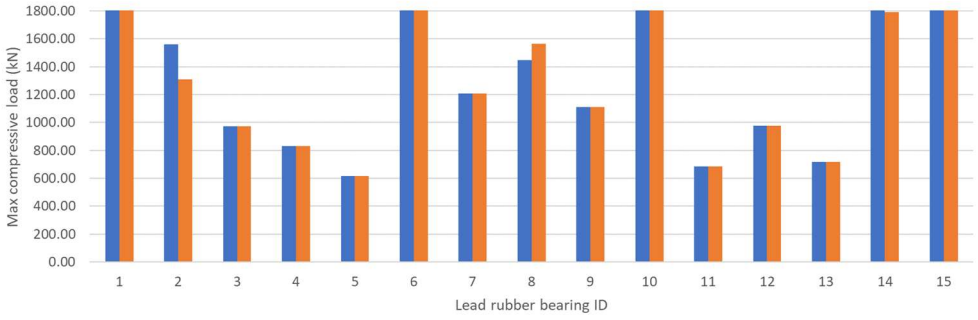

(b)

Figure 50. No gravity framing - Maximum compressive axial loads of the lead rubber bearings for the intensity levels of (a) 1 in 475 years and (b) 1 in 2475 years

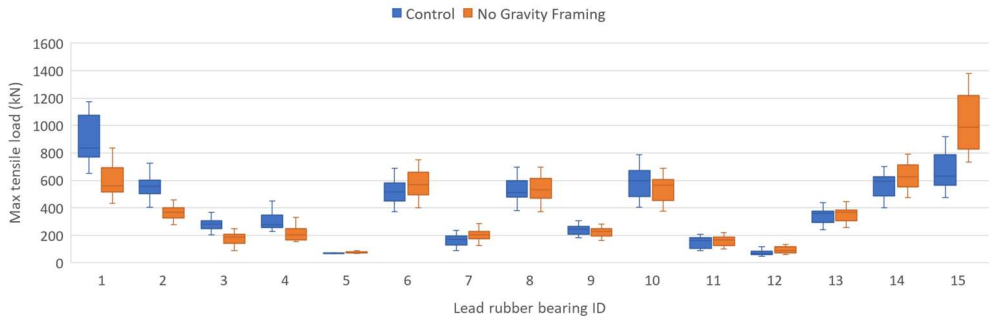

(a)

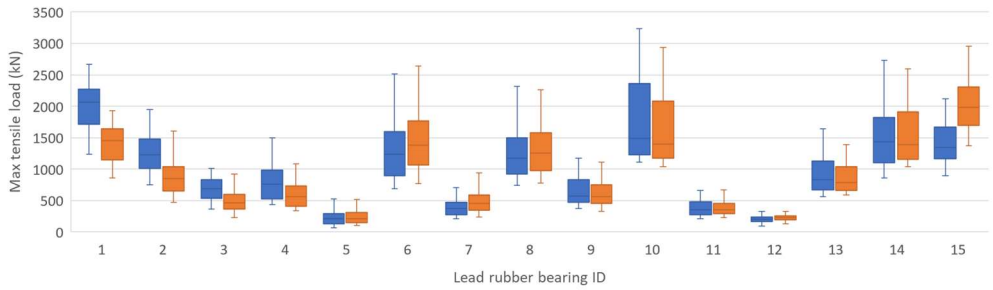

(b)

Figure 51. No gravity framing - Maximum tensile axial loads of the lead rubber bearings for the intensity levels of (a) 1 in 475 years and (b) 1 in 2475 years

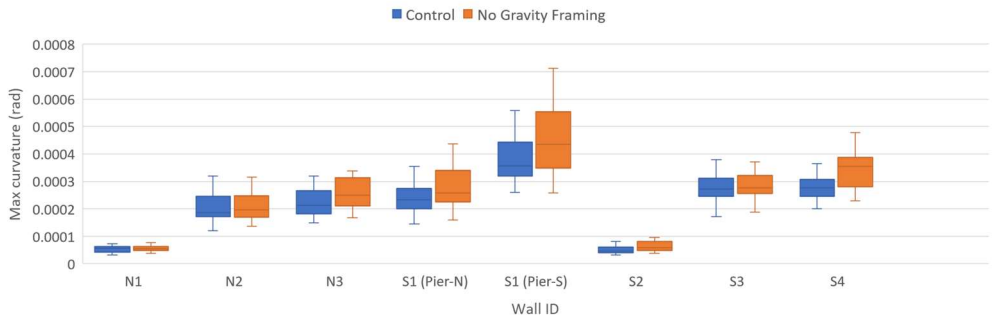

(a)

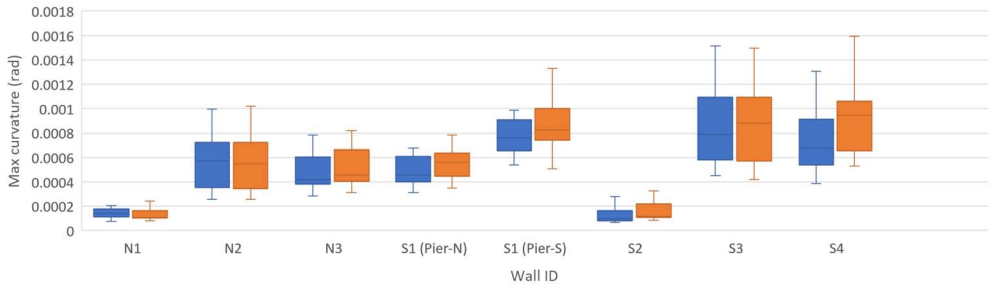

(b)

Figure 52. No gravity framing - Maximum curvature at the base of the walls for the intensity levels of (a) 1 in 475 years and (b) 1 in 2475 years

The removal of steel gravity framing from the structural model means that there is no lateral resistance contributed by the steel gravity framing. This corresponds to the perfectly pinned condition of the beam-column joints. From Figure 43 to Figure 52, it can be seen that certain EDPs are more affected than others. Notably, the IDR was the most affected. This could possibly be due to the change in torsional response of the superstructure. Since the gravity framing is not symmetrical about the centre of mass, it may have introduced some additional torsional eccentricity.

The drifts at the top storey in the Z-direction increased rather significantly without gravity framing. This is because the lightweight steel roof utilised a lot of steel gravity columns at this level that contributed to the lateral resisting system. However, the difference in global structural responses with or without the perfectly pinned assumption were not significant overall. This is also evident in the fact that the modal periods of the model without the gravity framing are very similar to the control model. Thus, the assumption of non-perfectly pinned beam-column joints is conservative, and it can also be concluded that the parameter α in Equation 3 is likely not significant.

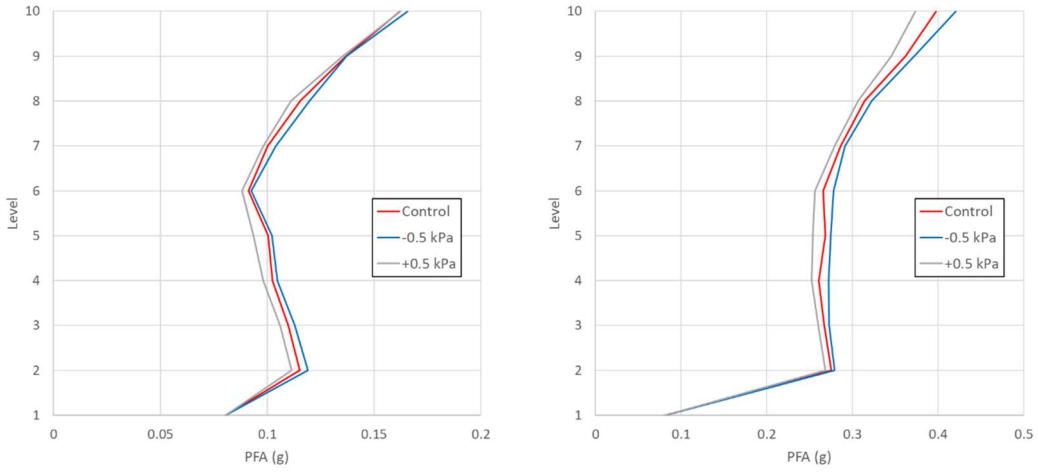

Figure 53. Slab weights - Peak floor accelerations (median) for the intensity levels of (a) 1 in 475 years and (b) 1 in 2475 years

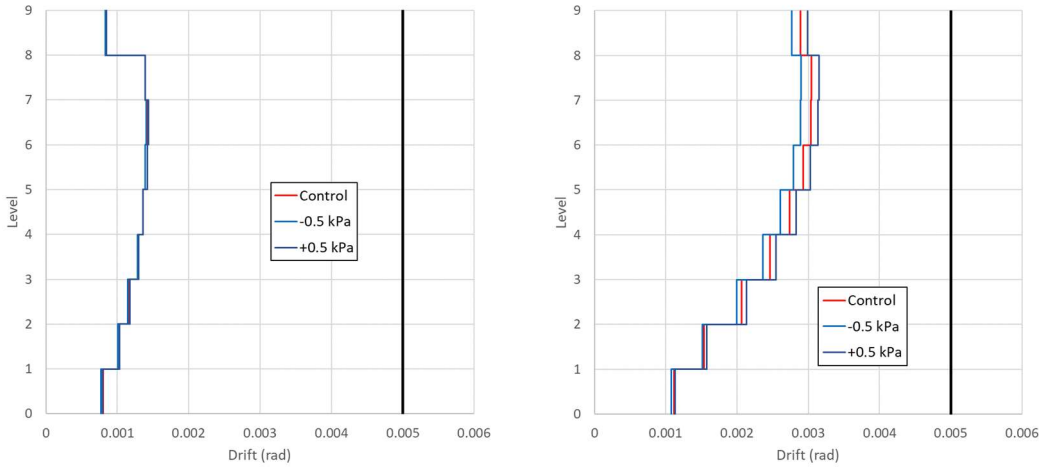

Figure 54. Slab weights - Inter-storey drift ratio (median) for the intensity level of 1 in 475 years in the (a) X-direction and (b) Z-direction

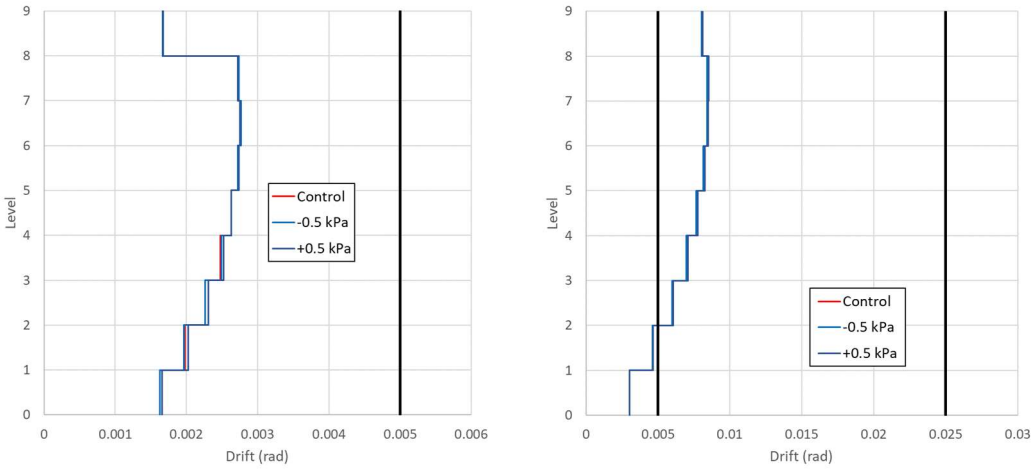

(a) (b)

Figure 55. Slab weights - Inter-storey drift ratio (median) for the intensity level of 1 in 2475 years in the (a) X-direction and (b) Z-direction

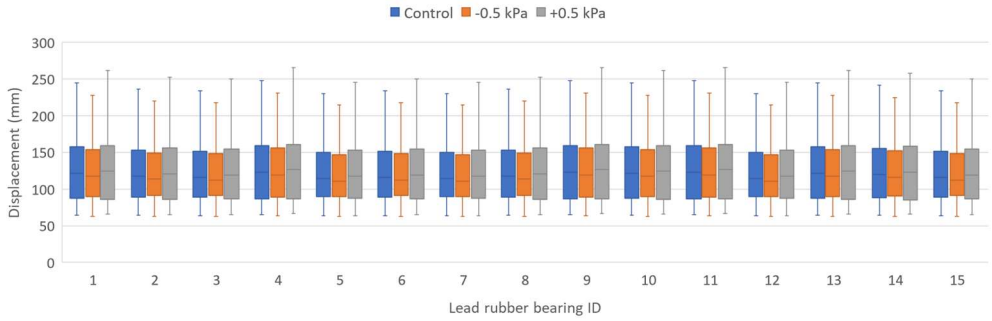

(a)

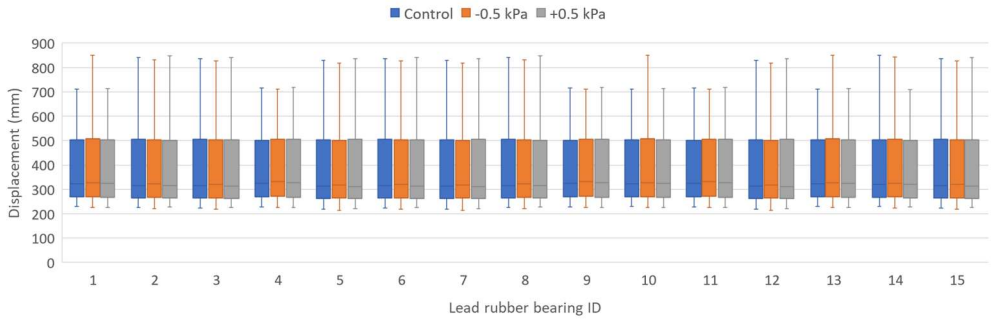

(b)

Figure 56. Slab weights - Maximum displacements of the lead rubber bearing in the X-direction for the intensity levels of (a) 1 in 475 years and (b) 1 in 2475 years

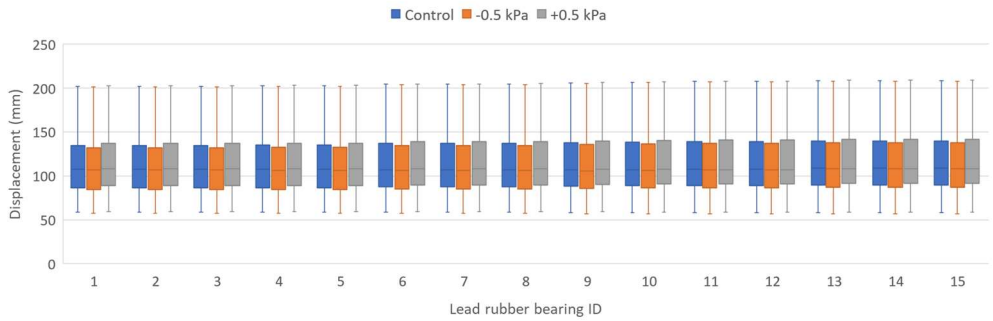

(a)

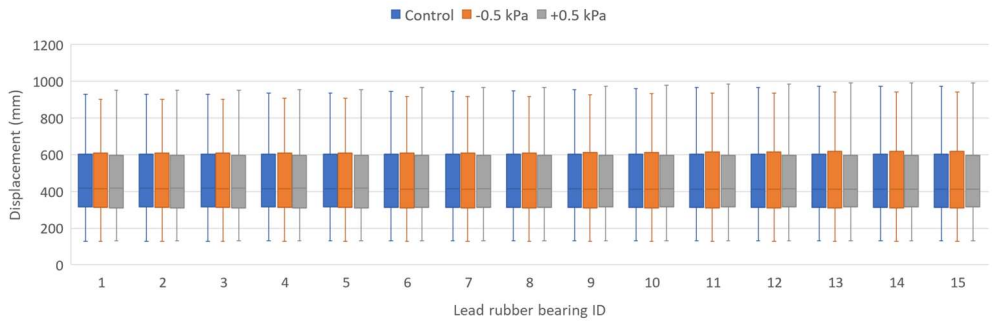

(b)

Figure 57. Slab weights - Maximum displacements of the lead rubber bearing in the Z-direction for the intensity levels of (a) 1 in 475 years and (b) 1 in 2475 years

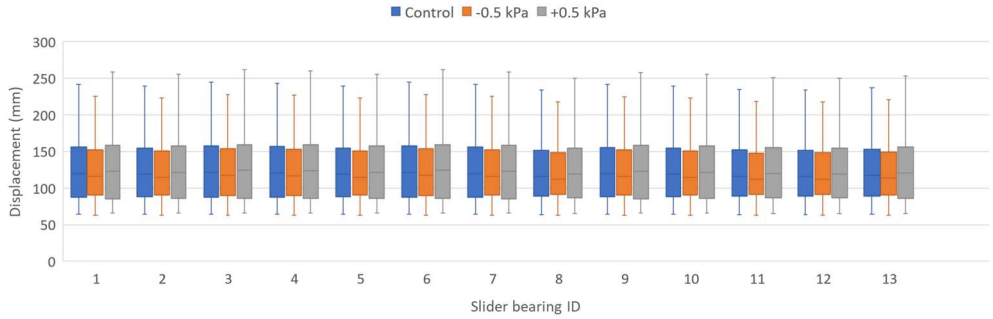

(a)

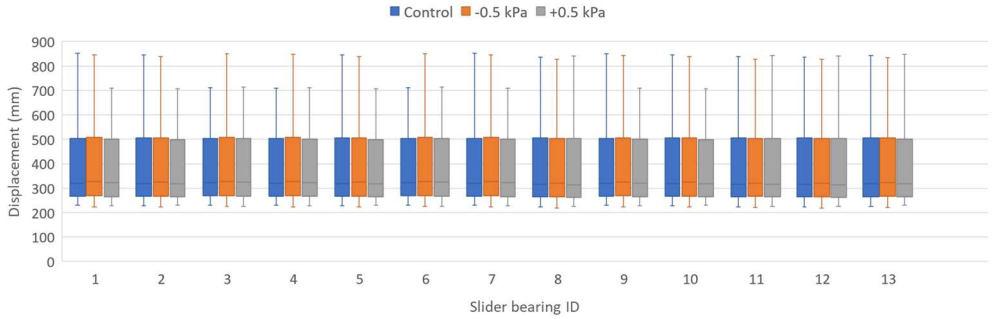

(b)

Figure 58. Slab weights - Maximum displacements of the slider bearing in the X-direction for the intensity levels of (a) 1 in 475 years and (b) 1 in 2475 years

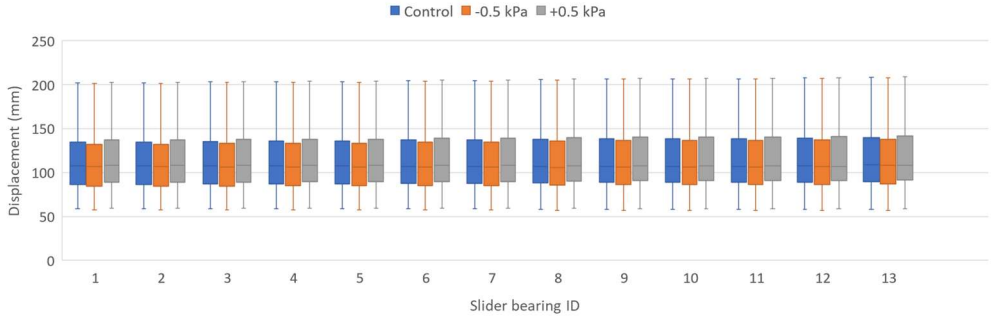

(a)

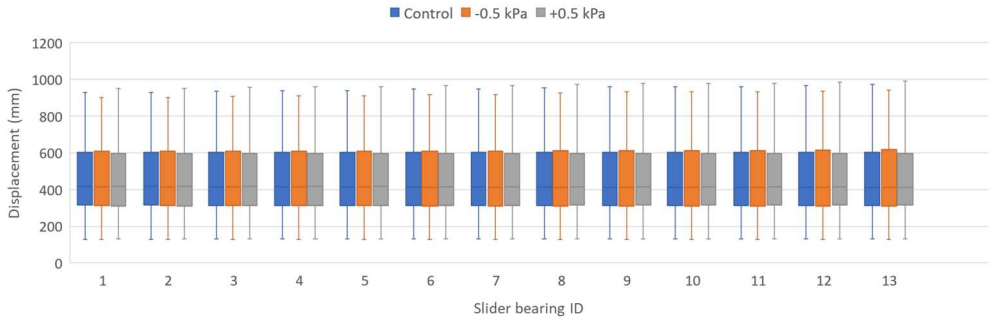

(b)

Figure 59. Slab weights - Maximum displacements of the slider bearing in the Z-direction for the intensity levels of (a) 1 in 475 years and (b) 1 in 2475 years

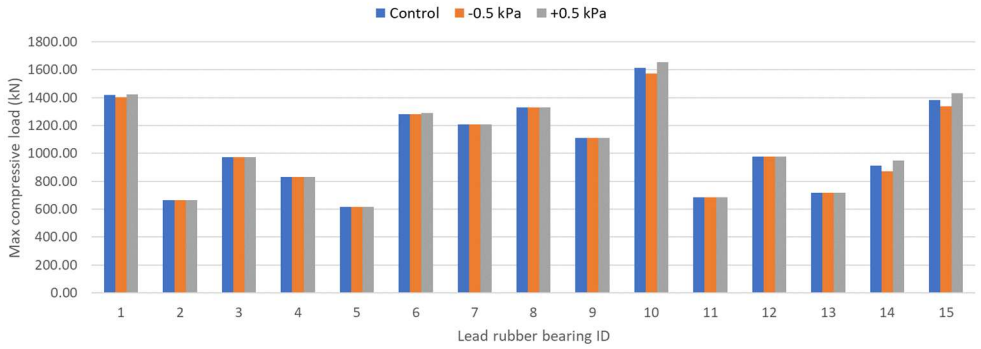

(a)

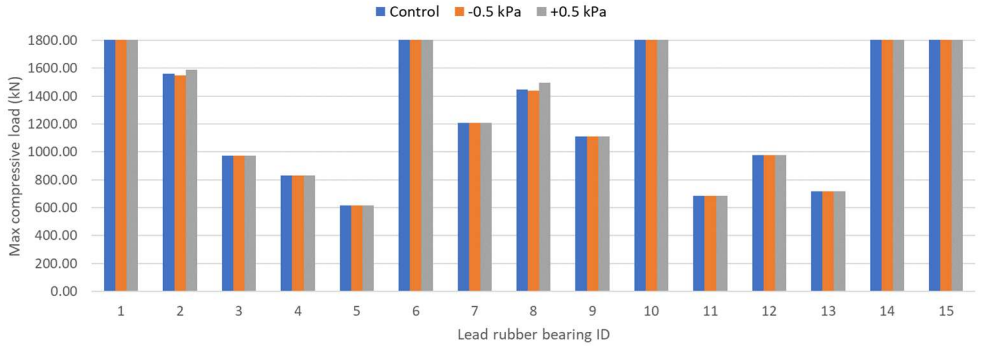

(b)

Figure 60. Slab weights - Maximum compressive axial loads of the lead rubber bearings for the intensity levels of (a) 1 in 475 years and (b) 1 in 2475 years

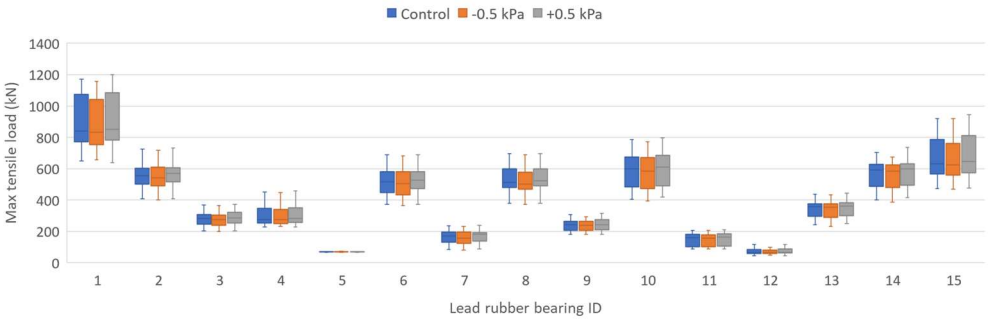

(a)

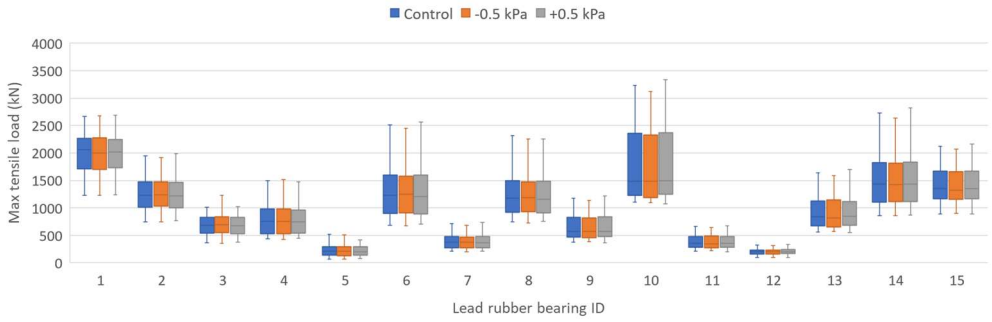

(b)

Figure 61. Slab weights - Maximum tensile axial loads of the lead rubber bearings for the intensity levels of (a) 1 in 475 years and (b) 1 in 2475 years

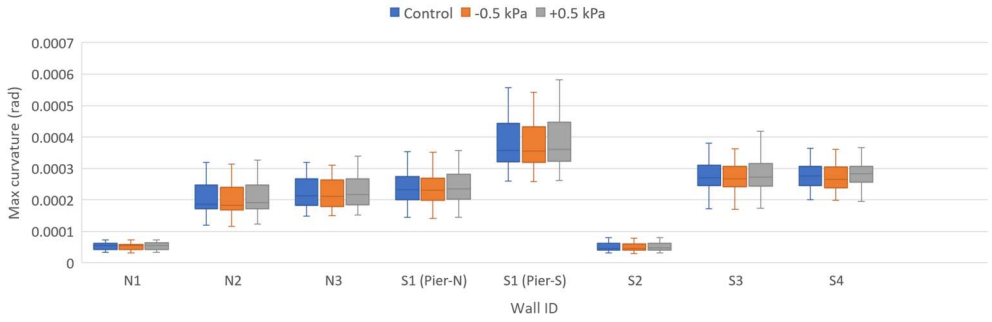

(a)

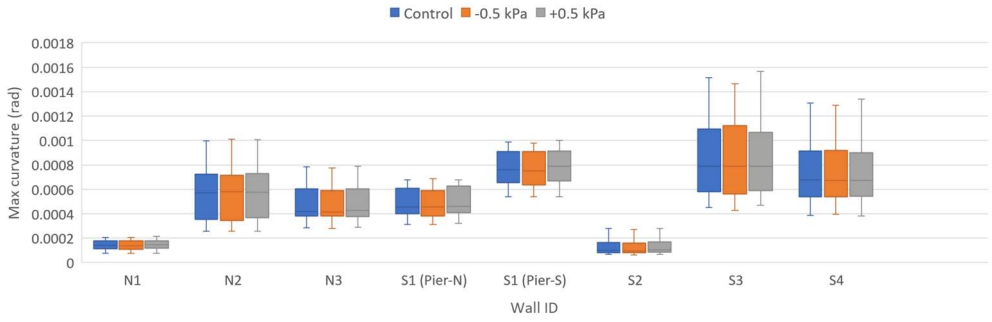

(b)

Figure 62. Slab weights - Maximum curvature at the base of the walls for the intensity levels of (a) 1 in 475 years and (b) 1 in 2475 years

Based on Figure 53 to Figure 62, varying the slab weights had almost no observable impact on the structural responses of interest. Thus, the control model will use the currently assumed service dead load on the slab.

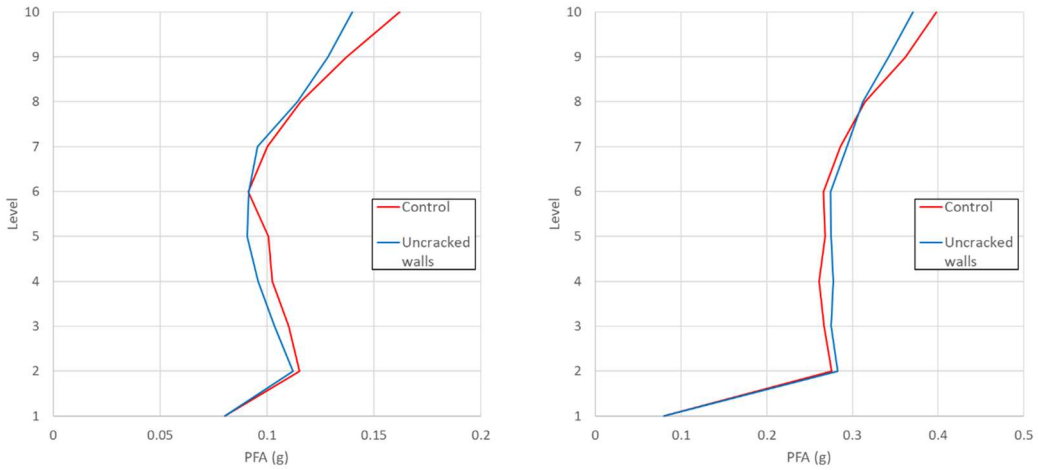

Figure 63. Uncracked walls - Peak floor accelerations (median) for the intensity levels of (a) 1 in 475 years and (b) 1 in 2475 years

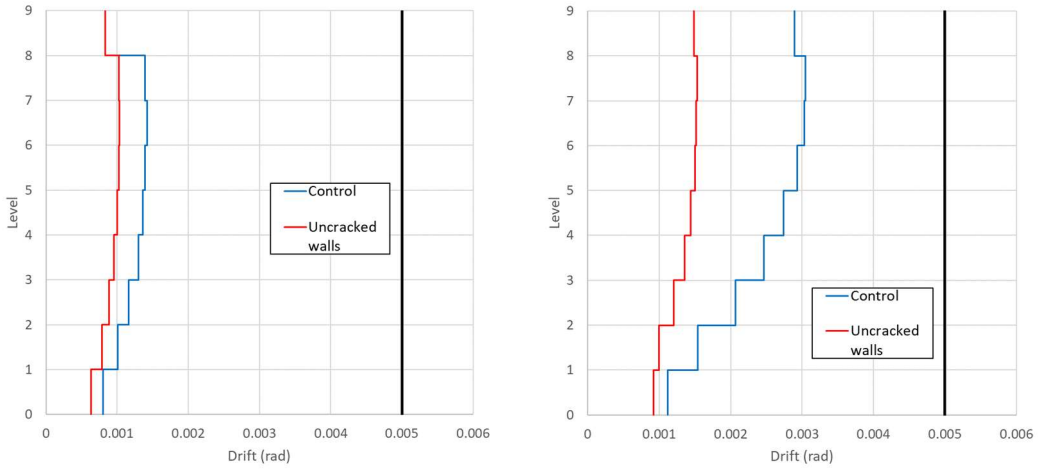

Figure 64. Uncracked walls - Inter-storey drift ratio (median) for the intensity level of 1 in 475 years in the (a) X-direction and (b) Z-direction

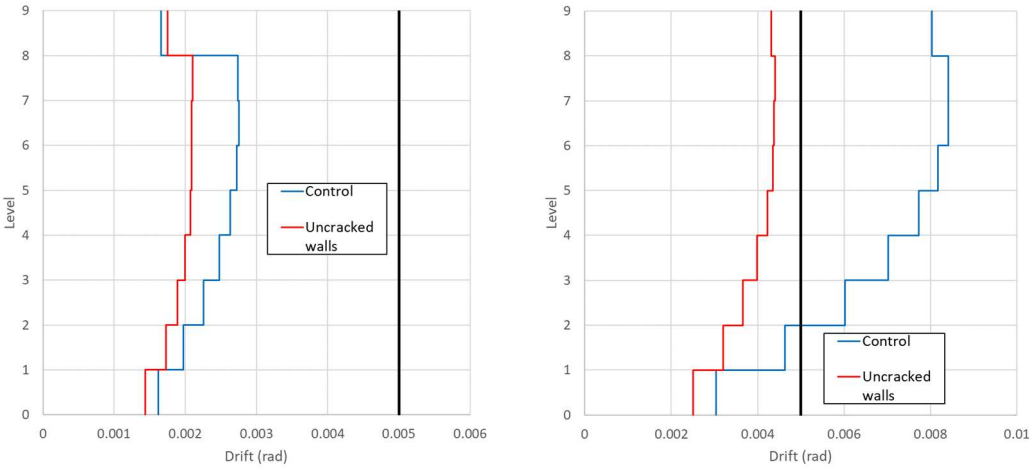

(a) (b)

Figure 65. Uncracked walls - Inter-storey drift ratio (median) for the intensity level of 1 in 2475 years in the (a) X-direction and (b) Z-direction

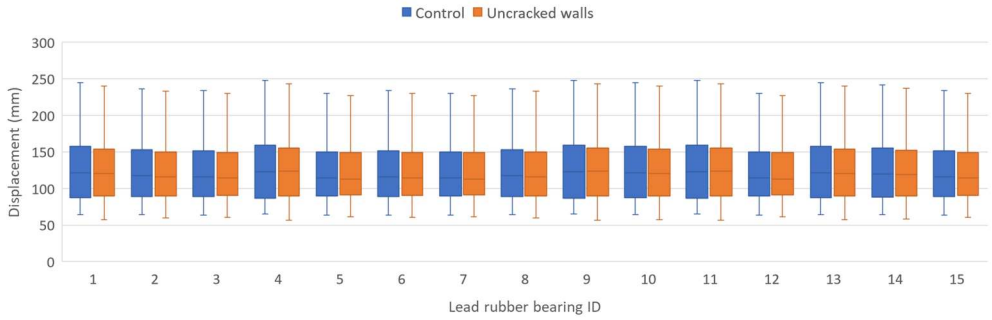

(a)

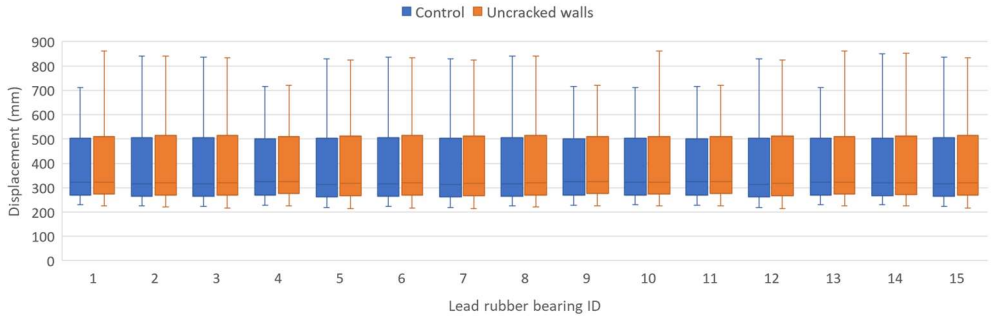

(b)

Figure 66. Uncracked walls - Maximum displacements of the lead rubber bearing in the X-direction for the intensity levels of (a) 1 in 475 years and (b) 1 in 2475 years

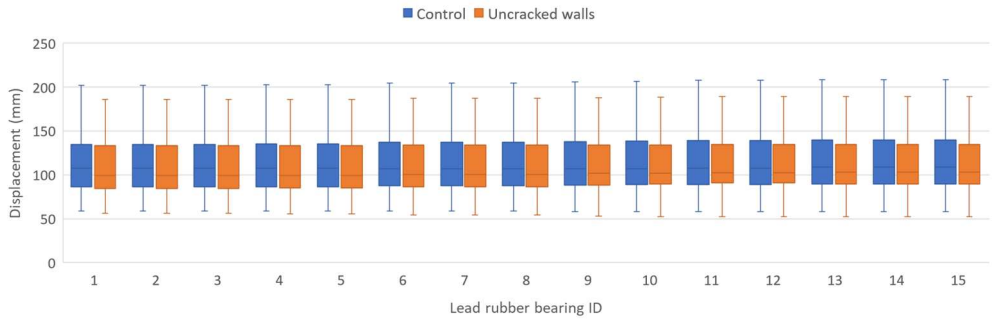

(a)

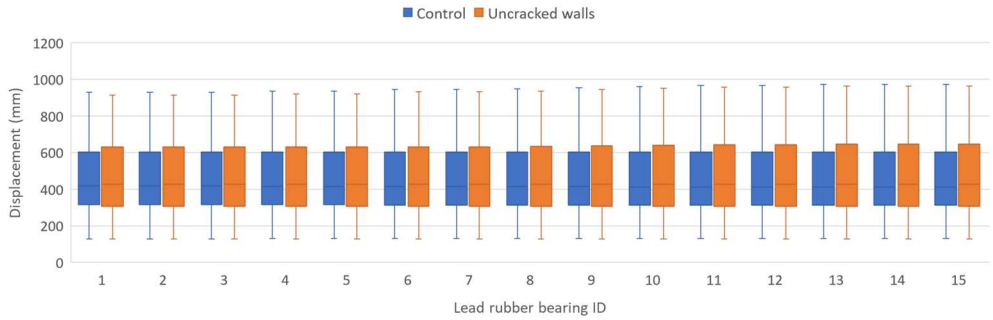

(b)

Figure 67. Uncracked walls - Maximum displacements of the lead rubber bearing in the Z-direction for the intensity levels of (a) 1 in 475 years and (b) 1 in 2475 years

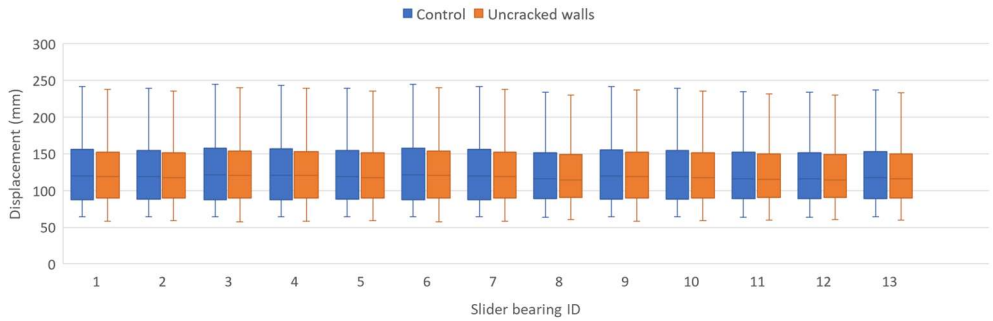

(a)

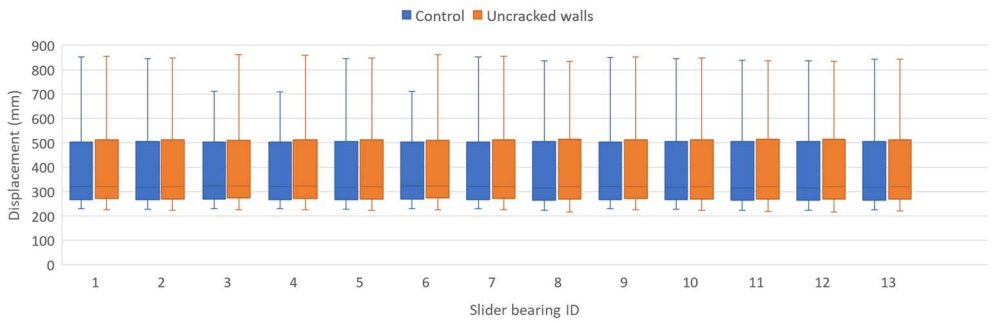

(b)

Figure 68. Uncracked walls - Maximum displacements of the slider bearing in the X-direction for the intensity levels of (a) 1 in 475 years and (b) 1 in 2475 years

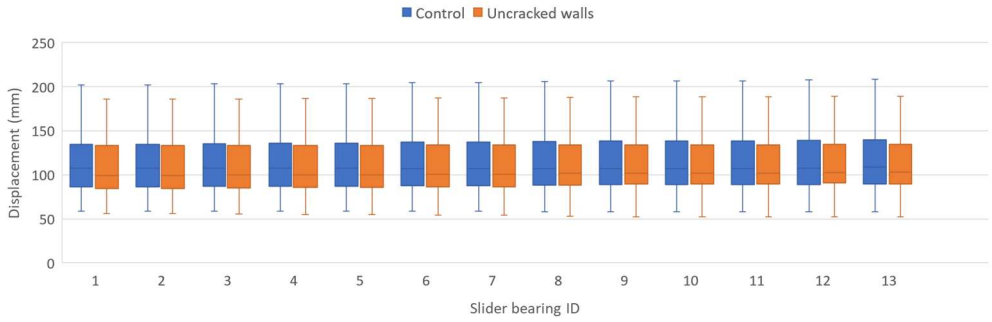

(a)

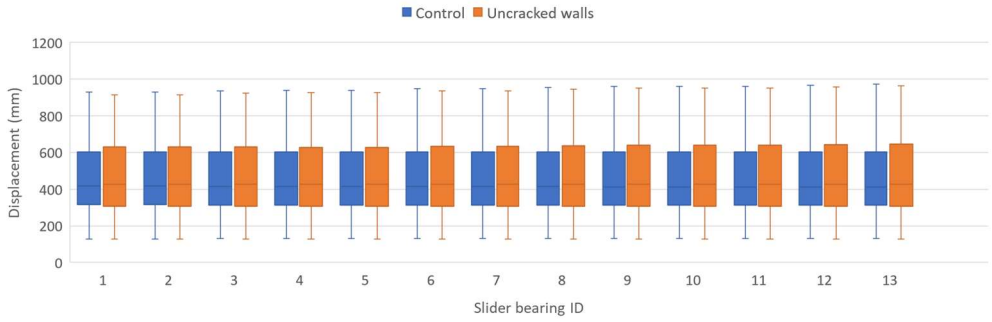

(b)

Figure 69. Uncracked walls - Maximum displacements of the slider bearing in the Z-direction for the intensity levels of (a) 1 in 475 years and (b) 1 in 2475 years

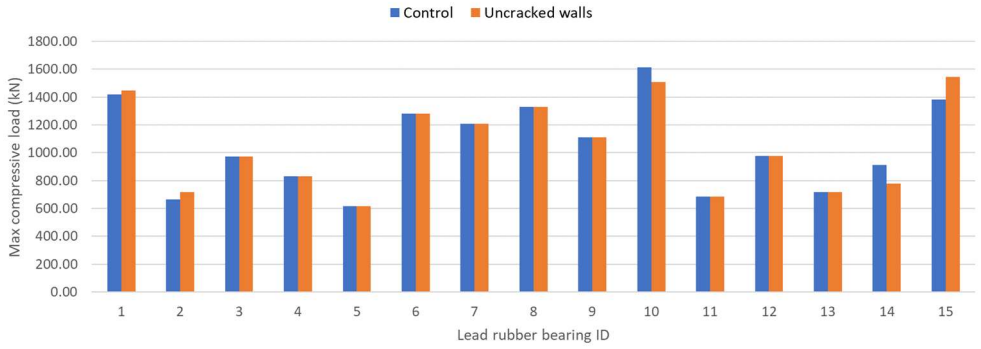

(a)

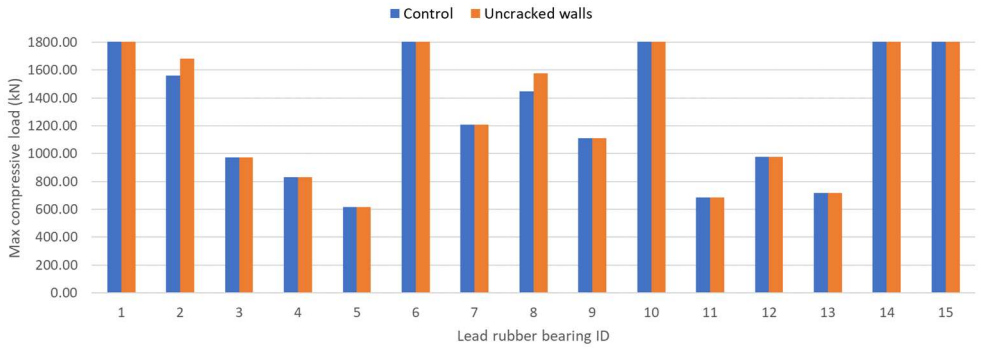

(b)

Figure 70. Uncracked walls - Maximum compressive axial loads of the lead rubber bearings for the intensity levels of (a) 1 in 475 years and (b) 1 in 2475 years

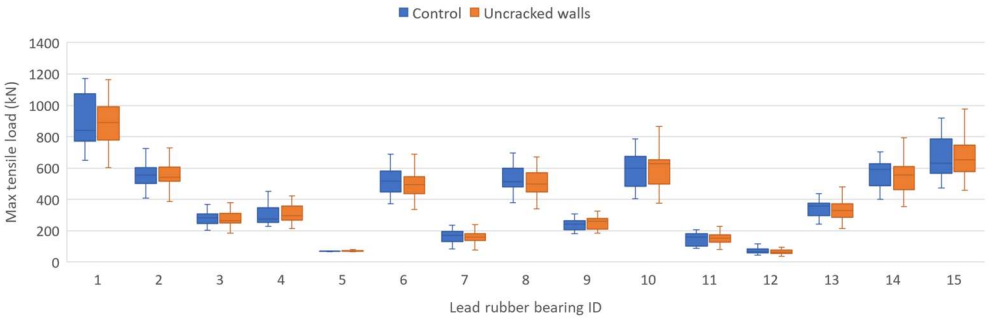

(a)

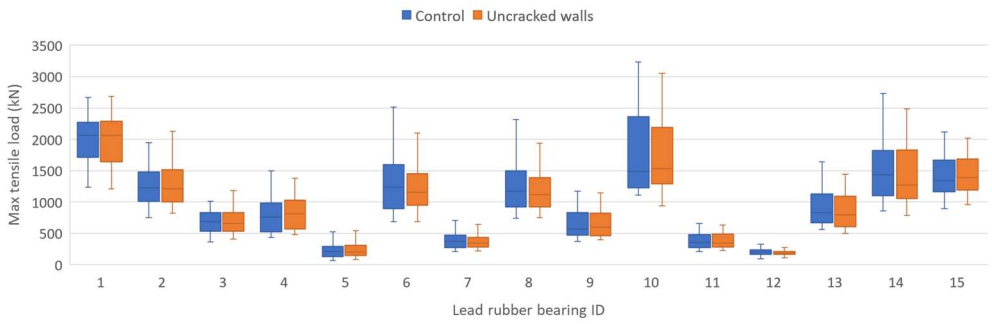

(b)

Figure 71. Uncracked walls - Maximum tensile axial loads of the lead rubber bearings for the intensity levels of (a) 1 in 475 years and (b) 1 in 2475 years

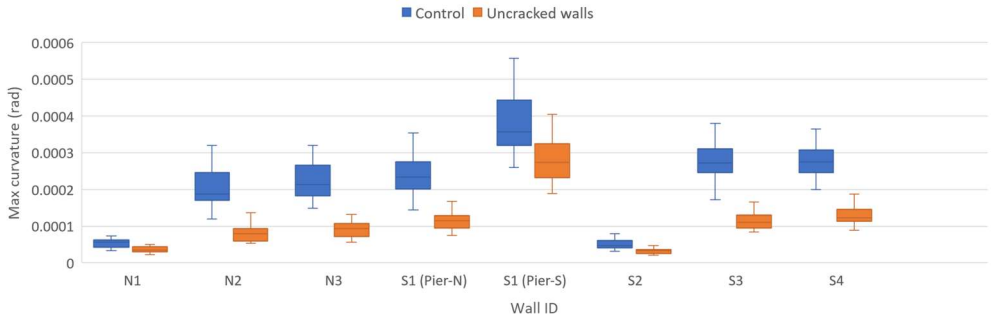

(a)

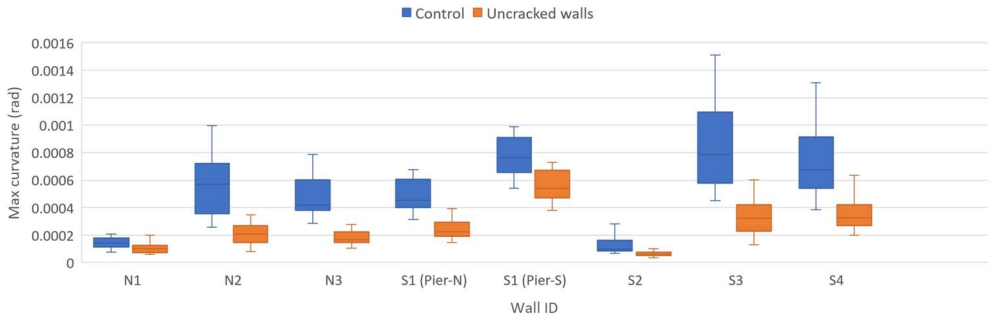

(b)

Figure 72. Uncracked walls - Maximum curvature at the base of the walls for the intensity levels of (a) 1 in 475 years and (b) 1 in 2475 years

Figure 63 to Figure 72 showed significant differences between the IDR of the control model and the model with uncracked wall stiffnesses. This may cause significant difference in the outputs of the loss analysis because IDR is an important EDP that has a potentially large contribution to the total direct loss. For this reason, it was decided that the cracked stiffness properties of the walls should be adopted.

This is justified for two reasons. Firstly, it is a conservative assumption, meaning that the computed direct loss would always be greater due to the increased IDR values. The second reason is that once a structural wall is cracked, it is not able to reverse its properties. Consequently, the less frequent an earthquake is, the greater the chance that the walls have been previously cracked after being subjected to smaller to moderate earthquakes preceding it.

3.4. Damage and Loss Analysis

3.4.1. Time-Based Loss Analysis

Time-based loss analysis was performed by using the Seismic Loss Analysis Tools or SLAT (Bradley, 2009) software and considering the structural analysis results from the twenty ground motion records of each intensity level, as described in Section 1.1.1. For this research, the downtime and deaths are not considered, and only the direct losses are computed with SLAT. Moreover, since this research is focused on comparing the direct losses of a base isolated building against traditionally constructed buildings in New Zealand, the collapse assessment will not be considered. In other words, the analysis will be restricted to damages to structural and non-structural components that are repairable or replaceable. This is deemed reasonable also considering that the likelihood of collapse would be very low for the building in question.

The engineering demand parameters (EDPs) from time-based structural analysis in Section 4.3.2 were first input into the SLAT software. A non-directional conversion factor of 1.2 is assumed as suggested by FEMA P-58. For example, the peak floor acceleration at each storey in the two horizontal directions was

obtained from the structural analysis results. The maximum of the two directions are multiplied by 1.2 to obtain the non-directional peak floor acceleration at each storey. In contrast, the inter-storey drift ratio in the two orthogonal horizontal directions are used. This is because drift sensitive components spanned along the major axes and are assumed to not be affected by out-of-plane deformations.

In addition to the engineering demand parameters (EDPs), time-based analysis also requires the hazard curve to be defined. The hazard curve models the relationship between the rate of exceedance (λ) and intensity measure (IM). In this case, the IM is set to the spectral acceleration at a conditioning period of 2.0 second, deemed to be close enough to the fundamental period of the case study building. The suite of ground motions inputted into SLAT were selected by Yeow et al. (2018) using the GCIM method proposed by Bradley (2010) based on the PSHA for the Central Business District in Christchurch, as mentioned earlier in Section 4.1.2.

SLAT uses direct numerical integration to solve the triple integrals of Equation 6. This contrasted to the PACT (Performance Assessment Calculation Tool) software, which utilises simulation (e.g. Monte Carlo) to evaluate the integrals (FEMA, 2012). An advantage of using numerical integration over simulation is its effective elimination of the uncertainty inherently associated with performing simulations with results depending on the random numbers used.

The Magnitude-oriented Adaptive Quadrature (MAQ) algorithm (Bradley et al., 2009) was used by SLAT. Its advantages over other numerical integration methods are accuracy, computational efficiency, as well as requiring no integration computation specifics (such as the step size and region of integration), other than the error tolerance and the maximum number of function evaluations.

The goal of this section is to compute the expected annual loss (EAL) of the base isolated building for the seismic hazard expected at Christchurch CBD. To

perform time-based loss analysis, SLAT was used to compute the triple integrals of the form shown below.

$$\lambda(DV) = \iiint_{0}^{\infty} G(DV|DM)\, dG(DM|EDP)\, dG(EDP|IM)\, d\lambda(IM) \quad \text{(Eq. 6)}$$

Where IM is intensity measure (e.g. spectral acceleration), EDP is engineering demand parameter (e.g. IDR, PFA), DM is damage measure (e.g. wall cracking), DV is decision variable (e.g. repair cost), and $\lambda(IM)$ is the annual rate of exceedance as a function of IM (i.e. the hazard curve). The terms relating to this equation will be expanded and explained in the next few sections.

3.4.2. Fragility Functions

A fragility function is a lognormal cumulative distributive function that returns the probability of exceeding a damage state (e.g., cracking of partition walls) for a given EDP (e.g., inter-storey drift). A component may also have multiple damage states with different probabilities of attaining for a given EDP. A fragility function can be derived experimentally or analytically if equations describing its failure modes are available.

The fragility functions from the FEMA P-58-3 database (FEMA, 2012) were generally adopted where available to represent the fragility of the non-structural components in the building. Table 9 summarises the fragility function for each structural and non-structural components considered in the case study building and their corresponding identifiers in the FEMA P-58-3 database.

Table 9. Fragility functions from FEMA P-58-3 (FEMA, 2012)

Component	Fragility Functions		
	DS1	**DS2**	**DS3**
HVAC - galvanised steel ducts (A < 6 ft^2)	D3041.011c, DS1	D3041.011c, DS2	
HVAC - compressor	D3032.013b, DS2		
HVAC - in-line fan	D3041.001c, DS1	D3041.001c, DS2	

HVAC - FCU (<5000 CFM)	D3052.013b, DS1	D3052.013b, DS2	
Water pipe system	D2021.012b, DS1	D2021.012a, DS1	D2021.012a, DS2
Sanitary pipe system	D2031.013b, DS1		
Fire sprinklers - pipes	D4011.023a, DS1	D4011.023a, DS2	
Fire sprinklers - drops	D4011.033a, DS1		
Traction elevators	D1014.011, DS1		
Stairs	C2011.001b, DS1	C2011.001b, DS2	C2011.001b, DS3

For components specific to New Zealand construction practice or unique to this building, representative fragility and loss functions from previous studies were adopted. These fragility functions will be outlined in the following.

Table 10 summarises the damage states of each component and their corresponding median and dispersion (in bracket) EDPs. Note that a fragility function is described by two parameters; the lognormal mean and standard deviation. The lognormal mean is the mean of a normal distribution in the lognormal scale. It corresponds to the median value of EDP resulting in a damage state. Meanwhile, the standard deviation quantifies the dispersion of the EDP values that resulted in a damage state.

Table 10. Summary of the median and dispersion values obtained from the literature

Component	DS1	
	Median	**Dispersion**
Ceiling (A < 20 m^2) Grid size: 0.9 x 0.6	0.452g [1]	0.37
Ceiling (A < 20 m^2) Grid size: 1.2 x 0.6	0.773g [1]	0.37
Ceiling (A < 23.2 m^2) - bracing	1.17g [2]	0.3
Ceiling (23.2 m^2 < A < 93 m^2) - bracing	1.15g [2]	0.3
Wall S2 (curvature)	0.000652	0.3
Wall S3 (curvature)	0.00092	0.3
Wall S4 (curvature)	0.00122	0.3
LRB (displacement)	0.655	0.3
LRB (compressive)	3087	0.3

[1] These values were obtained from Yeow, Sullivan, et al. (2018)
[2] These values were obtained from Soroushian (2016)

LRB (tensile)	4530	0.3
SB (displacement)	0.45	0

There are two types of suspended ceilings used in the building. The first being the fixed-floating ceiling primarily used in rooms with small ceiling area. For suspended ceilings of this type, the two sides are fixed to the adjacent walls, while the other two sides are floating by allowing gaps between the end of each ceiling batten and the wall. The reason for the gaps is to prevent the movements of adjacent walls during earthquake to impart compressive force on the suspended ceiling grid.

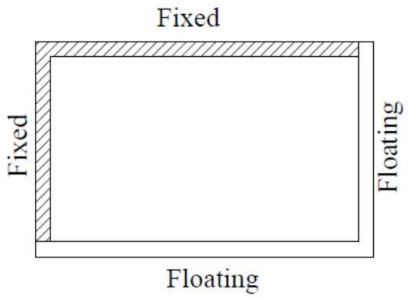

Figure 73. Plan view of the fixed-floating type (Dhakal, MacRae, et al., 2016)

A typical fixed-floating suspended ceiling for a rectangular room, as shown in Figure 73. Plan view of the fixed-floating type (Dhakal, MacRae, et al., 2016), is considered to fail when its weakest component reached its strength capacity. In the study by Dhakal et al. (2016), the governing components in an order from the weakest to strongest were found to be: single rivet connections (3.2 mm), cross tee connections under compression, main tee splices under tension, cross tee connections under tension and double rivet connections (3.2 mm). The fragility function of the suspended ceiling system is thus taken as equal the fragility function of the weakest component. The reasoning behind this is that the brittle failure of a single ceiling component would cause cascading failure

of other elements due to redistribution of load paths, which will consequently require the entire ceiling to be replaced.

Because of this, the fragility function of a fixed-floating suspended ceiling is a function of the ceiling tile weight, total ceiling area, and the grid spacings. The fragility functions of suspended ceilings suited for New Zealand condition and adopted in this study is summarised below. Note that suspended ceilings are sensitive to peak floor accelerations.

Table 11. Adopted fragility function for fixed-floating suspended ceilings (Yeow, Sullivan, et al., 2018)

Ceiling size	0.6 m by 0.6 m grid		1.2 m by 0.6 m grid	
	Median	Dispersion	Median	Dispersion
$A < 20$ m^2	12.4 g.kg/m^2	0.37	9.28 g.kg/m^2	0.37
20 m^2 $< A <$ 30 m^2	9.45 g.kg/m^2		7.08 g.kg/m^2	
30 m^2 $< A <$ 40 m^2	7.95 g.kg/m^2		6.02 g.kg/m^2	
40 m^2 $< A$	6.18 g.kg/m^2		4.63 g.kg/m^2	

When a given ceiling area is too large, the connections between the suspended ceiling and walls become insufficient to resist the force generated by its seismic weight. In such cases, suspended ceilings that are fully floating on all sides with back bracing are used. The lateral resistance is provided by diagonal splay wires connecting the slab above and the batten in a forty-five degrees angle along with a vertical strut. The purpose of a vertical strut is to provide resistance against the tensile force generated by the splay wires.

Figure 74. Typical back bracing consisting of four splay wires and a vertical strut

In contrast to the fixed-floating type, ceilings with back bracing have higher capacity because the splay wires are typically stronger than the grid connections (Ryu & Reinhorn, 2019). The fragility function of suspended ceilings with back bracing used in the analysis is based on the study by Soroushian (2016). The adopted fragility function was derived by considering a 6.8 kg/m^2 ceiling mass, however the tile mass used in the case study building is 12 kg/m^2 with the grids assumed to be weightless. To account for this difference, the median PFA is adjusted by multiplying it with the ratio of masses.

According to Yeow et al. (2018), the use of linear regression to fit the experimental relationship between median PFA of failure versus ceiling area is unconservative for a larger ceiling area because it means higher capacity than the actual for the larger ceiling area, whereas the relationship should be negative hyperbolic because the ceiling components only have fixed capacity based on the principle of capacity design (Dhakal, MacRae, et al., 2016). However, the use of linear regression should actually be conservative when the ceiling area is small, as found in the apartment building, because it will return a lower capacity than actual.

Most of the partition walls in the apartment building are full-height, timber-framed plasterboard partitions. For the loss analysis, it was assumed that doors do not act as partitions and were excluded in the overall length of the partition wall. Since there are some differences between the US and New Zealand practice, the fragility functions suited for New Zealand condition provided by Yeow et al. (2018) were adopted. Although the fragility functions were derived for steel-framed plasterboard partitions, it is assumed that their behaviours would be similar enough.

There are four damage states of interest for the partition walls (Mosqueda, 2016). Table 12 summarises the different damage states and their associated medians and dispersions in terms of inter-storey drift ratio. It is noteworthy that according to Mosqueda (2016), the damage state 0 may not necessarily require

repairs for functionality. However, because of the insurance industry in New Zealand, people are likely to conduct repairs for the DS0 damage state as they have been for single dwelling houses. As such, the fragility function and loss function will be defined for damage state 0.

Table 12. Damage states of partition walls (Mosqueda, 2016; Yeow, Sullivan, et al., 2018)

Damage state	**Description of damage**	**IDR**
DS0	Minor cosmetic damage, such as hairline cracking of wall board or joints, visible screw pop out, light warping or cracking of tape. Damage could be taken for normal wear and tear.	0.0029 (0.5)
DS1	Significant screw pop-out, cracking of wall board, cracking of tape, slight crushing of wall panel at corners.	0.0056 (0.43)
DS2	Moderate cracking or crushing of gypsum wall boards (typically in corners). Moderate corner gap openings, Bending of boundary studs.	0.0105 (0.31)
DS3	Buckling of studs and tearing of tracks. Tearing or bending of top track, tearing at corners with transverse walls, large gap openings, and walls displaced.	0.0234 (0.19)

At the time of this research, no studies were found on the fragility and loss functions for structural RC walls in the elastic range and for base isolators. For the interest of this research, the fragility and loss functions for these components were constructed based on expert opinions. The main assumption is that these components are not expected to contribute significantly to the estimated EAL.

For the lead rubber bearings, a prototype testing report from Robinson Seismic (2016) indicated the units suffered no apparent damage or degradation of their hysteretic properties when pushed significantly up to 415 mm under the design axial loads. In order to derive the fragility function of the LRB under shear displacement, it was assumed that there is a 5% chance of damage requiring replacement when the shear displacement reached 425 mm. Thus, this value is taken to equal the 5th percentile value in the fragility function. By assuming a dispersion value of 0.3, the lognormal mean was computed to equal 655 mm.

The compressive capacity of lead rubber bearing is coupled with its shear deformation. Compressive failure is associated with the buckling of lead core and shear displacement may reduce the critical buckling load due a decrease in the overlapping area between the uppermost and lowermost layers. The reduced buckling load of an LRB under shear deformation is given by (Yang & Zhang, 2018):

$$P_{cr} = P_{cr0}\frac{A_r}{A_b} \quad \text{(Eq. 7)}$$

Where P_{cr0} is the critical buckling load in its undeformed state, A_b is the net area of bearing, and A_r is the reduced area corresponding to the shaded area in Figure 75.

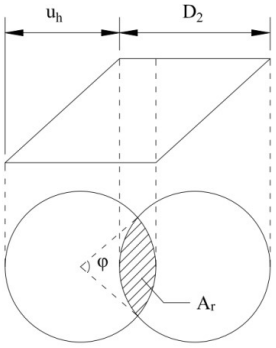

Figure 75. Overlapping area between top and bottom layers (Yang & Zhang, 2018)

While compressive failures are possible, LRBs should not lose their stability when the overlapping area is equal to zero. A lower bound of the critical buckling load can be taken as 20% of the undeformed critical buckling load (Warn & Ryan, 2012). Since the lead rubber bearings at the foundation of the apartment building are all of the same type, the lower bound critical buckling load was computed to equal 1,884 kN.

As there are no available fragility functions to model the compressive failure of lead rubber bearings, one was derived by setting the 5^{th} percentile value of the fragility function to equal 1,884 kN. In other words, there is a 5% probability that the LRB will be damaged and require replacement when its maximum compressive load reaches 1,884 kN. By assuming a dispersion of 0.3, the lognormal mean was computed to equal 3,087 kN.

The tensile capacity of lead rubber bearings, similar to the compressive capacity, is coupled with its shear deformation. When the shear strain increases, the tensile yield stress will simultaneously decrease. Moreover, the inner plates can generate rotation due to the increase of bending deformation in the rubber sheets that results in uneven strain distribution in the rubber layers, which would in effect increase the slope of the stress-deformation curves (Takayama et al., 2004).

Takayama et al. (2004) found through testing that failure was observed only when the shear strain was 300% and the breaking tensile strain was 48%. In another study (Iwabe et al., 2000), the LRB was found to not rupture even if it was subjected to 100% in tensile strain at an offset shear strain of 200%. In addition, the prototype testing subjected the LRB to 0.8% tensile strain without observing damage. Based on the results of the time history analyses at the highest intensity level obtained in Section 4.3.1, the maximum recorded tensile strain is 12% and the shear strain is 400%. Note that these values are observed from different ground motions.

As there are no available fragility functions on the tensile failure of lead rubber bearings, one was derived by setting the 95th percentile value of the fragility function to a value corresponding to 20% of tensile strain. The lognormal mean was computed to be 4,530 kN by assuming a dispersion of 0.3.

The slider bearings have a maximum displacement of 450 mm. Once the displacement exceeded this limit, the slider bearings will lose their vertical support capacity requiring it to be replaced. Thus, the damage state is set to a lognormal mean of 0.45 m with a dispersion of zero.

The fragility function corresponding to damage requiring repair of each RC wall is derived by setting the analytical yield curvature as the lognormal mean and assuming a dispersion of 0.3. Priestley (2003) indicated that the yield curvature of cantilevered rectangular walls can be approximated as a function of the geometric properties:

$$\phi_y = 2.00\frac{\epsilon_y}{l_w} \quad \text{(Eq. 8)}$$

Here, ϵ_y is the yield strain of the longitudinal reinforcement bar at the extreme fibre and l_w is the wall length.

The façades of the apartment building are unitised curtain walls consisting of the glazing unit and neolith slab unit. The neolith slab unit is made up of aluminium brackets supporting a 10 mm thick neolith slab. Both the glazing and neolith slab units are hung like curtains by outriggers cast into the concrete slab.

Each unit is supported by three outriggers, two at the upper left and right, and one at the bottom centre. The bottom connection is fully pinned to the outrigger; hence, it is not allowed any movement and is designed just to hold the unit in place to prevent out of plane deformation. The two upper connections are allowed to slide horizontally. These are called rear splices and they are fixed to the outrigger connecting to the main structure. The sliding capacity at each side is 23 mm, summing to a total of 46 mm of sliding distance.

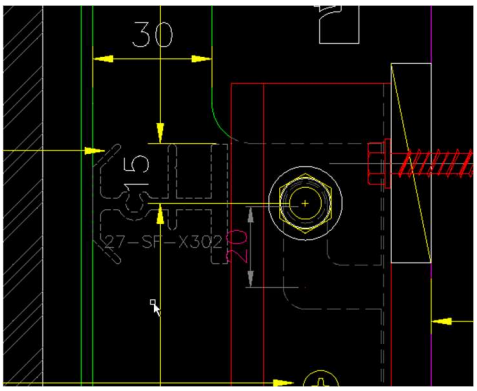

Figure 76. Detail of the rear splices located at the upper section of each unit

In addition to the curtain walls, rainscreen neolith panels were attached on the structural walls located at the southern side of the building. Since these neolith panels are directly glued to the structural walls, thermal expansion movements of 20 mm are allowed at each side of the panel.

Building façades are typically drift sensitive components. Excessive drift demand to a curtain wall can cause tearing of the air-seals and, in some cases, disengagement of the bottom panel. However, since both the curtain walls and rainscreen neolith panels were given large displacement allowances, they are assumed to not be damageable when subjected to the range of ground motions used in this study. Thus, the façades will not be considered in subsequent loss analysis. This assumption is further supported by the fact that this type of façade was not damaged in the Christchurch earthquake of 2011 meaning that they are quite robust.

3.4.3. Loss Functions

A loss function quantifies the direct loss due to the repair or replacement of a component after attaining a damage state. It is a function of the number of units and the uncertainty associated with the loss per unit. Since it became more economical, in terms of labour and material costs, to repair components in bulk, the cost of repair or replacement per unit would decrease when more of the same

units at the same storey are damaged. For example, the cost to repair damaged sprinkler pipes must account for the cost to remove the suspended ceilings and provide water protection covering on the floor. As the length of damaged pipes increases, the cost to replace them would not increase linearly because the repairs can become more efficient.

The information required to develop loss functions can come from a variety of sources, including construction estimating documents, experimental studies, and professional surveys (FEMA, 2012). Several loss functions for the non-structural components were adopted from the FEMA P-58-3 database (FEMA, 2012). Note that all values of costs are in 2011 US$.

Table 13. Repair costs obtained from the Background Documents (FEMA, 2012)

Component	Loss Functions		
	DS1	**DS2**	**DS3**
HVAC - galvanised steel ducts (A < 6 ft^2)	D3041.011c, DS1	D3041.011c, DS2	
HVAC - compressor	D3032.013b, DS2		
HVAC - in-line fan	D3041.001c, DS1	D3041.001c, DS2	
HVAC - FCU (<5000 CFM)	D3052.013b, DS1	D3052.013b, DS2	
Water pipe system	D2021.012b, DS1	D2021.012a, DS1	D2021.012a, DS2
Sanitary pipe system	D2031.013b, DS1		
Fire sprinklers - pipes	D4011.023a, DS1	D4011.023a, DS2	
Fire sprinklers - drops	D4011.033a, DS1		
Traction elevators	D1014.011, DS1		
Stairs	C2011.001b, DS1	C2011.001b, DS2	C2011.001b, DS3

The loss functions deemed more representative for New Zealand constructions are used where available from the literature and are summarised below in Table 14. Repair costs have been obtained from the literature. Note that all values of costs had been converted to 2011 US$ to match the costs provided by the FEMA P-58 database.

Table 14. Repair costs obtained from the literature

Component	Loss Functions
	DS1
Ceiling (A < 20 m^2) Grid size: 0.9 x 0.6	93.5 (5.83)[3]
Ceiling (A < 20 m^2) Grid size: 1.2 x 0.6	93.5 (5.83)[3]
Ceiling (A < 23.2 m^2) – bracing	93.5 (5.83)[3]
Ceiling (23.2 m^2 < A < 93 m^2) – bracing	93.5 (5.83)[3]
Wall S2	140 (0.4)
Wall S3	200 (0.4)
Wall S4	150 (0.4)
LRB (displacement)	3000 (0.4)
LRB (compressive)	3000 (0.4)
LRB (tensile)	3000 (0.4)
SB (displacement)	4800 (0.4)

The costs to repair damage states 1 to 3 of the partition walls are adopted from the study by Dhakal et al. (2016) to reflect the definitions provided by Mosqueda (2016) for full height partitions. For the damage state 0, the repair action required is light pasting and repainting mainly around the corners and edges of wall, such as in the door or window corners and the wall corners. According to the rates of painters provided by Resene Group, the cost to paint a square meter of wall in New Zealand, when accounting for material and labour, can be taken to equal 2011 US$ 8.15 (Resene Paints Ltd, 2020).

Table 15. Repair costs of partition walls (Dhakal, Pourali, et al., 2016)

Damage state	Repair action	Repair cost (2011 US$ per m^2)
DS0	Localized repair mainly around corners and edges of wall. May require light pasting and repainting.	8.15 (4)

[3] These values were obtained from Yeow, Sullivan, et al. (2018)

DS1	Re-tape joints, past and repaint. May require cutting and replacing corner sections of board. Repair 5% wallboard, 10% re-tape, 25% paint.	17.58 (4.62)
DS2	Remove and replace 10% of wall board (both sides), re-tape and paste 25% of wall, paint 50% of wall. Replace boundary studs ~ 5 intersections per 100 ft of wall.	40.85 (4.14)
DS3	Remove and replace 50% length of metal stud wall, both sides of the gypsum wall board and any embedded utilities, and tape, paste and repaint. 50% wall replacement, 100% paint	76.59 (13.92)

Due to base isolation, the demands on the walls are significantly reduced compared to traditional construction. Hence, the only damage states considered is cracking of the walls requiring cosmetic repair. Only the three walls at the southern side of the building surrounding the stairwell are considered in the loss analysis because they are the only ones not hidden behind partition walls. The cost to perform cosmetic repair on cracked walls is taken at 2011 US$ 8.15 (Resene Paints Ltd, 2020), which accounted the cost for painting. The cost may have been underestimated and future research could investigate the impact of this on the EAL. Despite this, it was found that this is not a significant contribution to the loss analysis.

There are fifteen lead rubber bearings and thirteen slider bearing units in the foundation. Based on a discussion with the manufacturer of the isolators, the replacement costs are US$3,000 and US$4,800 per unit, respectively. An additional US$1,000 was added to the replacement costs to account for post-earthquake engineering inspection and labour costs.

3.4.4. Deaggregated Losses

In order to analyse the contribution of specific components and performance groups on the total loss, SLAT (Bradley, 2009) was used to evaluate the losses of specific components at certain intensity levels. Since the final goal is to compute the expected annual loss (EAL), the losses can be obtained from intermediate calculations.

Firstly, the mean repair or replacement cost of the ith component due to it being subjected to a specific EDP (e.g. peak floor acceleration) can be computed through Equation 9 (Bradley, 2009),

$$\mu_{L_i|EDP} = \sum_{j=1}^{N_{DS}} \mu_{L_i|DS_j} P\left(DS_j \middle| EDP\right) \quad \text{(Eq. 9)}$$

Where N_{DS} is the number of damage states associated with the ith component. The term $\mu_{L_i|DS_j}$ is the mean repair or replacement cost of a damage state and can be directly obtained from the loss functions aforementioned in Section 4.4.2. Meanwhile, the term $P\left(DS_j \middle| EDP\right)$ is the probability of a damage state occurring under the given EDP, which can be easily derived from the fragility functions aforementioned in Section 4.4.1. This equation represents the mean loss of a component for a given EDP as the sum of the products between the loss and probability of damage over all damage states.

Next, the component loss at a given intensity level is needed. This can be computed using Equation 10 (Bradley, 2009),

$$\mu_{L_i|IM} = \int_0^{\infty} \mu_{L_i|EDP} \left| \frac{dG(EDP|IM)}{dEDP} \right| dEDP \quad \text{(Eq. 10)}$$

Here, $\mu_{L_i|EDP}$ is the mean loss of the ith component considering all damage states as computed previously from Equation 9. Note that $G(x|y) = G(X \geq x|Y = y)$ is the complementary cumulative distribution function (CCDF) of X given Y,

while $dG(x|y)$ is the differentials of $G(x|y)$. Therefore, Equation 10 is the mean loss of the ith component over a range of plausible EDPs at a given IM, with the assumption that the probability density function of the EDP at a given IM has a lognormal distribution.

The mean total loss of the entire structure for a given IM and considering no collapse is simply the sum of losses over all components, as described by Equation 11 (Bradley, 2009) while its variance can be computed using Equation 12 (Bradley, 2009),

$$\mu_{L_T|IM} = \sum_{i=1}^{N} \mu_{L_i|IM} \quad \text{(Eq. 11)}$$

$$\sigma^2_{L_T|IM} = \sum_{i=1}^{N} \sigma^2_{L_i|IM} + 2\sum_{i=1}^{N}\sum_{j=1}^{i-1} \rho_{L_i,L_j|IM}\, \sigma_{L_i|IM}\, \sigma_{L_j|IM} \quad \text{(Eq. 12)}$$

Equation 11 is equal to the sum of the losses contributed by every component given the IM. Meanwhile, Equation 12 is a function of the variances of the losses of individual components and the covariances of the losses between every pair of components. The term $\rho_{L_i,L_j|IM}$ is the correlation coefficient between any two components, namely the ith and jth components. It defines the linear dependency between different components in terms of their loss-damage relationships (e.g., costs to repair different components may be correlated), damage-EDP relationships (e.g., damage in different components due to the same EDP may be correlated), and EDP-IM relationships (e.g., larger than average displacement at one level may imply larger than average displacements at other levels). Due to the difficulty in quantifying the correlation coefficients, it is simply assumed that all components are mutually independent and thus are uncorrelated. However, this assumption leads to the implication that the calculated loss is at a lower bound (Bradley et al., 2008).

Figure 77 presents the losses for each component type against a range of intensity levels. Although only nine unique intensity levels are provided as

inputs to SLAT, logarithmic interpolation between the values is used to obtain the values in between. In addition, Table 16 summarises the losses of major components at discrete IM values corresponding to the nine intensity levels input into SLAT. Note that Table 16 does not show components which contribute less than 5% of the total loss (e.g., stairs, ceilings).

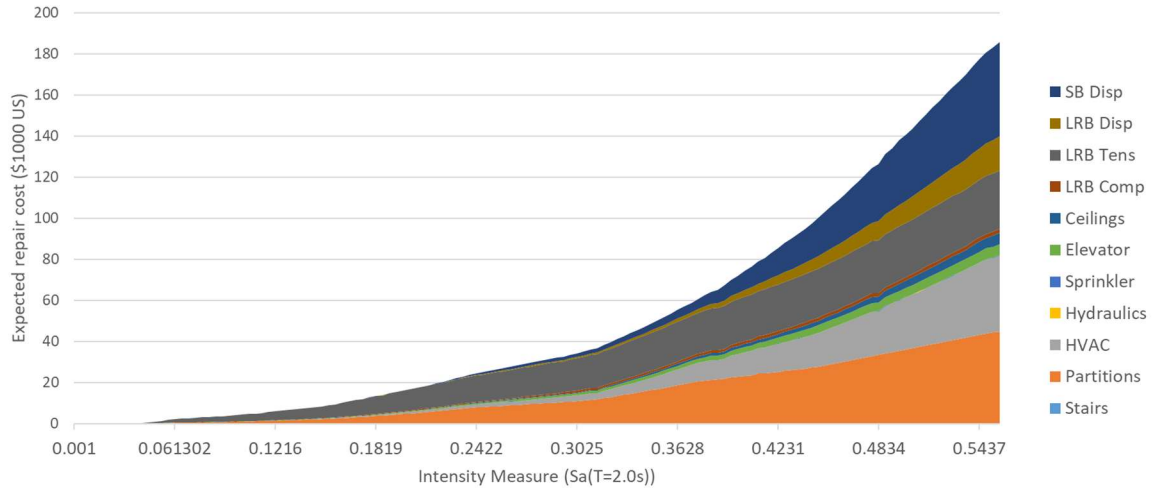

Figure 77. Expected losses de-aggregated based on type against intensity measure

Table 16. Significant component losses for each of the nine intensity levels

		Repair cost ($1000 US)					
Return period (1/years)	Sa(2.0s) (g)	Partitions	HVAC	LRB Tens	LRB Disp	SB Disp	**Total**
30	0.060	0.41	0.04	1.57	0.00	0.00	**2.01**
70	0.093	0.75	0.10	2.83	0.00	0.00	**3.68**
225	0.148	2.04	0.26	5.58	0.00	0.00	**7.88**
475	0.190	4.08	0.67	9.34	0.01	0.01	**14.11**
975	0.237	7.62	1.38	12.49	0.29	0.72	**22.50**
2475	0.311	11.68	3.10	16.16	0.75	1.92	**33.60**
4975	0.374	20.28	8.98	19.84	1.78	4.80	**55.68**
10000	0.446	27.49	16.25	23.79	6.02	18.23	**91.78**
25000	0.555	44.68	36.75	28.41	16.52	45.56	**171.92**

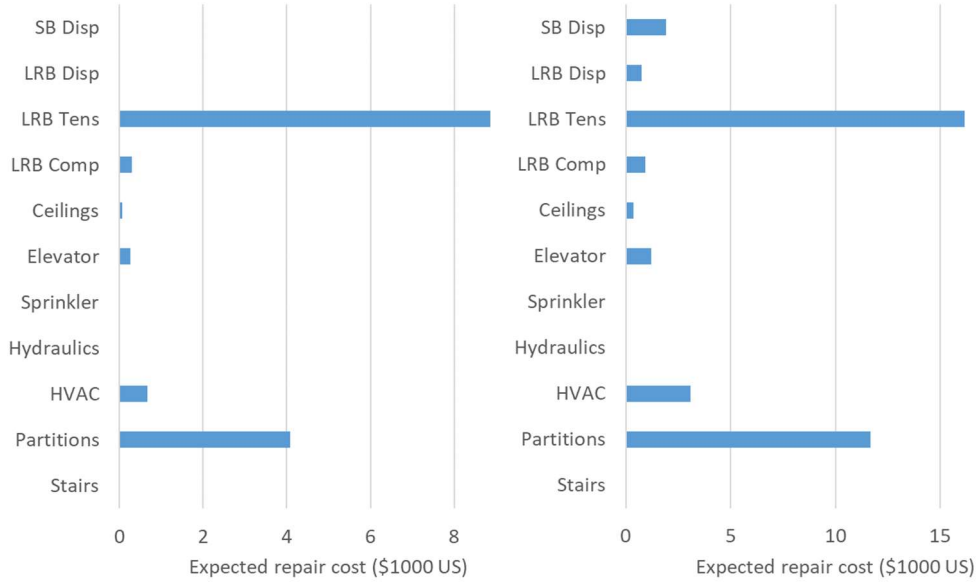

(a) (b)

Figure 78. Expected losses de-aggregated for (a) 1 in 475 years and (b) 1 in 2475 years

Notice that the contribution of RC walls has not been included in Figure 78 because it was found to be negligible. This is expected because the total area of exposed RC walls that would need a cosmetic repair after an earthquake is quite small.

Figure 79 displays the deaggregation of loss due to storey drift over the height of the structure for the return periods of 475 years and 2475 years. The two profiles are quite similar except for their difference in magnitudes. It can be seen that loss increased with height up to level 5-PG before reducing at the roof level. This is because the drift profile increases approximately linearly with height as shown in Figure 25 as a result of the cantilever action of the structural walls and since the upper two levels have less partition walls.

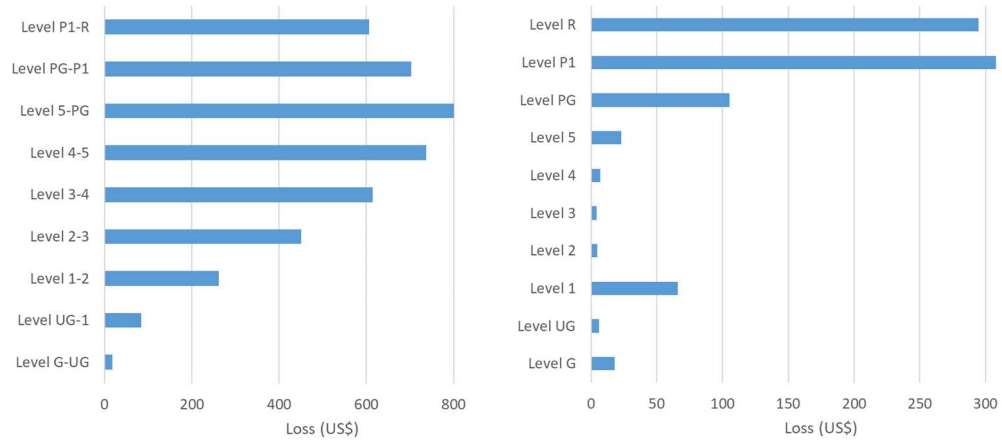

(a) (b)

Figure 79. Storey losses due to IDR for (a) 1 in 475 years and (b) 1 in 2475 years

Figure 80 displays the deaggregation of loss due to peak floor acceleration over the height of the structure for the return periods of 475 years and 2475 years. Once again, the two profiles are quite similar except for their difference in magnitudes. This has to be expected because the superstructure remains elastic throughout the analysis. The losses at level P1 and roof level are significantly greater than the other levels. It was found that the main contribution of the losses at these two levels are due to HVAC damage because of the higher number of fan coil unit (FCU) at these two levels.

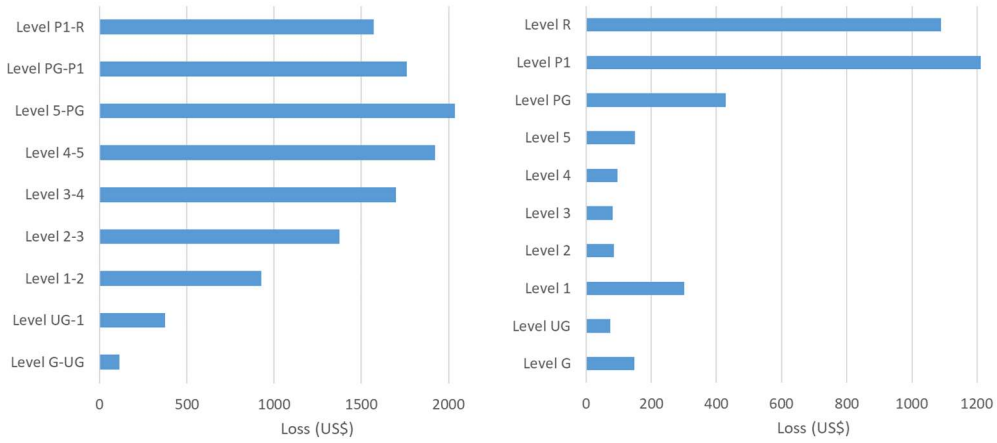

(a) (b)

Figure 80. Storey losses due to PFA for (a) 1 in 475 years and (b) 1 in 2475 years

3.4.5. Expected Annual Loss

Finally, the expected annual loss (EAL) can be computed by combining the total component loss for every intensity level and the annual exceedance rate from the hazard curve. The expected value, μ_{L_T}, can be obtained by integrating the following equation,

$$\mu_{L_T} = \int_0^\infty \mu_{L_T|IM} \left|\frac{d\lambda_{IM}}{dIM}\right| dIM \qquad \text{(Eq. 13)}$$

Applying Equation 13 to the component losses returns the expected value of 2020 of NZ$330. This is the expected annual loss (EAL) of the base isolated building. The building replacement cost is usually estimated at around 15% more than the building construction cost to allow for demolition and post-earthquake inflation. Since the initial construction cost is 2020 NZ$ 24 million, the building replacement cost is estimated to be 2020 NZ$ 27.6 million. The EAL can be expressed as a percentage of the building replacement cost, which is 0.0012%.

In comparison, the EAL of a code-complying case study building performed by Bradley et al. (2008) was 2008 NZ$11,700 which relates to 0.08% of the replacement cost of the structure. It was noted that the main contribution of economic loss in structures during small to moderate ground motions is dominated by damage to non-structural components and contents rather than structural components. Because of the base isolation, a cost saving by almost a hundred orders of magnitude was achieved through significantly lowering the non-structural damages.

The EAL is uncertain due to the fact that the damage and cost itself is uncertain. For example, two units of LRB may have different failure criteria due to inherent variability in material and construction. Hence, to get a sense of the uncertainty of EAL, the standard deviation was computed using Equation 14, which is equal to NZ$77 (0.00028% of building replacement cost).

$$\sigma_{L_T} = \sqrt{\mu_{L_T^2} - \left(\mu_{L_T}\right)^2} \quad \text{(Eq. 14)}$$

The net-present-cost (NPC) assessment provides an indication of the expected cumulative losses over time (i.e., discounted future losses), in addition to the initial construction cost, converted to the net present value. This metric is useful to identify whether base isolation is likely to pay off for a given duration of the building in service. It can be computed through the following equation,

$$NPC = \frac{\left(1 - e^{-\lambda t}\right)}{\lambda} EAL + C_i \quad \text{(Eq. 15)}$$

Where C_i is the building value or the initial cost of construction, λ is the discount rate, and t is the duration that the building has been in service in years.

The discount rate controls the rate of loss over time and in practice, it could reasonably vary between 1% and 7% (Beck et al., 2002). A high discount rate will reduce the loss over time compared to a low discount rate. For this apartment building, a discount rate of 4% was assumed as it is neither a high

priority building (e.g., hospital) nor a low priority building (e.g., single residential structure).

Since the initial cost of constructing the apartment building is approximately NZ$ 24 million, the expected loss of the building for 50 years can be computed through Equation 15 and is displayed in Figure 81. In order to display the uncertainty associated with the choice of discount rate, the lower and upper bounds corresponding to 1% and 7% discount rate, respectively, are also plotted.

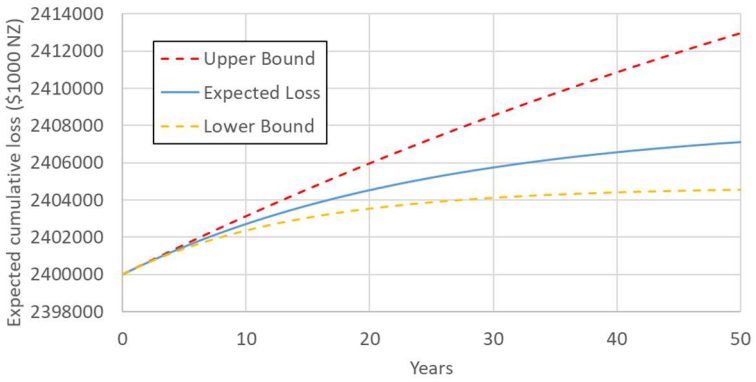

Figure 81. Expected cumulative loss for 50 years

3.4.6. Loss assessment assumptions

So far, the losses are assumed to be independent of the time of occurrence of the earthquakes. This means that it does not consider the effect of aftershocks that may result in direct loss greater than that predicted. This assumption would be reasonable, for example, if the seismic hazard is time-independent and the building will always be restored to its original state before the next damaging event, so that the building vulnerability remained the same.

The structural model also did not account for seismic pounding that resulted from the horizontal displacements of the grillage beams exceeding the allowable gap. Although it was exceeded in some ground motions at the highest intensity levels, no fragility functions were found that could account for damage in the

grillage beams from pounding. However, because of the rarity of the highest intensity levels, it is unlikely to contribute significantly to the estimated EAL.

3.5. Seismic Performance Comparison with a Fixed Base Building

3.5.1. Case Study Buildings

The study by Yeow et al. (2018) investigated the relative performance and cost-effectiveness of implementing friction beam-column and column-base joints in steel moment-resisting frame office buildings compared to those possessing traditional joints. This section aims to provide a direct comparison between these fixed base structures against the base isolated apartment building.

The study by Yeow et al. (2018) considered 4-storey and 12-storey buildings designed to the minimum requirements of New Zealand standards for Auckland, Christchurch, and Wellington. For the interest of this research, only the buildings designed for Christchurch will be considered. An iterative process was used to obtain the lightest steel frame possible while satisfying minimum serviceability and ultimate limit state requirements for both wind actions and earthquake actions.

The layout of the case study buildings is shown in Figure 82. Both the 4-storey and 12-storey buildings are designed with a perimeter lateral load resisting frame along each side of the building, and interior gravity beams and columns.

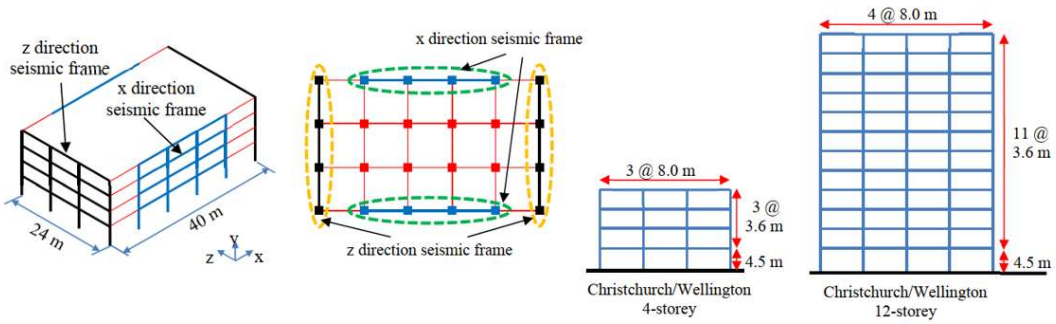

Figure 82. Layout of the case study buildings designed for Christchurch/Wellington conditions (Yeow, Orumiyehei, et al., 2018)

The case study buildings allowed for inelastic behaviour in the beam and column base, as well as in the friction connection in the case of the structure with non-"traditional connection". Modal analysis was performed for both traditional frame and friction connections. The fundamental periods of the 4-storey building are 1.4 s and 1.3 s, respectively, whereas the fundamental periods of the 12-storey building are 2.9 s and 2.6 s, respectively.

In contrast, the fundamental period of the superstructure of the apartment building is closer to that of the 4-storey building than to the 12-storey building. This is to be expected because the superstructure was designed to be much stiffer than an equivalent fixed base building of the same height so that displacements would concentrate at the base isolation layer.

3.5.2. Comparing Seismic Losses

To perform the loss analysis, Yeow et al. (2018) based the quantities of non-structural components by reviewing plans of similar building types and usage in Christchurch and using PACT's (FEMA, 2012) "Normative Quantity Estimation Tool" where information was not readily available elsewhere.

In addition, the building's value is required to estimate the full-replacement cost, which was assumed to be 20% greater than the building value to account for the price of demolition among other things. The total values of the buildings for both traditional frame and friction connections were estimated to be NZ$ 8.917 million and NZ$ 8.931 million, respectively, for the 4-storey building, and NZ$ 42.56 million and NZ$ 42.69 million, respectively, for the 12-storey building.

Time-based loss analysis was performed for the four case study buildings. Note that collapse was not considered for these buildings. The computed expected annual loss for each building, expressed as both absolute cost and as a percentage of full replacement cost (FRC) are shown in Table 17.

Table 17. Expected annual loss of each building in Christchurch

	Traditional frame		Friction connections	
	EAL (NZD)	EAL (% of FRC)	EAL (NZD)	EAL (% of FRC)
4-storey	11400	0.107	9030	0.084
12-storey	25800	0.05	22100	0.043

It can be observed that EAL is larger for the taller buildings in terms of absolute cost but is smaller in terms of percentage of full-replacement cost. The authors noted that this is because the responses of the 12-storey building are generally lower than that of the 4-storey building due to stricter drift requirements for taller buildings. Another observation is that the friction connections have consistently lower EAL than traditional connections. This is because the main cost saving of using friction connections is the reduction to the repair costs to the connections itself.

In comparison, the EAL that was computed for the base isolated apartment building was NZ$ 330 with the percentage of FRC as 0.0012%. When comparing cost effectiveness in terms of the percentage of FRC, the base isolated building is almost fifty times lower than the 12-storey buildings and almost one hundred times lower than the 4-storey buildings, regardless of connection type. As was noted by Yeow et al. (2018), 40-80% of contributions to the EAL in their study arise from seismic intensities smaller than a 10% in 50 year probability of exceedance event. This observation is consistent with past studies (Aslani & Miranda, 2005; Bradley et al., 2009). Therefore, it can be concluded that the main reason that the apartment building consistently have significantly lower EAL percentages of FRC is because base isolation provides a significant performance improvement for events below or equivalent to this shaking intensity.

It is also important to address some drawbacks and limitations from doing this kind of comparison. Firstly, the case study buildings were designed by Yeow et al. (2018) to obtain the lightest steel frame possible while meeting the minimum allowable standards. This would have the effect of reducing the initial cost,

while increasing the loss due to having a lower performance. Contrast this to a stronger building with a greater initial cost, but better seismic performances leading to a lower overall loss. Secondly, there is a significant variation in annual losses arising from the various assumptions made during the modelling and loss analysis stages in the Yeow et al. (2018) study and in this study. As such, the focus on EAL when making comparisons between base isolation and traditional fixed base structures in this way may hide the underlying large uncertainty.

3.6. Conclusions

A 3D structural model of the case study building was developed in Ruaumoko 3D (Carr, 2005). The main lateral resisting system is the reinforced concrete structural walls, which were modelled using the equivalent frame method based on the cracked section properties of the walls. The steel framing whose primary purpose is to resist gravity loads was also included in the model, although it was found the effects of including it were negligible. The case study building is base isolated with two different types of isolators: Lead Rubber Bearings (LRBs) and Steel-PTFE Slider Bearings (SBs). They were modelled as spring elements in Ruaumoko 3D (Carr, 2005) with section properties derived from the experimental results of prototype testing done by Robinson Seismic Limited.

The structural model was subjected to a suite of 20 ground motions over a range of 9 intensity levels derived from the PSHA by Yeow et al. (2018). For each ground motion analysis, the engineering demand parameters (EDP) of interest, including the peak floor accelerations (PFA), inter-storey drift ratio (IDR), the maximum displacements of the LRBs and SBs, the maximum compressive and tensile loads of the LRBs, and maximum wall curvatures at the base, were recorded.

Time-based loss analysis was then performed using SLAT (Bradley, 2009) by inputting the EDPs generated by the structural analyses stage. The fragility and loss functions for structural and non-structural components from previous

studies specific to New Zealand construction practice were adopted wherever available. Otherwise, fragility and loss functions from the FEMA P-58-3 database (FEMA, 2012) were adopted. Finally, the expected annual loss (EAL) was computed for this case study building, which amounts to $330 (0.0012% of replacement cost) with a standard deviation of $70 (0.00028% of replacement cost).

Direct comparison in terms of the expected annual loss (EAL) between the case study building and a hypothetical building with traditional foundation was done. The hypothetical building was designed for Christchurch conditions as a steel moment-resisting frame structure to satisfy the minimum allowable standards (Yeow, Orumiyehei, et al., 2018). It was found that the EAL of the case study, base isolated building is almost fifty times lower than the 12-storey buildings and almost one hundred times lower than the 4-storey buildings, regardless of connections type. However, such direct comparison may be limited in usefulness since the designs of the two buildings are quite different. A suggestion for future work is to compare the EALs of the case study building and a redesign with fixed foundation with increased strength for the reinforced concrete structural walls in order to satisfy the performance objectives.

4. Seismic Instrumentation

4.1. Introduction

The value of having seismic instrumentation will be investigated from a cost saving point of view. This will be done by rerunning the loss analysis with and without seismic instrumentation to investigate how it affected the decision to perform visual inspection after an earthquake. Thus, there will be two cases to investigate. One is the hypothetical scenario where the apartment building is not instrumented, which may increase the expected annual loss (EAL) due to an increase in the likelihood of inviting engineers for inspection. Another is when the building is instrumented.

Ultimately, having the instrumentation information after an earthquake allows a significant number of earthquakes to be filtered out without needing response from the structural engineer, such as when the ground motion at the site is known to be too small to have activated the structural response. Moreover, for a further range of events this information can offset the time-frame for the engineer to get to the site. One scenario is when there is the potential for damage in the structure that is unlikely to have significantly reduced the structural capacity of the building, and hence a visit three to four days after is acceptable to the owner or tenants.

In addition to reducing the need for manual inspection, seismic instrumentation also provides many benefits. As mentioned previously, seismic instrumentation can potentially avoid costly demolition due to a general lack of information resulting in difficulty when assessing the structural integrity. This lack of information might lead to the engineers making conservative decisions as were observed for many buildings after the 2011 Christchurch earthquake.

The triggers for getting a structural engineering visual inspection of the building will depend on the building type and age, the owner and tenants, and the ground motion. This might be earthquake magnitude based for a given epicentral

distance, or from using nearby instruments or on-site instruments to compare against the design spectrum.

Another trigger for an inspection is the development of non-structural or structural damage that aligns with the owner or tenants comfort level for continual occupancy or to use the building with safe occupancy. The public generally struggle to separate GIB wall damage from concrete wall damage as they generally do not have a background in how they are essentially unrelated, which may consequently result in a premature visual inspection to happen. To incorporate this phenomena, the fragility functions of the partition wall in the loss analysis will be updated accordingly.

An estimate of the cost of a typical visual inspection is assumed to equal the hourly rate of hiring the structural engineer multiplied by the total hours required for an inspection. According to a survey of an engineer based in Christchurch, a brief visual inspection of the apartment building would involve a walk-around of the building. Assuming easy access to key areas and only one visit, a site visit of four hours on site in addition to some time for writing up the site report, possibly checking information on file, might lead to eight to ten hours in total.

The inspection could also be set based on evaluating the nearest three Geonet station spectra. A potential inspection trigger might be set at a return period of 1 in 1000 years. A lower return period (e.g., 1 in 250 years) could also potentially trigger an investigation. However, based on the performance levels (i.e., drifts and isolation displacements), lower intensity levels had elastic wall response which from a structural perspective would not raise issues. Note, however, this ignores any issues around liquefaction at the site, which is assumed to not occur.

In the case of the apartment building, with instrumentation above and below ground, the structural engineering and inspection response can be somewhat independent of magnitude and distance. This is coupled with the fact that the

building is isolated with comparatively well understood performance under a range of ground motions.

The data recorded from an earthquake can be used by the engineer to rapidly compare site or building response against predetermined demands, beyond which the engineer is asked to visit the site and carry out a visual inspection of critical locations. This allows opportunity to immediately check against known performance limits for the building thereby reducing downtime and potentially inspection duration. The predetermined demands might be:

1. Check the isolation plane peak acceleration and integrated peak displacement against the design movements.
2. Check the penthouse acceleration and integrated peak displacement against the design movements.

In addition, the instrumentation could be connected to an automatic processing system that can immediately inform the tenants about the high-level overview of the structural health of the building after a relatively large earthquake or aftershock. With this, the client or tenants may feel more assured and a potentially unneeded visual inspections can be avoided.

To investigate the value of using seismic instrumentation, the expected annual loss (EAL) of the apartment building without instrumentation will be recomputed. This time it is assumed that a 1 in 250 years intensity earthquake, a 1 in 1000 years intensity earthquake, or cracking in the partition walls could trigger a visual inspection. In contrast, it is assumed that the instrumented building will only be inspected when the peak displacements at the isolation plane and penthouse ground floor exceeded the design movements.

Based on expert opinion and survey from structural engineers, the 1 in 250 years intensity earthquake will likely trigger an inspection of the base isolators at the basement of the building, which will cost approximately $3500. Meanwhile, the 1 in 1000 years intensity earthquake will likely trigger a more comprehensive inspection of the entire structure, which will cost approximately $8500. It is also

assumed that cracking of the partition walls at around 50% of the total partition walls length will also trigger an inspection of the entire structure.

The EAL of the apartment building without instrumentation was computed to be NZ$370 with a standard deviation of NZ$79. The net-present-cost (NPC) analysis can be seen in Figure 83 by assuming a discount rate of 4%. This can be compared with the EAL of the building with instrumentation, which is NZ$330 with a standard deviation of NZ$77. Note that inspections of the instrumented building only occurred at very high intensity levels, hence its contributions to the EAL are negligible. Therefore, an annual cost saving of NZ$40 is expected from having the building instrumented.

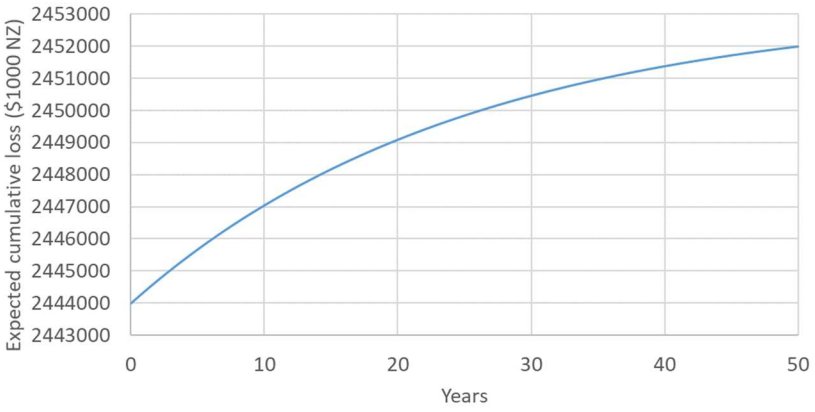

Figure 83. NPC analysis of the apartment building with no instrumentation

Since the total cost of the instrumentation is NZ$44,000, it is clear that instrumentation is not cost effective in terms of direct loss. However, this conclusion neglected the consideration of downtime and global collapse. Building instrumentation can also provide many advantages, such as providing more accurate diagnostics of the structural integrity after a potentially damaging earthquake. This can allow a better decision to be made regarding whether the building is still occupiable, or whether it will require demolition after a large damaging earthquake.

There have been several studies in the past (Cremen & Baker, 2018; Porter et al., 2006) that incorporated accelerometer data from instrumented buildings to produce rapid estimates of repair cost and probable locations of damage. In particular, the study by Cremen & Baker (2018) investigated the correlation between the number of sensors and accuracy in predicting consequences after a given earthquake. The study focused on computing direct losses using scenario-based and intensity-based assessments by following the FEMA P-58 Seismic Assessment procedure. It was found that increasing the number of sensors helped to reduce the uncertainty in the Intensity Measures (IMs) and Engineering Demand Parameters (EDPs) when undertaking the FEMA P-58 procedure. When at least one floor is instrumented and that floor is at the foundation level, then the uncertainty associated with IM for a given earthquake became zero. Likewise, if some floors of the structure are instrumented, then those floors will have zero uncertainty with regards to their EDPs.

The EDPs at non-instrumented floors could then be interpolated based on the EDPs of the instrumented floors, such as by using spline interpolations (Limongelli, 2003). These EDPs were then directly input into the fragility functions and subsequent loss functions to get the direct losses. It was found that the variance of losses generally decreases as the number of sensors increased. In addition, the reduction in variance is substantial as soon as more than a small number of floors are instrumented (Cremen & Baker, 2018).

In order to reduce the cost of instrumenting the buildings, smartphones may be used as a cheaper alternative. A second-hand smartphone in New Zealand can cost approximately NZ$100 based on the market at the time of this research. Since there are six sensors in the apartment building, the total cost to instrumenting the apartment building will be NZ$600. It can be seen from Figure 84 that NPC analyses suggests that the instrumented building is likely to be more economically beneficial than the non-instrumented building at 23 years.

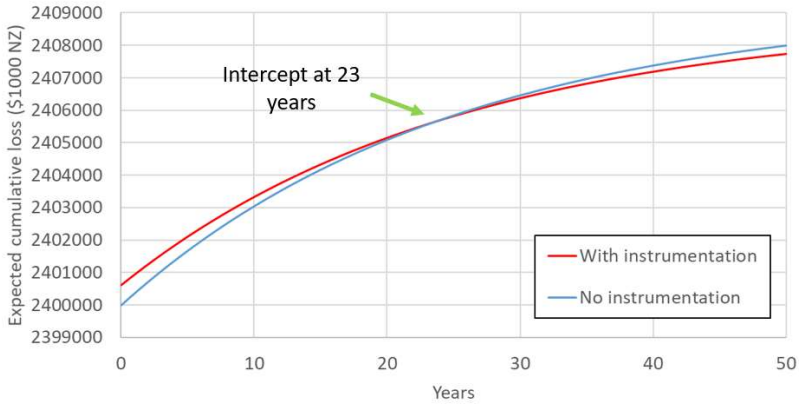

Figure 84. Net-present-cost analyses with and without instrumentation.

4.2. Smartphone Sensors

The previous section dealt with the reason of wanting seismic monitoring for the apartment building. Moreover, the study by Cremen & Baker (2018) showed that having a greater number of sensors can decrease the uncertainty associated with carrying out loss analysis after an earthquake. However, seismic instrumentation is very costly and hence are not as cost effective in terms of direct loss when considering inspection costs. This section will investigate how smartphone sensors can be used as a cheaper alternative to the accelerometer sensors used by the industry.

In order for the smartphones to become alternative to industrial accelerometers for recording seismic data, they must have sufficient sampling rates and accuracy. Many industrial accelerometers that are used for building instrumentation have sampling rate of 200 Hz. Although the accelerometers in most modern smartphones tend to have a high sampling rate in the tri-axial directions, at this time of writing, the authors are only aware of a few high-spec smartphones that can achieve a sampling rate of 200 Hz in terms of hardware. Moreover, there usually exists a ceiling of sampling rate in the smartphone arising from the overhead of its operating system.

An experiment was conducted to compare the accuracy of three smartphones against industrial accelerometers by subjecting them to a simulated ground motion on a 1-D shaketable. The smartphones used for this experiment are two Vodafone C9 that costed NZ$60 each and a LG Nexus 5 that costed NZ$100. Although they have theoretical or hardware sampling rates of 100 Hz and 200 Hz, respectively, the practical sampling rate for both types was found to be 40-50 Hz due to the overhead from the Android operating system. Despite this, however, a sampling rate of at least 20 Hz was deemed sufficient for the purpose of recording seismic data (Bolt & Hudson, 1975).

4.3. Automated MDOF System

The goal of this section is to create a simple automatic procedure to estimate the stiffness matrix of the apartment building after an earthquake occurs. The main motivation is to provide valuable information in the form of a full history of the structural stiffness to the engineers performing post-earthquake inspection. In this way, the amount of time needed to spend on inspection will be lessened, thereby reducing the potential downtime. Moreover, decisions on repairability and cost can be made with greater accuracy.

There are certainly many techniques of Structural Health Monitoring (SHM) that have been studied in the past. Early research mainly focused on estimating the modal properties (i.e., natural frequencies, mode shapes, and damping ratios) through system identification algorithms. There have been methods introduced to estimate the stiffness matrix (Salawu & Williams, 1993), however this class of methods generally suffer from a lack of accuracy due to difficulty in capturing high-order modes. Another class of methods to estimate stiffness matrix is based on model updating of a numerical model (Brownjohn et al., 2001; Friswell & Mottershead, 2013). The main drawback is that they can produce erroneous results when the numerical model it relied upon is not well defined.

Compared to these methods, the technique used here does not require estimating modal properties, nor does it require a numerical model of the structure to be known beforehand to estimate the stiffness time history. Instead, it relies on statistical methods to derive the stiffness time history by treating the acceleration data outputted by the sensors as sample points to perform regressions over.

The apartment building can be idealised into a simple Multiple Degree of Freedom (MDOF) system, as shown in Figure 85. In this system, the lumped mass assumption will be used. A mass will represent the grillage beams just above the isolation plane, and another to represent the superstructure entirely. The ground below the isolation plane has triaxial accelerometers recording the ground motions variation with time, i.e. $\{\ddot{u}(t)\}$.

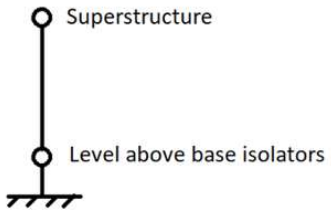

Figure 85. MDOF representation of the case study building

The equations of motion that describes this MDOF system is shown in Equation 16, where DOF 1 represents the mass at the grillage beams level and DOF 2 represents the mass of superstructure. Note that m_1 and m_2 are the masses, c_1 and c_2 are the damping coefficients, k_1 and k_2 are the stiffness coefficients, x_1 and x_2 are the displacements of DOF 1 and DOF 2, respectively.

$$\begin{bmatrix} m_1 & 0 \\ 0 & m_2 \end{bmatrix} \begin{Bmatrix} \ddot{x}_1 \\ \ddot{x}_2 \end{Bmatrix} + \begin{bmatrix} c_1 + c_2 & -c_2 \\ -c_2 & c_2 \end{bmatrix} \begin{Bmatrix} \dot{x}_1 \\ \dot{x}_2 \end{Bmatrix} + \begin{bmatrix} k_1 + k_2 & -k_2 \\ -k_2 & k_2 \end{bmatrix} \begin{Bmatrix} x_1 \\ x_2 \end{Bmatrix} = -\begin{bmatrix} m_1 & 0 \\ 0 & m_2 \end{bmatrix} \ddot{x}_g \quad \text{(Eq. 16)}$$

Since the two orthogonal horizontal axes can be computed in the same manner, the discussion herein will be restricted to only one horizontal axis because an identical procedure can be applied to the other horizontal axis. Furthermore, the behaviour of the MDOF in the vertical axis can also be formulated with the same equation of motion, Equation 16.

The main aim is to implement a procedure that can automatically compute the stiffness time history from the recorded sensor data of an earthquake event. The sensors will start recording acceleration when they detect motions greater than a specified minimum threshold. This will be done via majority voting when at least three out of the six sensors must exceed their minimum threshold to trigger the recording. A rolling buffer of thirty seconds is programmed into the sensors to preserve data from thirty seconds before the trigger and thirty seconds after the earthquake. This will be important in signal processing for estimating the signal to noise ratio.

Once the time history of the accelerations is obtained, a numerical integration method can be used to integrate once to derive the velocities time history and twice to derive the displacements time history. However, the main challenge is that the velocities and displacements are sensitive to noise. When integrating the time history twice, the ground motion along with the noise will get integrated twice. Therefore, it is important that a suitable filtering technique is employed before the numerical integration.

The algorithm developed by Sakkas & Sakellariou (2018) will be utilised in this study to perform automatic correction of the accelerograms. The main reason it is used is that the algorithm can automatically select the frequency band width to filter from the recorded time history by estimating the signal-to-noise ratio using pre-event and post-event data. Moreover, the algorithm was found to be computationally efficient which is crucial for post-earthquake decision making.

This approach will automatically consider the pre-event and post-event time to detect the noise in the data. The algorithm would then compute 4 different low

cut-off frequencies for the acceleration and velocity time histories. The high cut-off frequency was set to the recommended value of 45 Hz for newer digital instruments (Sakkas & Sakellariou, 2018). A Butterworth filter based on low and high cut-off frequencies would then be applied to the acceleration time histories. Finally, velocities and displacements could be computed through numerical integration using the trapezoidal rule.

The superstructure is only instrumented at a single level located at the Penthouse Ground floor. Hence, only the responses at this PG floor are known. With the MDOF assumption, the superstructure mass must be lumped into a single level and that location does not necessarily have to be at the PG level. The effective height of the superstructure can be computed using Equation 17, where Δ_i is the displacement of storey i from a pushover analysis, m_i is the mass of storey i, and H_i is the height of storey i.

$$H_e = \sum_{i=1}^{n} \frac{m_i \Delta_i H_i}{m_i \Delta_i} \qquad \text{(Eq. 17)}$$

There are several approaches to derive the responses at the lumped mass location of the superstructure based on the responses at the PG floor. The first approach assumes that the superstructure is dominated by first mode behaviour. In this case, the displacements at the effective height can be linearly interpolated between the two instrumented levels, namely the ground floor and the PG floor. However, such assumption might be too simplistic, especially if the building response is dominated by higher modes.

The second approach is to use the cubic spline function to interpolate the absolute acceleration along the height of the building (Limongelli, 2003). The spline functions are able to provide a more complex displacement shape compared to first mode response. At the same time, it does not rely on directly measuring the mode shapes and frequencies, which are more susceptible to noises as mentioned previously. The interpolation of spline function is done by

solving for the unknown coefficients for each time interval based on continuity, interpolation, and boundary conditions (Limongelli, 2003).

In order to compute the stiffness time history for a single axis from the recorded sensor data after an earthquake event, the equations of motion shall be solved using the known acceleration, velocity, and displacement at each DOF. To get a unique solution at each time step, a mass-invariant constraint will be assumed. Moreover, the damping constants shall be assumed to not vary significantly for the duration of the earthquake.

Firstly, the response history will be discretised into multiple bins with each bin associated to a set of equations of motion. The number of bins, n, will depend on the length of the data and the timestep. Next, the average responses, such as accelerations, will be computed for each bin. Now each bin can be described by a set of equations of motion.

For instance, Equation 18 shows the equations of motion for the first bin ($n = 1$) with vectors for the average acceleration, $\ddot{x}_{1,avg}$, average velocity, $\dot{x}_{1,avg}$, and average displacement, $x_{1,1}$. Given the mass-invariant constraint, there are four unknowns, namely $k_{1,1}$, $k_{2,1}$, $c_{1,1}$, and $c_{2,1}$.

$$\begin{bmatrix} m_1 & 0 \\ 0 & m_2 \end{bmatrix} \begin{Bmatrix} \ddot{x}_{1,1} \\ \ddot{x}_{2,1} \end{Bmatrix} + \begin{bmatrix} c_{1,avg} + c_{2,avg} & -c_{2,avg} \\ -c_{2,avg} & c_{2,avg} \end{bmatrix} \begin{Bmatrix} \dot{x}_{1,1} \\ \dot{x}_{2,1} \end{Bmatrix} + \begin{bmatrix} k_{1,avg} + k_{2,avg} & -k_{2,avg} \\ -k_{2,avg} & k_{2,avg} \end{bmatrix} \begin{Bmatrix} x_{1,1} \\ x_{2,1} \end{Bmatrix} = -\begin{bmatrix} m_1 & 0 \\ 0 & m_2 \end{bmatrix} \ddot{x}_{g,1} \quad \text{(Eq. 18)}$$

The equations below show the equation of motion for the second bin ($n = 2$).

$$\begin{bmatrix} m_1 & 0 \\ 0 & m_2 \end{bmatrix} \begin{Bmatrix} \ddot{x}_{1,2} \\ \ddot{x}_{2,2} \end{Bmatrix} + \begin{bmatrix} c_{1,avg} + c_{2,avg} & -c_{2,avg} \\ -c_{2,avg} & c_{2,avg} \end{bmatrix} \begin{Bmatrix} \dot{x}_{1,2} \\ \dot{x}_{2,2} \end{Bmatrix} + \begin{bmatrix} k_{1,avg} + k_{2,avg} & -k_{2,avg} \\ -k_{2,avg} & k_{2,avg} \end{bmatrix} \begin{Bmatrix} x_{1,2} \\ x_{2,2} \end{Bmatrix} = -\begin{bmatrix} m_1 & 0 \\ 0 & m_2 \end{bmatrix} \ddot{x}_{g,2} \quad \text{(Eq. 19)}$$

By assuming average values for the damping constants of the two DOFs, $c_{1,avg}$ and $c_{2,avg}$, and stiffnesses of the two DOFs, $k_{1,avg}$ and $k_{2,avg}$, across the two

bins, it is possible to solve for them using the four unique equations of motion, as shown above. However, the $k_{1,avg}$ and $k_{2,avg}$ are not of interest because their values would be smothered over a relatively large span of time. On the other hand, this is not a problem for the damping matrix, c_{avg}, since it was assumed that the damping matrix generally do not vary significantly relative to the stiffness matrix.

Figure 86 shows a time-series discretised into eight bins ($n = 4$) of equal durations. This gives eight equations of motion that can be used to solve for two non-overlapping sets of averaged damping constants, i.e. a set consisting of $c_{1,avg}$ and $c_{2,avg1}$, and another set of $c_{1,avg}$ and $c_{2,avg2}$. Note that the two sets of damping constants can perhaps be thought to correspond with pre-damage damping constants and post-damage damping constants.

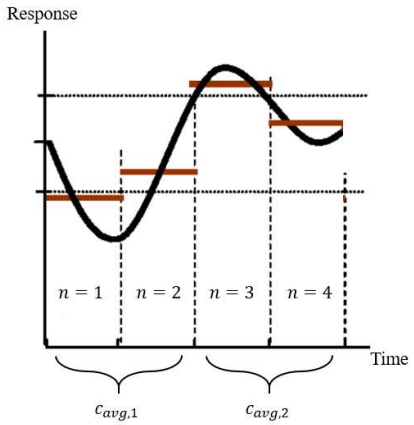

Figure 86. Response history discretised into $n = 4$ bins

As mentioned previously, the averaged stiffnesses across the four bins are not of interest because their resolutions are too low to be of any use. Hence, the analysis will be redone by solving the equation of motion at every time step of the response history to get the two stiffnesses shown in Figure 85, i.e. the values of k_1 and k_2, by using the two equations of motion (Equation 16). The difference with last time is that the damping coefficients to be used are the averaged values computed previously.

At every time step, Equation 20 will be used to compute the stiffness values (i.e. k_1 and k_2). Note that the masses, accelerations, velocities, and displacements are known beforehand. Moreover, the averaged damping constant, c_{i,avg_j}, as computed earlier using Equation 18 and Equation 19 will be substituted into the equations at the appropriate time span.

$$\begin{bmatrix} m_1 & 0 \\ 0 & m_2 \end{bmatrix} \begin{Bmatrix} \ddot{x}_1 \\ \ddot{x}_2 \end{Bmatrix} + \begin{bmatrix} c_{1,avg_i} + c_{2,avg_j} & -c_{2,avg_j} \\ -c_{2,avg_j} & c_{2,avg_j} \end{bmatrix} \begin{Bmatrix} \dot{x}_1 \\ \dot{x}_2 \end{Bmatrix} + \begin{bmatrix} k_1 + k_2 & -k_2 \\ -k_2 & k_2 \end{bmatrix} \begin{Bmatrix} x_1 \\ x_2 \end{Bmatrix} = - \begin{bmatrix} m_1 & 0 \\ 0 & m_2 \end{bmatrix} \ddot{x}_g \quad \text{(Eq. 20)}$$

Performing this will output the stiffness values at every time step, hence a time history of stiffness values is produced. However, the current stiffness values are susceptible to noise or outliers. A plot of these values over time may reveal random fluctuations around the underlying "true" stiffness values due to the errors that have been accumulated so far. The underlying curve can be recovered by performing regression analysis by treating each stiffness value in the time history as a sample point. A piecewise polynomial function can then be fitted over the values to recover the general shape of the stiffness time history.

A problem with this approach is that it might not be satisfactory to simply fit a single polynomial regression model over the entirety of the stiffness time history using the least-squares method since it may fail to accurately model localised area well. The solution to this is to discretize the stiffness time history and perform multiple polynomial regressions at various subintervals so that the local behaviour on the curve can be captured more accurately. This can be done by utilising an automatic Bayesian curve fitting algorithm (Denison et al., 1998).

The basic idea of this algorithm is to compose together several generally low order polynomials with each defined over a different subinterval, where the union of these subintervals is the full duration of the time-series. The points that separate the subintervals are known as the knots. In order to fit the curve, the algorithm requires prior knowledge in the form of the initial number of knots,

λ, the distribution of the number of knots, k, the order of the piecewise polynomial, l, and the degree of continuity, l_0. It was noted that the generated curves are generally not sensitive to the parameters λ and k, although λ does have some effect on the smoothness of the derived curve (Denison et al., 1998).

This method has been shown to be effective at approximating rapidly varying curves (Denison et al., 1998), which made it particularly suitable for modelling the stiffness time history. The authors of the study tested the algorithm on arbitrary test curves with added noise. They were able to remove the noise and recover the underlying curves approximately by setting $l_0 = 1$, $l = 2$, along with assigning a Poisson prior distribution for k, and $\lambda = 5$. However, further studies would be beneficial to investigate the application of this algorithm to derive the stiffness time history and to select the most suitable parameters for this purpose.

The procedure described so far is for estimating the stiffness time history of the simple MDOF system shown in Figure 85. This may already be sufficient to provide a quick overview on the structural integrity of the apartment building after an earthquake. If desired, it is also possible to recover the full structural stiffness using the condensed model identification and recovery method proposed by Koh et al. (2006). However, this method requires a numerical model of the apartment building to be known beforehand. This will not be considered further as it is outside the scope of this research.

4.4. Conclusions

The value of having seismic instrumentation was investigated. The primary focus was on the cost saving provided by lowering the reliance on post-earthquake inspection for the case study building. The expected annual loss (EAL) of the case study building without instrumentation was recomputed by assuming a 1 in 250 years intensity earthquake, a 1 in 1000 years intensity earthquake, or cracking in the partition walls could trigger a visual inspection.

The EAL of the apartment building without instrumentation was computed to be $330 (0.0012% of replacement cost) with a standard deviation of $70 (0.00028% of replacement cost). A net-present-cost (NPC) analysis was performed to determine the value of having instrumentation in terms of cost saving with respect to lowering the reliance on post-earthquake inspection. It was determined that, in this case, seismic instrumentation does not provide a cost saving benefit to the client.

As an alternative, cheap smartphone sensors could be used, which was shown to be more cost-effective as the building instrumented with smartphones is likely to be more economically beneficial than the non-instrumented building at 23 years.

Lastly, an automatic procedure to estimate the storey stiffnesses of an idealised MDOF representation of the case study building for post-earthquake structural assessment was discussed. The procedure differed from other SHM techniques since it does not rely on capturing frequencies and does not require a numerical model to be known beforehand. Instead, it relies on statistical learning techniques to fit a linear model on the recorded data from the seismic sensors installed on the case study building to estimate the time history of storey stiffnesses.

Unlike some other procedures that rely on more complex learning models, such as artificial neural networks, the procedure proposed herein fits a linear model to estimate storey stiffnesses. Although this might result in a lower prediction power than other state-of-the-art learning models, it has the benefit of being more interpretable, since it can output a time history of the storey stiffnesses. This is important because the main aim of this procedure is to aid the inspecting engineers in determining the global response of the structure.

5. Summary and Conclusions

This study performed a loss analysis of a multi-storey residential building in New Zealand with base isolation, made a comparison with a fixed base in terms of losses, and considered the value of using a seismic monitoring system. The findings are expressed in relation to the four main research questions below.

1. What is the expected annual loss of the base isolated building?

* A 3D structural model was developed and analysed under a suite of ground motions over a range of intensities. The PEER-PBEE framework was followed to compute the EAL of the base isolated building, which was found to be 0.0012% with a standard deviation of 0.00028% the building replacement cost.

2. How does the expected annual loss of this building compare with other structural typologies?

* The EAL of the base isolated building was found to be around 50-100 times lower than the EAL of a 12-storey and 4-storey traditional steel moment resisting frame office buildings.

3. Can seismic monitoring significantly reduce cost and downtime associated with manual inspection of a building after earthquakes?

* It was determined that conventional seismic instrumentation does not provide a reduction in cost associated with manual post-earthquake inspection due to the high initial cost of the instrumentation. However, a reduction in the initial cost of instrumenting may result in a reduction in the cost of manual inspection. This study investigated the potential use of smartphones as an alternative to conventional accelerometers. It was found that using smartphones is likely to be economically beneficial after 23 years. In addition, a procedure to estimate the structural stiffness from data outputted by seismic sensors are described. The goal of this procedure is to

assist engineers in assessing the structure after an earthquake, thereby improving the accuracy of assessment and to reduce the potential for post-earthquake downtime.

5.1. Limitations and Future Work

Although this research covered the overall PEER-PBEE framework (Deierlein et al., 2003), there are some limitations in this study such as:

- Only one case study building was considered to represent base isolated buildings.
- Comparison with fixed base structures only included a study of office buildings with steel moment resisting frames rather than reinforced concrete structural walls as the main lateral resisting system.
- The accuracy of smartphone sensors was not assessed in comparison to conventional accelerometers.
- There are uncertainties in the fragility and repair cost functions assumed.

As such, as a suggestion for future research on the topic of this research, the following topics are highlighted:

- Obtain robust fragility and repair cost functions through consultation with the industry and then repeat the loss assessment.
- Redesign the case study building as a fixed base building and redo the loss analysis to get a fairer comparison between base isolation and fixed base buildings in terms of losses.
- Perform experimental study on the accuracy of using smartphones for recording seismic data.

References

Al-Azawi, T., AlMusaui, A. I., & Al-Zaidee, S. R. (2017). Global Journal of Engineering Science and Research Management.

Arnott, K. (2005). Shear wall analysis- new modelling, same answers. *Structural Engineer, 83*(3), 20-22.

Aslani, H., & Miranda, E. (2005). Probability-based seismic response analysis. *Engineering Structures, 27*(8), 1151-1163.

Bathe, K. J., & Dvorkin, E. N. (1986). A formulation of general shell elements—the use of mixed interpolation of tensorial components. *International Journal for Numerical Methods in Engineering, 22*(3), 697-722.

Beck, J. L., Porter, K. A., Shaikhutdinov, R., Au, S., Mizukoshi, K., Miyamura, M., . . . Masuda, M. (2002). Impact of seismic risk on lifetime property values.

Beyer, K., Dazio, A., & Priestley, M. (2008). Inelastic wide-column models for U-shaped reinforced concrete walls. *Journal of Earthquake Engineering, 12*(S1), 1-33.

Bolt, B. A., & Hudson, D. E. (1975). Seismic instrumentation of dams. *Journal of Geotechnical and Geoenvironmental Engineering, 101*(ASCE# 11697 Proceeding).

Bradley, B. A. (2009). User manual for SLAT: seismic loss assessment tool version 1.14.

Bradley, B. A. (2010). A generalized conditional intensity measure approach and holistic ground-motion selection. *Earthquake engineering & structural dynamics, 39*(12), 1321-1342.

Bradley, B. A., Dhakal, R. P., Cubrinovski, M., MacRae, G. A., & Lee, D. S. (2008). Seismic loss estimation for efficient decision making.

Bradley, B. A., Lee, D. S., Broughton, R., & Price, C. (2009). Efficient evaluation of performance-based earthquake engineering equations. *Structural Safety, 31*(1), 65-74.

Brown, C., Seville, E., & Vargo, J. (2013). The role of insurance in organisational recovery following the 2010 and 2011 Canterbury earthquakes.

Brownjohn, J. M., Xia, P.-Q., Hao, H., & Xia, Y. (2001). Civil structure condition assessment by FE model updating:: methodology and case studies. *Finite elements in analysis and design, 37*(10), 761-775.

Buckle, I. G., & Liu, H. (1994). Critical loads of elastomeric isolators at high shear strain. In *Technical Report NCEER* (Vol. 94, pp. 4-85, 84-99): US National Center for Earthquake Engineering Research.

Carr, A. (2005). 3D RUAUMOKO: inelastic three-dimensional dynamic analysis program.

Celebi, M. (1996). Successful performance of a base-isolated hospital building during the 17 January 1994 Northridge earthquake. *The Structural Design of Tall Buildings, 5*(2), 95-109.

Celebi, M. (2002). *Seismic instrumentation of buildings (with emphasis on federal buildings)*. Retrieved from

Chang, C.-M., Lin, T.-K., & Chang, C.-W. (2018). Applications of neural network models for structural health monitoring based on derived modal properties. *Measurement, 129*, 457-470.

Christchurch City Council. (2016a). *166 Gloucester St. - Construction Documents*. Retrieved from

Christchurch City Council. (2016b). 166 Gloucester St. - Structural Drawings. In. Christchurch, New Zealand.

Constantinou, M., Caccese, J., & Harris, H. (1987). Frictional characteristics of Teflon–steel interfaces under dynamic conditions. *Earthquake engineering & structural dynamics, 15*(6), 751-759.

Constantinou, M., Mokha, A., & Reinhorn, A. (1990). Teflon bearings in base isolation II: Modeling. *Journal of structural engineering, 116*(2), 455-474.

Cremen, G., & Baker, J. W. (2018). Quantifying the benefits of building instruments to FEMA P-58 rapid post-earthquake damage and loss predictions. *Engineering Structures, 176*, 243-253.

Cutfield, M., Ma, Q., & Ryan, K. (2014). *Cost-benefit analysis of base isolated and conventional buildings: A case study.* Paper presented at the Proceedings of the 2014 New Zealand Society for Earthquake Engineering Conference, Paper O.

Deierlein, G., Krawinkler, H., & Cornell, C. (2003). *A Framework for Performance-Based Earthquake Engineering.* Paper presented at the Pacific Conference on Earthquake Engineering.

Deirlein, G., Krawinkler, H., & Cornell, C. (2003). *A framework for performance-based earthquake engineering.* Paper presented at the Proc., 2003 Pacific Conference on Earthquake Engineering.

Denison, D., Mallick, B., & Smith, A. (1998). Automatic Bayesian curve fitting. *Journal of the Royal Statistical Society: Series B (Statistical Methodology), 60*(2), 333-350.

Dhakal, R. P., MacRae, G. A., Pourali, A., & Paganotti, G. (2016). Seismic fragility of suspended ceiling systems used in NZ based on component tests.

Dhakal, R. P., Pourali, A., & Saha, S. K. (2016). Simplified seismic loss functions for suspended ceilings and drywall partitions. *Bulletin of the New Zealand Society for Earthquake Engineering, 49*(1), 64-78.

Dolce, M., Cardone, D., & Croatto, F. (2005). Frictional behavior of steel-PTFE interfaces for seismic isolation. *Bulletin of earthquake engineering, 3*(1), 75-99.

Dolce, M., Cardone, D., & Palermo, G. (2007). Seismic isolation of bridges using isolation systems based on flat sliding bearings. *Bulletin of earthquake engineering, 5*(4), 491-509.

Elwood, K., Marder, K., Pampanin, S., Ramirez, A. C., Kral, M., Smith, P., . . . Stannard, M. (2016). *Draft framework for assessing residual capacity of earthquake-damaged concrete buildings.* Paper presented at the

Proceedings of The New Zealand Society for Earthquake Engineering Annual Technical Conference.

Elwood, K., Marquis, F., & Kim, J. (2015). *Post-earthquake assessment and repairability of RC buildings: lessons from Canterbury and emerging challenges.* Paper presented at the Proceedings of the tenth pacific conference on earthquake engineering, Sydney, Australia.

Fahjan, Y., Kubin, J., & Tan, M. (2010). *Nonlinear analysis methods for reinforced concrete buildings with shear walls.* Paper presented at the 14th European Conference on Earthquake Engineering.

Farrar, C. R., & Worden, K. (2006). An introduction to structural health monitoring. *Philosophical Transactions of the Royal Society A: Mathematical, Physical and Engineering Sciences, 365*(1851), 303-315.

FEMA. (2012). *Seismic Performance Assessment of Buildings, Volume 3 – Supporting Electronic Materials and Background Documentation*.

Friswell, M., & Mottershead, J. E. (2013). *Finite element model updating in structural dynamics* (Vol. 38): Springer Science & Business Media.

Giberson, M. F. (1969). Two nonlinear beams with definitions of ductility. *Journal of the Structural Division*.

Homan, J. (2018). What is the Difference between Low & High Cycle Fatigue? Retrieved from https://www.fatec-engineering.com/2018/08/23/what-is-the-difference-between-low-high-cycle-fatigue/

Iwabe, N., Takayama, M., Kani, N., & Wada, A. (2000). *Experimental study on the effect of tension for rubber bearings.* Paper presented at the Proceedings: 12th World Conference on Earthquake Engineering.

Kam, W. Y., Pampanin, S., & Elwood, K. (2011). Seismic performance of reinforced concrete buildings in the 22 February Christchurch (Lyttelton) earthquake. *Bulletin of the New Zealand Society for Earthquake Engineering, 44*(4), 239-278.

Koh, C., Tee, K., & Quek, S. (2006). Condensed model identification and recovery for structural damage assessment. *Journal of structural engineering, 132*(12), 2018-2026.

Koh, C. G., & Kelly, J. M. (1988). A simple mechanical model for elastomeric bearings used in base isolation. *International journal of mechanical sciences, 30*(12), 933-943.

Kwan, A. (1993). Improved wide-column-frame analogy for shear/core wall analysis. *Journal of structural engineering, 119*(2), 420-437.

Lamonaca, F., Sciammarella, P., Scuro, C., Carnì, D., & Olivito, R. (2018). *Internet of things for structural health monitoring.* Paper presented at the 2018 Workshop on Metrology for Industry 4.0 and IoT.

Lau, S. L., & David, K. (2010). *Movement recognition using the accelerometer in smartphones.* Paper presented at the 2010 Future Network & Mobile Summit.

Limongelli, M. P. (2003). Optimal location of sensors for reconstruction of seismic responses through spline function interpolation. *Earthquake engineering & structural dynamics, 32*(7), 1055-1074.

Livigni, F. (2016). Turn your smartphone into a sensor and an actuator. Retrieved from https://developer.ibm.com/tutorials/iot-smartphone-sensor-actuator-bluemix-apps-trs/

Loporcaro, G., Pampanin, S., & Kral, M. (2015). *Experimental validation of "the hardness method" to estimate the residual ductility of plastically deformed steel reinforcement.* Paper presented at the Proc., 2015 New Zealand Society of Earthquake Engineering Conference.

Marquis, F., Kim, J. J., Elwood, K. J., & Chang, S. E. (2017). Understanding post-earthquake decisions on multi-storey concrete buildings in Christchurch, New Zealand. *Bulletin of earthquake engineering, 15*(2), 731-758.

Mazars, J., Kotronis, P., Ragueneau, F., & Casaux, G. (2006). Using multifiber beams to account for shear and torsion: Applications to concrete structural elements. *Computer Methods in Applied Mechanics and Engineering, 195*(52), 7264-7281.

Mokha, A., Constantinou, M., & Reinhorn, A. (1990). Teflon bearings in base isolation I: testing. *Journal of structural engineering, 116*(2), 438-454.

Mosqueda, G. (2016). Interior Cold-framed Steel Framed Gypsum Partition Walls. *Background Document FEMA P-58/BD-3.9.32*.

Nagarajaiah, S., Reinhorn, A. M., & Constantinou, M. C. (1991). 3D-BASIS-nonlinear dynamic analysis of three-dimensional base isolated structures: Part II.

Newmark, N. M. (1959). *A method of computation for structural dynamics*.

O'Reilly, G. J., & Sullivan, T. J. (2016). Fragility functions for eccentrically braced steel frame structures. *Earthquakes and Structures, 10*(2), 367-388.

Oliver, S. (2016). Armagh Apartments Structural Project Features Report. In: Holmes Consulting Group LP.

Pekelnicky, R., & Poland, C. (2012). *ASCE 41-13: Seismic Evaluation and Retrofit Rehabilitation of Existing Buildings.* Paper presented at the Proceedings, SEAOC 2012 Convention.

Pietra, D., & Park, A. (2017). *Behaviour and Modelling of Lead-Rubber Bearings Subjected to Tensile Actions.* Paper presented at the Proceedings from the 16th World Conference on Earthquake Engineering, Santiago Chile, Paper.

Porter, K., Mitrani-Reiser, J., & Beck, J. L. (2006). Near-real-time loss estimation for instrumented buildings. *The Structural Design of Tall and Special Buildings, 15*(1), 3-20.

Porter, K. A. (2003). *An overview of PEER's performance-based earthquake engineering methodology.* Paper presented at the Proceedings of ninth international conference on applications of statistics and probability in civil engineering.

Priestley, M. (2003). *Myths and Fallacies in Earthquake Engineering, Revisited: The Ninth Mallet Milne Lecture, 2003*: Istituto Universitario di Studi Superiori di Pavia.

Ramirez, C. M. (2009). *Building-specific loss estimation methods & tools for simplified performance-based earthquake engineering*: Stanford University.
Resene Paints Ltd. (2020). Average rates for painting. In Resene Group (Ed.). New Zealand.
Rosenblatt, F. (1958). The perceptron: a probabilistic model for information storage and organization in the brain. *Psychological review, 65*(6), 386.
Ryu, K. P., & Reinhorn, A. M. (2019). Experimental study of large area suspended ceilings. *Journal of Earthquake Engineering, 23*(6), 1001-1032.
Sakkas, G., & Sakellariou, N. (2018). An algorithm developed in Matlab for the automatic selection of cut-off frequencies, in the correction of strong motion data. *Acta Geophysica, 66*(4), 425-448.
Salawu, O., & Williams, C. (1993). *Structural Damage Detection Using Experimental Modal Analysis A Comparison of Some Methods.* Paper presented at the PROCEEDINGS OF THE INTERNATIONAL MODAL ANALYSIS CONFERENCE.
Sanchez, J., Masroor, A., Mosqueda, G., & Ryan, K. (2012). Static and dynamic stability of elastomeric bearings for seismic protection of structures. *Journal of structural engineering, 139*(7), 1149-1159.
SAP, C. (2013). Computers and structures Inc. *Berkeley, CA, USA*.
Soroushian, S. (2016). Acoustical Tile or Lay-in Panel Suspended Ceilings. *Background Document FEMA P-58/BD-3.9.31*.
Standards New Zealand. (2004). NZS1170. 5: 2004. In *Struct. Des. Actions-Part* (Vol. 5).
Standards New Zealand. (2006). NZS3101:1: 2006. In.
Su, L., Ahmadi, G., & Tadjbakhsh, I. G. (1990). A comparative study of performances of various base isolation systems, Part II: Sensitivity analysis. *Earthquake engineering & structural dynamics, 19*(1), 21-33.
Sullivan, T. (2020). Post-Earthquake Reparability of Buildings: The Role of Non-Structural Elements. *Structural Engineering International, 30*(2), 217-223.
Sullivan, T., Welch, D. P., & Calvi, G. M. (2014). Simplified seismic performance assessment and implications for seismic design. *Earthquake Engineering and Engineering Vibration, 13*(1), 95-122.
Takayama, M., Oka, K., & Kato, R. (2004). *The tensile tests of natural rubber bearing focused on the effect of the steel flange plates.* Paper presented at the 13th World Conference on Earthquake Engineering.
Warn, G. P., & Ryan, K. L. (2012). A review of seismic isolation for buildings: historical development and research needs. *Buildings, 2*(3), 300-325.
Worden, K., & Manson, G. (2006). The application of machine learning to structural health monitoring. *Philosophical Transactions of the Royal Society A: Mathematical, Physical and Engineering Sciences, 365*(1851), 515-537.
Yang, T., & Zhang, H. (2018). Seismic safety assessment of base isolated buildings using lead-rubber bearings. *Earthquake Spectra*.

Yeow, T., Orumiyehei, A., Sullivan, T., MacRae, G., Clifton, G., & Elwood, K. (2018). Seismic performance of steel friction connections considering direct-repair costs. *Bulletin of earthquake engineering, 16*(12), 5963-5993.

Yeow, T., Sullivan, T., & Elwood, K. (2018). Evaluation of fragility functions with potential relevance for use in New Zealand. *Bulletin of the New Zealand Society for Earthquake Engineering, 51*(3), 127-144.

Ying, Y., Garrett Jr, J. H., Oppenheim, I. J., Soibelman, L., Harley, J. B., Shi, J., & Jin, Y. (2012). Toward data-driven structural health monitoring: application of machine learning and signal processing to damage detection. *Journal of Computing in Civil Engineering, 27*(6), 667-680.

Zhang, Y., Burton, H. V., Sun, H., & Shokrabadi, M. (2018). A machine learning framework for assessing post-earthquake structural safety. *Structural Safety, 72*, 1-16.

Appendix A

Structural analysis results for other intensity levels

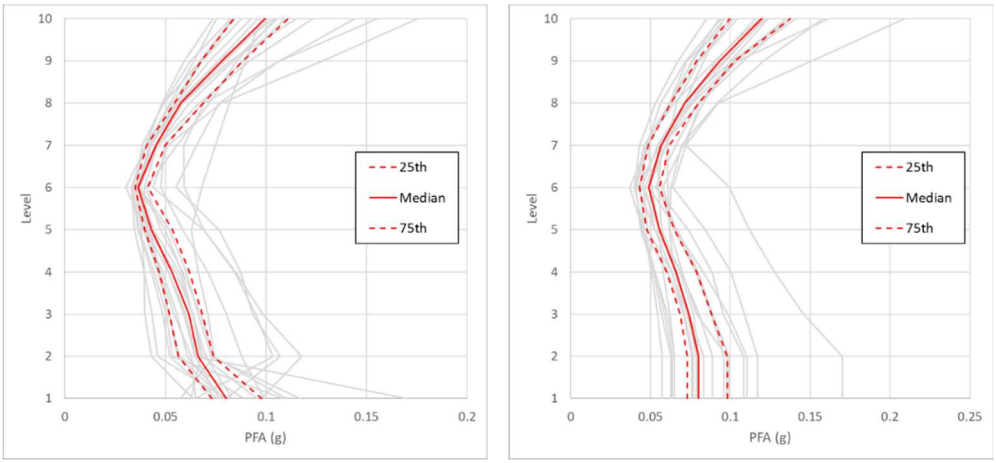

(a) (b)

Figure A1. Peak floor accelerations (PFA) of the control structural model subjected to 20 ground motions for the intensity levels of (a) 1 in 30 years and (b) 1 in 75 years

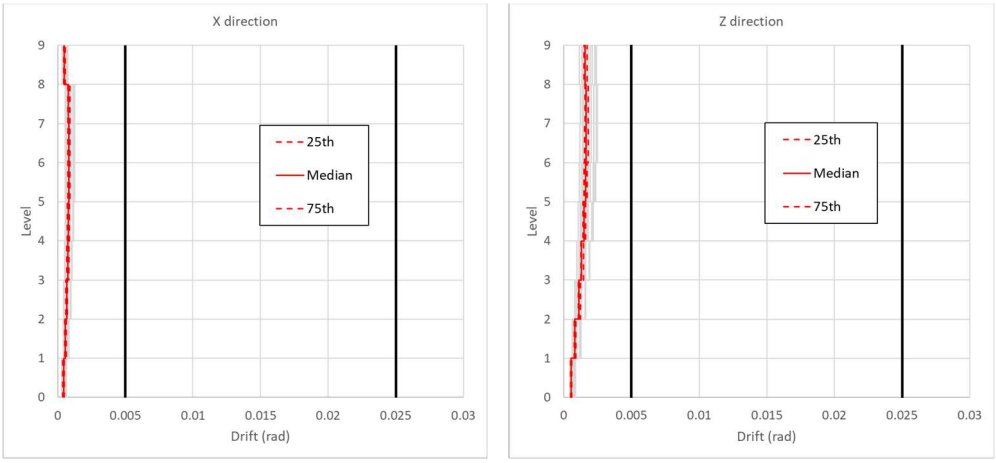

(a) (b)

Figure A2. Inter-storey drift ratio (IDR) of the control structural model subjected to 20 ground motions for the intensity level of 1 in 30 years in the (a) X-direction and (b) Z-direction

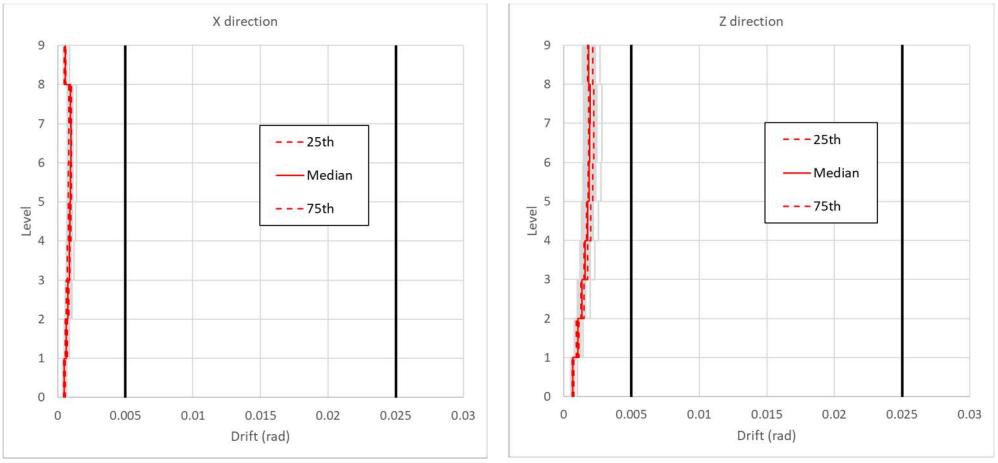

(a) (b)

Figure A3. Inter-storey drift ratio (IDR) of the control structural model subjected to 20 ground motions for the intensity level of 1 in 75 years in the (a) X-direction and (b) Z-direction

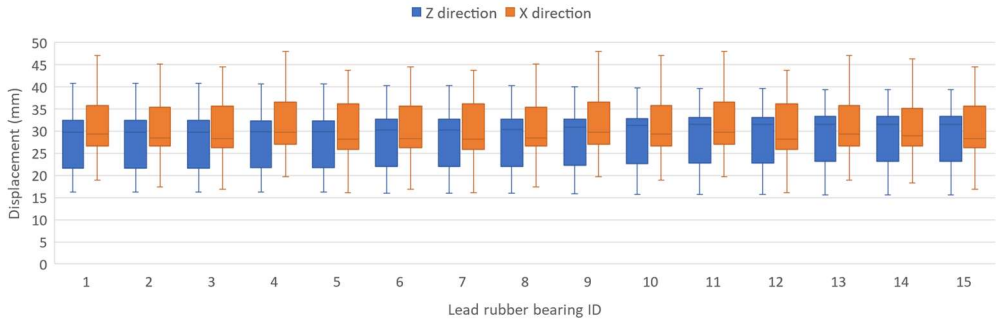

(a)

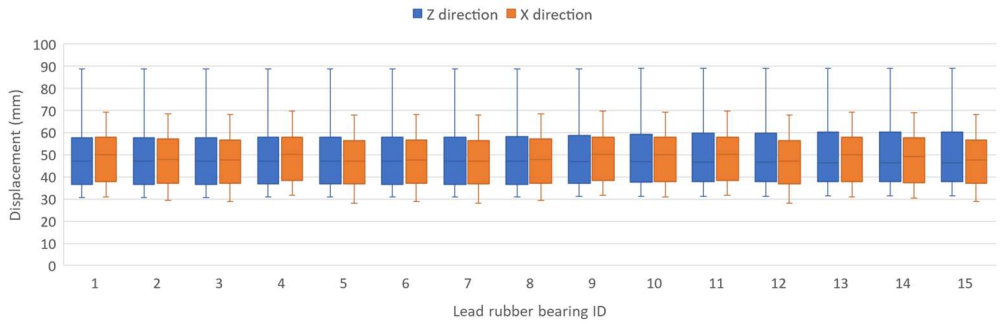

(b)

Figure A4. Maximum displacements of the lead rubber bearing (LRB) in the two horizontal directions for the intensity levels of (a) 1 in 30 years and (b) 1 in 75 years

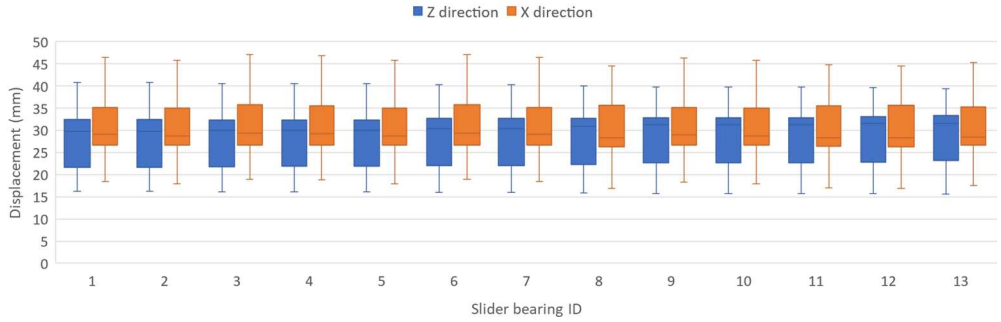

(a)

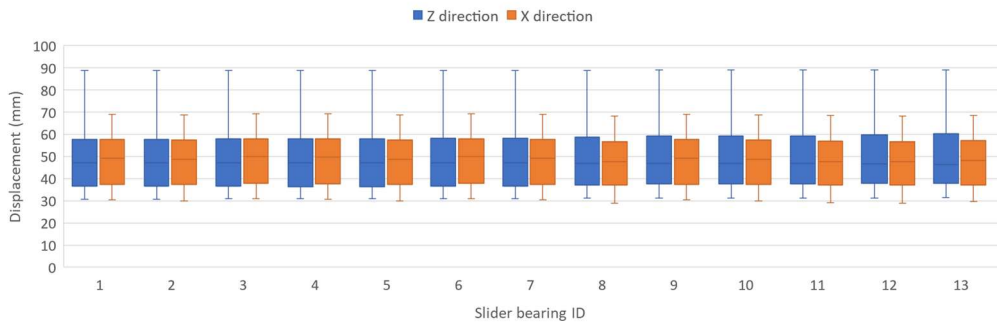

(b)

Figure A5. Maximum displacements of the slider bearing (SB) in the two horizontal directions for the intensity levels of (a) 1 in 30 years and (b) 1 in 75 years

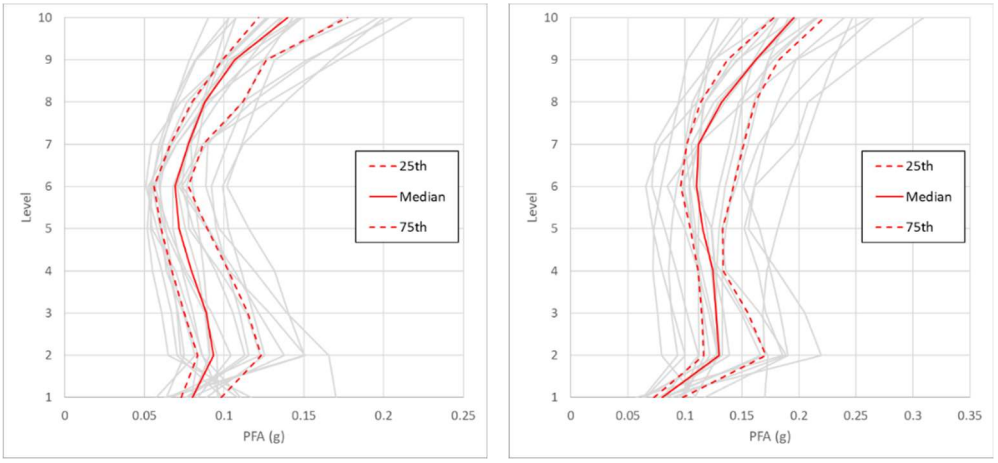

(a) (b)

Figure A6. Peak floor accelerations (PFA) of the control structural model subjected to 20 ground motions for the intensity levels of (a) 1 in 250 years and (b) 1 in 975 years

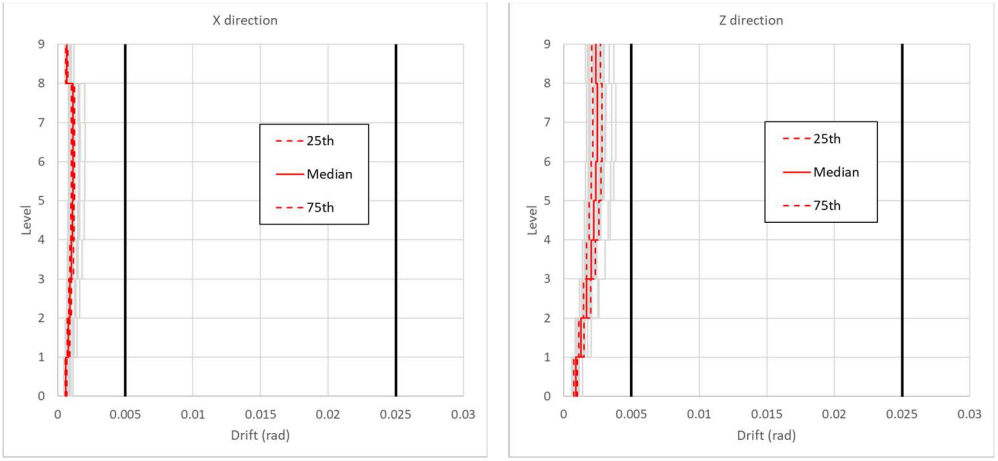

(a) (b)

Figure A7. Inter-storey drift ratio (IDR) of the control structural model subjected to 20 ground motions for the intensity level of 1 in 250 years in the (a) X-direction and (b) Z-direction

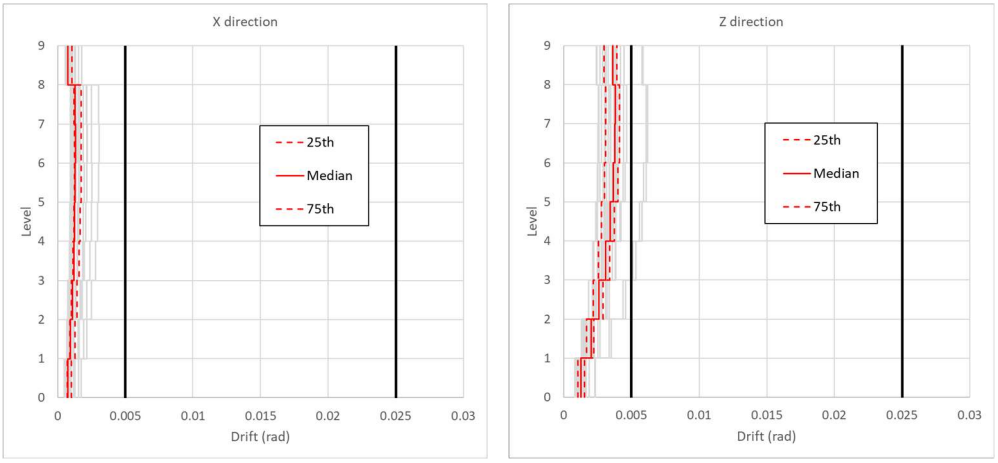

(a) (b)

Figure A8. Inter-storey drift ratio (IDR) of the control structural model subjected to 20 ground motions for the intensity level of 1 in 975 years in the (a) X-direction and (b) Z-direction

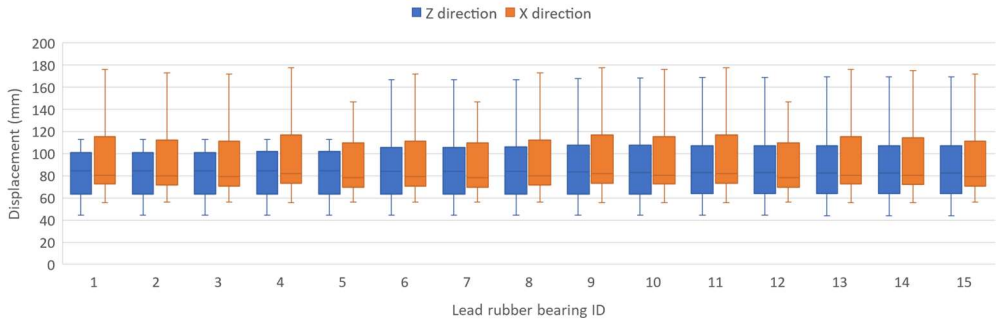

(a)

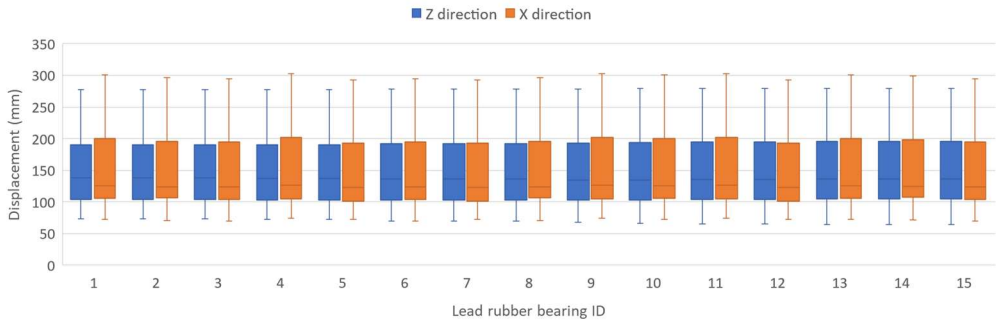

(b)

Figure A9. Maximum displacements of the lead rubber bearing (LRB) in the two horizontal directions for the intensity levels of (a) 1 in 250 years and (b) 1 in 975 years

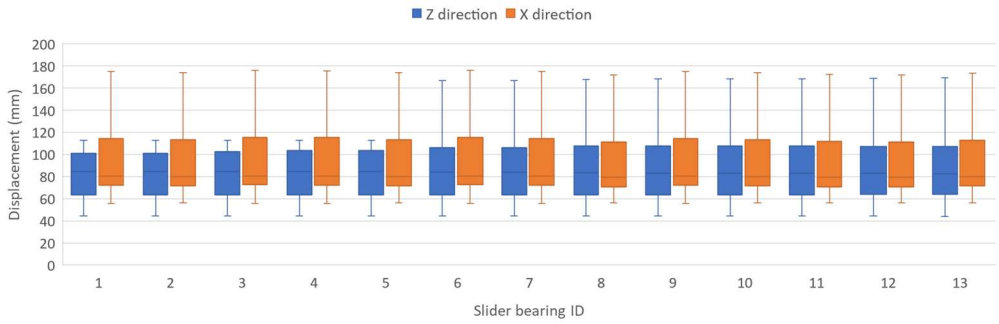

(a)

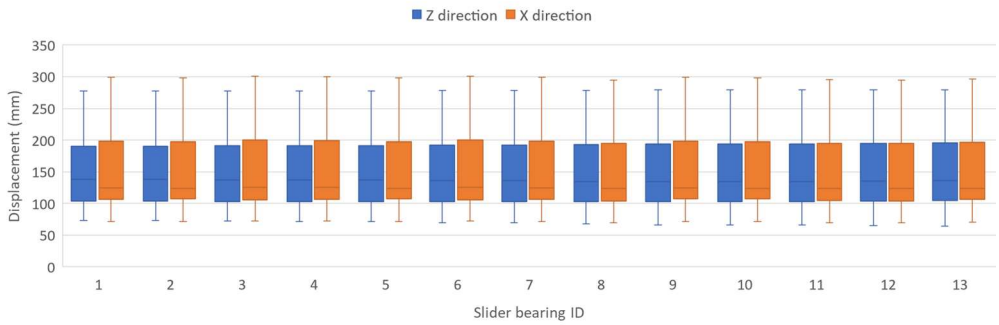

(b)

Figure A10. Maximum displacements of the slider bearing (SB) in the two horizontal directions for the intensity levels of (a) 1 in 250 years and (b) 1 in 975 years

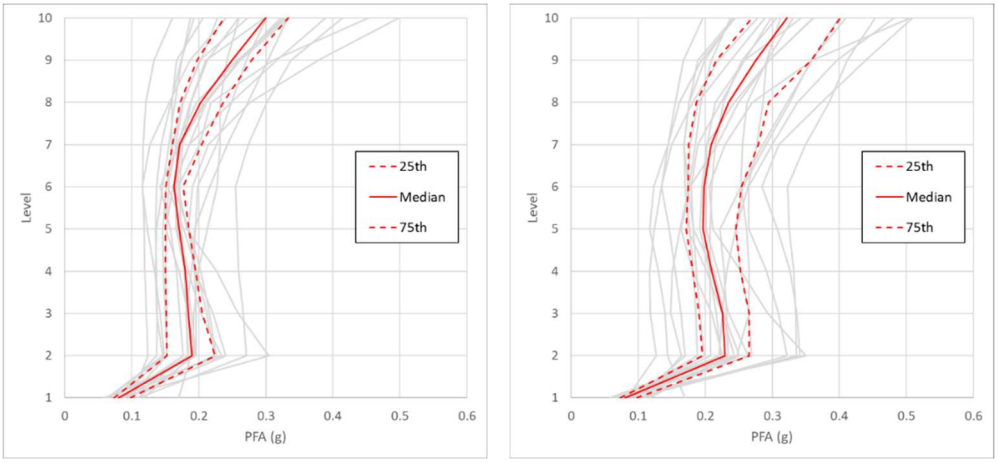

(a) (b)

Figure A11. Peak floor accelerations (PFA) of the control structural model subjected to 20 ground motions for the intensity levels of (a) 1 in 4,975 years and (b) 1 in 10,000 years

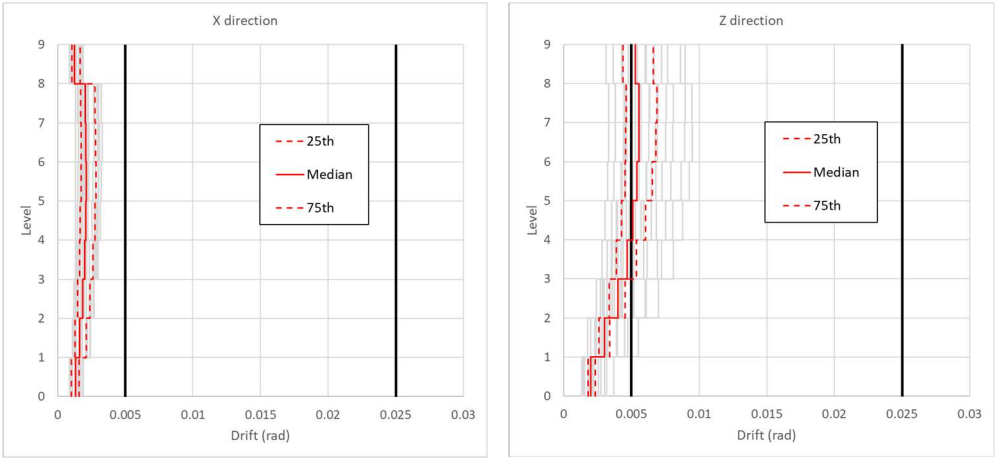

(a) (b)

Figure A12. Inter-storey drift ratio (IDR) of the control structural model subjected to 20 ground motions for the intensity level of 1 in 4,975 years in the (a) X-direction and (b) Z-direction

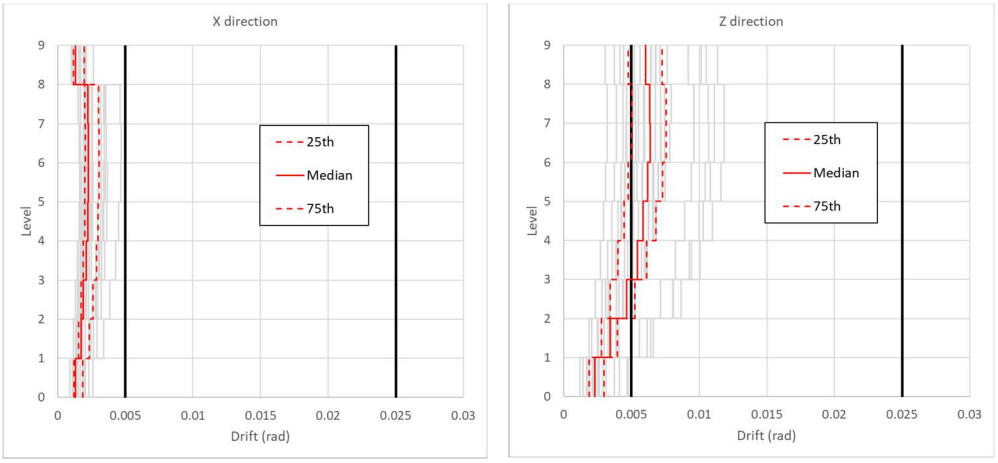

(a) (b)

Figure A13. Inter-storey drift ratio (IDR) of the control structural model subjected to 20 ground motions for the intensity level of 1 in 10,000years in the (a) X-direction and (b) Z-direction

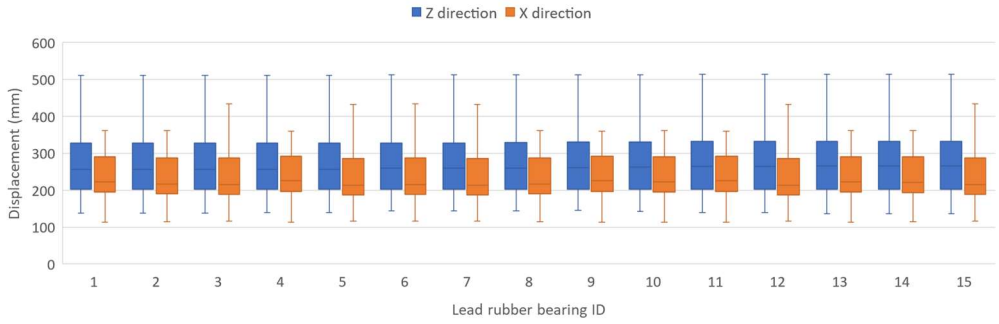

(a)

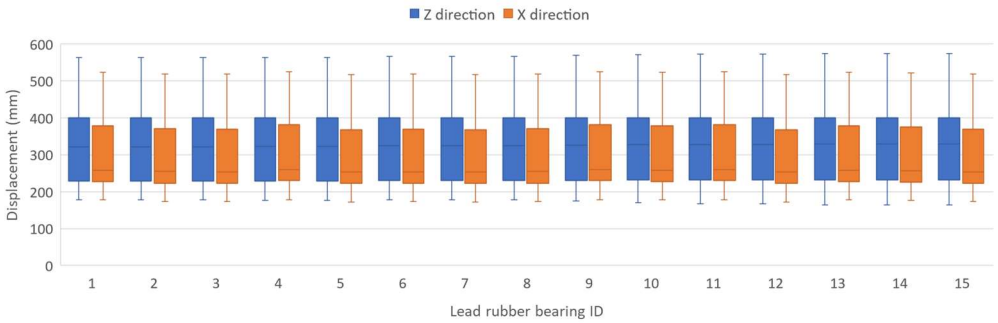

(b)

Figure A14. Maximum displacements of the lead rubber bearing (LRB) in the two horizontal directions for the intensity levels of (a) 1 in 4,975 years and (b) 1 in 10,000years

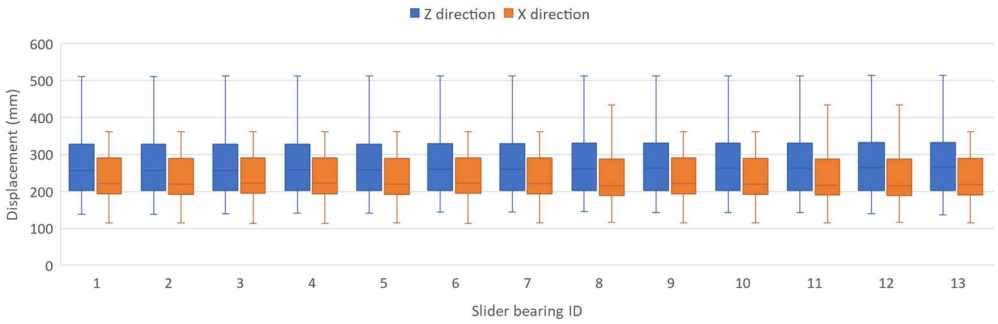

(a)

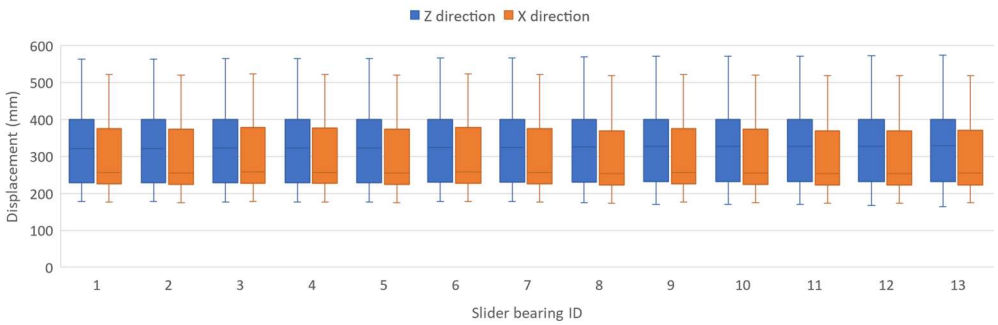

(b)

Figure A15. Maximum displacements of the slider bearing (SB) in the two horizontal directions for the intensity levels of (a) 1 in 4,975 years and (b) 1 in 10,000 years

Appendix B

Ruaumoko 3D input file

The model of the apartment building developed in Ruaumoko 3D (Carr, 2005) is shown below.

```
Base-isolated Apartment Building 63 Armagh St, Units: kN, m, sec.
2 1 0 2 2 2
1 0 0 0 0 1 0 0 0
539 796 197 20  1   5   9.81    5   5   0.01    1000    1
0 100 0 1 0.5 0.5 0.5 0 10 2 1 0
D D D D D D
0 0

NODES
1   9.7 15.75   11.242  0   1   0   1   0   1   0   0   0
2   10.4948 15.75   11.1525 1   2   1   1   1   1   1   0   0
3   10.4948 18.98   11.1525 0   2   0   1   0   1   2   0   0
4   10.0099 18.98   11.2878 1   2   1   1   1   1   3   0   0
5   10.0099 22.04   11.2878 0   2   0   1   0   1   4   0   0
6   10.0123 22.04   11.2961 1   2   1   1   1   1   5   0   0
7   10.0123 25.27   11.2961 0   2   0   1   0   1   6   0   0
8   10.0123 25.27   11.2961 1   2   1   1   1   1   7   0   0
9   10.0123 28.5    11.2961 0   2   0   1   0   1   8   0   0
10  10.0125 28.5    11.2964 1   2   1   1   1   1   9   0   0
11  10.0125 31.73   11.2964 0   2   0   1   0   1   10  0   0
12  10.0125 31.73   11.2964 1   2   1   1   1   1   11  0   0
13  10.0125 34.96   11.2964 0   2   0   1   0   1   12  0   0
14  9.988   34.96   11.3064 1   2   1   1   1   1   13  0   0
15  9.988   38.19   11.3064 0   2   0   1   0   1   14  0   0
16  9.9203  38.19   11.247  1   2   1   1   1   1   15  0   0
17  9.9203  41.42   11.247  0   2   0   1   0   1   16  0   0
18  9.8819  41.42   11.0197 1   2   1   1   1   1   17  0   0
19  9.8819  45.21   11.0197 0   2   0   1   0   1   18  0   0
20  1.36    15.74   4.6 1   1   1   1   1   1   0   0   0
21  1.36    15.75   4.6 2   0   2   0   2   0   1   0   0
22  1.36    15.74   14.59   1   1   1   1   1   1   0   0   0
23  1.36    15.75   14.59   2   0   2   0   2   0   1   0   0
24  1.36    15.74   17.99   1   1   1   1   1   1   0   0   0
25  1.36    15.75   17.99   2   0   2   0   2   0   1   0   0
26  3.235   15.74   0   1   1   1   1   1   1   0   0   0
27  3.235   15.75   0   2   0   2   0   2   0   1   0   0
28  3.235   15.74   22.59   1   1   1   1   1   1   0   0   0
29  3.235   15.75   22.59   2   0   2   0   2   0   1   0   0
30  7.715   15.74   17.99   1   1   1   1   1   1   0   0   0
31  7.715   15.75   17.99   2   0   2   0   2   0   1   0   0
32  7.715   15.74   22.59   1   1   1   1   1   1   0   0   0
33  7.715   15.75   22.59   2   0   2   0   2   0   1   0   0
34  8.19    15.74   14.59   1   1   1   1   1   1   0   0   0
35  8.19    15.75   14.59   2   0   2   0   2   0   1   0   0
36  11.405  15.74   0   1   1   1   1   1   1   0   0   0
37  11.405  15.75   0   2   0   2   0   2   0   1   0   0
38  13.86   15.74   4.6 1   1   1   1   1   1   0   0   0
39  13.86   15.75   4.6 2   0   2   0   2   0   1   0   0
40  15.885  15.74   0   1   1   1   1   1   1   0   0   0
41  15.885  15.75   0   2   0   2   0   2   0   1   0   0
42  15.885  15.74   22.59   1   1   1   1   1   1   0   0   0
43  15.885  15.75   22.59   2   0   2   0   2   0   1   0   0
44  18.5    15.74   4.6 1   1   1   1   1   1   0   0   0
45  18.5    15.75   4.6 2   0   2   0   2   0   1   0   0
46  18.5    15.74   8.46    1   1   1   1   1   1   0   0   0
47  18.5    15.75   8.46    2   0   2   0   2   0   1   0   0
48  18.5    15.74   17.99   1   1   1   1   1   1   0   0   0
49  18.5    15.75   17.99   2   0   2   0   2   0   1   0   0
50  1.36    15.74   7.86    1   1   1   1   1   1   0   0   0
51  1.36    15.745  7.86    2   0   2   1   2   1   1   0   0
52  1.36    15.74   11.07   1   1   1   1   1   1   0   0   0
53  1.36    15.745  11.07   2   0   2   1   2   1   1   0   0
```

54	4.015	15.74	4.6 1	1	1	1	1	1	0	0	0	
55	4.015	15.745	4.6 2	0	2	1	2	1	1	0	0	
56	5.11	15.74	5.8 1	1	1	1	1	1	0	0	0	
57	5.11	15.745	5.8 2	0	2	1	2	1	1	0	0	
58	5.11	15.74	11.07	1	1	1	1	1	1	0	0	0
59	5.11	15.745	11.07	2	0	2	1	2	1	1	0	0
60	8.19	15.74	4.6 1	1	1	1	1	1	0	0	0	
61	8.19	15.745	4.6 2	0	2	1	2	1	1	0	0	
62	8.19	15.74	7.86	1	1	1	1	1	1	0	0	0
63	8.19	15.745	7.86	2	0	2	1	2	1	1	0	0
64	11.405	15.74	17.99	1	1	1	1	1	1	0	0	0
65	11.405	15.745	17.99	2	0	2	1	2	1	1	0	0
66	13.86	15.74	8.46	1	1	1	1	1	1	0	0	0
67	13.86	15.745	8.46	2	0	2	1	2	1	1	0	0
68	13.86	15.74	11.07	1	1	1	1	1	1	0	0	0
69	13.86	15.745	11.07	2	0	2	1	2	1	1	0	0
70	13.86	15.74	16.79	1	1	1	1	1	1	0	0	0
71	13.86	15.745	16.79	2	0	2	1	2	1	1	0	0
72	15.885	15.74	17.99	1	1	1	1	1	1	0	0	0
73	15.885	15.745	17.99	2	0	2	1	2	1	1	0	0
74	18.5	15.74	13.71	1	1	1	1	1	1	0	0	0
75	18.5	15.745	13.71	2	0	2	1	2	1	1	0	0
76	1.36	15.75	7.86	2	0	2	0	2	0	1	0	0
77	1.36	15.75	11.07	2	0	2	0	2	0	1	0	0
78	4.015	15.75	4.6 2	0	2	0	2	0	1	0	0	
79	5.11	15.75	5.8 2	0	2	0	2	0	1	0	0	
80	5.11	15.75	11.07	2	0	2	0	2	0	1	0	0
81	8.19	15.75	4.6 2	0	2	0	2	0	1	0	0	
82	8.19	15.75	7.86	2	0	2	0	2	0	1	0	0
83	11.405	15.75	17.99	2	0	2	0	2	0	1	0	0
84	13.86	15.75	8.46	2	0	2	0	2	0	1	0	0
85	13.86	15.75	11.07	2	0	2	0	2	0	1	0	0
86	13.86	15.75	16.79	2	0	2	0	2	0	1	0	0
87	15.885	15.75	17.99	2	0	2	0	2	0	1	0	0
88	18.5	15.75	13.71	2	0	2	0	2	0	1	0	0
89	3.235	15.75	4.6 2	0	2	0	2	0	1	0	0	
90	3.235	15.75	17.99	2	0	2	0	2	0	1	0	0
91	15.885	15.75	4.6 2	0	2	0	2	0	1	0	0	
92	8.19	15.75	13.71	2	0	2	0	2	0	1	0	0
93	8.19	15.75	17.99	2	0	2	0	2	0	1	0	0
94	11.405	15.75	13.71	2	0	2	0	2	0	1	0	0
95	11.405	15.75	4.6 2	0	2	0	2	0	1	0	0	
96	18.5	15.75	11.07	2	0	2	0	2	0	1	0	0
97	9.84	15.75	8.0454	2	0	2	0	2	0	1	0	0
98	11.18	15.75	8.196	2	0	2	0	2	0	1	0	0
99	13.53	15.75	8.46	2	0	2	0	2	0	1	0	0
100	5.11	15.75	14.59	2	0	2	0	2	0	1	0	0
101	5.27	15.75	17.99	2	0	2	0	2	0	1	0	0
102	5.59	15.75	0 2	0	2	0	2	0	1	0	0	
103	7.86	15.75	0 2	0	2	0	2	0	1	0	0	
104	11.25	15.75	22.59	2	0	2	0	2	0	1	0	0
105	13.53	15.75	4.6 2	0	2	0	2	0	1	0	0	
106	4	15.75	11.07	0	0	0	0	0	0	0	0	
107	7.715	15.75	7.86	2	0	2	0	2	0	1	0	0
108	5.11	15.75	7.86	2	0	2	0	2	0	1	0	0
109	7.715	15.75	14.59	2	0	2	0	2	0	1	0	0
110	9.7 15.75	13.71	2	0	2	0	2	0	1	0	0	
111	9.84	15.75	13.71	2	0	2	0	2	0	1	0	0
112	11.18	15.75	13.71	2	0	2	0	2	0	1	0	0
113	13.86	15.75	13.71	2	0	2	0	2	0	1	0	0
114	16.6	15.75	17.99	0	0	0	0	0	0	0	0	0
115	9.7 15.75	17.99	2	0	2	0	2	0	1	0	0	
116	13.86	15.75	17.99	2	0	2	0	2	0	1	0	0
117	5.11	15.75	4.6 2	0	2	0	2	0	1	0	0	
118	9.7 15.75	15.85	2	0	2	0	2	0	1	0	0	
119	9.84	15.75	8.73	2	0	2	0	2	0	1	0	0
120	5.11	15.75	8.575	2	0	2	0	2	0	1	0	0
121	5.54	15.75	8.31	2	0	2	0	2	0	1	0	0
122	5.54	15.75	8.575	2	2	2	2	2	2	120	0	0
123	13.86	15.75	13.4	2	2	2	2	2	2	128	0	0

```
124 3.29    15.75   7.86    2   0   2   0   2   0   1   0   0
125 3.29    15.75   8.31    2   2   2   2   2   2   124 0   0
126 6.495   15.75   4.6 2   0   2   0   2   0   1   0   0
127 16.05   15.75   13.4    2   0   2   0   2   0   1   0   0
128 13.43   15.75   13.4    2   0   2   0   2   0   1   0   0
129 16.05   15.75   13.71   2   2   2   2   2   2   127 0   0
130 2.1 15.75   11.07   2   0   2   0   2   0   1   0   0
131 16.05   18.98   13.4    2   0   2   0   2   0   3   0   0
132 16.05   22.04   13.4    2   0   2   0   2   0   5   0   0
133 16.05   25.27   13.4    2   0   2   0   2   0   7   0   0
134 16.05   28.5    13.4    2   0   2   0   2   0   9   0   0
135 16.05   31.73   13.4    2   0   2   0   2   0   11  0   0
136 16.05   34.96   13.4    2   0   2   0   2   0   13  0   0
137 16.05   38.19   13.4    2   0   2   0   2   0   15  0   0
138 16.05   41.42   13.4    2   0   2   0   2   0   17  0   0
139 13.43   18.98   13.4    2   0   2   0   2   0   3   0   0
140 13.43   22.04   13.4    2   0   2   0   2   0   5   0   0
141 13.43   25.27   13.4    2   0   2   0   2   0   7   0   0
142 13.43   28.5    13.4    2   0   2   0   2   0   9   0   0
143 13.43   31.73   13.4    2   0   2   0   2   0   11  0   0
144 13.43   34.96   13.4    2   0   2   0   2   0   13  0   0
145 13.43   38.19   13.4    2   0   2   0   2   0   15  0   0
146 13.43   41.42   13.4    2   0   2   0   2   0   17  0   0
147 13.86   18.98   17.99   2   0   2   0   2   0   3   0   0
148 15.885  22.04   17.99   2   0   2   0   2   0   5   0   0
149 15.885  18.98   17.99   2   0   2   0   2   0   3   0   0
150 12.4075 22.04   17.99   2   0   2   0   2   0   5   0   0
151 12.4075 18.98   17.99   2   0   2   0   2   0   3   0   0
152 13.86   25.27   17.99   2   0   2   0   2   0   7   0   0
153 13.86   22.04   17.99   2   0   2   0   2   0   5   0   0
154 13.86   28.5    17.99   2   0   2   0   2   0   9   0   0
155 13.86   31.73   17.99   2   0   2   0   2   0   11  0   0
156 13.86   34.96   17.99   2   0   2   0   2   0   13  0   0
157 13.86   38.19   17.99   2   0   2   0   2   0   15  0   0
158 6.495   18.98   4.6 2   0   2   0   2   0   3   0   0
159 3.235   18.98   4.6 2   0   2   0   2   0   3   0   0
160 8.195   22.04   4.6 2   0   2   0   2   0   5   0   0
161 8.195   18.98   4.6 2   0   2   0   2   0   3   0   0
162 4.9 22.04   4.6 2   0   2   0   2   0   5   0   0
163 4.9 18.98   4.6 2   0   2   0   2   0   3   0   0
164 5.69    25.27   4.6 2   0   2   0   2   0   7   0   0
165 5.69    22.04   4.6 2   0   2   0   2   0   5   0   0
166 5.69    28.5    4.6 2   0   2   0   2   0   9   0   0
167 5.69    31.73   4.6 2   0   2   0   2   0   11  0   0
168 5.69    34.96   4.6 2   0   2   0   2   0   13  0   0
169 5.69    38.19   4.6 2   0   2   0   2   0   15  0   0
170 3.29    18.98   8.31    2   0   2   0   2   0   3   0   0
171 3.29    22.04   8.31    2   0   2   0   2   0   5   0   0
172 3.29    25.27   8.31    2   0   2   0   2   0   7   0   0
173 3.29    28.5    8.31    2   0   2   0   2   0   9   0   0
174 3.29    31.73   8.31    2   0   2   0   2   0   11  0   0
175 3.29    34.96   8.31    2   0   2   0   2   0   13  0   0
176 3.29    38.19   8.31    2   0   2   0   2   0   15  0   0
177 3.29    41.42   8.31    2   0   2   0   2   0   17  0   0
178 5.54    18.98   8.575   2   0   2   0   2   0   3   0   0
179 5.54    22.04   8.575   2   0   2   0   2   0   5   0   0
180 5.54    25.27   8.575   2   0   2   0   2   0   7   0   0
181 5.54    28.5    8.575   2   0   2   0   2   0   9   0   0
182 5.54    31.73   8.575   2   0   2   0   2   0   11  0   0
183 5.54    34.96   8.575   2   0   2   0   2   0   13  0   0
184 5.54    38.19   8.575   2   0   2   0   2   0   15  0   0
185 5.54    41.42   8.575   2   0   2   0   2   0   17  0   0
186 2.1 18.98   11.145  2   0   2   0   2   0   3   0   0
187 2.1 15.75   11.145  2   2   2   2   2   2   130 0   0
188 2.1 22.04   11.145  2   0   2   0   2   0   5   0   0
189 2.1 25.27   11.145  2   0   2   0   2   0   7   0   0
190 2.1 28.5    11.145  2   0   2   0   2   0   9   0   0
191 2.1 31.73   11.145  2   0   2   0   2   0   11  0   0
192 2.1 34.96   11.145  2   0   2   0   2   0   13  0   0
193 2.1 38.19   11.145  2   0   2   0   2   0   15  0   0
194 2.1 41.42   11.145  2   0   2   0   2   0   17  0   0
```

195	5.54	18.98	8.31	2	0	2	0	2	0	3	0	0
196	13.43	18.98	10.35	2	0	2	0	2	0	3	0	0
197	13.43	18.98	14.59	2	0	2	0	2	0	3	0	0
198	13.43	18.98	16.79	2	0	2	0	2	0	3	0	0
199	13.53	18.98	10.35	2	0	2	0	2	0	3	0	0
200	5.54	22.04	8.31	2	0	2	0	2	0	5	0	0
201	5.54	22.04	11.07	2	0	2	0	2	0	5	0	0
202	13.43	22.04	10.35	2	0	2	0	2	0	5	0	0
203	13.43	22.04	14.59	2	0	2	0	2	0	5	0	0
204	5.54	25.27	8.31	2	0	2	0	2	0	7	0	0
205	5.54	25.27	11.07	2	0	2	0	2	0	7	0	0
206	13.43	25.27	10.35	2	0	2	0	2	0	7	0	0
207	13.43	25.27	14.59	2	0	2	0	2	0	7	0	0
208	5.54	28.5	8.31	2	0	2	0	2	0	9	0	0
209	5.54	28.5	11.07	2	0	2	0	2	0	9	0	0
210	13.43	28.5	10.35	2	0	2	0	2	0	9	0	0
211	13.43	28.5	14.59	2	0	2	0	2	0	9	0	0
212	5.54	31.73	8.31	2	0	2	0	2	0	11	0	0
213	5.54	31.73	11.07	2	0	2	0	2	0	11	0	0
214	13.43	31.73	10.35	2	0	2	0	2	0	11	0	0
215	13.43	31.73	14.59	2	0	2	0	2	0	11	0	0
216	5.54	34.96	8.31	2	0	2	0	2	0	13	0	0
217	5.54	34.96	11.07	2	0	2	0	2	0	13	0	0
218	13.43	34.96	10.35	2	0	2	0	2	0	13	0	0
219	13.43	34.96	14.59	2	0	2	0	2	0	13	0	0
220	5.54	38.19	8.31	2	0	2	0	2	0	15	0	0
221	5.54	38.19	11.07	2	0	2	0	2	0	15	0	0
222	13.43	38.19	10.35	2	0	2	0	2	0	15	0	0
223	13.43	38.19	14.59	2	0	2	0	2	0	15	0	0
224	5.54	41.42	8.31	2	0	2	0	2	0	17	0	0
225	5.54	41.42	9.645	2	0	2	0	2	0	17	0	0
226	13.43	41.42	10.35	2	0	2	0	2	0	17	0	0
227	13.43	41.42	11.75	2	0	2	0	2	0	17	0	0
228	1.36	18.98	8.31	2	0	2	0	2	0	3	0	0
229	2.91	18.98	4.6 2	0	2	0	2	0	3	0	0	
230	3.635	18.98	4.6 2	0	2	0	2	0	3	0	0	
231	3.635	18.98	8.31	2	0	2	0	2	0	3	0	0
232	5.3546	18.98	8.31	2	0	2	0	2	0	3	0	0
233	8.47	18.98	4.6 2	0	2	0	2	0	3	0	0	
234	11.2225	18.98	17.99	2	0	2	0	2	0	3	0	0
235	13.43	18.98	17.99	2	0	2	0	2	0	3	0	0
236	15.45	18.98	13.4	2	0	2	0	2	0	3	0	0
237	15.45	18.98	17.99	2	0	2	0	2	0	3	0	0
238	16.4975	18.98	17.99	2	0	2	0	2	0	3	0	0
239	18.5	18.98	13.4	2	0	2	0	2	0	3	0	0
240	1.36	22.04	8.31	2	0	2	0	2	0	5	0	0
241	2.91	22.04	4.6 2	0	2	0	2	0	5	0	0	
242	8.47	22.04	4.6 2	0	2	0	2	0	5	0	0	
243	11.2225	22.04	17.99	2	0	2	0	2	0	5	0	0
244	16.4975	22.04	17.99	2	0	2	0	2	0	5	0	0
245	18.5	22.04	13.4	2	0	2	0	2	0	5	0	0
246	1.36	25.27	8.31	2	0	2	0	2	0	7	0	0
247	3.235	25.27	4.6 2	0	2	0	2	0	7	0	0	
248	2.91	25.27	4.6 2	0	2	0	2	0	7	0	0	
249	8.47	25.27	4.6 2	0	2	0	2	0	7	0	0	
250	11.2225	25.27	17.99	2	0	2	0	2	0	7	0	0
251	15.885	25.27	17.99	2	0	2	0	2	0	7	0	0
252	16.4975	25.27	17.99	2	0	2	0	2	0	7	0	0
253	18.5	25.27	13.4	2	0	2	0	2	0	7	0	0
254	1.36	28.5	8.31	2	0	2	0	2	0	9	0	0
255	3.235	28.5	4.6 2	0	2	0	2	0	9	0	0	
256	2.91	28.5	4.6 2	0	2	0	2	0	9	0	0	
257	8.47	28.5	4.6 2	0	2	0	2	0	9	0	0	
258	11.2225	28.5	17.99	2	0	2	0	2	0	9	0	0
259	15.885	28.5	17.99	2	0	2	0	2	0	9	0	0
260	16.4975	28.5	17.99	2	0	2	0	2	0	9	0	0
261	18.5	28.5	13.4	2	0	2	0	2	0	9	0	0
262	1.36	31.73	8.31	2	0	2	0	2	0	11	0	0
263	3.235	31.73	4.6 2	0	2	0	2	0	11	0	0	
264	2.91	31.73	4.6 2	0	2	0	2	0	11	0	0	

```
265 8.47    31.73   4.6 2   0   2   0   2   0   11  0   0
266 11.2225 31.73   17.99   2   0   2   0   2   0   11  0   0
267 15.885  31.73   17.99   2   0   2   0   2   0   11  0   0
268 16.4975 31.73   17.99   2   0   2   0   2   0   11  0   0
269 18.5    31.73   13.4    2   0   2   0   2   0   11  0   0
270 1.36    34.96   8.31    2   0   2   0   2   0   13  0   0
271 3.235   34.96   4.6 2   0   2   0   2   0   13  0   0
272 2.91    34.96   4.6 2   0   2   0   2   0   13  0   0
273 8.47    34.96   4.6 2   0   2   0   2   0   13  0   0
274 11.2225 34.96   17.99   2   0   2   0   2   0   13  0   0
275 15.885  34.96   17.99   2   0   2   0   2   0   13  0   0
276 16.4975 34.96   17.99   2   0   2   0   2   0   13  0   0
277 18.5    34.96   13.4    2   0   2   0   2   0   13  0   0
278 1.36    38.19   8.31    2   0   2   0   2   0   15  0   0
279 3.235   38.19   4.6 2   0   2   0   2   0   15  0   0
280 2.91    38.19   4.6 2   0   2   0   2   0   15  0   0
281 7.715   38.19   4.6 2   0   2   0   2   0   15  0   0
282 8.47    38.19   4.6 2   0   2   0   2   0   15  0   0
283 11.2225 38.19   17.99   2   0   2   0   2   0   15  0   0
284 15.185  38.19   17.99   2   0   2   0   2   0   15  0   0
285 15.885  38.19   17.99   2   0   2   0   2   0   15  0   0
286 16.4975 38.19   17.99   2   0   2   0   2   0   15  0   0
287 18.5    38.19   13.4    2   0   2   0   2   0   15  0   0
288 2.1055  41.42   8.31    2   0   2   0   2   0   17  0   0
289 1.36    41.42   8.31    2   0   2   0   2   0   17  0   0
290 4.19    41.42   8.31    2   0   2   0   2   0   17  0   0
291 18.5    41.42   13.4    2   0   2   0   2   0   17  0   0
292 2.74    18.98   11.145  2   0   2   0   2   0   3   0   0
293 1.36    22.04   11.145  2   0   2   0   2   0   5   0   0
294 1.36    25.27   11.145  2   0   2   0   2   0   7   0   0
295 1.36    28.5    11.145  2   0   2   0   2   0   9   0   0
296 1.36    31.73   11.145  2   0   2   0   2   0   11  0   0
297 1.36    34.96   11.145  2   0   2   0   2   0   13  0   0
298 1.36    38.19   11.145  2   0   2   0   2   0   15  0   0
299 1.36    41.42   11.145  2   0   2   0   2   0   17  0   0
300 2.1 45.21   11.145  2   0   2   0   2   0   19  0   0
301 1.36    45.21   11.145  2   0   2   0   2   0   19  0   0
302 2.1055  45.21   8.31    2   0   2   0   2   0   19  0   0
303 1.36    45.21   8.31    2   0   2   0   2   0   19  0   0
304 5.54    45.21   9.645   2   0   2   0   2   0   19  0   0
305 13.43   45.21   11.75   2   0   2   0   2   0   19  0   0
306 15.185  41.42   17.99   2   1   2   0   2   0   17  0   0
307 1.36    41.42   5.94    2   0   2   0   2   0   17  0   0
308 1.36    45.21   5.94    2   0   2   0   2   0   19  0   0
309 1.36    45.21   13.47   2   0   2   0   2   0   19  0   0
310 1.36    41.42   13.47   2   0   2   0   2   0   17  0   0
311 3.2348  41.42   17.99   2   1   2   0   2   0   17  0   0
312 3.2348  45.21   17.99   2   0   2   0   2   0   19  0   0
313 5.72    45.21   17.99   2   0   2   0   2   0   19  0   0
314 5.28    41.42   4.6 2   1   2   0   2   0   17  0   0
315 3.235   45.21   4.6 2   0   2   0   2   0   19  0   0
316 5.28    45.21   4.6 2   0   2   0   2   0   19  0   0
317 5.7198  41.42   17.99   2   1   2   0   2   0   17  0   0
318 5.28    41.42   2.302   2   1   2   0   2   0   17  0   0
319 5.28    45.21   2.302   2   0   2   0   2   0   19  0   0
320 5.72    41.42   20.3    2   1   2   0   2   0   17  0   0
321 5.72    45.21   20.3    2   0   2   0   2   0   19  0   0
322 7.715   45.21   8.33    2   0   2   0   2   0   19  0   0
323 7.715   41.42   8.31    2   0   2   0   2   0   17  0   0
324 9.16    41.42   20.3    2   1   2   0   2   0   17  0   0
325 9.16    45.21   20.3    2   0   2   0   2   0   19  0   0
326 10.01   41.42   2.302   2   1   2   0   2   0   17  0   0
327 10.01   45.21   2.302   2   0   2   0   2   0   19  0   0
328 10.01   45.21   4.6 2   0   2   0   2   0   19  0   0
329 10.01   41.42   4.6 2   1   2   0   2   0   17  0   0
330 10.23   41.42   6.67    2   1   2   0   2   0   17  0   0
331 10.23   45.21   6.67    2   0   2   0   2   0   19  0   0
332 13.53   45.21   6.67    2   0   2   0   2   0   19  0   0
333 13.53   41.42   6.67    2   1   2   0   2   0   17  0   0
334 18.5    45.21   11.7531 2   0   2   0   2   0   19  0   0
335 13.78   41.42   17.99   2   1   2   0   2   0   17  0   0
```

```
336 13.78   45.21   17.99   2   0   2   0   2   0   19  0   0
337 16.58   45.21   17.99   2   0   2   0   2   0   19  0   0
338 13.78   41.42   20.3    2   1   2   0   2   0   17  0   0
339 13.78   45.21   20.3    2   0   2   0   2   0   19  0   0
340 16.58   41.42   17.99   2   1   2   0   2   0   17  0   0
341 15.885  41.42   2.302   2   1   2   0   2   0   17  0   0
342 15.885  45.21   2.302   2   0   2   0   2   0   19  0   0
343 15.885  41.42   4.6 2   1   2   0   2   0   17  0   0
344 15.885  45.21   4.6 2   0   2   0   2   0   19  0   0
345 18.5    41.42   11.753  2   0   2   0   2   0   17  0   0
346 18.5    41.42   5.957   2   0   2   0   2   0   17  0   0
347 18.5    45.21   5.957   2   0   2   0   2   0   19  0   0
348 18.5    45.21   8.46    2   0   2   0   2   0   19  0   0
349 18.5    45.21   13.4    2   0   2   0   2   0   19  0   0
350 1.36    18.98   4.6 2   0   2   0   2   0   3   0   0
351 1.36    18.98   14.59   2   0   2   0   2   0   3   0   0
352 1.36    18.98   17.99   2   0   2   0   2   0   3   0   0
353 2.74    18.98   14.59   2   0   2   0   2   0   3   0   0
354 3.235   18.98   17.99   2   0   2   0   2   0   3   0   0
355 3.235   18.98   0   2   0   2   0   2   0   3   0   0
356 3.235   18.98   22.59   2   0   2   0   2   0   3   0   0
357 3.635   18.98   3.4 2   0   2   0   2   0   3   0   0
358 5.27    18.98   17.99   2   0   2   0   2   0   3   0   0
359 5.59    18.98   0   2   0   2   0   2   0   3   0   0
360 7.715   18.98   14.59   2   0   2   0   2   0   3   0   0
361 7.715   18.98   22.59   2   0   2   0   2   0   3   0   0
362 6.38    18.98   17.99   2   0   2   0   2   0   3   0   0
363 7.715   18.98   8.31    2   0   2   0   2   0   3   0   0
364 7.86    18.98   0   2   0   2   0   2   0   3   0   0
365 7.715   18.98   17.99   2   0   2   0   2   0   3   0   0
366 7.715   18.98   21.8    2   0   2   0   2   0   3   0   0
367 9.7 18.98   17.99   2   0   2   0   2   0   3   0   0
368 9   18.98   4.6 2   0   2   0   2   0   3   0   0
369 11.25   18.98   14.59   2   0   2   0   2   0   3   0   0
370 11.25   18.98   22.59   2   0   2   0   2   0   3   0   0
371 11.405  18.98   0   2   0   2   0   2   0   3   0   0
372 11.405  18.98   4.6 2   0   2   0   2   0   3   0   0
373 13.53   18.98   8.46    2   0   2   0   2   0   3   0   0
374 13.53   18.98   4.6 2   0   2   0   2   0   3   0   0
375 15.885  18.98   22.59   2   0   2   0   2   0   3   0   0
376 15.885  18.98   0   2   0   2   0   2   0   3   0   0
377 15.885  18.98   4.6 2   0   2   0   2   0   3   0   0
378 18.5    18.98   8.46    2   0   2   0   2   0   3   0   0
379 18.5    18.98   4.6 2   0   2   0   2   0   3   0   0
380 18.5    18.98   17.99   2   0   2   0   2   0   3   0   0
381 18.5    18.98   12.5    2   0   2   0   2   0   3   0   0
382 1.36    22.04   4.6 2   0   2   0   2   0   5   0   0
383 1.36    22.04   14.59   2   0   2   0   2   0   5   0   0
384 1.36    22.04   17.99   2   0   2   0   2   0   5   0   0
385 3.235   22.04   17.99   2   0   2   0   2   0   5   0   0
386 3.235   22.04   0   2   0   2   0   2   0   5   0   0
387 3.235   22.04   4.6 2   0   2   0   2   0   5   0   0
388 3.235   22.04   22.59   2   0   2   0   2   0   5   0   0
389 5.59    22.04   0   2   0   2   0   2   0   5   0   0
390 7.715   22.04   14.59   2   0   2   0   2   0   5   0   0
391 7.715   22.04   17.99   2   0   2   0   2   0   5   0   0
392 7.715   22.04   22.59   2   0   2   0   2   0   5   0   0
393 7.715   22.04   8.31    2   0   2   0   2   0   5   0   0
394 7.86    22.04   0   2   0   2   0   2   0   5   0   0
395 11.25   22.04   22.59   2   0   2   0   2   0   5   0   0
396 11.405  22.04   0   2   0   2   0   2   0   5   0   0
397 13.53   22.04   8.46    2   0   2   0   2   0   5   0   0
398 13.53   22.04   4.6 2   0   2   0   2   0   5   0   0
399 15.885  22.04   22.59   2   0   2   0   2   0   5   0   0
400 15.885  22.04   0   2   0   2   0   2   0   5   0   0
401 15.885  22.04   4.6 2   0   2   0   2   0   5   0   0
402 18.5    22.04   8.46    2   0   2   0   2   0   5   0   0
403 18.5    22.04   4.6 2   0   2   0   2   0   5   0   0
404 18.5    22.04   17.99   2   0   2   0   2   0   5   0   0
405 18.5    22.04   12.5    2   0   2   0   2   0   5   0   0
```

```
406 1.36    25.27   4.6 2   0   2   0   2   0   7   0   0
407 1.36    25.27   14.59   2   0   2   0   2   0   7   0   0
408 1.36    25.27   17.99   2   0   2   0   2   0   7   0   0
409 3.235   25.27   17.99   2   0   2   0   2   0   7   0   0
410 3.235   25.27   0   2   0   2   0   2   0   7   0   0
411 3.235   25.27   22.59   2   0   2   0   2   0   7   0   0
412 7.715   25.27   14.59   2   0   2   0   2   0   7   0   0
413 7.715   25.27   17.99   2   0   2   0   2   0   7   0   0
414 7.715   25.27   22.59   2   0   2   0   2   0   7   0   0
415 7.715   25.27   8.31    2   0   2   0   2   0   7   0   0
416 11.405  25.27   0   2   0   2   0   2   0   7   0   0
417 13.53   25.27   8.46    2   0   2   0   2   0   7   0   0
418 13.53   25.27   4.6 2   0   2   0   2   0   7   0   0
419 15.885  25.27   22.59   2   0   2   0   2   0   7   0   0
420 15.885  25.27   0   2   0   2   0   2   0   7   0   0
421 15.885  25.27   4.6 2   0   2   0   2   0   7   0   0
422 18.5    25.27   8.46    2   0   2   0   2   0   7   0   0
423 18.5    25.27   4.6 2   0   2   0   2   0   7   0   0
424 18.5    25.27   17.99   2   0   2   0   2   0   7   0   0
425 18.5    25.27   12.5    2   0   2   0   2   0   7   0   0
426 1.36    28.5    4.6 2   0   2   0   2   0   9   0   0
427 1.36    28.5    14.59   2   0   2   0   2   0   9   0   0
428 1.36    28.5    17.99   2   0   2   0   2   0   9   0   0
429 3.235   28.5    17.99   2   0   2   0   2   0   9   0   0
430 3.235   28.5    0   2   0   2   0   2   0   9   0   0
431 3.235   28.5    22.59   2   0   2   0   2   0   9   0   0
432 7.715   28.5    14.59   2   0   2   0   2   0   9   0   0
433 7.715   28.5    17.99   2   0   2   0   2   0   9   0   0
434 7.715   28.5    22.59   2   0   2   0   2   0   9   0   0
435 7.715   28.5    8.31    2   0   2   0   2   0   9   0   0
436 11.405  28.5    0   2   0   2   0   2   0   9   0   0
437 13.53   28.5    8.46    2   0   2   0   2   0   9   0   0
438 13.53   28.5    4.6 2   0   2   0   2   0   9   0   0
439 15.885  28.5    22.59   2   0   2   0   2   0   9   0   0
440 15.885  28.5    0   2   0   2   0   2   0   9   0   0
441 15.885  28.5    4.6 2   0   2   0   2   0   9   0   0
442 18.5    28.5    8.46    2   0   2   0   2   0   9   0   0
443 18.5    28.5    4.6 2   0   2   0   2   0   9   0   0
444 18.5    28.5    17.99   2   0   2   0   2   0   9   0   0
445 18.5    28.5    12.5    2   0   2   0   2   0   9   0   0
446 1.36    31.73   4.6 2   0   2   0   2   0   11  0   0
447 1.36    31.73   14.59   2   0   2   0   2   0   11  0   0
448 1.36    31.73   17.99   2   0   2   0   2   0   11  0   0
449 3.235   31.73   17.99   2   0   2   0   2   0   11  0   0
450 3.235   31.73   0   2   0   2   0   2   0   11  0   0
451 3.235   31.73   22.59   2   0   2   0   2   0   11  0   0
452 7.715   31.73   14.59   2   0   2   0   2   0   11  0   0
453 7.715   31.73   17.99   2   0   2   0   2   0   11  0   0
454 7.715   31.73   22.59   2   0   2   0   2   0   11  0   0
455 7.715   31.73   8.31    2   0   2   0   2   0   11  0   0
456 11.405  31.73   0   2   0   2   0   2   0   11  0   0
457 13.53   31.73   8.46    2   0   2   0   2   0   11  0   0
458 13.53   31.73   4.6 2   0   2   0   2   0   11  0   0
459 15.885  31.73   22.59   2   0   2   0   2   0   11  0   0
460 15.885  31.73   0   2   0   2   0   2   0   11  0   0
461 15.885  31.73   4.6 2   0   2   0   2   0   11  0   0
462 18.5    31.73   8.46    2   0   2   0   2   0   11  0   0
463 18.5    31.73   4.6 2   0   2   0   2   0   11  0   0
464 18.5    31.73   17.99   2   0   2   0   2   0   11  0   0
465 18.5    31.73   12.5    2   0   2   0   2   0   11  0   0
466 1.36    34.96   4.6 2   0   2   0   2   0   13  0   0
467 1.36    34.96   14.59   2   0   2   0   2   0   13  0   0
468 1.36    34.96   17.99   2   0   2   0   2   0   13  0   0
469 3.235   34.96   17.99   2   0   2   0   2   0   13  0   0
470 3.235   34.96   0   2   0   2   0   2   0   13  0   0
471 3.235   34.96   22.59   2   0   2   0   2   0   13  0   0
472 7.715   34.96   14.59   2   0   2   0   2   0   13  0   0
473 7.715   34.96   17.99   2   0   2   0   2   0   13  0   0
474 7.715   34.96   22.59   2   0   2   0   2   0   13  0   0
475 7.715   34.96   8.31    2   0   2   0   2   0   13  0   0
476 11.405  34.96   0   2   0   2   0   2   0   13  0   0
```

```
477 13.53   34.96   8.46    2   0   2   0   2   0   13  0   0
478 13.53   34.96   4.6 2   0   2   0   2   0   13  0   0
479 15.885  34.96   22.59   2   0   2   0   2   0   13  0   0
480 15.885  34.96   0   2   0   2   0   2   0   13  0   0
481 15.885  34.96   4.6 2   0   2   0   2   0   13  0   0
482 18.5    34.96   8.46    2   0   2   0   2   0   13  0   0
483 18.5    34.96   4.6 2   0   2   0   2   0   13  0   0
484 18.5    34.96   17.99   2   0   2   0   2   0   13  0   0
485 18.5    34.96   12.5    2   0   2   0   2   0   13  0   0
486 1.36    38.19   4.6 2   0   2   0   2   0   15  0   0
487 1.36    38.19   14.59   2   0   2   0   2   0   15  0   0
488 1.36    38.19   17.99   2   0   2   0   2   0   15  0   0
489 3.235   38.19   17.99   2   0   2   0   2   0   15  0   0
490 3.235   38.19   0   2   0   2   0   2   0   15  0   0
491 3.235   38.19   22.59   2   0   2   0   2   0   15  0   0
492 7.715   38.19   14.59   2   0   2   0   2   0   15  0   0
493 7.715   38.19   17.99   2   0   2   0   2   0   15  0   0
494 7.715   38.19   22.59   2   0   2   0   2   0   15  0   0
495 7.715   38.19   8.31    2   0   2   0   2   0   15  0   0
496 11.405  38.19   0   2   0   2   0   2   0   15  0   0
497 13.53   38.19   8.46    2   0   2   0   2   0   15  0   0
498 13.53   38.19   4.6 2   0   2   0   2   0   15  0   0
499 15.885  38.19   22.59   2   0   2   0   2   0   15  0   0
500 15.885  38.19   0   2   0   2   0   2   0   15  0   0
501 15.885  38.19   4.6 2   0   2   0   2   0   15  0   0
502 18.5    38.19   8.46    2   0   2   0   2   0   15  0   0
503 18.5    38.19   4.6 2   0   2   0   2   0   15  0   0
504 18.5    38.19   17.99   2   0   2   0   2   0   15  0   0
505 18.5    38.19   12.5    2   0   2   0   2   0   15  0   0
506 1.36    41.42   4.6 2   0   2   0   2   0   17  0   0
507 1.36    41.42   13.17   2   0   2   0   2   0   17  0   0
508 1.36    41.42   14.59   2   0   2   0   2   0   17  0   0
509 1.36    41.42   16.7    2   0   2   0   2   0   17  0   0
510 1.36    41.42   17.99   2   0   2   0   2   0   17  0   0
511 5.28    41.42   0   2   0   2   0   2   0   17  0   0
512 3.235   41.42   0   2   0   2   0   2   0   17  0   0
513 3.235   41.42   22.59   2   0   2   0   2   0   17  0   0
514 5.72    41.42   22.59   2   0   2   0   2   0   17  0   0
515 7.715   41.42   22.59   2   0   2   0   2   0   17  0   0
516 10.01   41.42   0   2   0   2   0   2   0   17  0   0
517 11.405  41.42   0   2   0   2   0   2   0   17  0   0
518 13.78   41.42   22.59   2   0   2   0   2   0   17  0   0
519 13.53   41.42   0   2   0   2   0   2   0   17  0   0
520 15.885  41.42   0   2   0   2   0   2   0   17  0   0
521 15.885  41.42   22.59   2   0   2   0   2   0   17  0   0
522 18.5    41.42   4.6 2   0   2   0   2   0   17  0   0
523 18.5    41.42   8.46    2   0   2   0   2   0   17  0   0
524 18.5    41.42   17.99   2   0   2   0   2   0   17  0   0
525 1.36    45.21   4.6 2   0   2   0   2   0   19  0   0
526 1.36    45.21   14.59   2   0   2   0   2   0   19  0   0
527 1.36    45.21   17.99   2   0   2   0   2   0   19  0   0
528 5.59    45.21   4.6 2   0   2   0   2   0   19  0   0
529 7.715   45.21   4.6 2   0   2   0   2   0   19  0   0
530 9.16    45.21   17.99   2   0   2   0   2   0   19  0   0
531 9.51    45.21   17.99   2   0   2   0   2   0   19  0   0
532 10.23   45.21   4.6 2   0   2   0   2   0   19  0   0
533 13.53   45.21   17.99   2   0   2   0   2   0   19  0   0
534 13.53   45.21   2.302   2   0   2   0   2   0   19  0   0
535 13.53   45.21   4.6 2   0   2   0   2   0   19  0   0
536 18.5    45.21   4.6 2   0   2   0   2   0   19  0   0
537 18.5    45.21   17.99   2   0   2   0   2   0   19  0   0
538 3.235   41.42   4.6 2   1   2   0   2   0   17  0   0
539 7.715   15.75   8.31    2   2   2   2   2   2   107 0   0

DRIFT ANGLE
1   3   5   7   9   11  13  15  17  19

ELEMENTS
1   1   2   3   0   0   X   0   0       ! Gravity column G-UG
2   1   4   5   0   0   X   0   0       ! Gravity column UG-1
```

```
3   1   6   7   0   0   X   0   0       ! Gravity column 1-2
4   1   8   9   0   0   X   0   0       ! Gravity column 2-3
5   1   10  11  0   0   X   0   0       ! Gravity column 3-4
6   1   12  13  0   0   X   0   0       ! Gravity column 4-5
7   1   14  15  0   0   X   0   0       ! Gravity column 5-PG
8   1   16  17  0   0   X   0   0       ! Gravity column PG-P1
9   1   18  19  0   0   X   0   0       ! Gravity column P1-R
10  2   20  21  0   0   X   0   0       ! LRB 1
11  3   22  23  0   0   X   0   0       ! LRB 2
12  4   24  25  0   0   X   0   0       ! LRB 3
13  5   26  27  0   0   X   0   0       ! LRB 4
14  6   28  29  0   0   X   0   0       ! LRB 5
15  7   30  31  0   0   X   0   0       ! LRB 6
16  8   32  33  0   0   X   0   0       ! LRB 7
17  9   34  35  0   0   X   0   0       ! LRB 8
18  10  36  37  0   0   X   0   0       ! LRB 9
19  11  38  39  0   0   X   0   0       ! LRB 10
20  12  40  41  0   0   X   0   0       ! LRB 11
21  13  42  43  0   0   X   0   0       ! LRB 12
22  14  44  45  0   0   X   0   0       ! LRB 13
23  15  46  47  0   0   X   0   0       ! LRB 14
24  16  48  49  0   0   X   0   0       ! LRB 15
25  17  50  51  0   0   X   0   0       ! SB 1
26  18  52  53  0   0   X   0   0       ! SB 2
27  19  54  55  0   0   X   0   0       ! SB 3
28  20  56  57  0   0   X   0   0       ! SB 4
29  21  58  59  0   0   X   0   0       ! SB 5
30  22  60  61  0   0   X   0   0       ! SB 6
31  23  62  63  0   0   X   0   0       ! SB 7
32  24  64  65  0   0   X   0   0       ! SB 8
33  25  66  67  0   0   X   0   0       ! SB 9
34  26  68  69  0   0   X   0   0       ! SB 10
35  27  70  71  0   0   X   0   0       ! SB 11
36  28  72  73  0   0   X   0   0       ! SB 12
37  29  74  75  0   0   X   0   0       ! SB 13
38  30  51  76  0   0   X   0   0       ! SB Axial
39  30  53  77  0   0   X   0   0       ! SB Axial
40  30  55  78  0   0   X   0   0       ! SB Axial
41  30  57  79  0   0   X   0   0       ! SB Axial
42  30  59  80  0   0   X   0   0       ! SB Axial
43  30  61  81  0   0   X   0   0       ! SB Axial
44  30  63  82  0   0   X   0   0       ! SB Axial
45  30  65  83  0   0   X   0   0       ! SB Axial
46  30  67  84  0   0   X   0   0       ! SB Axial
47  30  69  85  0   0   X   0   0       ! SB Axial
48  30  71  86  0   0   X   0   0       ! SB Axial
49  30  73  87  0   0   X   0   0       ! SB Axial
50  30  75  88  0   0   X   0   0       ! SB Axial
51  31  45  47  0   0   X   0   0       ! Grillage
52  32  27  89  0   0   X   0   0       ! Grillage
53  32  90  29  0   0   X   0   0       ! Grillage
54  32  41  91  0   0   X   0   0       ! Grillage
55  32  87  43  0   0   X   0   0       ! Grillage
56  33  23  25  0   0   X   0   0       ! Grillage
57  34  82  92  0   0   X   0   0       ! Grillage
58  34  92  35  0   0   X   0   0       ! Grillage
59  34  35  93  0   0   X   0   0       ! Grillage
60  35  83  94  0   0   X   0   0       ! Grillage
61  36  82  81  0   0   X   0   0       ! Grillage
62  37  31  33  0   0   X   0   0       ! Grillage
63  37  37  95  0   0   X   0   0       ! Grillage
64  38  47  84  0   0   Z   0   0       ! Grillage
65  38  96  85  0   0   Z   0   0       ! Grillage
66  39  82  97  0   0   Z   0   0       ! Grillage
67  39  97  98  0   0   Z   0   0       ! Grillage
68  39  98  99  0   0   Z   0   0       ! Grillage
69  39  84  99  0   0   Z   0   0       ! Grillage
70  40  91  39  0   0   Z   0   0       ! Grillage
71  40  45  91  0   0   Z   0   0       ! Grillage
72  41  100 23  0   0   Z   0   0       ! Grillage
73  42  101 90  0   0   Z   0   0       ! Grillage
```

```
74  42  31  101 0   0   Z   0   0       ! Grillage
75  43  90  25  0   0   Z   0   0       ! Grillage
76  44  102 27  0   0   Z   0   0       ! Grillage
77  44  33  29  0   0   Z   0   0       ! Grillage
78  44  103 102 0   0   Z   0   0       ! Grillage
79  44  104 33  0   0   Z   0   0       ! Grillage
80  44  37  103 0   0   Z   0   0       ! Grillage
81  44  43  104 0   0   Z   0   0       ! Grillage
82  44  41  37  0   0   Z   0   0       ! Grillage
83  45  21  76  0   0   X   0   0       ! Grillage
84  45  76  77  0   0   X   0   0       ! Grillage
85  45  77  23  0   0   X   0   0       ! Grillage
86  45  96  47  0   0   X   0   0       ! Grillage
87  45  88  96  0   0   X   0   0       ! Grillage
88  45  49  88  0   0   X   0   0       ! Grillage
89  46  84  39  0   0   X   0   0       ! Grillage
90  47  95  81  0   0   Z   0   0       ! Grillage
91  47  105 95  0   0   Z   0   0       ! Grillage
92  47  39  105 0   0   Z   0   0       ! Grillage
93  48  89  21  0   0   Z   0   0       ! Grillage
94  49  106 80  0   0   Z   0   0       ! Grillage
95  50  107 108 0   0   Z   0   0       ! Grillage
96  50  100 109 0   0   Z   0   0       ! Grillage
97  50  82  107 0   0   Z   0   0       ! Grillage
98  50  109 35  0   0   Z   0   0       ! Grillage
99  51  110 92  0   0   Z   0   0       ! Grillage
100 51  111 110 0   0   Z   0   0       ! Grillage
101 51  112 111 0   0   Z   0   0       ! Grillage
102 51  94  112 0   0   Z   0   0       ! Grillage
103 51  113 94  0   0   Z   0   0       ! Grillage
104 52  49  114 0   0   Z   0   0       ! Grillage
105 53  31  93  0   0   Z   0   0       ! Grillage
106 53  93  115 0   0   Z   0   0       ! Grillage
107 53  115 83  0   0   Z   0   0       ! Grillage
108 54  84  85  0   0   X   0   0       ! Grillage
109 54  86  116 0   0   X   0   0       ! Grillage
110 55  117 79  0   0   X   0   0       ! Grillage
111 55  80  100 0   0   X   0   0       ! Grillage
112 56  118 110 0   0   X   0   0       ! Grillage
113 56  115 118 0   0   X   0   0       ! Grillage
114 56  97  119 0   0   X   0   0       ! Grillage
115 56  119 111 0   0   X   0   0       ! Grillage
116 57  112 98  0   0   X   0   0       ! Grillage
117 58  79  108 0   0   X   0   0       ! Wall links at ground (connecting to
grillage)
118 58  108 120 0   0   X   0   0       ! Wall links at ground (connecting to
grillage)
119 58  120 80  0   0   X   0   0       ! Wall links at ground (connecting to
grillage)
120 58  121 122 0   0   X   0   0       ! Wall links at ground (connecting to
grillage)
121 58  85  123 0   0   X   0   0       ! Wall links at ground (connecting to
grillage)
122 58  123 113 0   0   X   0   0       ! Wall links at ground (connecting to
grillage)
123 58  113 86  0   0   X   0   0       ! Wall links at ground (connecting to
grillage)
124 59  124 76  0   0   Z   0   0       ! Wall links at ground (connecting to
grillage)
125 59  78  89  0   0   Z   0   0       ! Wall links at ground (connecting to
grillage)
126 59  108 124 0   0   Z   0   0       ! Wall links at ground (connecting to
grillage)
127 59  125 121 0   0   Z   0   0       ! Wall links at ground (connecting to
grillage)
128 59  117 78  0   0   Z   0   0       ! Wall links at ground (connecting to
grillage)
129 59  126 117 0   0   Z   0   0       ! Wall links at ground (connecting to
grillage)
```

```
130 59  81  126 0   0   Z   0   0       ! Wall links at ground (connecting to
grillage)
131 59  83  116 0   0   Z   0   0       ! Wall links at ground (connecting to
grillage)
132 59  127 128 0   0   Z   0   0       ! Wall links at ground (connecting to
grillage)
133 59  87  116 0   0   Z   0   0       ! Wall links at ground (connecting to
grillage)
134 59  129 113 0   0   Z   0   0       ! Wall links at ground (connecting to
grillage)
135 59  114 87  0   0   Z   0   0       ! Wall links at ground (connecting to
grillage)
136 59  88  129 0   0   Z   0   0       ! Wall links at ground (connecting to
grillage)
137 60  77  130 0   0   Z   0   0       ! Wall links at ground (connecting to
grillage)
138 60  130 106 0   0   Z   0   0       ! Wall links at ground (connecting to
grillage)
139 61  131 127 0   0   Z   0   0      ! Wall N1 (G-UG)
140 61  132 131 0   0   Z   0   0      ! Wall N1 (UG-1)
141 61  133 132 0   0   Z   0   0      ! Wall N1 (1-2)
142 61  134 133 0   0   Z   0   0      ! Wall N1 (2-3)
143 61  135 134 0   0   Z   0   0      ! Wall N1 (3-4)
144 62  136 135 0   0   Z   0   0      ! Wall N1 (4-5)
145 62  137 136 0   0   Z   0   0      ! Wall N1 (5-PG)
146 62  138 137 0   0   Z   0   0      ! Wall N1 (PG-P1)
147 63  139 128 0   0   X   0   0      ! Wall N2 (G-UG)
148 63  140 139 0   0   X   0   0      ! Wall N2 (UG-1)
149 63  141 140 0   0   X   0   0      ! Wall N2 (1-2)
150 63  142 141 0   0   X   0   0      ! Wall N2 (2-3)
151 63  143 142 0   0   X   0   0      ! Wall N2 (3-4)
152 64  144 143 0   0   X   0   0      ! Wall N2 (4-5)
153 64  145 144 0   0   X   0   0      ! Wall N2 (5-PG)
154 64  146 145 0   0   X   0   0      ! Wall N2 (PG-P1)
155 65  147 116 0   0   Z   0   0      ! Wall N3 (G-UG)
156 66  148 149 0   0   Z   0   0      ! Wall N3 (UG-1) Pier-N
157 67  150 151 0   0   Z   0   0      ! Wall N3 (UG-1) Pier-S
158 68  152 153 0   0   Z   0   0      ! Wall N3 (1-2)
159 68  154 152 0   0   Z   0   0      ! Wall N3 (2-3)
160 68  155 154 0   0   Z   0   0      ! Wall N3 (3-4)
161 69  156 155 0   0   Z   0   0      ! Wall N3 (4-5)
162 69  157 156 0   0   Z   0   0      ! Wall N3 (5-PG)
163 70  158 126 0   0   Z   0   0      ! Wall S1 (G-UG) Pier-N
164 71  159 89  0   0   Z   0   0      ! Wall S1 (G-UG) Pier-S
165 72  160 161 0   0   Z   0   0      ! Wall S1 (UG-1) Pier-N
166 73  162 163 0   0   Z   0   0      ! Wall S1 (UG-1) Pier-S
167 74  164 165 0   0   Z   0   0      ! Wall S1 (1-2)
168 75  166 164 0   0   Z   0   0      ! Wall S1 (2-3)
169 75  167 166 0   0   Z   0   0      ! Wall S1 (3-4)
170 76  168 167 0   0   Z   0   0      ! Wall S1 (4-5)
171 76  169 168 0   0   Z   0   0      ! Wall S1 (5-PG)
172 77  170 125 0   0   Z   0   0      ! Wall S2 (G-UG)
173 77  171 170 0   0   Z   0   0      ! Wall S2 (UG-1)
174 77  172 171 0   0   Z   0   0      ! Wall S2 (1-2)
175 77  173 172 0   0   Z   0   0      ! Wall S2 (2-3)
176 77  174 173 0   0   Z   0   0      ! Wall S2 (3-4)
177 78  175 174 0   0   Z   0   0      ! Wall S2 (4-5)
178 78  176 175 0   0   Z   0   0      ! Wall S2 (5-PG)
179 78  177 176 0   0   Z   0   0      ! Wall S2 (PG-P1)
180 79  178 122 0   0   X   0   0      ! Wall S3 (G-UG)
181 79  179 178 0   0   X   0   0      ! Wall S3 (UG-1)
182 79  180 179 0   0   X   0   0      ! Wall S3 (1-2)
183 79  181 180 0   0   X   0   0      ! Wall S3 (2-3)
184 79  182 181 0   0   X   0   0      ! Wall S3 (3-4)
185 80  183 182 0   0   X   0   0      ! Wall S3 (4-5)
186 80  184 183 0   0   X   0   0      ! Wall S3 (5-PG)
187 80  185 184 0   0   X   0   0      ! Wall S3 (PG-P1)
188 81  186 187 0   0   Z   0   0      ! Wall S4 (G-UG)
189 81  186 188 0   0   Z   0   0      ! Wall S4 (UG-1)
190 82  189 188 0   0   Z   0   0      ! Wall S4 (1-2)
191 82  190 189 0   0   Z   0   0      ! Wall S4 (2-3)
```

```
192 82  191 190 0   0   Z   0   0       ! Wall S4 (3-4)
193 83  192 191 0   0   Z   0   0       ! Wall S4 (4-5)
194 83  193 192 0   0   Z   0   0       ! Wall S4 (5-PG)
195 83  194 193 0   0   Z   0   0       ! Wall S4 (PG-P1)
196 84  195 178 0   0   X   0   0       ! Wall Link W1 (UG-1)
197 84  196 139 0   0   X   0   0
198 84  139 197 0   0   X   0   0
199 84  197 198 0   0   X   0   0
200 84  199 196 0   0   Z   0   0
201 84  200 179 0   0   X   0   0
202 84  179 201 0   0   X   0   0
203 84  202 140 0   0   X   0   0
204 84  140 203 0   0   X   0   0
205 85  204 180 0   0   X   0   0       ! Wall Link W1 (2-PG)
206 85  180 205 0   0   X   0   0
207 85  206 141 0   0   X   0   0
208 85  141 207 0   0   X   0   0
209 85  208 181 0   0   X   0   0
210 85  181 209 0   0   X   0   0
211 85  210 142 0   0   X   0   0
212 85  142 211 0   0   X   0   0
213 85  212 182 0   0   X   0   0
214 85  182 213 0   0   X   0   0
215 85  214 143 0   0   X   0   0
216 85  143 215 0   0   X   0   0
217 85  216 183 0   0   X   0   0
218 85  183 217 0   0   X   0   0
219 85  218 144 0   0   X   0   0
220 85  144 219 0   0   X   0   0
221 85  220 184 0   0   X   0   0
222 85  184 221 0   0   X   0   0
223 85  222 145 0   0   X   0   0
224 85  145 223 0   0   X   0   0
225 86  224 185 0   0   X   0   0       ! Wall Link W1 (P1)
226 86  185 225 0   0   X   0   0
227 86  226 227 0   0   X   0   0
228 86  227 146 0   0   X   0   0
229 87  170 228 0   0   Z   0   0       ! Wall Link W2 (UG-1)
230 87  229 159 0   0   Z   0   0
231 87  159 230 0   0   Z   0   0
232 87  231 170 0   0   Z   0   0
233 87  230 163 0   0   Z   0   0
234 87  232 231 0   0   Z   0   0
235 87  195 232 0   0   Z   0   0
236 87  163 158 0   0   Z   0   0
237 87  161 158 0   0   Z   0   0
238 87  233 161 0   0   Z   0   0
239 87  234 151 0   0   Z   0   0
240 87  151 235 0   0   Z   0   0
241 87  235 147 0   0   Z   0   0
242 87  236 139 0   0   Z   0   0
243 87  237 147 0   0   Z   0   0
244 87  237 149 0   0   Z   0   0
245 87  131 236 0   0   Z   0   0
246 87  149 238 0   0   Z   0   0
247 87  239 131 0   0   Z   0   0
248 87  171 240 0   0   Z   0   0
249 87  162 241 0   0   Z   0   0
250 87  200 171 0   0   Z   0   0
251 87  165 162 0   0   Z   0   0
252 87  160 165 0   0   Z   0   0
253 87  242 160 0   0   Z   0   0
254 87  243 150 0   0   Z   0   0
255 87  150 153 0   0   Z   0   0
256 87  132 140 0   0   Z   0   0
257 87  148 153 0   0   Z   0   0
258 87  244 148 0   0   Z   0   0
259 87  245 132 0   0   Z   0   0
260 88  172 246 0   0   Z   0   0       ! Wall Link W2 (2-PG)
261 88  247 248 0   0   Z   0   0
```

```
262 88  204 172 0   0   Z   0   0
263 88  164 247 0   0   Z   0   0
264 88  249 164 0   0   Z   0   0
265 88  250 152 0   0   Z   0   0
266 88  133 141 0   0   Z   0   0
267 88  152 251 0   0   Z   0   0
268 88  251 252 0   0   Z   0   0
269 88  253 133 0   0   Z   0   0
270 88  173 254 0   0   Z   0   0
271 88  255 256 0   0   Z   0   0
272 88  208 173 0   0   Z   0   0
273 88  166 255 0   0   Z   0   0
274 88  257 166 0   0   Z   0   0
275 88  258 154 0   0   Z   0   0
276 88  134 142 0   0   Z   0   0
277 88  154 259 0   0   Z   0   0
278 88  259 260 0   0   Z   0   0
279 88  261 134 0   0   Z   0   0
280 88  174 262 0   0   Z   0   0
281 88  263 264 0   0   Z   0   0
282 88  212 174 0   0   Z   0   0
283 88  167 263 0   0   Z   0   0
284 88  265 167 0   0   Z   0   0
285 88  266 155 0   0   Z   0   0
286 88  135 143 0   0   Z   0   0
287 88  155 267 0   0   Z   0   0
288 88  267 268 0   0   Z   0   0
289 88  269 135 0   0   Z   0   0
290 88  175 270 0   0   Z   0   0
291 88  271 272 0   0   Z   0   0
292 88  216 175 0   0   Z   0   0
293 88  168 271 0   0   Z   0   0
294 88  273 168 0   0   Z   0   0
295 88  274 156 0   0   Z   0   0
296 88  136 144 0   0   Z   0   0
297 88  156 275 0   0   Z   0   0
298 88  275 276 0   0   Z   0   0
299 88  277 136 0   0   Z   0   0
300 88  176 278 0   0   Z   0   0
301 88  279 280 0   0   Z   0   0
302 88  220 176 0   0   Z   0   0
303 88  169 279 0   0   Z   0   0
304 88  281 169 0   0   Z   0   0
305 88  282 281 0   0   Z   0   0
306 88  283 157 0   0   Z   0   0
307 88  157 284 0   0   Z   0   0
308 88  137 145 0   0   Z   0   0
309 88  284 285 0   0   Z   0   0
310 88  285 286 0   0   Z   0   0
311 88  287 137 0   0   Z   0   0
312 89  288 289 0   0   Z   0   0       ! Wall Link W2 (P1)
313 89  177 288 0   0   Z   0   0
314 89  290 177 0   0   Z   0   0
315 89  224 290 0   0   Z   0   0
316 89  146 138 0   0   Z   0   0
317 89  138 291 0   0   Z   0   0
318 90  292 186 0   0   Z   0   0       ! Wall Link W3 (UG-1)
319 90  188 293 0   0   Z   0   0
320 91  189 294 0   0   Z   0   0       ! Wall Link W3 (2-PG)
321 91  190 295 0   0   Z   0   0
322 91  191 296 0   0   Z   0   0
323 91  192 297 0   0   Z   0   0
324 91  193 298 0   0   Z   0   0
325 92  194 299 0   0   Z   0   0       ! Wall Link W3 (P1)
326 96  300 194 0   0   Z   0   0       ! Roof level - Walls
327 97  300 301 0   0   Z   0   0
328 98  302 303 0   0   Z   0   0
329 94  302 288 0   0   Z   0   0
330 95  304 225 0   0   X   0   0
331 93  305 227 0   0   X   0   0
332 99  306 284 0   0   X   0   0       ! Roof level
```

```
333 100 307 308 0   0   X   0   0
334 101 307 303 0   0   Z   0   0
335 101 289 308 0   0   Z   0   0
336 101 299 309 0   0   Z   0   0
337 101 310 301 0   0   Z   0   0
338 100 310 309 0   0   X   0   0
339 100 311 312 0   0   X   0   0
340 101 311 313 0   0   Z   0   0
341 101 314 315 0   0   Z   0   0
342 100 314 316 0   0   X   0   0
343 101 317 312 0   0   Z   0   0
344 100 317 313 0   0   X   0   0
345 102 318 319 0   0   X   0   0
346 102 320 321 0   0   X   0   0
347 104 322 323 0   0   X   0   0
348 102 324 325 0   0   X   0   0
349 102 326 327 0   0   X   0   0
350 100 328 329 0   0   X   0   0
351 100 330 331 0   0   X   0   0
352 101 330 332 0   0   X   0   0
353 101 333 331 0   0   X   0   0
354 100 333 332 0   0   X   0   0
355 101 227 334 0   0   Z   0   0
356 100 335 336 0   0   X   0   0
357 101 335 337 0   0   Z   0   0
358 102 338 339 0   0   X   0   0
359 101 340 336 0   0   Z   0   0
360 100 340 337 0   0   X   0   0
361 102 341 342 0   0   X   0   0
362 100 343 344 0   0   X   0   0
363 101 345 305 0   0   Z   0   0
364 100 345 334 0   0   X   0   0
365 100 346 347 0   0   X   0   0
366 101 346 348 0   0   Z   0   0
367 103 291 349 0   0   X   0   0
368 109 350 228 0   0   X   0   0       ! Steel framing
369 104 351 352 0   0   X   0   0
370 110 351 353 0   0   Z   0   0
371 111 350 229 0   0   Z   0   0
372 112 352 354 0   0   Z   0   0
373 113 355 159 0   0   X   0   0
374 113 354 356 0   0   X   0   0
375 114 230 357 0   0   X   0   0
376 115 230 231 0   0   X   0   0
377 116 354 358 0   0   Z   0   0
378 117 359 355 0   0   Z   0   0
379 118 353 360 0   0   Z   0   0
380 119 361 356 0   0   Z   0   0
381 116 358 362 0   0   Z   0   0
382 120 363 195 0   0   Z   0   0
383 121 364 359 0   0   Z   0   0
384 122 365 362 0   0   Z   0   0
385 123 365 366 0   0   X   0   0
386 124 366 361 0   0   X   0   0
387 125 365 367 0   0   Z   0   0
388 126 368 233 0   0   Z   0   0
389 127 360 369 0   0   Z   0   0
390 128 370 361 0   0   Z   0   0
391 129 371 364 0   0   Z   0   0
392 116 372 368 0   0   Z   0   0
393 130 367 234 0   0   Z   0   0
394 131 373 363 0   0   -Z  0   0
395 132 369 197 0   0   Z   0   0
396 112 374 372 0   0   Z   0   0
397 114 235 198 0   0   X   0   0
398 133 373 374 0   0   X   0   0
399 111 373 199 0   0   X   0   0
400 134 375 370 0   0   Z   0   0
401 119 376 371 0   0   Z   0   0
402 130 377 374 0   0   Z   0   0
```

```
403 135 237 236 0   0   X   0   0
404 113 376 377 0   0   X   0   0
405 113 149 375 0   0   X   0   0
406 136 373 378 0   0   Z   0   0
407 137 379 377 0   0   Z   0   0
408 111 380 238 0   0   Z   0   0
409 138 379 378 0   0   X   0   0
410 139 378 381 0   0   X   0   0
411 140 381 239 0   0   X   0   0
412 141 239 380 0   0   X   0   0
413 109 382 240 0   0   X   0   0
414 144 383 293 0   0   X   0   0
415 145 383 384 0   0   X   0   0
416 111 382 241 0   0   Z   0   0
417 112 384 385 0   0   Z   0   0
418 146 386 387 0   0   X   0   0
419 146 388 385 0   0   X   0   0
420 147 389 386 0   0   Z   0   0
421 148 383 390 0   0   Z   0   0
422 149 385 391 0   0   Z   0   0
423 146 392 388 0   0   Z   0   0
424 111 393 200 0   0   Z   0   0
425 150 394 389 0   0   Z   0   0
426 151 391 243 0   0   Z   0   0
427 147 395 392 0   0   Z   0   0
428 152 396 394 0   0   Z   0   0
429 127 390 203 0   0   Z   0   0
430 131 397 393 0   0   -Z  0   0
431 136 398 242 0   0   Z   0   0
432 152 399 395 0   0   Z   0   0
433 146 400 396 0   0   Z   0   0
434 132 401 398 0   0   Z   0   0
435 146 400 401 0   0   X   0   0
436 146 148 399 0   0   X   0   0
437 136 397 402 0   0   Z   0   0
438 153 403 401 0   0   Z   0   0
439 111 404 244 0   0   Z   0   0
440 138 403 402 0   0   X   0   0
441 139 402 405 0   0   X   0   0
442 140 405 245 0   0   X   0   0
443 141 245 404 0   0   X   0   0
444 109 406 246 0   0   X   0   0
445 144 407 294 0   0   X   0   0
446 145 407 408 0   0   X   0   0
447 111 406 248 0   0   Z   0   0
448 112 408 409 0   0   Z   0   0
449 146 410 247 0   0   X   0   0
450 146 411 409 0   0   X   0   0
451 148 407 412 0   0   Z   0   0
452 149 409 413 0   0   Z   0   0
453 146 414 411 0   0   Z   0   0
454 111 415 204 0   0   Z   0   0
455 154 416 410 0   0   Z   0   0
456 155 413 250 0   0   Z   0   0
457 156 412 207 0   0   Z   0   0
458 131 417 415 0   0   -Z  0   0
459 157 418 249 0   0   Z   0   0
460 154 419 414 0   0   Z   0   0
461 146 420 416 0   0   Z   0   0
462 132 421 418 0   0   Z   0   0
463 146 420 421 0   0   X   0   0
464 146 251 419 0   0   X   0   0
465 136 417 422 0   0   Z   0   0
466 153 423 421 0   0   Z   0   0
467 111 424 252 0   0   Z   0   0
468 138 423 422 0   0   X   0   0
469 139 422 425 0   0   X   0   0
470 140 425 253 0   0   X   0   0
471 141 253 424 0   0   X   0   0
472 109 426 254 0   0   X   0   0
473 144 427 295 0   0   X   0   0
```

```
474 145 427 428 0   0   X   0   0
475 111 426 256 0   0   Z   0   0
476 112 428 429 0   0   Z   0   0
477 146 430 255 0   0   X   0   0
478 146 431 429 0   0   X   0   0
479 148 427 432 0   0   Z   0   0
480 149 429 433 0   0   Z   0   0
481 146 434 431 0   0   Z   0   0
482 111 435 208 0   0   Z   0   0
483 154 436 430 0   0   Z   0   0
484 155 433 258 0   0   Z   0   0
485 156 432 211 0   0   Z   0   0
486 131 437 435 0   0   -Z  0   0
487 157 438 257 0   0   Z   0   0
488 154 439 434 0   0   Z   0   0
489 146 440 436 0   0   Z   0   0
490 132 441 438 0   0   Z   0   0
491 146 440 441 0   0   X   0   0
492 146 259 439 0   0   X   0   0
493 136 437 442 0   0   Z   0   0
494 153 443 441 0   0   Z   0   0
495 111 444 260 0   0   Z   0   0
496 138 443 442 0   0   X   0   0
497 139 442 445 0   0   X   0   0
498 140 445 261 0   0   X   0   0
499 141 261 444 0   0   X   0   0
500 109 446 262 0   0   X   0   0
501 144 447 296 0   0   X   0   0
502 145 447 448 0   0   X   0   0
503 111 446 264 0   0   Z   0   0
504 112 448 449 0   0   Z   0   0
505 146 450 263 0   0   X   0   0
506 146 451 449 0   0   X   0   0
507 148 447 452 0   0   Z   0   0
508 149 449 453 0   0   Z   0   0
509 146 454 451 0   0   Z   0   0
510 111 455 212 0   0   Z   0   0
511 154 456 450 0   0   Z   0   0
512 155 453 266 0   0   Z   0   0
513 156 452 215 0   0   Z   0   0
514 131 457 455 0   0   -Z  0   0
515 157 458 265 0   0   Z   0   0
516 154 459 454 0   0   Z   0   0
517 146 460 456 0   0   Z   0   0
518 132 461 458 0   0   Z   0   0
519 146 460 461 0   0   X   0   0
520 146 267 459 0   0   X   0   0
521 136 457 462 0   0   Z   0   0
522 153 463 461 0   0   Z   0   0
523 111 464 268 0   0   Z   0   0
524 138 463 462 0   0   X   0   0
525 139 462 465 0   0   X   0   0
526 140 465 269 0   0   X   0   0
527 141 269 464 0   0   X   0   0
528 109 466 270 0   0   X   0   0
529 144 467 297 0   0   X   0   0
530 145 467 468 0   0   X   0   0
531 111 466 272 0   0   Z   0   0
532 112 468 469 0   0   Z   0   0
533 146 470 271 0   0   X   0   0
534 146 471 469 0   0   X   0   0
535 148 467 472 0   0   Z   0   0
536 149 469 473 0   0   Z   0   0
537 146 474 471 0   0   Z   0   0
538 111 475 216 0   0   Z   0   0
539 154 476 470 0   0   Z   0   0
540 155 473 274 0   0   Z   0   0
541 156 472 219 0   0   Z   0   0
542 131 477 475 0   0   -Z  0   0
543 157 478 273 0   0   Z   0   0
```

```
544 154 479 474 0   0   Z   0   0
545 146 480 476 0   0   Z   0   0
546 132 481 478 0   0   Z   0   0
547 146 480 481 0   0   X   0   0
548 146 275 479 0   0   X   0   0
549 136 477 482 0   0   Z   0   0
550 153 483 481 0   0   Z   0   0
551 111 484 276 0   0   Z   0   0
552 138 483 482 0   0   X   0   0
553 139 482 485 0   0   X   0   0
554 140 485 277 0   0   X   0   0
555 141 277 484 0   0   X   0   0
556 109 486 278 0   0   X   0   0
557 144 487 298 0   0   X   0   0
558 145 487 488 0   0   X   0   0
559 111 486 280 0   0   Z   0   0
560 112 488 489 0   0   Z   0   0
561 146 490 279 0   0   X   0   0
562 146 491 489 0   0   X   0   0
563 148 487 492 0   0   Z   0   0
564 149 489 493 0   0   Z   0   0
565 146 494 491 0   0   Z   0   0
566 111 495 220 0   0   Z   0   0
567 154 496 490 0   0   Z   0   0
568 158 495 281 0   0   X   0   0
569 159 493 492 0   0   X   0   0
570 155 493 283 0   0   Z   0   0
571 160 492 223 0   0   Z   0   0
572 131 497 495 0   0   -Z  0   0
573 157 498 282 0   0   Z   0   0
574 154 499 494 0   0   Z   0   0
575 161 498 497 0   0   X   0   0
576 146 500 496 0   0   Z   0   0
577 132 501 498 0   0   Z   0   0
578 146 500 501 0   0   X   0   0
579 146 285 499 0   0   X   0   0
580 136 497 502 0   0   Z   0   0
581 153 503 501 0   0   Z   0   0
582 111 504 286 0   0   Z   0   0
583 138 503 502 0   0   X   0   0
584 139 502 505 0   0   X   0   0
585 140 505 287 0   0   X   0   0
586 141 287 504 0   0   X   0   0
587 162 506 307 0   0   X   0   0
588 163 307 289 0   0   X   0   0
589 164 507 299 0   0   X   0   0
590 165 310 507 0   0   X   0   0
591 166 508 310 0   0   X   0   0
592 164 509 508 0   0   X   0   0
593 167 510 509 0   0   X   0   0
594 168 511 512 0   0   Z   0   0
595 137 513 514 0   0   Z   0   0
596 111 323 224 0   0   Z   0   0
597 130 514 515 0   0   Z   0   0
598 150 516 511 0   0   Z   0   0
599 169 517 516 0   0   Z   0   0
600 170 515 518 0   0   Z   0   0
601 130 519 517 0   0   Z   0   0
602 125 520 519 0   0   Z   0   0
603 168 518 521 0   0   Z   0   0
604 167 522 346 0   0   X   0   0
605 171 346 523 0   0   X   0   0
606 172 523 345 0   0   X   0   0
607 173 345 291 0   0   X   0   0
608 174 291 524 0   0   X   0   0
609 175 308 525 0   0   X   0   0
610 176 303 308 0   0   X   0   0
611 177 309 301 0   0   X   0   0
612 178 526 309 0   0   X   0   0
613 179 526 527 0   0   X   0   0
614 180 315 525 0   0   Z   0   0
```

```
615 180 312 527 0   0   Z   0   0
616 181 316 315 0   0   Z   0   0
617 176 313 312 0   0   Z   0   0
618 182 319 316 0   0   X   0   0
619 183 316 528 0   0   Z   0   0
620 182 313 321 0   0   X   0   0
621 184 528 529 0   0   Z   0   0
622 185 313 530 0   0   Z   0   0
623 186 325 321 0   0   Z   0   0
624 187 327 319 0   0   Z   0   0
625 188 529 328 0   0   Z   0   0
626 189 325 530 0   0   X   0   0
627 184 530 531 0   0   Z   0   0
628 189 327 328 0   0   X   0   0
629 190 532 328 0   0   Z   0   0
630 191 339 325 0   0   Z   0   0
631 184 531 533 0   0   Z   0   0
632 182 534 327 0   0   Z   0   0
633 184 535 532 0   0   Z   0   0
634 192 534 535 0   0   X   0   0
635 190 533 336 0   0   Z   0   0
636 182 339 336 0   0   X   0   0
637 181 342 534 0   0   Z   0   0
638 193 344 535 0   0   Z   0   0
639 194 336 337 0   0   Z   0   0
640 182 342 344 0   0   X   0   0
641 195 344 536 0   0   Z   0   0
642 180 337 537 0   0   Z   0   0
643 175 347 536 0   0   X   0   0
644 176 348 347 0   0   X   0   0
645 186 334 348 0   0   X   0   0
646 196 349 334 0   0   X   0   0
647 197 349 537 0   0   X   0   0
648 105 350 21  0   0   Z   0   0
649 104 382 350 0   0   Z   0   0
650 104 406 382 0   0   Z   0   0
651 104 426 406 0   0   Z   0   0
652 104 446 426 0   0   Z   0   0
653 104 466 446 0   0   Z   0   0
654 104 486 466 0   0   Z   0   0
655 104 506 486 0   0   Z   0   0
656 104 525 506 0   0   Z   0   0
657 106 351 23  0   0   X   0   0
658 142 383 351 0   0   X   0   0
659 142 407 383 0   0   X   0   0
660 142 427 407 0   0   X   0   0
661 142 447 427 0   0   X   0   0
662 142 467 447 0   0   X   0   0
663 142 487 467 0   0   X   0   0
664 142 508 487 0   0   X   0   0
665 142 526 508 0   0   X   0   0
666 105 352 25  0   0   X   0   0
667 104 384 352 0   0   X   0   0
668 104 408 384 0   0   X   0   0
669 104 428 408 0   0   X   0   0
670 104 448 428 0   0   X   0   0
671 104 468 448 0   0   X   0   0
672 104 488 468 0   0   X   0   0
673 104 510 488 0   0   X   0   0
674 104 527 510 0   0   X   0   0
675 105 355 27  0   0   Z   0   0
676 104 386 355 0   0   Z   0   0
677 104 410 386 0   0   Z   0   0
678 104 430 410 0   0   Z   0   0
679 104 450 430 0   0   Z   0   0
680 104 470 450 0   0   Z   0   0
681 104 490 470 0   0   Z   0   0
682 104 512 490 0   0   Z   0   0
683 100 538 315 0   0   X   0   0
684 101 538 316 0   0   Z   0   0
```

```
685 105 356 29  0   0   Z   0   0
686 104 388 356 0   0   Z   0   0
687 104 411 388 0   0   Z   0   0
688 104 431 411 0   0   Z   0   0
689 104 451 431 0   0   Z   0   0
690 104 471 451 0   0   Z   0   0
691 104 491 471 0   0   Z   0   0
692 104 513 491 0   0   Z   0   0
693 107 358 101 0   0   X   0   0
694 108 359 102 0   0   X   0   0
695 143 389 359 0   0   X   0   0
696 105 363 539 0   0   X   0   0
697 104 393 363 0   0   X   0   0
698 104 415 393 0   0   X   0   0
699 104 435 415 0   0   X   0   0
700 104 455 435 0   0   X   0   0
701 104 475 455 0   0   X   0   0
702 104 495 475 0   0   X   0   0
703 104 323 495 0   0   X   0   0
704 105 360 109 0   0   X   0   0
705 104 390 360 0   0   X   0   0
706 104 412 390 0   0   X   0   0
707 104 432 412 0   0   X   0   0
708 104 452 432 0   0   X   0   0
709 104 472 452 0   0   X   0   0
710 104 492 472 0   0   X   0   0
711 106 365 31  0   0   Z   0   0
712 142 391 365 0   0   Z   0   0
713 142 413 391 0   0   Z   0   0
714 142 433 413 0   0   Z   0   0
715 142 453 433 0   0   Z   0   0
716 142 473 453 0   0   Z   0   0
717 142 493 473 0   0   Z   0   0
718 106 361 33  0   0   Z   0   0
719 142 392 361 0   0   Z   0   0
720 142 414 392 0   0   Z   0   0
721 142 434 414 0   0   Z   0   0
722 142 454 434 0   0   Z   0   0
723 142 474 454 0   0   Z   0   0
724 142 494 474 0   0   Z   0   0
725 142 515 494 0   0   Z   0   0
726 108 364 103 0   0   X   0   0
727 143 394 364 0   0   X   0   0
728 107 367 115 0   0   X   0   0
729 108 370 104 0   0   X   0   0
730 143 395 370 0   0   X   0   0
731 105 371 37  0   0   Z   0   0
732 104 396 371 0   0   Z   0   0
733 104 416 396 0   0   Z   0   0
734 104 436 416 0   0   Z   0   0
735 104 456 436 0   0   Z   0   0
736 104 476 456 0   0   Z   0   0
737 104 496 476 0   0   Z   0   0
738 104 517 496 0   0   Z   0   0
739 105 374 105 0   0   Z   0   0
740 104 398 374 0   0   Z   0   0
741 104 418 398 0   0   Z   0   0
742 104 438 418 0   0   Z   0   0
743 104 458 438 0   0   Z   0   0
744 104 478 458 0   0   Z   0   0
745 104 498 478 0   0   Z   0   0
746 105 373 99  0   0   Z   0   0
747 104 397 373 0   0   Z   0   0
748 104 417 397 0   0   Z   0   0
749 104 437 417 0   0   Z   0   0
750 104 457 437 0   0   Z   0   0
751 104 477 457 0   0   Z   0   0
752 104 497 477 0   0   Z   0   0
753 105 376 41  0   0   Z   0   0
754 104 400 376 0   0   Z   0   0
755 104 420 400 0   0   Z   0   0
```

```
756 104 440 420 0   0   Z   0   0
757 104 460 440 0   0   Z   0   0
758 104 480 460 0   0   Z   0   0
759 104 500 480 0   0   Z   0   0
760 104 520 500 0   0   Z   0   0
761 105 375 43  0   0   Z   0   0
762 104 399 375 0   0   Z   0   0
763 104 419 399 0   0   Z   0   0
764 104 439 419 0   0   Z   0   0
765 104 459 439 0   0   Z   0   0
766 104 479 459 0   0   Z   0   0
767 104 499 479 0   0   Z   0   0
768 104 521 499 0   0   Z   0   0
769 105 379 45  0   0   Z   0   0
770 104 403 379 0   0   Z   0   0
771 104 423 403 0   0   Z   0   0
772 104 443 423 0   0   Z   0   0
773 104 463 443 0   0   Z   0   0
774 104 483 463 0   0   Z   0   0
775 104 503 483 0   0   Z   0   0
776 104 522 503 0   0   Z   0   0
777 104 536 522 0   0   Z   0   0
778 105 378 47  0   0   Z   0   0
779 104 402 378 0   0   Z   0   0
780 104 422 402 0   0   Z   0   0
781 104 442 422 0   0   Z   0   0
782 104 462 442 0   0   Z   0   0
783 104 482 462 0   0   Z   0   0
784 104 502 482 0   0   Z   0   0
785 104 523 502 0   0   Z   0   0
786 101 523 347 0   0   Z   0   0
787 104 348 523 0   0   Z   0   0
788 105 380 49  0   0   Z   0   0
789 104 404 380 0   0   Z   0   0
790 104 424 404 0   0   Z   0   0
791 104 444 424 0   0   Z   0   0
792 104 464 444 0   0   Z   0   0
793 104 484 464 0   0   Z   0   0
794 104 504 484 0   0   Z   0   0
795 104 524 504 0   0   Z   0   0
796 104 537 524 0   0   Z   0   0

PROPS
1   FRAME   Gravity Column
    1   3   3   0   0   0   0   0   0
    248211284     103421368.3  0.0112243     9.30E-07      0.000140676  4.84E-05
0.007381333 0.00273 0   0   0
    0   0   0   0   0   0   0   0   0   0
2   SPRING  LRB 1
    1   2   0   0   1   0   0   0   0   0
    894000  6563    6563    0   10290   10290   0   0.13036 0
    -347    0   0   0   0   0   0
    175 -2500   42  -42 42  -42
    0   0   0   0   0   0
3   SPRING  LRB 2
    1   2   0   0   1   0   0   0   0   0
    894000  6563    6563    0   10290   10290   0   0.13036 0
    -667    0   0   0   0   0   0
    175 -2500   42  -42 42  -42
    0   0   0   0   0   0
4   SPRING  LRB 3
    1   2   0   0   1   0   0   0   0   0
    894000  6563    6563    0   10290   10290   0   0.13036 0
    -973    0   0   0   0   0   0
    175 -2500   42  -42 42  -42
    0   0   0   0   0   0
5   SPRING  LRB 4
    1   2   0   0   1   0   0   0   0   0
    894000  6563    6563    0   10290   10290   0   0.13036 0
    -832    0   0   0   0   0   0
```

```
    175 -2500   42  -42 42  -42
    0   0   0   0   0   0
6   SPRING  LRB 5
    1   2   0   0   1   0   0   0   0   0
    894000  6563    6563    0   10290   10290   0   0.13036 0
    -615    0   0   0   0   0   0
    175 -2500   42  -42 42  -42
    0   0   0   0   0   0
7   SPRING  LRB 6
    1   2   0   0   1   0   0   0   0   0
    894000  6563    6563    0   10290   10290   0   0.13036 0
    -1280   0   0   0   0   0   0
    175 -2500   42  -42 42  -42
    0   0   0   0   0   0
8   SPRING  LRB 7
    1   2   0   0   1   0   0   0   0   0
    894000  6563    6563    0   10290   10290   0   0.13036 0
    -1210   0   0   0   0   0   0
    175 -2500   42  -42 42  -42
    0   0   0   0   0   0
9   SPRING  LRB 8
    1   2   0   0   1   0   0   0   0   0
    894000  6563    6563    0   10290   10290   0   0.13036 0
    -1330   0   0   0   0   0   0
    175 -2500   42  -42 42  -42
    0   0   0   0   0   0
10  SPRING  LRB 9
    1   2   0   0   1   0   0   0   0   0
    894000  6563    6563    0   10290   10290   0   0.13036 0
    -1110   0   0   0   0   0   0
    175 -2500   42  -42 42  -42
    0   0   0   0   0   0
11  SPRING  LRB 10
    1   2   0   0   1   0   0   0   0   0
    894000  6563    6563    0   10290   10290   0   0.13036 0
    -1510   0   0   0   0   0   0
    175 -2500   42  -42 42  -42
    0   0   0   0   0   0
12  SPRING  LRB 11
    1   2   0   0   1   0   0   0   0   0
    894000  6563    6563    0   10290   10290   0   0.13036 0
    -687    0   0   0   0   0   0
    175 -2500   42  -42 42  -42
    0   0   0   0   0   0
13  SPRING  LRB 12
    1   2   0   0   1   0   0   0   0   0
    894000  6563    6563    0   10290   10290   0   0.13036 0
    -977    0   0   0   0   0   0
    175 -2500   42  -42 42  -42
    0   0   0   0   0   0
14  SPRING  LRB 13
    1   2   0   0   1   0   0   0   0   0
    894000  6563    6563    0   10290   10290   0   0.13036 0
    -720    0   0   0   0   0   0
    175 -2500   42  -42 42  -42
    0   0   0   0   0   0
15  SPRING  LRB 14
    1   2   0   0   1   0   0   0   0   0
    894000  6563    6563    0   10290   10290   0   0.13036 0
    -776    0   0   0   0   0   0
    175 -2500   42  -42 42  -42
    0   0   0   0   0   0
16  SPRING  LRB 15
    1   2   0   0   1   0   0   0   0   0
    894000  6563    6563    0   10290   10290   0   0.13036 0
    -373    0   0   0   0   0   0
    175 -2500   42  -42 42  -42
    0   0   0   0   0   0
17  SPRING  SB 1
    5   1   0   0   0   0   0   0   0   0
    8940000 0   0   0   0   0   0   0   0
```

```
    148.2   0.04    0   0
18  SPRING  SB 2
    5   1   0   0   0   0   0   0   0   0
    8940000 0   0   0   0   0   0   0   0
    113.84  0.04    0   0
19  SPRING  SB 3
    5   1   0   0   0   0   0   0   0   0
    8940000 0   0   0   0   0   0   0   0
    59.87   0.04    0   0
20  SPRING  SB 4
    5   1   0   0   0   0   0   0   0   0
    8940000 0   0   0   0   0   0   0   0
    246.9   0.04    0   0
21  SPRING  SB 5
    5   1   0   0   0   0   0   0   0   0
    8940000 0   0   0   0   0   0   0   0
    213.72  0.04    0   0
22  SPRING  SB 6
    5   1   0   0   0   0   0   0   0   0
    8940000 0   0   0   0   0   0   0   0
    130.76  0.04    0   0
23  SPRING  SB 7
    5   1   0   0   0   0   0   0   0   0
    8940000 0   0   0   0   0   0   0   0
    130.52  0.04    0   0
24  SPRING  SB 8
    5   1   0   0   0   0   0   0   0   0
    8940000 0   0   0   0   0   0   0   0
    71.66   0.04    0   0
25  SPRING  SB 9
    5   1   0   0   0   0   0   0   0   0
    8940000 0   0   0   0   0   0   0   0
    67.98   0.04    0   0
26  SPRING  SB 10
    5   1   0   0   0   0   0   0   0   0
    8940000 0   0   0   0   0   0   0   0
    296.39  0.04    0   0
27  SPRING  SB 11
    5   1   0   0   0   0   0   0   0   0
    8940000 0   0   0   0   0   0   0   0
    347.2   0.04    0   0
28  SPRING  SB 12
    5   1   0   0   0   0   0   0   0   0
    8940000 0   0   0   0   0   0   0   0
    104.16  0.04    0   0
29  SPRING  SB 13
    5   1   0   0   0   0   0   0   0   0
    8940000 0   0   0   0   0   0   0   0
    146.75  0.04    0   0
30  SPRING  SB Axial Element
    1   15  0   0   0   0   0   0   0   0
    8940000 8940000 8940000 0   0   0
    1   -11000  0   0   0   0
    0   0   0   0   0   0
31  FRAME   Grillage 1
    1   0   0   0   0   0   0   0   0
    27897000     11623750     1.295    0.167711     0.09382 0.250268     0.96011
0.790724    0   0   0
    0   0   0   0   0   0   0   0   0   0
32  FRAME   Grillage 2
    1   0   0   0   0   0   0   0   0
    27897000    11623750    1.3745  0.168312    0.100717    0.456894    0.967926
0.630488    0   0   0
    0   0   0   0   0   0   0   0   0   0
33  FRAME   Grillage 3
    1   0   0   0   0   0   0   0   0
    27897000     11623750     1.295    0.167711     0.09379 0.250268     0.96011
0.790724    0   0   0
    0   0   0   0   0   0   0   0   0   0
34  FRAME   Grillage 4
```

```
    1   0   0   0   0   0   0   0   0
    27897000    11623750    1.3655  0.168244    0.101819    0.337122    0.967171
0.939722    0   0   0
    0   0   0   0   0   0   0   0   0   0
35  FRAME   Grillage 5
    1   0   0   0   0   0   0   0   0
    27897000    11623750    1.22    0.167049    0.087195    0.144348    0.949376
1.074524    0   0   0
    0   0   0   0   0   0   0   0   0   0
36  FRAME   Grillage 6
    1   0   0   0   0   0   0   0   0
    27897000     11623750     1.3655  0.168244     0.10011 0.337122     0.967171
0.939722    0   0   0
    0   0   0   0   0   0   0   0   0   0
37  FRAME   Grillage 7
    1   0   0   0   0   0   0   0   0
    27897000     11623750     1.265   0.167486     0.092022     0.18721 0.956315
1.045839    0   0   0
    0   0   0   0   0   0   0   0   0   0
38  FRAME   Grillage 8
    1   0   0   0   0   0   0   0   0
    27897000    11623750    1.326   0.180716    0.103785    0.206314    0.998567
1.064014    0   0   0
    0   0   0   0   0   0   0   0   0   0
39  FRAME   Grillage 9
    1   0   0   0   0   0   0   0   0
    27897000     11623750     1.3575  0.180952     0.107269     0.24782 1.002313
1.02303 0   0   0
    0   0   0   0   0   0   0   0   0   0
40  FRAME   Grillage 10
    1   0   0   0   0   0   0   0   0
    27897000     11623750     1.35    0.180892     0.105348     0.26915 1.001473
0.786268    0   0   0
    0   0   0   0   0   0   0   0   0   0
41  FRAME   Grillage 11
    1   0   0   0   0   0   0   0   0
    27897000    11623750    1.3785  0.181197    0.108093    0.279859    1.00451
0.997245    0   0   0
    0   0   0   0   0   0   0   0   0   0
42  FRAME   Grillage 12
    1   0   0   0   0   0   0   0   0
    27897000    11623750    1.455   0.181801    0.115702    0.429678    1.010981
0.931383    0   0   0
    0   0   0   0   0   0   0   0   0   0
43  FRAME   Grillage 13
    1   0   0   0   0   0   0   0   0
    27897000     11623750     1.35    0.180892     0.104857     0.26915 1.001473
0.786268    0   0   0
    0   0   0   0   0   0   0   0   0   0
44  FRAME   Grillage 14
    1   0   0   0   0   0   0   0   0
    27897000     11623750     1.35    0.180892     0.105925     0.26915 1.001473
0.786268    0   0   0
    0   0   0   0   0   0   0   0   0   0
45  FRAME   Grillage 15
    1   0   0   0   0   0   0   0   0
    27897000    11623750    2.0325  0.448667    0.247514    0.513747    1.569223
1.198973    0   0   0
    0   0   0   0   0   0   0   0   0   0
46  FRAME   Grillage 16
    1   0   0   0   0   0   0   0   0
    27897000     11623750     2.16    0.449624     0.268453     0.7776  1.583636
1.356777    0   0   0
    0   0   0   0   0   0   0   0   0   0
47  FRAME   Grillage 17
    1   0   0   0   0   0   0   0   0
    27897000      11623750     2.22     0.47644 0.307719     0.7848  1.635467
1.382535    0   0   0
    0   0   0   0   0   0   0   0   0   0
48  FRAME   Grillage 18
    1   0   0   0   0   0   0   0   0
```

```
    27897000    11623750    2.0925  0.475483    0.282753    0.521381    1.62072
1.228123    0   0   0
    0   0   0   0   0   0   0   0   0   0
49  FRAME   Grillage 19
    1   0   0   0   0   0   0   0   0
    27897000    11623750    1.953   0.474365    0.254267    0.276957    1.591738
1.709864    0   0   0
    0   0   0   0   0   0   0   0   0   0
50  FRAME   Grillage 20
    1   0   0   0   0   0   0   0   0
    27897000      11623750      2.0985   0.475531      0.28435  0.47307  1.621602
1.628597    0   0   0
    0   0   0   0   0   0   0   0   0   0
51  FRAME   Grillage 21
    1   0   0   0   0   0   0   0   0
    27897000      11623750      2.22      0.47644  0.308367      0.7848   1.635467
1.382535    0   0   0
    0   0   0   0   0   0   0   0   0   0
52  FRAME   Grillage 23
    1   0   0   0   0   0   0   0   0
    27897000    11623750    2.0925  0.475483    0.283341    0.521381    1.62072
1.228123    0   0   0
    0   0   0   0   0   0   0   0   0   0
53  FRAME   Grillage 24
    1   0   0   0   0   0   0   0   0
    27897000      11623750      2.22      0.47644  0.308367      0.7848   1.635467
1.382535    0   0   0
    0   0   0   0   0   0   0   0   0   0
54  FRAME   Grillage 25
    1   0   0   0   0   0   0   0   0
    27897000     11623750     2.46     0.586025     0.432458     0.8136  1.843123
1.485803    0   0   0
    0   0   0   0   0   0   0   0   0   0
55  FRAME   Grillage 26
    1   0   0   0   0   0   0   0   0
    27897000     11623750     2.46     0.586025     0.432483     0.8136  1.843123
1.485803    0   0   0
    0   0   0   0   0   0   0   0   0   0
56  FRAME   Grillage 27
    1   0   0   0   0   0   0   0   0
    27897000    11623750    0.285   0.004458    0.003955    0.017538    0.16502
0.224027    0   0   0
    0   0   0   0   0   0   0   0   0   0
57  FRAME   Grillage 28
    1   0   0   0   0   0   0   0   0
    27897000    11623750    0.41    0.010099    0.008728    0.036967    0.246907
0.310096    0   0   0
    0   0   0   0   0   0   0   0   0   0
58  FRAME   Link W1 (G)
    1   0   0   0   0   0   0   0   0
    28241000     11767083.33 0.56525 0.001993     12.2858 0.00577 0    0.471042
0   0   0
    0   0   0   0   0   0   0   0   0   0
59  FRAME   Link W2 (G)
    1   0   0   0   0   0   0   0   0
    28241000    11767083.33 0.4845  0.001283    10.5307 0.003634    0   0.40375
0   0   0
    0   0   0   0   0   0   0   0   0   0
60  FRAME   Link W3 (G)
    1   0   0   0   0   0   0   0   0
    28241000    11767083.33 0.40375 0.000759    8.7756  0.002103    0   0.336458
0   0   0
    0   0   0   0   0   0   0   0   0   0
61  FRAME   Wall N1 (G-4)
    1   0   0   0   0   0   0   0   0
    25000000    10416666.67 1.220928339 0.045414    1.99    0.011779    1.30875
1.30875 0   0   0
    0   0   0   0   0   0   0   0   0   0
62  FRAME   Wall N1 (4-P1)
    1   0   0   0   0   0   0   0   0
```

```
    25000000    10416666.67 1.058917299 0.045414    1.25    0.011779    1.30875
1.30875 0   0   0
    0   0   0   0   0   0   0   0   0   0
63  FRAME   Wall N2 (G-4)
    1   0   0   0   0   0   0   0   0
    25000000     10416666.67 1.56023951  0.089459     2.983    0.023153     1.89
1.89    0   0   0
    0   0   0   0   0   0   0   0   0   0
64  FRAME   Wall N2 (4-P1)
    1   0   0   0   0   0   0   0
    25000000     10416666.67 1.423065548 0.089459     2.023    0.023153     1.89
1.89    0   0   0
    0   0   0   0   0   0   0   0   0   0
65  FRAME   Wall N3 (G-1)
    1   0   0   0   0   0   0   0   0
    25000000    10416666.67 1.038791899 0.045774    1.148   0.011869    1.31875
1.31875 0   0   0
    0   0   0   0   0   0   0   0   0   0
66  FRAME   Wall N3 (UG) Pier-N
    1   0   0   0   0   0   0   0   0
    25000000    10416666.67 0.247339286 0.00928 0.016   0.002745    0.305   0.305
0   0   0
    0   0   0   0   0   0   0   0   0   0
67  FRAME   Wall N3 (UG) Pier-S
    1   0   0   0   0   0   0   0   0
    25000000    10416666.67 0.471676973 0.019629    0.109   0.005333    0.5925
0.5925  0   0   0
    0   0   0   0   0   0   0   0   0   0
68  FRAME   Wall N3 (1-4)
    1   0   0   0   0   0   0   0   0
    25000000    10416666.67 0.975397023 0.045774    0.854   0.011869    1.31875
1.31875 0   0   0
    0   0   0   0   0   0   0   0   0   0
69  FRAME   Wall N3 (4-PG)
    1   0   0   0   0   0   0   0   0
    25000000    10416666.67 0.913727177 0.045774    0.568   0.011869    1.31875
1.31875 0   0   0
    0   0   0   0   0   0   0   0   0   0
70  FRAME   Wall S1 (G) Pier-N
    1   0   0   0   0   0   0   0   0
    25000000    10416666.67 0.762862498 0.033849    0.443   0.008888    0.9875
0.9875  0   0   0
    0   0   0   0   0   0   0   0   0   0
71  FRAME   Wall S1 (G) Pier-S
    1   0   0   0   0   0   0   0   0
    25000000    10416666.67 0.11025 0.002729    0.0014705   0.001103    0.1225
0.1225  0   0   0
    0   0   0   0   0   0   0   0   0   0
72  FRAME   Wall S1 (UG) Pier-N
    1   0   0   0   0   0   0   0   0
    25000000    10416666.67 0.12375 0.003262    0.0020795   0.001238    0.1375
0.1375  0   0   0
    0   0   0   0   0   0   0   0   0   0
73  FRAME   Wall S1 (UG) Pier-S
    1   0   0   0   0   0   0   0   0
    25000000     10416666.67 0.764422118 0.034119    0.442   0.008955    0.995
0.995   0   0   0
    0   0   0   0   0   0   0   0   0   0
74  FRAME   Wall S1 (1-2)
    1   0   0   0   0   0   0   0   0
    25000000    10416666.67 1.052738189 0.048339    1.127   0.01251 1.39    1.39
0   0   0
    0   0   0   0   0   0   0   0   0   0
75  FRAME   Wall S1 (2-4)
    1   0   0   0   0   0   0   0   0
    25000000    10416666.67 0.995093786 0.048339    0.83    0.01251 1.39    1.39
0   0   0
    0   0   0   0   0   0   0   0   0   0
76  FRAME   Wall S1 (4-PG)
    1   0   0   0   0   0   0   0   0
```

```
    25000000    10416666.67 0.944242495 0.048339    0.568   0.01251 1.39    1.39
0   0   0
    0   0   0   0   0   0   0   0   0   0
77  FRAME   Wall S2 (G-4)
    1   0   0   0   0   0   0   0   0
    25000000    10416666.67 1.078752363 0.039699    1.371   0.01035 1.15    1.15
0   0   0
    0   0   0   0   0   0   0   0   0   0
78  FRAME   Wall S2 (4-P1)
    1   0   0   0   0   0   0   0   0
    25000000    10416666.67 0.93584121  0.039699    0.867   0.01035 1.15    1.15
0   0   0
    0   0   0   0   0   0   0   0   0   0
79  FRAME   Wall S3 (G-4)
    1   0   0   0   0   0   0   0   0
    25000000    10416666.67 1.305288066 0.074024    1.751   0.019294    1.575
1.575   0   0   0
    0   0   0   0   0   0   0   0   0   0
80  FRAME   Wall S3 (4-P1)
    1   0   0   0   0   0   0   0   0
    25000000    10416666.67 1.188004115 0.074024    1.181   0.019294    1.575
1.575   0   0   0
    0   0   0   0   0   0   0   0   0   0
81  FRAME   Wall S4 (G-1)
    1   0   0   0   0   0   0   0   0
    25000000    10416666.67 0.500162095 0.015794    0.172   0.004154    0.664583
0.664583    0   0   0
    0   0   0   0   0   0   0   0   0   0
82  FRAME   Wall S4 (1-4)
    1   0   0   0   0   0   0   0   0
    25000000    10416666.67 0.554166667 0.01793 0.148231    0.004688    0.75
0.75    0   0   0
    0   0   0   0   0   0   0   0   0   0
83  FRAME   Wall S4 (4-P1)
    1   0   0   0   0   0   0   0   0
    25000000    10416666.67 0.524074074 0.01793 0.094816    0.004688    0.75
0.75    0   0   0
    0   0   0   0   0   0   0   0   0   0
84  FRAME   Link W1 (UG-1)
    1   0   0   0   0   0   0   0   0
    28241000    11767083.33 1.10075 0.00418 90.7295 0.011237    0   0.917292
0   0   0
    0   0   0   0   0   0   0   0   0   0
85  FRAME   Link W1 (2-PG)
    1   0   0   0   0   0   0   0   0
    28241000    11767083.33 1.1305  0.004301    98.2866 0.011541    0   0.942083
0   0   0
    0   0   0   0   0   0   0   0   0   0
86  FRAME   Link W1 (P1)
    1   0   0   0   0   0   0   0   0
    28241000    11767083.33 0.56525 0.001993    12.2858 0.00577 0   0.471042
0   0   0
    0   0   0   0   0   0   0   0   0   0
87  FRAME   Link W2 (UG-1)
    1   0   0   0   0   0   0   0   0
    28241000    11767083.33 0.9435  0.00266 77.7682 0.007076    0   0.78625 0
0   0
    0   0   0   0   0   0   0   0   0   0
88  FRAME   Link W2 (2-PG)
    1   0   0   0   0   0   0   0   0
    28241000    11767083.33 0.969   0.002737    84.2457 0.007268    0   0.8075
0   0   0
    0   0   0   0   0   0   0   0   0   0
89  FRAME   Link W2 (P1)
    1   0   0   0   0   0   0   0   0
    28241000    11767083.33 0.4845  0.001283    10.5307 0.003634    0   0.40375
0   0   0
    0   0   0   0   0   0   0   0   0   0
90  FRAME   Link W3 (UG-1)
    1   0   0   0   0   0   0   0   0
```

```
    28241000    11767083.33 0.78625 0.001556    64.8068 0.004095    0   0.655208
0   0   0
    0   0   0   0   0   0   0   0   0   0
91  FRAME   Link W3 (2-PG)
    1   0   0   0   0   0   0   0   0
    28241000     11767083.33 0.8075  0.0016  70.2047 0.004206     0    0.672917
0   0   0
    0   0   0   0   0   0   0   0   0   0
92  FRAME   Link W3 (P1)
    1   0   0   0   0   0   0   0   0
    28241000    11767083.33 0.40375 0.000759    8.7756  0.002103    0   0.336458
0   0   0
    0   0   0   0   0   0   0   0   0   0
93  FRAME   Wall N2 (R)
    1   0   0   0   0   0   0   0   0
    25000000     10416666.67 0.656333333 0.039724     0.197    0.010719     0.875
0.875   0   0   0
    0   0   0   0   0   0   0   0   0   0
94  FRAME   Wall S2 (R)
    1   0   0   0   0   0   0   0   0
    25000000    10416666.67 0.455050663 0.018594    0.099   0.005074    0.56375
0.56375 0   0   0
    0   0   0   0   0   0   0   0   0   0
95  FRAME   Wall S3 (R)
    1   0   0   0   0   0   0   0   0
    25000000     10416666.67 0.709384711 0.04344 0.246    0.011648     0.950833
0.950833    0   0   0
    0   0   0   0   0   0   0   0   0   0
96  FRAME   Wall S4 (R)
    1   0   0   0   0   0   0   0   0
    25000000     10416666.67 0.351131087 0.011992    0.044   0.003203     0.5125
0.5125  0   0   0
    0   0   0   0   0   0   0   0   0   0
97  FRAME   Link W3 (Roof)
    1   0   0   0   0   0   0   0   0
    28241000    11767083.33 0.47375 0.000905    14.1771 0.002467    0   0.394792
0   0   0
    0   0   0   0   0   0   0   0   0   0
98  FRAME   Link W2 (Roof)
    1   0   0   0   0   0   0   0   0
    28241000    11767083.33 0.5685  0.001535    17.0125 0.004264    0   0.47375
0   0   0
    0   0   0   0   0   0   0   0   0   0
99  FRAME   125x9 SHS, joint flexibility: [1-Z=0.0017 1-Y=0.0017 2-Z=0.0017 2-
Y=0.0017 ]
    1   0   0   0   0   0   0   0   0
    205000000   78846153.85 0.004176   1.40E-05   9.42E-06   9.42E-06   0.00225
0.00225 0   0   0
    0   0   0   0   0.0017  0.0017  0.0017  0.0017  0   0
100 FRAME    125x9 SHS, joint flexibility: [1-Z=0.002 1-Y=0.002 2-Z=0.002 2-
Y=0.002 ]
    1   0   0   0   0   0   0   0   0
    205000000   78846153.85 0.004176   1.40E-05   9.42E-06   9.42E-06   0.00225
0.00225 0   0   0
    0   0   0   0   0.002   0.002   0.002   0.002   0   0
101 FRAME   130x10 FL, pinned (major), pinned (minor)
    1   3   3   0   0   0   0   0   0
    205000000   78846153.85 0.0013  4.12E-08   1.08E-08   1.83E-06   0.001083333
0.001083333 0   0   0
    0   0   0   0   0   0   0   0   0   0
102 FRAME    89x6 SHS, joint flexibility: [1-Z=0.0083 1-Y=0.0083 2-Z=0.0083 2-
Y=0.0083 ]
    1   0   0   0   0   0   0   0   0
    205000000     78846153.85  0.001992      3.43E-06      2.30E-06      2.30E-06
0.001068    0.001068    0   0   0
    0   0   0   0   0.0083  0.0083  0.0083  0.0083  0   0
103 FRAME    250UC90, joint flexibility: [1-Z=0.0001 1-Y=0.0004 2-Z=0.0001 2-
Y=0.0004 ]
    1   0   0   0   0   0   0   0   0
    205000000   78846153.85 0.0112243  9.30E-07   0.000140676 4.84E-05   0.00273
0.007381333 0   0   0
```

```
    0   0   0   0   0.0001  0.0001  0.0004  0.0004  0   0
104 FRAME   250UC90
    1   0   0   0   0   0   0   0   0
    205000000   78846153.85 0.0112243   9.30E-07    0.000140676 4.84E-05    0.00273
0.007381333 0   0   0
    0   0   0   0   0   0   0   0   0
105 FRAME   250UC90, hinged-J (major), hinged-J (minor)
    1   2   2   0   0   0   0   0   0
    205000000   78846153.85 0.0112243   9.30E-07    0.000140676 4.84E-05    0.00273
0.007381333 0   0   0
    0   0   0   0   0   0   0   0   0   0
106 FRAME   250UC90, hinged-J (major), hinged-J (minor), offset: y=0 z=0
    1   2   2   0   0   0   0   0   0
    205000000   78846153.85 0.0112243   9.30E-07    0.000140676 4.84E-05    0.00273
0.007381333 0   0   0
    0   0   0   0   0   0   0   0   0   0
107 FRAME   125x75x6 RHS, pinned (major), pinned (minor)
    1   3   3   0   0   0   0   0   0
    205000000   78846153.85 0.002256    4.30E-06    4.63E-06    2.04E-06    0.0015
0.0009  0   0   0
    0   0   0   0   0   0   0   0   0   0
108 FRAME   125x75x6 RHS, hinged-J (major), hinged-J (minor)
    1   2   2   0   0   0   0   0   0
    205000000   78846153.85 0.002256    4.30E-06    4.63E-06    2.04E-06    0.0015
0.0009  0   0   0
    0   0   0   0   0   0   0   0   0   0
109 FRAME    250UB26, joint flexibility: [1-Z=0.0005 1-Y=0.0073 2-Z=0.0005 2-
Y=0.0073 ]
    1   0   0   0   0   0   0   0   0
    205000000   78846153.85 0.003144    5.01E-08    3.38E-05    2.54E-06    0.00124
0.001653333 0   0   0
    0   0   0   0   0.0005  0.0005  0.0073  0.0073  0   0
110 FRAME   250UC90 (P15), joint flexibility: [1-Z=0.0 1-Y=0.0001 ]
    1   0   0   0   0   0   0   0   0
    205000000   78846153.85 0.0112243   9.30E-07    0.000140676 4.84E-05    0.00273
0.007381333 0   0   0
    0   0   0   0   0   0   0.0001  0   0   0
111 FRAME    250UC90, joint flexibility: [1-Z=0.0001 1-Y=0.0002 2-Z=0.0001 2-
Y=0.0002 ]
    1   0   0   0   0   0   0   0   0
    205000000   78846153.85 0.0112243   9.30E-07    0.000140676 4.84E-05    0.00273
0.007381333 0   0   0
    0   0   0   0   0.0001  0.0001  0.0002  0.0002  0   0
112 FRAME   250UC90 # (P15), joint flexibility: [1-Z=0.0001 1-Y=0.0002 ]
    1   0   0   0   0   0   0   0   0
    205000000   78846153.85 0.0112243   9.30E-07    0.000140676 4.84E-05    0.00273
0.007381333 0   0   0
    0   0   0   0   0.0001  0   0.0002  0   0   0
113 FRAME   152x76x6 RHS, joint flexibility: [1-Z=0.003 1-Y=0.0092 2-Z=0.003 2-
Y=0.0092 ]
    1   0   0   0   0   0   0   0   0
    205000000    78846153.85  0.002592     5.80E-06     7.61E-06     2.50E-06
0.001824    0.000912    0   0   0
    0   0   0   0   0.003   0.003   0.0092  0.0092  0   0
114 FRAME   250UC90, joint flexibility: [2-Z=0.0 2-Y=0.0001 ]
    1   0   0   0   0   0   0   0   0
    205000000   78846153.85 0.0112243   9.30E-07    0.000140676 4.84E-05    0.00273
0.007381333 0   0   0
    0   0   0   0   0   0   0   0.0001  0   0
115 FRAME   250UC90, joint flexibility: [2-Z=0.0001 2-Y=0.0004 ]
    1   0   0   0   0   0   0   0   0
    205000000   78846153.85 0.0112243   9.30E-07    0.000140676 4.84E-05    0.00273
0.007381333 0   0   0
    0   0   0   0   0   0.0001  0   0.0004  0   0
116 FRAME   250UC90 # (P15)
    1   0   0   0   0   0   0   0   0
    205000000   78846153.85 0.0112243   9.30E-07    0.000140676 4.84E-05    0.00273
0.007381333 0   0   0
    0   0   0   0   0   0   0   0   0   0
```

```
117 FRAME   152x76x6 RHS, joint flexibility: [1-Z=0.0015 1-Y=0.0047 2-Z=0.0015
2-Y=0.0047 ]
    1   0   0   0   0   0   0   0   0
    205000000     78846153.85  0.002592      5.80E-06      7.61E-06      2.50E-06
0.001824    0.000912    0   0   0
    0   0   0   0   0.0015  0.0015  0.0047  0.0047  0   0
118 FRAME   250UC90 (P15), joint flexibility: [2-Z=0.0002 2-Y=0.0005 ]
    1   0   0   0   0   0   0   0   0
    205000000   78846153.85 0.0112243   9.30E-07   0.000140676 4.84E-05   0.00273
0.007381333 0   0   0
    0   0   0   0   0   0.0002  0   0.0005  0   0
119 FRAME   152x76x6 RHS, joint flexibility: [1-Z=0.0029 1-Y=0.0089 2-Z=0.0029
2-Y=0.0089 ]
    1   0   0   0   0   0   0   0   0
    205000000     78846153.85  0.002592      5.80E-06      7.61E-06      2.50E-06
0.001824    0.000912    0   0   0
    0   0   0   0   0.0029  0.0029  0.0089  0.0089  0   0
120 FRAME    200UC52, joint flexibility: [1-Z=0.0002 1-Y=0.0006 2-Z=0.0002 2-
Y=0.0006 ]
    1   0   0   0   0   0   0   0   0
    205000000     78846153.85  0.006548      2.85E-07      5.18E-05      1.77E-05
0.001648    0.00425 0   0   0
    0   0   0   0   0.0002  0.0002  0.0006  0.0006  0   0
121 FRAME   152x76x6 RHS, joint flexibility: [1-Z=0.0015 1-Y=0.0045 2-Z=0.0015
2-Y=0.0045 ]
    1   0   0   0   0   0   0   0   0
    205000000     78846153.85  0.002592      5.80E-06      7.61E-06      2.50E-06
0.001824    0.000912    0   0   0
    0   0   0   0   0.0015  0.0015  0.0045  0.0045  0   0
122 FRAME   250UC90 # (P15), joint flexibility: [1-Z=0.0 1-Y=0.0001 ]
    1   0   0   0   0   0   0   0   0
    205000000   78846153.85 0.0112243   9.30E-07   0.000140676 4.84E-05   0.00273
0.007381333 0   0   0
    0   0   0   0   0   0   0.0001  0   0   0
123 FRAME   310UC137, joint flexibility: [1-Z=0.0001 1-Y=0.0002 ]
    1   0   0   0   0   0   0   0   0
    205000000    78846153.85 0.0175  2.52E-06    0.000329    0.000107    0.0044298
0.0111755   0   0   0
    0   0   0   0   0.0001  0   0.0002  0   0   0
124 FRAME   310UC137, joint flexibility: [2-Z=0.0 2-Y=0.0 ]
    1   0   0   0   0   0   0   0   0
    205000000    78846153.85 0.0175  2.52E-06    0.000329    0.000107    0.0044298
0.0111755   0   0   0
    0   0   0   0   0   0   0   0   0   0
125 FRAME   250UC90, joint flexibility: [1-Z=0.0001 1-Y=0.0002 ]
    1   0   0   0   0   0   0   0   0
    205000000   78846153.85 0.0112243   9.30E-07   0.000140676 4.84E-05   0.00273
0.007381333 0   0   0
    0   0   0   0   0.0001  0   0.0002  0   0   0
126 FRAME   250UC90 # (P15), joint flexibility: [2-Z=0.0 2-Y=0.0 ]
    1   0   0   0   0   0   0   0   0
    205000000   78846153.85 0.0112243   9.30E-07   0.000140676 4.84E-05   0.00273
0.007381333 0   0   0
    0   0   0   0   0   0   0   0   0   0
127 FRAME   250UC90 (P15), joint flexibility: [1-Z=0.0001 1-Y=0.0004 ]
    1   0   0   0   0   0   0   0   0
    205000000   78846153.85 0.0112243   9.30E-07   0.000140676 4.84E-05   0.00273
0.007381333 0   0   0
    0   0   0   0   0.0001  0   0.0004  0   0   0
128 FRAME   152x76x6 RHS, joint flexibility: [1-Z=0.0023 1-Y=0.007 2-Z=0.0023 2-
Y=0.007 ]
    1   0   0   0   0   0   0   0   0
    205000000     78846153.85  0.002592      5.80E-06      7.61E-06      2.50E-06
0.001824    0.000912    0   0   0
    0   0   0   0   0.0023  0.0023  0.007   0.007   0   0
129 FRAME   152x76x6 RHS, joint flexibility: [1-Z=0.0023 1-Y=0.0071 2-Z=0.0023
2-Y=0.0071 ]
    1   0   0   0   0   0   0   0   0
    205000000     78846153.85  0.002592      5.80E-06      7.61E-06      2.50E-06
0.001824    0.000912    0   0   0
    0   0   0   0   0.0023  0.0023  0.0071  0.0071  0   0
```

```
130 FRAME   250UC90, joint flexibility: [2-Z=0.0001 2-Y=0.0002 ]
    1   0   0   0   0   0   0   0   0
    205000000   78846153.85 0.0112243   9.30E-07    0.000140676 4.84E-05    0.00273
0.007381333 0   0   0
    0   0   0   0   0   0.0001  0   0.0002  0   0
131 FRAME   460UB67 (P15)
    1   0   0   0   0   0   0   0   0
    205000000     78846153.85  0.0084691     3.35E-07       0.000290795  1.45E-05
0.003859    0.004021667 0   0   0
    0   0   0   0   0   0   0   0   0   0
132 FRAME   250UC90 (P15), joint flexibility: [2-Z=0.0001 2-Y=0.0002 ]
    1   0   0   0   0   0   0   0   0
    205000000   78846153.85 0.0112243   9.30E-07    0.000140676 4.84E-05    0.00273
0.007381333 0   0   0
    0   0   0   0   0   0.0001  0   0.0002  0   0
133 FRAME   327FB234, joint flexibility: [1-Z=0.0 1-Y=0.0001 ]
    1   0   0   0   0   0   0   0   0
    205000000   78846153.85 0.02982 1.28E-05    0.000540768 0.0002007   0.00654
0.020733333 0   0   0
    0   0   0   0   0   0   0.0001  0   0   0
134 FRAME   152x76x6 RHS, joint flexibility: [1-Z=0.003 1-Y=0.0093 2-Z=0.003 2-
Y=0.0093 ]
    1   0   0   0   0   0   0   0   0
    205000000     78846153.85  0.002592      5.80E-06      7.61E-06      2.50E-06
0.001824    0.000912    0   0   0
    0   0   0   0   0.003   0.003   0.0093  0.0093  0   0
135 FRAME   250UC90, joint flexibility: [2-Z=0.0002 2-Y=0.0005 ]
    1   0   0   0   0   0   0   0   0
    205000000   78846153.85 0.0112243   9.30E-07    0.000140676 4.84E-05    0.00273
0.007381333 0   0   0
    0   0   0   0   0   0.0002  0   0.0005  0   0
136 FRAME   250UC90 (P15), joint flexibility: [1-Z=0.0002 1-Y=0.0005 2-Z=0.0002
2-Y=0.0005 ]
    1   0   0   0   0   0   0   0   0
    205000000   78846153.85 0.0112243   9.30E-07    0.000140676 4.84E-05    0.00273
0.007381333 0   0   0
    0   0   0   0   0.0002  0.0002  0.0005  0.0005  0   0
137 FRAME   250UC90, joint flexibility: [1-Z=0.0001 1-Y=0.0003 ]
    1   0   0   0   0   0   0   0   0
    205000000   78846153.85 0.0112243   9.30E-07    0.000140676 4.84E-05    0.00273
0.007381333 0   0   0
    0   0   0   0   0.0001  0   0.0003  0   0   0
138 FRAME    250UB26, joint flexibility: [1-Z=0.0006 1-Y=0.0076 2-Z=0.0006 2-
Y=0.0076 ]
    1   0   0   0   0   0   0   0   0
    205000000   78846153.85 0.003144    5.01E-08    3.38E-05    2.54E-06    0.00124
0.001653333 0   0   0
    0   0   0   0   0.0006  0.0006  0.0076  0.0076  0   0
139 FRAME   250UB26, joint flexibility: [1-Z=0.0006 1-Y=0.0079 ]
    1   0   0   0   0   0   0   0   0
    205000000   78846153.85 0.003144    5.01E-08    3.38E-05    2.54E-06    0.00124
0.001653333 0   0   0
    0   0   0   0   0.0006  0   0.0079  0   0   0
140 FRAME   250UB26, joint flexibility: [2-Z=0.0001 2-Y=0.0018 ]
    1   0   0   0   0   0   0   0   0
    205000000   78846153.85 0.003144    5.01E-08    3.38E-05    2.54E-06    0.00124
0.001653333 0   0   0
    0   0   0   0   0   0.0001  0   0.0018  0   0
141 FRAME    250UB26, joint flexibility: [1-Z=0.0007 1-Y=0.009 2-Z=0.0007 2-
Y=0.009 ]
    1   0   0   0   0   0   0   0   0
    205000000   78846153.85 0.003144    5.01E-08    3.38E-05    2.54E-06    0.00124
0.001653333 0   0   0
    0   0   0   0   0.0007  0.0007  0.009   0.009   0   0
142 FRAME   250UC90, offset: y=0 z=0
    1   0   0   0   0   0   0   0   0
    205000000   78846153.85 0.0112243   9.30E-07    0.000140676 4.84E-05    0.00273
0.007381333 0   0   0
    0   0   0   0   0   0   0   0   0   0
143 FRAME   125x75x6 RHS, hinged-I (major), hinged-I (minor)
```

```
    1   1   1   0   0   0   0   0   0
    205000000   78846153.85 0.002256    4.30E-06    4.63E-06    2.04E-06    0.0015
0.0009  0   0   0
    0   0   0   0   0   0   0   0   0   0
144 FRAME    250UB26, joint flexibility: [1-Z=0.0005 1-Y=0.0068 2-Z=0.0005 2-
Y=0.0068 ]
    1   0   0   0   0   0   0   0   0
    205000000   78846153.85 0.003144    5.01E-08    3.38E-05    2.54E-06    0.00124
0.001653333 0   0   0
    0   0   0   0   0.0005  0.0005  0.0068  0.0068  0   0
145 FRAME    250UB26, joint flexibility: [1-Z=0.0005 1-Y=0.0067 2-Z=0.0005 2-
Y=0.0067 ]
    1   0   0   0   0   0   0   0   0
    205000000   78846153.85 0.003144    5.01E-08    3.38E-05    2.54E-06    0.00124
0.001653333 0   0   0
    0   0   0   0   0.0005  0.0005  0.0067  0.0067  0   0
146 FRAME    250UC90, joint flexibility: [1-Z=0.0002 1-Y=0.0005 2-Z=0.0002 2-
Y=0.0005 ]
    1   0   0   0   0   0   0   0   0
    205000000   78846153.85 0.0112243   9.30E-07    0.000140676 4.84E-05    0.00273
0.007381333 0   0   0
    0   0   0   0   0.0002  0.0002  0.0005  0.0005  0   0
147 FRAME   250UC90 #, hinged-J (major), hinged-J (minor)
    1   2   2   0   0   0   0   0   0
    205000000   78846153.85 0.0112243   9.30E-07    0.000140676 4.84E-05    0.00273
0.007381333 0   0   0
    0   0   0   0   0   0   0   0   0   0
148 FRAME   250UC90 # (P15), joint flexibility: [1-Z=0.0002 1-Y=0.0007 2-Z=0.0002
2-Y=0.0007 ]
    1   0   0   0   0   0   0   0   0
    205000000   78846153.85 0.0112243   9.30E-07    0.000140676 4.84E-05    0.00273
0.007381333 0   0   0
    0   0   0   0   0.0002  0.0002  0.0007  0.0007  0   0
149 FRAME   250UC90 # (P15), joint flexibility: [2-Z=0.0002 2-Y=0.0005 ]
    1   0   0   0   0   0   0   0   0
    205000000   78846153.85 0.0112243   9.30E-07    0.000140676 4.84E-05    0.00273
0.007381333 0   0   0
    0   0   0   0   0   0.0002  0   0.0005  0   0
150 FRAME   250UC90 #
    1   0   0   0   0   0   0   0   0
    205000000   78846153.85 0.0112243   9.30E-07    0.000140676 4.84E-05    0.00273
0.007381333 0   0   0
    0   0   0   0   0   0   0   0   0   0
151 FRAME   250UC90 (P15), joint flexibility: [1-Z=0.0001 1-Y=0.0004 2-Z=0.0001
2-Y=0.0004 ]
    1   0   0   0   0   0   0   0   0
    205000000   78846153.85 0.0112243   9.30E-07    0.000140676 4.84E-05    0.00273
0.007381333 0   0   0
    0   0   0   0   0.0001  0.0001  0.0004  0.0004  0   0
152 FRAME   250UC90 #, hinged-I (major), hinged-I (minor)
    1   1   1   0   0   0   0   0   0
    205000000   78846153.85 0.0112243   9.30E-07    0.000140676 4.84E-05    0.00273
0.007381333 0   0   0
    0   0   0   0   0   0   0   0   0   0
153 FRAME   250UC90 (P15), joint flexibility: [1-Z=0.0001 1-Y=0.0003 ]
    1   0   0   0   0   0   0   0   0
    205000000   78846153.85 0.0112243   9.30E-07    0.000140676 4.84E-05    0.00273
0.007381333 0   0   0
    0   0   0   0   0.0001  0   0.0003  0   0   0
154 FRAME   250UC90 #, joint flexibility: [1-Z=0.0003 1-Y=0.0008 2-Z=0.0003 2-
Y=0.0008 ]
    1   0   0   0   0   0   0   0   0
    205000000   78846153.85 0.0112243   9.30E-07    0.000140676 4.84E-05    0.00273
0.007381333 0   0   0
    0   0   0   0   0.0003  0.0003  0.0008  0.0008  0   0
155 FRAME   460UB67 (P15), joint flexibility: [1-Z=0.0001 1-Y=0.0012 2-Z=0.0001
2-Y=0.0012 ]
    1   0   0   0   0   0   0   0   0
    205000000     78846153.85  0.0084691     3.35E-07      0.000290795  1.45E-05
0.003859    0.004021667 0   0   0
    0   0   0   0   0.0001  0.0001  0.0012  0.0012  0   0
```

```
156 FRAME   460UB67 (P15), joint flexibility: [1-Z=0.0001 1-Y=0.0012 ]
    1   0   0   0   0   0   0   0   0
    205000000     78846153.85  0.0084691     3.35E-07      0.000290795  1.45E-05
0.003859    0.004021667 0   0   0
    0   0   0   0   0.0001  0   0.0012  0   0   0
157 FRAME   460UB67 (P15), joint flexibility: [1-Z=0.0001 1-Y=0.0017 2-Z=0.0001
2-Y=0.0017 ]
    1   0   0   0   0   0   0   0   0
    205000000     78846153.85  0.0084691     3.35E-07      0.000290795  1.45E-05
0.003859    0.004021667 0   0   0
    0   0   0   0   0.0001  0.0001  0.0017  0.0017  0   0
158 FRAME   460UB67 (P15), joint flexibility: [1-Z=0.0 1-Y=0.0008 ]
    1   0   0   0   0   0   0   0   0
    205000000     78846153.85  0.0084691     3.35E-07      0.000290795  1.45E-05
0.003859    0.004021667 0   0   0
    0   0   0   0   0   0   0.0008  0   0   0
159 FRAME   460UB67 (P15), joint flexibility: [1-Z=0.0 1-Y=0.0004 ]
    1   0   0   0   0   0   0   0   0
    205000000     78846153.85  0.0084691     3.35E-07      0.000290795  1.45E-05
0.003859    0.004021667 0   0   0
    0   0   0   0   0   0   0.0004  0   0   0
160 FRAME   460UB67 (P15), joint flexibility: [1-Z=0.0 1-Y=0.0006 ]
    1   0   0   0   0   0   0   0   0
    205000000     78846153.85  0.0084691     3.35E-07      0.000290795  1.45E-05
0.003859    0.004021667 0   0   0
    0   0   0   0   0   0   0.0006  0   0   0
161 FRAME    460UB67, joint flexibility: [1-Z=0.0001 1-Y=0.0013 2-Z=0.0001 2-
Y=0.0013 ]
    1   0   0   0   0   0   0   0   0
    205000000     78846153.85  0.0084691     3.35E-07      0.000290795  1.45E-05
0.003859    0.004021667 0   0   0
    0   0   0   0   0.0001  0.0001  0.0013  0.0013  0   0
162 FRAME   250UB26, joint flexibility: [1-Z=0.0002 1-Y=0.0026 ]
    1   0   0   0   0   0   0   0   0
    205000000   78846153.85 0.003144   5.01E-08   3.38E-05   2.54E-06   0.00124
0.001653333 0   0   0
    0   0   0   0   0.0002  0   0.0026  0   0   0
163 FRAME   250UB26, joint flexibility: [2-Z=0.0004 2-Y=0.0047 ]
    1   0   0   0   0   0   0   0   0
    205000000   78846153.85 0.003144   5.01E-08   3.38E-05   2.54E-06   0.00124
0.001653333 0   0   0
    0   0   0   0   0   0.0004  0   0.0047  0   0
164 FRAME   200UC52, joint flexibility: [2-Z=0.0002 2-Y=0.0006 ]
    1   0   0   0   0   0   0   0   0
    205000000     78846153.85  0.006548      2.85E-07      5.18E-05      1.77E-05
0.001648    0.00425 0   0   0
    0   0   0   0   0   0.0002  0   0.0006  0   0
165 FRAME   200UC52
    1   0   0   0   0   0   0   0   0
    205000000     78846153.85  0.006548      2.85E-07      5.18E-05      1.77E-05
0.001648    0.00425 0   0   0
    0   0   0   0   0   0   0   0   0   0
166 FRAME   200UC52, joint flexibility: [1-Z=0.0001 1-Y=0.0003 ]
    1   0   0   0   0   0   0   0   0
    205000000     78846153.85  0.006548      2.85E-07      5.18E-05      1.77E-05
0.001648    0.00425 0   0   0
    0   0   0   0   0.0001  0   0.0003  0   0   0
167 FRAME   200UC52, joint flexibility: [1-Z=0.0001 1-Y=0.0004 ]
    1   0   0   0   0   0   0   0   0
    205000000     78846153.85  0.006548      2.85E-07      5.18E-05      1.77E-05
0.001648    0.00425 0   0   0
    0   0   0   0   0.0001  0   0.0004  0   0   0
168 FRAME   250UC90 #, joint flexibility: [2-Z=0.0001 2-Y=0.0002 ]
    1   0   0   0   0   0   0   0   0
    205000000   78846153.85 0.0112243  9.30E-07   0.000140676 4.84E-05   0.00273
0.007381333 0   0   0
    0   0   0   0   0   0.0001  0   0.0002  0   0
169 FRAME   250UC90 #, joint flexibility: [1-Z=0.0 1-Y=0.0001 ]
    1   0   0   0   0   0   0   0   0
```

```
    205000000   78846153.85 0.0112243   9.30E-07    0.000140676 4.84E-05    0.00273
0.007381333 0    0    0
    0    0    0    0    0    0    0.0001   0    0    0
170 FRAME    250UC90 #, joint flexibility: [1-Z=0.0002 1-Y=0.0006 ]
    1    0    0    0    0    0    0    0    0
    205000000   78846153.85 0.0112243   9.30E-07    0.000140676 4.84E-05    0.00273
0.007381333 0    0    0
    0    0    0    0    0.0002   0    0.0006   0    0    0
171 FRAME    200UC52, joint flexibility: [2-Z=0.0002 2-Y=0.0007 ]
    1    0    0    0    0    0    0    0    0
    205000000     78846153.85  0.006548      2.85E-07      5.18E-05      1.77E-05
0.001648     0.00425 0    0    0
    0    0    0    0    0    0.0002   0    0.0007   0    0
172 FRAME    200UC52, joint flexibility: [1-Z=0.0003 1-Y=0.0009 ]
    1    0    0    0    0    0    0    0    0
    205000000     78846153.85  0.006548      2.85E-07      5.18E-05      1.77E-05
0.001648     0.00425 0    0    0
    0    0    0    0    0.0003   0    0.0009   0    0    0
173 FRAME    200UC52, joint flexibility: [2-Z=0.0002 2-Y=0.0005 ]
    1    0    0    0    0    0    0    0    0
    205000000     78846153.85  0.006548      2.85E-07      5.18E-05      1.77E-05
0.001648     0.00425 0    0    0
    0    0    0    0    0    0.0002   0    0.0005   0    0
174 FRAME     200UC52, joint flexibility: [1-Z=0.0004 1-Y=0.0013 2-Z=0.0004 2-
Y=0.0013 ]
    1    0    0    0    0    0    0    0    0
    205000000     78846153.85  0.006548      2.85E-07      5.18E-05      1.77E-05
0.001648     0.00425 0    0    0
    0    0    0    0    0.0004   0.0004   0.0013   0.0013   0    0
175 FRAME    250x150x6 RHS, joint flexibility: [2-Z=0.0002 2-Y=0.0004 ]
    1    0    0    0    0    0    0    0    0
    205000000   78846153.85 0.004656    3.82E-05    4.03E-05    1.82E-05    0.003
0.0018   0    0    0
    0    0    0    0    0    0.0002   0    0.0004   0    0
176 FRAME    250x150x6 RHS, joint flexibility: [1-Z=0.0003 1-Y=0.0007 ]
    1    0    0    0    0    0    0    0    0
    205000000   78846153.85 0.004656    3.82E-05    4.03E-05    1.82E-05    0.003
0.0018   0    0    0
    0    0    0    0    0.0003   0    0.0007   0    0    0
177 FRAME    250x150x6 RHS, joint flexibility: [2-Z=0.0003 2-Y=0.0006 ]
    1    0    0    0    0    0    0    0    0
    205000000   78846153.85 0.004656    3.82E-05    4.03E-05    1.82E-05    0.003
0.0018   0    0    0
    0    0    0    0    0    0.0003   0    0.0006   0    0
178 FRAME    250x150x6 RHS, joint flexibility: [1-Z=0.0001 1-Y=0.0003 ]
    1    0    0    0    0    0    0    0    0
    205000000   78846153.85 0.004656    3.82E-05    4.03E-05    1.82E-05    0.003
0.0018   0    0    0
    0    0    0    0    0.0001   0    0.0003   0    0    0
179 FRAME    250x150x6 RHS, joint flexibility: [1-Z=0.0004 1-Y=0.0009 ]
    1    0    0    0    0    0    0    0    0
    205000000   78846153.85 0.004656    3.82E-05    4.03E-05    1.82E-05    0.003
0.0018   0    0    0
    0    0    0    0    0.0004   0    0.0009   0    0    0
180 FRAME    250x150x6 RHS, joint flexibility: [2-Z=0.0002 2-Y=0.0005 ]
    1    0    0    0    0    0    0    0    0
    205000000   78846153.85 0.004656    3.82E-05    4.03E-05    1.82E-05    0.003
0.0018   0    0    0
    0    0    0    0    0    0.0002   0    0.0005   0    0
181 FRAME    250x150x6 RHS, joint flexibility: [1-Z=0.0003 1-Y=0.0006 ]
    1    0    0    0    0    0    0    0    0
    205000000   78846153.85 0.004656    3.82E-05    4.03E-05    1.82E-05    0.003
0.0018   0    0    0
    0    0    0    0    0.0003   0    0.0006   0    0    0
182 FRAME    250x150x6 RHS
    1    0    0    0    0    0    0    0    0
    205000000   78846153.85 0.004656    3.82E-05    4.03E-05    1.82E-05    0.003
0.0018   0    0    0
    0    0    0    0    0    0    0    0    0    0
183 FRAME    360UB51, joint flexibility: [1-Z=0.0 1-Y=0.0002 ]
    1    0    0    0    0    0    0    0    0
```

```
    205000000     78846153.85  0.0063639     2.09E-07      0.000139199  9.59E-06
0.0025988   0.0032775   0   0   0
    0   0   0   0   0   0   0.0002  0   0   0
184 FRAME   360UB51
    1   0   0   0   0   0   0   0   0
    205000000     78846153.85  0.0063639     2.09E-07      0.000139199  9.59E-06
0.0025988   0.0032775   0   0   0
    0   0   0   0   0   0   0   0   0   0
185 FRAME   360UB51, joint flexibility: [1-Z=0.0001 1-Y=0.0018 ]
    1   0   0   0   0   0   0   0   0
    205000000     78846153.85  0.0063639     2.09E-07      0.000139199  9.59E-06
0.0025988   0.0032775   0   0   0
    0   0   0   0   0.0001  0   0.0018  0   0   0
186 FRAME   250x150x6 RHS, joint flexibility: [2-Z=0.0004 2-Y=0.0009 ]
    1   0   0   0   0   0   0   0   0
    205000000   78846153.85 0.004656    3.82E-05    4.03E-05    1.82E-05    0.003
0.0018  0   0   0
    0   0   0   0   0   0.0004  0   0.0009  0   0
187 FRAME   250x150x6 RHS, joint flexibility: [2-Z=0.0006 2-Y=0.0013 ]
    1   0   0   0   0   0   0   0   0
    205000000   78846153.85 0.004656    3.82E-05    4.03E-05    1.82E-05    0.003
0.0018  0   0   0
    0   0   0   0   0   0.0006  0   0.0013  0   0
188 FRAME   360UB51, joint flexibility: [2-Z=0.0001 2-Y=0.0012 ]
    1   0   0   0   0   0   0   0   0
    205000000     78846153.85  0.0063639     2.09E-07      0.000139199  9.59E-06
0.0025988   0.0032775   0   0   0
    0   0   0   0   0   0.0001  0   0.0012  0   0
189 FRAME   310UB32
    1   0   0   0   0   0   0   0   0
    205000000     78846153.85  0.003935      6.46E-08      6.04E-05      4.41E-06
0.001639    0.001986667 0   0   0
    0   0   0   0   0   0   0   0   0   0
190 FRAME   360UB51, joint flexibility: [2-Z=0.0 2-Y=0.0001 ]
    1   0   0   0   0   0   0   0   0
    205000000     78846153.85  0.0063639     2.09E-07      0.000139199  9.59E-06
0.0025988   0.0032775   0   0   0
    0   0   0   0   0   0   0   0.0001  0   0
191 FRAME   250x150x6 RHS, joint flexibility: [1-Z=0.0006 1-Y=0.0013 ]
    1   0   0   0   0   0   0   0   0
    205000000   78846153.85 0.004656    3.82E-05    4.03E-05    1.82E-05    0.003
0.0018  0   0   0
    0   0   0   0   0.0006  0   0.0013  0   0   0
192 FRAME    310UB32, joint flexibility: [1-Z=0.0002 1-Y=0.0026 2-Z=0.0002 2-
Y=0.0026 ]
    1   0   0   0   0   0   0   0   0
    205000000     78846153.85  0.003935      6.46E-08      6.04E-05      4.41E-06
0.001639    0.001986667 0   0   0
    0   0   0   0   0.0002  0.0002  0.0026  0.0026  0   0
193 FRAME   360UB51, joint flexibility: [1-Z=0.0001 1-Y=0.0012 ]
    1   0   0   0   0   0   0   0   0
    205000000     78846153.85  0.0063639     2.09E-07      0.000139199  9.59E-06
0.0025988   0.0032775   0   0   0
    0   0   0   0   0.0001  0   0.0012  0   0   0
194 FRAME   250x150x6 RHS, joint flexibility: [1-Z=0.0003 1-Y=0.0008 ]
    1   0   0   0   0   0   0   0   0
    205000000   78846153.85 0.004656    3.82E-05    4.03E-05    1.82E-05    0.003
0.0018  0   0   0
    0   0   0   0   0.0003  0   0.0008  0   0   0
195 FRAME   250x150x6 RHS, joint flexibility: [1-Z=0.0003 1-Y=0.0007 2-Z=0.0003
2-Y=0.0007 ]
    1   0   0   0   0   0   0   0   0
    205000000   78846153.85 0.004656    3.82E-05    4.03E-05    1.82E-05    0.003
0.0018  0   0   0
    0   0   0   0   0.0003  0.0003  0.0007  0.0007  0   0
196 FRAME   250x150x6 RHS, joint flexibility: [1-Z=0.0002 1-Y=0.0005 ]
    1   0   0   0   0   0   0   0   0
    205000000   78846153.85 0.004656    3.82E-05    4.03E-05    1.82E-05    0.003
0.0018  0   0   0
    0   0   0   0   0.0002  0   0.0005  0   0   0
```

```
197 FRAME   250x150x6 RHS, joint flexibility: [1-Z=0.0006 1-Y=0.0013 2-Z=0.0006
2-Y=0.0013 ]
    1   0   0   0   0   0   0   0   0
    205000000   78846153.85 0.004656    3.82E-05    4.03E-05    1.82E-05    0.003
0.0018  0   0   0
    0   0   0   0   0.0006  0.0006  0.0013  0.0013  0   0

WEIGHTS 0
1   8964.511514 0   8964.511514 0   600633.0107 0
3   2628.583222 0   2628.583222 0   150985.4824 0
5   3637.098113 0   3637.098113 0   268533.623  0
7   3678.34936  0   3678.34936  0   269952.1029 0
9   3678.34936  0   3678.34936  0   269952.1029 0
11  3678.17945  0   3678.17945  0   269938.3002 0
13  3678.17945  0   3678.17945  0   269938.3002 0
15  3724.109576 0   3724.109576 0   262866.4527 0
17  2935.586387 0   2935.586387 0   189057.0761 0
19  424.1989188 0   424.1989188 0   24938.23154 0

LOADS   0
1   0   8964.511514 0   0   0   0
3   0   2628.583222 0   0   0   0
5   0   3637.098113 0   0   0   0
7   0   3678.34936  0   0   0   0
9   0   3678.34936  0   0   0   0
11  0   3678.17945  0   0   0   0
13  0   3678.17945  0   0   0   0
15  0   3724.109576 0   0   0   0
17  0   2935.586387 0   0   0   0
19  0   424.1989188 0   0   0   0

EQUAKE
6 1 0.005 1 -1 0 0 1

EQUAKE
6 1 0.005 1 -1 0 0 1
```